Computations of Viscous Compressible Flows in h, p, k Finite Element Framework with Variationally Consistent Integral Forms

by
Srikanth Allu

B.Tech. (Mechanical), J.N.T.U., Hyderabad, India 2001
M.S. (Mechanical), University of Kansas, Kansas, U.S.A 2003

Submitted to the Department of Mechanical Engineering and the Faculty of the Graduate School of the University of Kansas in partial fulfillment of the requirements for the Degree of Philosophy

Dissertation Committee Members

Dr. Karan S.Surana (Advisor), Chairman

Dr. Peter W. Tenpas

Dr. Bedru Yimer

Dr. Albert Romkes

Dr. Ray Taghavi

Dissertation Defended on : January 22, 2008

The Dissertation Committee for Srikanth Allu certifies that this is the approved version of the following dissertation:

Computations of Viscous Compressible Flows in h, p, k Finite Element Framework with Variationally Consistent Integral Forms

Dissertation Committee :

Dr. Karan S.Surana (Advisor), Chairman

Dr. Peter W. Tenpas

Dr. Bedru Yimer

Dr. Albert Romkes

Dr. Ray Taghavi

Date Approved :

This work is dedicated to my parents.

Acknowledgements

I would like to take this opportunity to achnowledge the major contribution of my advisor Dr. Karan S. Surana. As a mentor, he has carefully threaded the research and had a clear vision during the initial stages of my work. This invaluable guidance and encouragement led to a fruitful completion of this thesis. I greatly appreciate his persistence in all aspects of research and aim towards perfection and consistency.

I am grateful to Dr. Peter W. Tenpas and Dr. Albert Romkes for their critic and reasoned judgement which always helped me improve on the quality of the research and thesis. I also thank Dr. Bedru Yimer and Dr. Ray Taghavi for serving on my committee and also for their support and encouragement.

The financial support provided by DEPSCoR/AFOSR through grant numbers F49620-03-0298 to the University of Kansas, Department of Mechanical Engineering and through grant number F49620-03-1-0201 to Texas A&M University are gratefully acknowledged. The seed grand provided by ARO through grant numbers FED46680 to the University of Kansas, Department of Mechanical Engineering is also acknowledged. The financial support from the Department of Mechanical Engineering of the University of Kansas to support this work is much appreciated. The computing facilities of the Computational Mechanics Laboratory (CML) of the Department of Mechanical Engineering and the software development infrastructure provided has been instrumental in conducting the numerical studies.

Many people are involved directly or indirectly in helping me during the course of study at KU. I owe many of my accomplishments to all of my friends and colleagues and also thank them for making my journey eventful.

Finally, I like to make a special mention about my parents for their unconditional love and support. I would have never achieved anything in life without the trust and confidence they have on me. I dedicate this work to them for their belief in me all these years.

Srikanth Allu
Kansas.

Abstract

This thesis presents mathematical models for time dependent and stationary viscous compressible flows based on conservation laws, constitutive equations and equations of state using Eulerian description. In the presence of physical viscosity, conductivity and other transport properties, the mathematical models are well recognized Navier-Stokes equations. Variable transport properties as well as ideal and real gas models are considered for equations of state. The mathematical models are a highly non-linear coupled partial differential equations in space and time. The mathematical and computational infrastructure using finite element method is presented for obtaining numerical solutions of the Boundary Value Problems and Initial Value Problems associated with the mathematical models. This infrastructure is based on h, p, k (h-characteristic length, p-degree of local approximation, k-order of approximation space) as independent computational parameters with an additional requirement that the integral form be variationally consistent in case of Boundary Value Problems and space-time variationally consistent in case of Initial Value Problems. All methods of approximation except Least Squares and Space-Time Least Squares Processes are Variationally Inconsistent. Variational Consistency and Space-Time Variational Consistency of integral forms ensure unconditionally stable computational processes.

A variety of numerical studies are presented for Initial Value Problems as well as Boundary Value Problems. 1-D transient viscous form of Burgers equation, 1-D Riemann shock tube with ideal and real gas models and Boundary Value Problems in 2-D compressible flow : Carter's plate with Mach 1, 2, 3 and 5 flows and Mach 1 flow past a circular cylinder are used as model problems. Shock evolution, propagation, interactions and reflection are quantified based on the rate of entropy production using Air as a medium for 1-D Riemann shock tube. It is clearly established that rarefaction shocks are not possible for FC70 for any choice of initial conditions. In all studies evolution of a shock is presented (unlike the published work). Its existence and sustained propagation is established based on S_r, the rate of entropy production per unit volume. In case of transient Burgers equation it is demonstrated that time accurate evolutions can be computed for any finite Reynolds number. Contrary to the common belief, the work presented here shows that solutions of Boundary Value Problems in compressible flows present no special problems.

In Summary : (i) the mathematical models for the compressible flow are based on Navier-Stokes equations. (ii) computational infrastructure is based on hpk

and unconditionally stable integral forms with higher order global differentiability in space and time. (iii) All numerical studies utilize actual transport properties of the medium. (iv) Up-winding methods such as SUPG, SUPG/DC, SUPG/DC/LS are neither needed nor used. (v) existence of shocks is established through evolution and not using Rankine-Hugoniot relations. (vi) Governing Differential Equations in the mathematical models are neither linearized nor altered in any form during the entire process of formulation and computations.

The work presented here clearly demonstrates that the numerical simulations of Boundary Value Problems and Initial Value Problems based on Navier-Stokes equations describing viscous compressible flows can be done in a straight forward manner in h, p, k framework with Variational Consistent and Space-Time Variationally Consistent integral forms. The computational processes always remain unconditionally stable. The mathematical models based on Euler's equations lack physics, computational methods for Euler's equations use problem dependent up-winding methods which lack mathematical basis and rigor and thus in our view are of little merit if at all for numerical simulations of Boundary Value Problems and Initial Value Problems in compressible flows.

Table of Contents

List of Tables **v**

List of Figures **vi**

Chapter 1. Introduction **1**

1.1 Introduction 1

1.2 Literature Review 5

1.2.1 1-D nonlinear conservation law : 1D time dependent Burgers equation 6

1.2.2 1-D Riemann shock tube 12

1.2.3 2-D compressible flows : BVPs 14

1.2.4 Mathematical and Computational methodologies for BVPs . . 15

1.2.5 Mathematical and Computational Methodologies for IVPs . . 17

1.2.6 Up-winding methods 32

1.2.7 Higher order smoothness or differentiability of approximations 34

1.3 Scope of work 36

Chapter 2. Mathematical Framework and Computational Infrastructure for BVPs and IVPs **41**

2.1 Introduction 41

2.2 Boundary value problems (BVPs) 41

2.3 Initial Value Problems (IVPs) 44

2.3.1 General Considerations 44

2.3.2 Mathematical classification of space-time differential operators 46

2.3.3 Space-time Integral forms and space-time methods of approximation 50

2.4 Higher order global differentiability approximation spaces 55

2.5 Calculus of variations and space-time variational consistency (STVC) or variational inconsistency (STVIC) of the space-time integral forms 56

2.5.1 Elements of calculus of variations 56
2.5.2 STVC or STVIC of space-time integral forms 58
2.6 Space-time mesh and space-time, time marching processes. 63
2.6.1 Space-time mesh : 64
2.6.2 Time marching using space-time strip or slab : 64
2.7 Summary 68

Chapter 3. Mathematical Models and Finite Element Formulations 72
3.1 Introduction 72
3.2 1-D Transient Viscous Burgers Equation 72
3.3 Literature Review 73
3.3.1 Present Study 79
3.4 1-D Transient Burgers equation 81
3.4.1 Strong form of the GDE 81
3.4.2 Weak form of the GDE 82
3.4.3 Space-time LSP in h, p, k framework 86
3.5 Mathematical model for viscous conducting compressible flows with variable transport properties 88
3.5.1 Weak form of GDEs 92
3.5.2 Strong form of GDEs 93
3.5.3 Dimensionless form of the GDEs for compressible flow . . . 94
3.5.4 Dimensionless form of GDEs (Weak form) 95
3.5.5 Dimensionless form of GDEs (Strong form) 96
3.5.6 General remark on the mathematical models : GDEs in weak and strong form 97
3.5.7 Equation of state : $p = p(\rho, T)$ 98
3.5.7.1 Perfect gas or ideal gas 98
3.5.7.2 Thermal equations of state for real gases or real gas models 99
3.5.8 Specific internal energy $\hat{e}$ and other transport properties : . . . 100
3.5.9 Specific choices of p_0, τ_0 : 102
3.5.9.1 Weak form of GDEs (dimensionless) : 102
3.5.9.2 Strong form of GDEs (dimensionless) : 103

3.6 1-D Riemann shock tube (IVP) . . . 104
3.6.1 Mathematical models . . . 105
3.6.2 Weak form of GDEs : 1-D Riemann shock tube . . . 105
3.6.3 Strong form of GDEs : 1-D Riemann shock tube . . . 109
3.7 2-D Compressible flow : BVPs . . . 111
3.7.1 Mathematical models (2-D BVPs) : . . . 112
3.7.1.1 Weak form of GDEs . . . 112
3.7.1.2 Strong form of GDEs . . . 115
3.7.2 Summary . . . 117

Chapter 4. Numerical Studies : 1-D Transient Viscous Burgers Equation 119
4.1 Introduction . . . 119
4.2 Numerical Studies . . . 119
4.2.1 Evolution and stationary states of a single shock . . . 120
4.2.1.1 Mathematical representation of step boundary condition and rationale for comparison between theoretical and numerical solutions. . . . 121
4.2.1.2 Evolution and its stationary state for Re = 100. . . . 124
4.2.1.3 Evolution and its stationary state for Re = 1000. . . . 125
4.2.1.4 Evolution and its stationary state for Re = 10000 . . 130
4.2.2 Evolution and stationary state of a double shock at $Re = 1000$ 130
4.2.3 Evolution of transonic shock at $Re = 1000$ . . . 137
4.2.4 Evolutions for progressively increasing CFL numbers : unconditional non-degeneracy and stability of STLSP . . . 139
4.3 Summary . . . 139

Chapter 5. Numerical Studies : 1-D Riemann Shock tube with Viscous and Conducting medium using ideal and real gas models for equation of state 146
5.1 Introduction . . . 146
5.2 Riemann shock tube : Ideal gas Law . . . 147
5.2.1 Definition of shock . . . 148
5.2.1.1 Numerical Studies : Ideal gas Law . . . 150
5.3 Riemann shock tube : Real gas Laws . . . 174

5.3.1 Real gas behavior and possibility of rarefaction shocks 174
5.3.2 Numerical Studies : Real gas model ; Van der Waals equation of state 180
5.4 Summary 207

Chapter 6. Numerical Studies for 2-D viscous compressible flows : BVPs 217
6.1 Introduction 217
6.2 Carter's plate 222
6.2.1 Mach 1 flow : 224
6.2.2 General consideration for higher Mach number flows : 227
6.2.3 Mach 2 flow 228
6.2.4 Mach 3 flow 231
6.2.5 Mach 5 flow 233
6.2.6 Comparison of results for Mach 1, 2, 3 and 5 flows 235
6.3 Flow past a circular cylinder 239
6.3.1 Starting or Initial solutions 243
6.3.2 Mach 1 flow past a circular cylinder 254
6.4 Summary 260

Chapter 7. Summary and Conclusions 262

List of Tables

6.1 Re, I, g for incompressible flow calculations 254

List of Figures

2.1 Space-time mesh and space-time strip or slab for an increment of time Δt 47

4.1 BC at x=0 i.e., $\varphi(0,t)$ 121
4.2 Descriptions of impulsive $\varphi(0,t)$ for $0 \leq t \leq \Delta t$ in spaces of progressively higher order global differentiability in time obtained using interpolants 123
4.3 Contours and profiles of φ_h in x-t domain for a single shock at $Re = 100$ 126
4.4 L_2-norms of the $\partial\varphi_h/\partial x$ and $\partial\varphi_h/\partial t$ versus time for a single shock at Re=100 using space-time strip with time marching 127
4.5 Contours and profiles of φ_h in x-t domain for a single shock at $Re = 1000$ 128
4.6 L_2-norms of the $\partial\varphi_h/\partial x$ and $\partial\varphi_h/\partial t$ versus time for a single shock at Re=1000 using space-time strip with time marching 129
4.7 Contours and profiles of φ_h in x-t domain for a single shock at $Re = 10000$ 131
4.8 IC and BC for double shock at $Re = 1000$ 133
4.9 Contours and profiles of φ_h in x-t domain for a double shock at $Re = 1000$ 135
4.10 L_2-norms of the $\partial\varphi_h/\partial x$ and $\partial\varphi_h/\partial t$ for solutions of class $C^{1,1}$ and $C^{2,1}$ for double shock at $Re = 1000$ 136
4.11 IC and BC for transonic shock at $Re = 1000$ 138
4.12 Contours and profiles of φ_h in x-t domain for a transonic shock at $Re = 1000$ 140
4.13 L_2-norms of the $\partial\varphi_h/\partial x$ and $\partial\varphi_h/\partial t$ for transonic shock problem at Re=1000 141
4.14 L_2-norms of the $\partial\varphi_h/\partial x$ and $\partial\varphi_h/\partial t$ for meshes of 200, 400, 800 elements in space with $h_t = \Delta t = 0.01$ and $Re = 1000$ 142

5.1 Schematic of Riemann shock tube for an increment of time Δt . . . 152
5.2 Distribution of density over an element at the diaphragm 152

5.3 Evolution of density ρ : $\rho_h/\rho_l = 20$; $\varphi_h^e \in C^{11}({}^n\bar{\Omega}_{xt}^e), p = 11$ . . . 153
5.4 Evolution of velocity u : $\rho_h/\rho_l = 20$; $\varphi_h^e \in C^{11}({}^n\bar{\Omega}_{xt}^e), p = 11$ . . . 154
5.5 Evolution of temperature T : $\rho_h/\rho_l = 20$; $\varphi_h^e \in C^{11}({}^n\bar{\Omega}_{xt}^e), p = 11$. 154
5.6 Space-time plot of evolution of S_r 157
5.7 Space-time plot of evolution of velocity, u 158
5.8 Space-time plot of evolution of density, ρ 159
5.9 Space-time plot of evolution of temperature, T 160
5.10 Evolution of density ρ : $\rho_h/\rho_l = 20$; $\varphi_h^e \in C^{21}({}^n\bar{\Omega}_{xt}^e), p = 5$ 162
5.11 Evolution of velocity u : $\rho_h/\rho_l = 20$; $\varphi_h^e \in C^{21}({}^n\bar{\Omega}_{xt}^e), p = 5$ 162
5.12 Evolution of temperature T : $\rho_h/\rho_l = 20$; $\varphi_h^e \in C^{21}({}^n\bar{\Omega}_{xt}^e), p = 5$ . . 163
5.13 Space-time plot of evolution of S_r 164
5.14 Space-time plot of evolution of velocity, u 165
5.15 Space-time plot of evolution of density, ρ 166
5.16 Space-time plot of evolution of temperature, T 167
5.17 Space-time plot of evolution of S_r 170
5.18 Space-time plot of evolution of velocity, u 171
5.19 Space-time plot of evolution of density, ρ 172
5.20 Space-time plot of evolution of temperature, T 173
5.21 Isentrope with anomalous convexity in Van der Waals equation of state 175
5.22 1D-Riemann shock tube with density distribution for some value ot time 178
5.23 p versus v for case(a) : Isothermal ; Initial Conditions inside the critical zone 183
5.24 Evolution of Density for case(a) : Isothermal ; Initial Conditions inside the critical zone 184
5.25 Evolution of Velocity for case(a) : Isothermal ; Initial Conditions inside the critical zone 185
5.26 Evolution of Temperature for case(a) : Isothermal ; Initial Conditions inside the critical zone 185
5.27 Space-time plot of evolution of S_r ; case(a) : Isothermal , Initial Conditions inside the critical zone 186
5.28 Space-time plot of evolution of velocity, u ; case(a) : Isothermal , Initial Conditions inside the critical zone 187

5.29 Space-time plot of evolution of density, ρ ; case(a) : Isothermal , Initial Conditions inside the critical zone 188
5.30 Space-time plot of evolution of temperature, T ; case(a) : Isothermal , Initial Conditions inside the critical zone 189
5.31 p versus v for case(b) : Non-isothermal ; Initial Conditions inside the critical zone 191
5.32 Evolution of Density for case(b) : Non-isothermal ; Initial Conditions inside the critical zone 192
5.33 Evolution of Velocity for case(b) : Non-isothermal ; Initial Conditions inside the critical zone 192
5.34 Evolution of Temperature for case(b) : Non-isothermal ; Initial Conditions inside the critical zone 193
5.35 Space-time plot of evolution of S_r ; case(b) : Non-isothermal , Initial Conditions inside the critical zone 194
5.36 Space-time plot of evolution of velocity, u ; case(b) : Non-isothermal , Initial Conditions inside the critical zone 195
5.37 Space-time plot of evolution of density, ρ ; case(b) : Non-isothermal , Initial Conditions inside the critical zone 196
5.38 Space-time plot of evolution of temperature, T ; case(b) : Non-isothermal , Initial Conditions inside the critical zone 197
5.39 p versus v for case(c) : Isothermal ; Initial Conditions outside the critical zone 199
5.40 Evolution of Density for case(c) : Isothermal ; Initial Conditions outside the critical zone 200
5.41 Evolution of Velocity for case(c) : Isothermal ; Initial Conditions outside the critical zone 200
5.42 Evolution of Temperature for case(c) : Isothermal ; Initial Conditions outside the critical zone 201
5.43 Space-time plot of evolution of S_r ; case(c) : Isothermal , Initial Conditions outside the critical zone 202
5.44 Space-time plot of evolution of velocity, u ; case(c) : Isothermal , Initial Conditions outside the critical zone 203
5.45 Space-time plot of evolution of density, ρ ; case(c) : Isothermal , Initial Conditions outside the critical zone 204
5.46 Space-time plot of evolution of temperature, T ; case(c) : Isothermal , Initial Conditions outside the critical zone 205
5.47 p vs v for case(d) : Non-isothermal ; Initial Conditions inside the critical zone 208

5.48 Evolution of Density for case(d) : Non-isothermal ; Initial Conditions inside the critical zone 209
5.49 Evolution of Velocity for case(d) : Isothermal ; Initial Conditions inside the critical zone 209
5.50 Evolution of Temperature for case(d) : Non-isothermal ; Initial Conditions inside the critical zone 210
5.51 Space-time plot of evolution of S_r ; case(d) : Non-isothermal , Initial Conditions inside the critical zone 211
5.52 Space-time plot of evolution of velocity, u ; case(d) : Non-isothermal , Initial Conditions inside the critical zone 212
5.53 Space-time plot of evolution of density, ρ ; case(d) : Non-isothermal , Initial Conditions inside the critical zone 213
5.54 Space-time plot of evolution of temperature, T ; case(d) : Non-isothermal , Initial Conditions inside the critical zone 214

6.1 Schematic of Carter's plate 223
6.2 Carter's plate Boundary conditions 223
6.3 Contour of the Density, ρ for Mach 1.0 flow 225
6.4 Contour of the Velocity, u for Mach 1.0 flow 226
6.5 Contour of the Temperature, T for Mach 1.0 flow 226
6.6 Contour of the Density, ρ for Mach 2.0 flow 229
6.7 Contour of the Velocity, u for Mach 2.0 flow 229
6.8 Contour of the Temperature, T for Mach 2.0 flow 230
6.9 Contour of the Density, ρ for Mach 3.0 flow 231
6.10 Contour of the Velocity, u for Mach 3.0 flow 232
6.11 Contour of the Temperature, T for Mach 3.0 flow 232
6.12 Contour of the Density, ρ for Mach 5.0 flow 233
6.13 Contour of the Velocity, u for Mach 5.0 flow 234
6.14 Contour of the Temperature, T for Mach 5.0 flow 234
6.15 Velocity u at the outflow for Mach 1, 2, 3 and 5 flows 236
6.16 Exploded View of Velocity u for Mach 1, 2, 3 and 5 flows 237
6.17 Density ρ at the outflow for Mach 1, 2, 3 and 5 flows 237
6.18 Temperature T at the outflow for Mach 1, 2, 3 and 5 flows 238
6.19 Velocity v at the outflow for Mach 1, 2, 3 and 5 flows 238
6.20 Schematic of Flow over circular cylinder 240

6.21 Boundary conditions for flow past a circular cylinder (compressible flow) 241
6.22 Discretizations for the two different domain lengths for flow past a cylinder 242
6.23 Comparison of Velocity component u for $Re = 10$ of lengths of 30.5 and 60.5 behind the cylinder (incompressible flow) 245
6.24 Comparison of Velocity component u for $Re = 20$ of lengths of 30.5 and 60.5 behind the cylinder (incompressible flow) 246
6.25 Comparison of Velocity component u for $Re = 40$ of lengths of 30.5 and 60.5 behind the cylinder (incompressible flow) 247
6.26 Comparison of Velocity component u for $Re = 60$ of lengths of 30.5 and 60.5 behind the cylinder (incompressible flow) 248
6.27 Comparison of Velocity component u for $Re = 80$ of lengths of 30.5 and 60.5 behind the cylinder (incompressible flow) 249
6.28 Comparison of Velocity component u for $Re = 100$ of lengths of 30.5 and 60.5 behind the cylinder (incompressible flow) 250
6.29 Comparison of Velocity component u for $Re = 200$ of lengths of 30.5 and 60.5 behind the cylinder (incompressible flow) 251
6.30 Comparison of Velocity component u for $Re = 500$ of lengths of 30.5 and 60.5 behind the cylinder (incompressible flow) 252
6.31 Contour plot of Velocity u for compressible flow past a cylinder of lengths of 30.5 256
6.32 Contour plot of Velocity v for compressible flow past a cylinder of lengths of 30.5 257
6.33 Contour plot of Density ρ for compressible flow past a cylinder of lengths of 30.5 258
6.34 Contour plot of Temperature T for compressible flow past a cylinder of lengths of 30.5 259

Nomenclature

Br	–	Brinkman Number $\left(\frac{\mu_0 u_0^2}{k_{x0} T_0}\right)$
c_p	–	Specific heat at constant pressure
c_v	–	Specific heat at constant volume
E_i^e	–	Error (or residual) equation for an element $'\mathrm{e}'$
Ec	–	Eckert Number $\left(\frac{u_0^2}{c_{v0} T_0}\right)$
I	–	Error Functional in Least Squares Finite Element Formulation
k_x	–	coefficient of thermal conductivity
L_o	–	Reference Length
$\hat{\mathrm{p}}$	–	Pressure
p	–	Dimensionless Pressure
q_x	–	heat flux
S_r	–	rate of entropy production per unit volume
R	–	gasconstant
Re	–	Reynolds Number $\left(\frac{\rho_0 L_0 u_0}{\mu_0}\right)$
T	–	Temperature
t	–	time
$\hat{u}$	–	Velocity in x direction
u	–	Dimensionless Velocity in x direction
u_o	–	Reference Velocity
$\hat{v}$	–	Velocity in y direction
v	–	Dimensionless Velocity in y direction
$\hat{w}$	–	Velocity in z direction
w	–	Dimensionless Velocity in z direction
$\hat{x}$	–	x coordinate
x	–	Dimensionless x coordinate
$\hat{y}$	–	y coordinate
y	–	Dimensionless y coordinate

Greek Symbols

$\hat{\rho}$	–	Density
ρ	–	Dimensionless Density
$\hat{\mu}$	–	Dynamic Viscosity
μ	–	Dimensionless Dynamic Viscosity
$\hat{\tau}$	–	Stress Tensor
τ	–	Dimensionless Stress Tensor
$\hat{\tau}_{xx}$	–	Normal Stress in x direction
τ_{xx}	–	Dimensionless Normal Stress in x direction
$\hat{\tau}_{yy}$	–	Normal Stress in y direction
τ_{yy}	–	Dimensionless Normal Stress in y direction
$\hat{\tau}_{zz}$	–	Normal Stress in z direction
τ_{zz}	–	Dimensionless Normal Stress in z direction
$\hat{\tau}_{xy}$	–	Shear Stress in xy plane
τ_{xy}	–	Dimensionless Shear Stress in xy plane
ϕ	–	Field Variable
Φ	–	Viscous Dissipation
τ_o	–	Reference Stress
ρ_o	–	Reference Density
μ_o	–	Reference Viscosity
$\dot{\gamma}$	–	ShearRate

Chapter 1

Introduction

1.1 Introduction

It is well known that numerical solutions of Boundary Value Problems and Initial Value Problems in viscous compressible flows are dominated by finite difference and finite volume methods. The mathematical models generally consists of Euler's equations derived from the corresponding Navier-Stokes equations by considering the medium inviscid and non-conducting. These mathematical models admit perfect shocks (step change) and hence suffer from non-uniqueness of the solutions. Using the idea of generalized solutions proposed by S.L. Sobolev, Godunov [1] showed that theory of generalized solutions leads to non-uniqueness of solutions for inviscid Burgers equation : $\partial\varphi/\partial t + \varphi\partial\varphi/\partial x = 0$. This situation can be corrected by imposing additional restrictions on the weak form used in generalized solutions. For the Burgers equation (and its generalization to quasi-linear systems), this restriction leads to the law of conservation of entropy. Thus, in gas dynamics equations describing reversible processes, the law of conservation of entropy must hold in the theory of generalized solutions, whereas in irreversible processes there must be entropy production which in physical systems under adiabatic conditions is only possible through dissipative mechanisms. In other words, in the theory of generalized solutions of gas dynamics equations, the law of

increase in entropy must be replaced by the law of dissipation of energy to ensure the uniqueness of generalized solutions. A rigorous mathematical exposition of the solutions of quasi-linear hyperbolic equations is presented by B.L. Rozhdestvenskii [2]. The findings are similar to those reported by Godunov and are summarized in reference [3]. The author shows that systems of linear equations are always conservative, while the systems of non-linear equations, generally speaking, are conservative only for $n \leq 2$ (two conservation laws).

The extension of Gudunov's findings for Euler's equations amounts to stating that in the absence of viscous dissipation the solutions of Euler's equations are non-unique regardless of the computational methodology employed. Thus, in order to make the solutions of the Euler's equations unique one must have some mechanism of viscous dissipation. This is done at present using what are known as up-winding methods. These methods add artificial diffusion to the Euler's equations (i.e., artificial mechanism of viscous dissipation) in some form or the other. Thus, in finite difference, finite volume and finite element methods (based on Galerkin method with weak form) Euler's equations are solved numerically using up-winding methods. In this approach : (i) the artificial diffusion is non-physical and rarely has a basis in view of the mathematical models based on viscous and conducting medium. (ii) The means by which up-winding is accomplished is problem dependent. Hence, making it not appealing as general approach for BVPs and IVPs. (iii) Due to non physical nature of the up-winding methods, evolutions are rarely time accurate. (iv) Up-winded numerical solutions are generally diffused, thus, some means must be employed to restore the sharpness of the fronts. In the

finite element method thus has given rise to a host of approaches such as SUPG, SUPG/DC, SUPG/DC/LS and others [4]. (v) Due to problem dependent nature of the up-winding methods, a general mathematical computational infrastructure for all BVPs and IVPs in which all mathematical models can be treated with the same rigor and same methodology cannot be constructed.

Inspite of all these short comings, the mathematical models based on Euler's equations with up-winding methods remain the dominant computational methodology for compressible flows. In many works it has been argued that resolution of viscous boundary layer, viscous shock structures is a time consuming and mesh intensive process that requires enormous computational resources. Hence, if these behaviors are isolated from the rest of the domain so that the lack of their resolution does not corrupt the solution elsewhere, then it may be possible to resolve the flow feature everywhere except in these isolated regions which are generally orders of magnitude smaller than the over all flow domain. This idea has lead to shock capturing methods, shock fitting methods etc, in which one only tries to obtain shock relations without shock structure resolution. This approach does have its own merits in the sense that in this methodology many useful quantities of interest to the designer may be obtained without paying attention to the small scale details.

These methods had utility and usefulness when the computational resources were limited and we had no choice but to do so in-order to obtain some meaningful solutions of practical problems of interest. However, this is not the case at present. Incredibly fast desktops, clusters with distributed computing capability and

supercomputers configured using clusters provide ample computing power so that perhaps the assumptions employed in the mathematical models (such as inviscid and non-conducting medium) may no longer be necessary. This approach opens the door for more precise mathematical models that are a closer representation of the true physics in the computational process and possibly provide an avenue in which we can avoid (to some extent) many of the ad-hoc and problem dependent treatments (such as up-winding methods). This is one aspect that is addressed carefully in the present research.

The other aspect is obtaining reliable and accurate numerical solutions of the mathematical models. This obviously requires a choice of prudent and problem independent strategy that has : (i) Sound mathematical infrastructure to allow us to ascertain a priori of computations regarding existence, necessary conditions, sufficient conditions for the numerical solution of a given BVP or IVP. (ii) Sound computational infrastructure that allows us to transform or translate the mathematical features and requirements into a workable computational framework to seek the numerical solutions of BVPs and IVPs. In view of (i) and (ii), finite difference and finite volume methods can be easily ruled out in the present work. Out of finite element method, boundary element method, mesh-less methods, mesh-less petrov Galerkin method etc, we choose finite element method in the present work. The compelling reasons for doing so will be clear in the following sections and chapters. Even in finite element method there are a host of choices : Galerkin method (Gal), Petrov Galerkin Method (PGM), Weighted Residual Method (WRM), Galerkin Method with Weak Form (Gal/WF) and Least Squares

method (or process) (LSP). We choose LSP for BVPs and space-time Least Squares Processes for IVPs. This choice is obvious based on the fact that partial differential equations (PDEs) in the mathematical models are always non-linear and hence LSP and STLSP are the only methods that would yield Variationally Consistent integral form [5], essential for unconditional stability of the computational processes for BVPs and IVPs.

1.2 Literature Review

A literature review of Finite difference and Finite volume methods is not presented here for obvious reasons. Even the published work on finite element methods in fluid mechanics and gas dynamics is voluminous and a comprehensive discussion of these would hardly serve any purpose. Instead we group the pertinent literature and provide a short discussion with appropriate references so that interested reader can search for desired information. Since 1-D conservation law, 1-D Riemann shock tube and 2-D compressible flows are specifically dealt with in this work, we provide references in these areas.

Euler's equations as a basis for Mathematical models

A compelling need for the use of Euler's equations as mathematical models for compressible viscous flows is elaborately described in [6]. The paper lists 183 references related to Euler's equations and many techniques of using them effectively in the computations of viscous compressible flows. Assured accuracy, acceptable computational and human costs and fast turn around are listed as the

three basic requirements of a computational method for industrial use. Euler's equations are assumed to be valid mathematical model for compressible flows. References [7]-[8] report various aspects of finite difference and finite volume numerical methods to obtain numerical solution of Euler's equations. Interested readers can search [6] for more work using Euler's equations. Our view of Euler's equations as mathematical models is rather simple : (i) Do these models have the right physics ? (ii) Are the solutions of the associated BVPs and IVPs based on Euler's equations unique ? (iii) Can the solutions of the Euler's equations be made unique (without going back to Navier-Stokes equations) using mathematically justifiable means ? The answers to all these fundamental questions raising intrinsically important and crucial aspects related to the mathematical model is of course 'NO'. Then why is it that we insist and continue to use these in CFD ? There is one more extremely important question for us to answer : Is there an alternative ? Answer to this question is 'Yes'. Alternative is use of full viscous form of Navier-Stokes equations for conducting medium that incorporates the desire physics, and investigation of BVPs and IVPs associated with these mathematical models to determine if these can be solved accurately and effectively in a problem independent mathematical computational infrastructure. In the following we present literature review pertinent to the model problems used in this study.

1.2.1 1-D nonlinear conservation law : 1D time dependent Burgers equation

Solution of non-linear hyperbolic systems has been reported by Glimm [3] and Smoller [3]-[9]. Grimm proposed an existence theorem and provided its

proof. Smoller reported general characteristics of these solutions with specific details and discussion of the Riemann problem and contact discontinuities. Hopf [10] presented a mathematical proof of the convergence of weak solutions of quasi-linear equations of first order with artificial viscosity to strong solutions as viscosity approaches zero. Friedrich and Lax [11] discussed first order conservative systems of non-linear conservation laws which have as a consequence an additional conservation law. They show that if the additional conserved quantity is a convex function of the original ones, the original system can be put into symmetric hyperbolic form. They also derive an entropy inequality which has also been suggested by Kruzhkov [12] for discontinuous solutions of the given system of conservation laws. Existence of discrete shocks, genuine non-linearity and the use of fourth order dissipation in a single conservation law have been reported by Mock [13]-[14]. A thorough mathematical exposition with theorems and proofs for uniqueness of the solutions of hyperbolic conservation laws has been reported by DiPerna [15]. Existence and uniqueness of entropy solutions to the Riemann problem for hyperbolic systems of two conservation laws has been reported by Keyfitz and Kranzer [16]. The paper presents proofs of existence and uniqueness of the solutions in one space variable. Only strictly hyperbolic and genuinely non-linear systems are investigated. Noh [17] reported an investigation of the errors introduced in the calculation of strong shocks using artificial viscosity of the type in reference [18] and artificial heat flux. An investigation of the errors introduced in the interaction of strong shocks due to the assumption of finite shock width has been reported by Menikoff [19].

There are many published works addressing numerical simulation of partial differential equations resulting from non-linear hyperbolic conservation laws. Here we primarily consider finite element approaches. Comprehensive literature review of published finite element approaches for convection-diffusion and Burgers equation can be found in references [20]-[21]. As pointed out in reference [2], for linear and non-linear hyperbolic systems based on one or two conservation laws it is possible to show the convergence of generalized solutions to strong solutions.

The one dimensional form of the time dependent momentum equation yields 1-D time dependent viscous form of the Burgers equation, which when non-dimensionalized, contains the dimensionless parameter, Reynolds number (Re). The viscosity of the medium is reflected in Re. For the viscous form of the Burgers equation the solutions are analytic with finite shock width dependent upon the Reynolds number. For higher Re, the shock width is approximately $O(1/Re)$ and hence remains finite for a finite value of Re. The shock structure resolution in this case requires prudent mesh refinements in the shock zone to accommodate the localized high gradients of the solution for high Re. The analytic solutions of the viscous form of the Burgers equation can be expressed as algebraic polynomials of infinite degree in space and time. Obviously, the best way to simulate such a solution is to use a single space-time element with p-levels in space and time approaching infinity, which of course is not possible. Thus, if we limit p-levels in space and time, then discretization of the domain in space and time is obviously necessary. For the converged numerical solutions to approach theoretical solutions (up to certain order derivatives), higher order global differentiability (smoothness)

of local approximation in space and time becomes essential. Hence, h, p, k mathematical framework is essential for numerical simulation of such processes.

Inviscid form of the Burgers equation is a special case of the viscous form in which $Re = \infty$ (zero viscosity). In this case shock width $O(1/Re)$ becomes zero (hence requiring discretization length of zero for its accurate resolution) and we have a perfect shock i.e. jump with non-unique values of the solution at the shock. Such solutions are non-analytic and singular at the shock and therefore the solution derivatives are not defined at the shock. These solutions cannot be simulated in this precise form using finite element processes employing algebraic monomials as basis functions. As pointed out in reference [1] an attempt to compute solutions of inviscid Burgers equation would lead to non-uniqueness of the solution and hence obviously the lack of convergence of the associated functionals (for example residual functional in least squares processes). The solutions of the inviscid Burgers equations can only be approached as a limiting case. For example:

(i) Artificial viscosity approach [1] in which case one shows that as the artificial viscosity approaches zero the solutions of the inviscid form can be visualized (but not possible to compute).

(ii) More recently $H(Div)$ least squares processes have been used in which the inviscid Burgers equation is recast as a first order system of coupled partial differential equations using auxiliary variables [22]-[23]. The authors recognize the non-uniqueness of the solution and lack of existence of unique first derivative at the shock and introduce the Frêchet derivative to restore

analyticity of the solution. Many theorems related to the convergence of the least squares functional, uniqueness of the solution of the reconstructed IVP and convergence of its weak solutions are presented. Some significant points are worth nothing: (a) As pointed out by Gudunov [1], the solutions of inviscid Burgers equation are non-unique and the uniqueness can only be restored by introducing some mechanism of viscosity (artificial or physical). (b) In the $H(Div)$ approach, mesh dependent artificial viscosity is introduced in the inviscid form of the Burgers equation such that with progressively refined meshes in the spatial direction yield progressively decreasing viscous dissipation mechanism and hence it is possible to argue that, in the limit the discretization length in space approaching zero, the solutions of the inviscid Burgers equation are possible to approach (but never possible to compute directly). (c) From (b) it is clear that in references [22]-[23] the authors only solve the viscous form of the Burgers equation in which the mechanism of viscous dissipation is artificial (non-physical) and not the inviscid form. (d) The viscous form of the Burgers equation resulting form the non-linear conservation law already has a physical mechanism of viscous dissipation which in the dimensionless form of the GDE is reflected in the Reynolds number (Re). (e) In view of (a)-(d) it is quite clear that here we have two possible propositions. Should the solutions of the inviscid Burgers equation be approached using the artificial viscosity approach (let it be $H(Div)$ or any other) or should these be approached using viscous form of the GDEs with progressively increasing Re thereby progressively diminishing viscosity.

First, we argue that the viscous form of the Burgers equation has a physical mechanism of viscosity and its solutions are always unique and that the computations using this form require no other artificial means. Secondly, we must show that the computations for the viscous form are possible with monotonic convergence of the least squares functional, accurate resolutions of the shock structure (depending upon Re) for discretizations that are no more refined than those employed in the artificial viscosity approaches (hence computationally competitive). For a given Re, the computed evolution is always time accurate and as Re is increased progressively the computed solutions indeed approach those of the inviscid form. (f) In reference [22] the solutions reported using $H(Div)$ approach for 16 x 16, 32 x 32, 64 x 64 and 256 x 256 space-time meshes show that these solutions correspond to progressively increasing Re, however, from this approach Re corresponding to these solutions can not be quantified.

Our view regarding $H(div)$ least squares methods and all others using artificial viscosity approaches is rather simple. If we are to diffuse the solutions in some form or the other, then, we may as well use the viscous form of the Burgers equation in which the diffusion is physical due to actual viscosity of the medium and is reflected in the Reynolds number. In this approach if one could show that:

(a) The solutions remain unique and convergent for any finite Reynolds number.

(b) The associated least squares functional shows monotonic convergence and indeed approaches zero.

(c) For progressively increasing Re the progressively reduced shock width ($O(1/Re)$) for high Re is achieved and that the computations are always time accurate.

Then, we indeed have a computational strategy in which the solutions of the inviscid Burgers equation can be visualized as a limiting case when the Reynolds number approaches infinity. This approach is much more appealing because of the fact that viscous form of the Burgers equation is in agreement with the physics, and, that it requires no other treatments to regularize singular solutions of the inviscid Burgers equation, as they are naturally analytic due to the physics of the viscous medium.

1.2.2 1-D Riemann shock tube

There is enormous literature present on 1-D Riemann shock tube simulations using Euler's equations as mathematical models [24]. In such approaches (i) shock evolution is not possible to determine (ii) shock structure is not possible to establish either (iii) only shock relations can be determined (iv) with shock fitting and shock capturing methods it is possible to create an illusion of a shock (with right shock relations) but total absence of the nature of shock structure.

Surana and Van Dyne [25]-[26] were perhaps the first one to report shock evolution, shock structure resolution, shock propagation and interaction in a 1-D Riemann shock tube using mathematical models based on viscous form of Navier-Stokes equations with conducting medium using ideal gas as equation of state. The authors utilized finite element method based on solution of class C^{11} in space and time using space-time integral form in space-time least squares processes.

Subsequently Surana and Allu reported solutions of classes $C^{ij}; i \geq 1, j \geq 1$ for 1-D Riemann shock tube using same mathematical models as in case of [27]. The authors in this work demonstrated: (i) The mathematical models based on first order PDEs (using stress and flux as variables) result in failure during evolution for Riemann shock tube. Thus, it is essential to eliminate viscous stress and flux as variables and instead use GDEs in ρ, u and T as a mathematical model for computations. The authors showed benefits of using $C^{ii}; i \geq 1$ local approximations of higher order global differentiability in spatial directions. Ideal gas was used as equation of state. In all these works [27], equation of state was based on ideal gas law and the shock formation, propagation and interaction was visual i.e., through graphical representations of ρ, u and T over the spatial domain of the shock tube during the evolution.

It has been reported in many published works [28] that heavy molecular weight gases with c_v/R ratios greater than 20, it is possible to have a shock in the rarefaction region when the initial conditions are partially or wholly lie within a zone bounded by saturation curve and $\partial^2 P/\partial v^2 = 0$($\Gamma$-curve) i.e., near the gas liquid critical point. In these works many theoretical and numerical results are presented based on Euler's equations. Shock relations are established based on Rankine-Hugoniot approach and then applied as initial conditions for Euler's equations to show that these propagate during evolution. To our knowledge, there is no published work demonstrating the evolution of a shock in the rarefaction region. Investigation of the compressible shocks in Riemann shock tube for ideal gas law and the possibility of the existence of rarefaction shocks as well

as compression shocks for heavy molecular weight gases using real gas model thermodynamic map (as opposed to graphical approach) are presented. Shock propagation, repeated shock reflections and interactions are the thrust of the work presented here. Mathematical models are based on Navier-Stokes equations with actual transport properties of the medium. We utilize space-time finite element process that yield space-time variationally consistent integral forms.

1.2.3 2-D compressible flows : BVPs

Compressible flows of practical interest are generally high Mach number flows associated with high Reynolds numbers. In such flows turbulence plays a significant role. Thus such flows must either be simulated using empirical models of turbulence with time averaged Navier-Stokes equations or using Direct numerical simulation (DNS) of time dependent Navier-Stokes equations. However, the solutions of BVPs in compressible flow has also been a subject of study for long time. Even though for real flow conditions, the BVPs do not describe the correct physics, but computations of their numerical solutions has been viewed as a challenge for computational methods. It has been generally concluded that BVPs for compressible flows can only be solved for low Reynolds numbers that are often well below the range of practical interest. We make some remarks regarding the state of computations for BVPs in compressible flows.

Remarks

(1) The mathematical models are generally Euler's equations and are rarely based on true Navier-Stokes equations incorporating the physical viscosity and the conductivity of the medium.

(2) Computational methods based on Finite difference and Finite Volume are generally accepted to be not able to simulate solutions for these mathematical models.

(3) In Finite element methods, generally Galerkin method with weak form is used. Since the mathematical models for 2D viscous compressible flows are a system of non-linear PDEs, Galerkin method with weak form results in integral forms that are variationally inconsistent. This necessitated the use of up-winding methods and hence there in lies the fundamental problem and difficulty in these methods.

In the work presented here we utilize Navier-Stokes equations and variationally consistent integral forms to present solutions of BVPs in 2D compressible flows for high Reynolds number.

1.2.4 Mathematical and Computational methodologies for BVPs

Even though Finite Difference and Finite Volume methods dominate computations in Computational Fluid Dynamics (CFD), due to the reasons mentioned earlier, here we only consider Finite Element method and the commonly used methodologies. We refer to all finite element methods of obtaining numerical

solutions of BVPs as methods of approximation. In finite element methods one constructs an integral form using PDEs from mathematical models. A link to these integral forms and Calculus of Variations [29], establishes which integral forms are variationally consistent and which ones are variationally inconsistent [30]. Surana et.al. [30, 31, 32], have shown that variationally consistent integral forms yield symmetric positive definite algebraic systems that have a unique solution. Variationally inconsistent integral forms on the other hand yield non-symmetric algebraic systems that may have partial or completely complex basis and unconditional positive definiteness of such algebraic systems can not be ensured. In variationally inconsistent integral forms the computations may even totally cease or degenerate.

Based on definition of VC and VIC integral form, Surana et.al. [30]-[32] evaluated various methods of approximation (also see chapter 2 for more details) and showed that when the PDEs in the mathematical models of the BVPs are non-linear only LSP using Newton's linear method for solving non-linear algebraic systems are variationally consistent. All other methods of approximations are VIC. Inspite of this, the most commonly used approach in the finite element method for nonlinear PDEs remains Galerkin method with weak form [33] in which the resulting integral forms are VIC. Hence, the use of stabilizing methods such as SUPG, SUPG/DC, SUPG/DC/LS and their many variations [4] becomes essential. For a comprehensive literature review of these methods see reference [34]. Use of stabilizing methods in the integral forms obviously produce resulting forms that are not in correspondence with the PDEs [35] and therefore the solutions from these

methods are rarely the solutions of PDEs of the mathematical model. A significant point to note here is that in context with BVPs for compressible flow, we wish to resolve the issue of whether the numerical solutions of these are possible or not. Thus, we must employ methods of approximations in which other factors influencing the solution are either absent or used minimally. Based on this, our view is that if Galerkin methods with weak form using stabilizing method fails to yield the solutions of BVPs for compressible flow, this is not conclusive enough to say that their solution can not be computed numerically because the computational methods used are questionable. This is the main motivation in the present work.

1.2.5 Mathematical and Computational Methodologies for IVPs

Since computations of evolution for IVPs (1-D conservation law, Riemann shock tube) is a significant aspect of the work presented here, it is perhaps fitting to present a detailed literature review of various methodologies for obtaining numerical solutions of IVPs.

A review of published pertinent literature and currently used finite element approaches for IVP is given in the following. Broadly speaking, the Finite Element techniques for time dependent processes can be categorized as either space-time decoupled methods or space-time coupled methods. In decoupled approaches a finite element discretization is performed in spatial direction independently from the finite element or finite difference discretization in time. In contrast, the space-time coupled approaches perform the discretization in space and time concurrently.

Time dependent problems represent evolutionary processes where the so-

lutions are naturally functions of both space and time. For such problems decoupled methods are used in an attempt to reduce computational effort. However, decoupling the simultaneous dependence on space and time may lead to loss of accuracy and usually small time steps may be required to ensure stability. As a result, the overall computational effort required by decoupled methods may actually be greater than that for coupled methods. The following is a brief discussion of the pertinent literature on decoupled formulations followed by a short review of the published work on coupled formulations. Lewis and Bruch [36] presented the application of least squares method to one-dimensional transient problems. For a fixed instant of time the Galerkin formulation is first constructed in space. The least squares method is then applied to the resulting ordinary differential equations to devise a time-stepping algorithm. Results are presented for one-dimensional heat conduction, convection-diffusion equation, and unsaturated flow problems. Donea [37] presented a Taylor-Galerkin finite element formulation for hyperbolic problems. The method involves retaining up to the third-order time derivative in the Taylor series expansion of the solution at time t^{n+1} about the solution at time t^n. The paper presents numerical examples in one- and two-dimensions and discusses phase and dispersion errors. Lohner et al. [38] presented a characteristics-based finite element method for the solution of non-linear hyperbolic equations. The solution at time step t^{n+1} is expanded in second-order accurate Taylor series about the solution at time t^n. The expressions for the first and the second time derivatives (derived using the hyperbolic equation) of the dependent variable are substituted in the Taylor series expansion to obtain a time discretized form of the hyperbolic

equation for which the finite element formulation is constructed in space using the Galerkin method. The paper demonstrates that this method is identical to the Taylor-Galerkin method for convection-diffusion problems. Time-step limits are discussed based on a stability analysis for linear problems. Numerical results are presented for one- and two-dimensional non-linear hyperbolic problems. Donea et al. [37] presented a Taylor-Galerkin finite element formulation for multi-dimensional advection-diffusion equations and one-dimensional Burgers equation. The paper discusses linear and parabolic finite element approximations in space and applications to transient problems reaching a steady state.

Kujawski and Wiberg [39] present a family of least squares time integration schemes for thermal problems. In this work, the Galerkin method is used to discretize in space first, resulting in a set of first-order ordinary differential equations in time. A least squares procedure, which includes weighting coefficients, is then applied to produce a general time-stepping scheme. The values of the weighting coefficients determine the accuracy, stability and convergence rate of the method. Carey and Jiang [40] presented a least squares finite element formulation for hyperbolic systems. For a given instant of time $t^* = t + \theta\Delta t, 0 \leq \theta \leq 1$ a least squares functional I is described purely in space. The Taylor series expansions about t^n are used to determine approximations to the space and temporal derivatives of the dependent variable appearing in the integrand of I. The variation of I at time $t+\Delta t$ is then evaluated and set to zero. This form is used to construct finite element approximation in space using the Galerkin method. The paper also demonstrates the relationship between this method and the Taylor-Galerkin procedure for $\theta = 1/2$.

The stability of the method is investigated and its extension to non-linear problems is presented.

Jiang and Carey [41] also presented a least squares finite element formulation for non-linear hyperbolic problems. In this work, the equations are first linearized over the time step $\Delta t = t^{n+1} - t^n$. A backward difference approximation is then used to obtain an implicit time-difference approximation for which the least-squares finite element formulation is constructed in space using the functional $I = \int_\Omega (R^2 + \beta(\partial R/\partial x)^2)\ d\Omega\ ;\ 0 \leq \beta \leq 1$ instead of $I = \int_\Omega R^2 d\Omega$, where R represents the residuals resulting from the linearized time-discretized equations. Numerical examples include inviscid Burgers equation, isothermal flow in a nozzle, and a shock tube problem. A Petrov-Galerkin/modified operator formulation for the convection diffusion problem is presented by Sampaio [42]. The equation is discretized in time and then integrated over an element using a weighting function. A suitable choice of weighting function is used to obtain the self-adjoint differential operator. The paper discusses the stability of the proposed scheme and presents one- and two-dimensional numerical examples. Sampaio [43] also presented a Petrov-Galerkin formulation for the incompressible Navier-Stokes equation using equal-order interpolation for velocity and pressure. First a linear forward difference discretization in time (Crank-Nicholson type) is used to eliminate time derivatives of the dependent variables. The resulting equations are used to construct a least squares finite element formulation in space using linear elements. The paper presents numerical results for steady state problems only.

An important feature of the formulations presented in References [38]-[43]

is that for a given increment of time the effects of time and space are assumed to be decoupled. Thus, the discretization in space and time are carried out non-concurrently. The various methods differ from each other in the manner in which these discretizations are performed. Due to decoupling of space and time, the stability of the numerical process must be examined. If the method is only conditionally stable then the size of the time step becomes very limited, otherwise the solution will grow without bounds. In unconditionally stable methods, the size of the time step is limited by the accuracy of the approximation of the temporal derivatives.

An alternative to decoupling space and time is to construct space-time integral forms which leads to space-time finite elements. Here, the effects of space and time are coupled. If the initial value problem requires a space-time mesh consisting of a large number of elements in time, the size of the resulting set of assembled equations can become enormous for two- and three-dimensional problems. To circumvent this, a marching or time-stepping procedure is used. The solution is obtained for only one layer of elements in time, at a time, in a sequential manner. The initial conditions for the current time step (length of the layer in time) are supplied by the solution from the previous time step. Thus, in this procedure an initial value problem can be solved for each time step and time marched only when the solution is converged for the current time step. This is in contrast to decoupled methods where each time step may represent a serious approximation. In space-time coupled methods the only restriction on the size of the time step is imposed by local or element approximation or the desired accuracy. In the following we

present a brief review of the published space-time finite element literature. The approximations and assumptions used in these formulations are examined in detail.

The concept of space-time finite elements was first proposed by Fried [44] and Oden [45] in 1969. Since then the space-time marching procedure has been applied to problems in solid mechanics [46]-[47] and heat conduction. Varoglu and Finn were the first to apply the space-time finite element procedure to the convection-diffusion [48]-[49] and Burgers equation [50]. Their formulations are based on the Galerkin method with weak form, which has been shown to produce spurious numerical oscillations for convection-dominated problems [51]-[52]. To eliminate these oscillations they employed the method of characteristics to modify the spatial discretization at each time step. Hughes et al. [33] and Shakib and Hughes [35] presented Galerkin least squares space-time finite elements for the convection-diffusion equation. In these formulations a least squares operator is added to the Galerkin formulation to improve stability and to minimize spurious oscillations resulting from the space-time Galerkin method with weak form.

A least squares based space-time finite element formulation was first presented by Nguyen and Reynen [53],[54] for the convection-diffusion and the Burgers equation. The authors begin the formulation procedures with a true least squares minimization statement in space and time. First, we note that for both convection-diffusion and Burgers equation, the expressions for E (error) involve second derivatives of the dependent variable. Thus, a linear finite element approximation for the dependent variable in space is unsuitable and will destroy the true form of the least squares minimization principle. It could be argued

that δE (variation of E) may be treated like a weight function w_j (which is a function of space and time) and that the least-squares method is a special case of the Petrov-Galerkin technique. Then of course any suitable form of w_j is permissible. However, the formulation resulting for any other w_j except δE will not represent a true least squares space-time finite element formulation. Second, the authors perform integration by parts for some terms and drop the others due to linear local approximation. Last, it is important to point out that the authors are able to make this procedure a marching procedure in time only by introducing $\Delta\varphi_i$ (change in dependent variable φ over the time step). This is only possible for a linear approximation in time. For higher degree approximations in time the procedure presented in references [35] and [53] cannot be utilized as a time-stepping procedure. In conclusion, the formulations presented in references [35] and [53] are not true least squares space-time formulations and the time stepping is possible only for linear local approximation in time.

In a series of papers, Kececioglu and Rubinsky [55]-[56] presented a mixed variable continuously deforming finite element method based on least squares approach for evolution problems. These papers discuss theoretical aspects, their application to problems of phase-change in least squares minimization approach in theory, but the effects of space and time are actually decoupled in the details of the specific formulation eventually presented and utilized in computations. The authors first discretize temporal derivatives using a differencing scheme and then construct a least squares minimization formulation of the resulting discretized equations in space. It is worth remarking again that the published formulations in this area

(cited above) actually represent various approximations to the true least squares space-time minimization procedure and furthermore in the literature cited above the use of p-version higher degree local approximations in both space and time has not been explored at all.

Bell and Surana [57, 58] presented C^0 p-version space-time least squares processes in connection with fluid dynamics using convection diffusion, Burgers equation and two dimensional laminar Newtonian fluid flows as model problems. Advantages of this approach over decoupled methods were clearly demonstrated. The papers also discuss serious shortcomings of space-time decoupled method (summarized in the conclusions of references [57, 58]). Further applications of C^0 and C^1 space-time LSP can also be found in references [25, 26, 59, 60, 61, 62]. C^1 space-time LSP have been used successfully by Surana et. al. [25]-[26] in gas dynamics applications. Riemann shock tube was used as a model problem to demonstrate the applications of the approach. Published work on space-time Galerkin processes is virtually non-existent. Fundamental reasons for this have been explored by Surana et al. [5]. It is rather clear that in IVP describing evolutions, dependent variables exhibit simultaneous dependence on space and time, hence space-time coupled approaches are a natural way to incorporate the correct physics and mathematics of IVP in the computational processes.

In the following we present some mathematical developments to demonstrate the difference between space-time decoupled methods and space-time coupled methods.

Space-Time decoupled methods

To illustrate the important features of both methodologies, we consider the initial value problems,

$$A\varphi(x,t) - f(x,t) = 0 \; \forall (x,t) \;\text{ in }\; \Omega_{xt} = \Omega_x \times \Omega_t \tag{1.1}$$

with some boundary conditions and initial conditions. In space-time decoupled methods, we construct a discretization $\bar{\Omega}_x^T$ of $\bar{\Omega}_x$ such that

$$\bar{\Omega}_x^T = \bigcup_e \bar{\Omega}_x^e; \; \bar{\Omega}_x^e = \Omega_x^e \bigcup \Gamma^e \tag{1.2}$$

where $\bar{\Omega}_x^e$ is a sub-domain e or an element e in space only. If we assume that at an instant of time and in its small neighborhood Δt, φ is only a function of x, then using fundamental Lemma [29, 63]-[64, 65] an integral form of (1.1) in space alone is possible,

$$\int_{\bar{\Omega}_x} (A\varphi(x,t) - f(x,t))v(x,t)dx = 0 \tag{1.3}$$

where $v(x)$ is a test function. If $v = \delta\varphi$ then (1.3) is Galerkin method in space. If $v \neq \delta\varphi$ but $v = 0$ where $\varphi = \varphi_0$(given), then (1.3) represents Petrov Galerkin method or method of weighted residuals. If one transfers some differentiation (with respect to space coordinates only) from φ to v in (1.3), then we have Galerkin method with weak form in space. In all these methods we finally have,

$$B(v,\varphi) = l(v) \tag{1.4}$$

If φ_h is an approximation of φ in $\bar{\Omega}_x^T$, then (1.4) for $\bar{\Omega}_x^T$ becomes,

$$B(v,\varphi_h) = l(v) \tag{1.5}$$

For the discretization $\bar{\Omega}_x^T$ (1.5) can be written as (provided appropriate continuity and differentiability requirements in x are satisfied),

$$\sum_{e=1}^{M_x} B^e(v, \varphi_h^e) = \sum_{e=1}^{M_x} l^e(v) \tag{1.6}$$

Where M_x are the number of sub-domain in $\bar{\Omega}_x^T$ and φ_h^e is the local approximation of φ over $\bar{\Omega}_x^e$ such that

$$\varphi_h = \bigcup_e \bar{\varphi}_h^e \tag{1.7}$$

From (1.6) for a sub-domain $\bar{\Omega}_x^e$, we have,

$$B^e(v, \varphi_h^e) = l^e(v) \tag{1.8}$$

The approximation φ_h^e is constructed using,

$$\varphi_h^e(x,t) = \sum_{i=1}^{N} N_i(x)\varphi_i^e(t) \tag{1.9}$$

In which $N_i(x)$ are basis functions and $\varphi_i^e(t)$ are nodal degrees of freedom. When (1.9) is substituted in (1.8), integrated with respect to x over $\bar{\Omega}_x^e$ and then assembled using (1.6), we obtain a system of ordinary differential equation in $\{\delta\}, \{\dot{\delta}\}, ...$ etc. where the $\{\delta\}$ are nodal dofs for the discretization $\bar{\Omega}_x^T$. Thus,

$$\{\delta\} = \bigcup_e \{\varphi^e\} \tag{1.10}$$

The evolution is then obtained from these ordinary differential equations in time using: implicit, explicit time integration methods or finite elements in time. We make following remarks:

(1) IVP (1.1) describes evolution in which $\varphi = \varphi(x, t)$, i.e., φ is simultaneously dependent on x and t, hence integral form (1.3) is only valid for infinitely small neighborhood of time t. For a finite Δt (neighborhood of t), the time integration strategies for the resulting ordinary differential equation in time are obviously in error.

(2) Concepts of VC and VIC introduced by Surana et.al. [30]-[32] for BVP cannot be applied to the integral form (1.3), hence the well posedness and the stability of the algebraic systems in time integration schemes must be established on problem by problem basis.

(3) Decoupling of space and time is inherent in (1.3). Local approximation (1.9) is similar to separation of variables which is not valid for all IVP [66]-[67].

(4) Due to decoupling of space and time CFL number ($\Delta t/\Delta x$ or h_t/h_x) limitation must be observed to ensure that time integration schemes yield bounded evolution. This generally limits the choice of Δt for a given Δx.

(5) Evolutions in this approach are only time accurate for infinitely small increment of time in the time integration schemes. Inaccuracies and errors introduced due to decoupling of space and time can be minimized by prudent choices of Δx and Δt (problem dependent), but can never be eliminated.

(6) Space-time decoupled approach is also possible in the least squares framework. In this case generally a time approximation is constructed first for a given x and its infinitely small neighborhood Δx, then the LSP is applied

to the resulting ODEs or PDEs in space to obtain algebraic systems. This approach also suffers from most of the same drawbacks as described in remarks above. However, the resulting coefficient matrices in the algebraic systems are symmetric and positive definite, which is a distinct advantage of this method over the others.

(7) Since the differential operators A (as in (1.1)) in IVPs are space-time differential operators, development of a general mathematical and computational framework requires their mathematical classification over $\bar{\Omega}_{xt}$ (or space-time strip $\bar{\Omega}^n_{xt}$ as in chapter 2). In the space-time decoupled method this is not possible. Hence, these methods cannot provide a general mathematical and computational framework for all IVP. This necessitates that in these methods each IVP must be viewed on individual basis to ensure a meaningful formulation and solution.

A comprehensive literature review of the standard space-time decoupled approaches [36]-[43] based on the details presented here (and some variations of these) can be found in papers by Bell and Surana [57]-[58].

Space-time coupled methods

In the following we consider space-time coupled methodology for IVP. Consider IVP (1.1). We assume that $\varphi = \varphi(x,t)\ \forall\ x,t \in \Omega_{xt}$. Let $\bar{\Omega}^T_{xt}$ be a space-time discretization of $\bar{\Omega}_{xt}$ such that,

$$\bar{\Omega}^T_{xt} = \bigcup_e \bar{\Omega}^e_{xt} \tag{1.11}$$

where $\bar{\Omega}_{xt}^{e}$ is a space-time sub-domain e (or an element e) of $\bar{\Omega}_{xt}^{T}$. Using fundamental lemma [29]-[65], a space-time integral form of (1.1) is possible over $\bar{\Omega}_{xt}$,

$$\int_{\bar{\Omega}_{xt}} (A\varphi(x,t) - f(x,t))v(x,t)d\Omega_{xt} = 0 \tag{1.12}$$

Where $v(x,t)$ is the test function. If $v = \delta\varphi$ but $v = 0$ where $\varphi = \varphi_0$ (specified), then (1.3) represents space-time Petrov Galerkin (STPGM) or space-time weighted residual method (STWRM). If one transfers some differentiation from φ to v with respect to space and/or time, then we have Galerkin method with weak form (GM/WF). In all these methods we finally have

$$B(v(x,t), \varphi(x,t)) = l(v(x,t)) \tag{1.13}$$

If $\varphi_h(x,t)$ is an approximation of $\varphi(x,t)$ in $\bar{\Omega}_{xt}^{T}$, then (1.13) for $\bar{\Omega}_{xt}^{T}$ becomes,

$$B(v(x,t), \varphi_h(x,t)) = l(v(x,t)) \tag{1.14}$$

using (1.12) and (1.14), we can write the following (provided appropriate continuity and differentiability requirements are satisfied),

$$\sum_{e=1}^{M_{xt}} B^e(v(x,t), \varphi_h^e(x,t)) = \sum_{e=1}^{M_{xt}} l^e(v(x,t)) \tag{1.15}$$

where M_{xt} are number of space-time sub-domains or elements in the space-time discretization $\bar{\Omega}_{xt}^{T}$ and $\varphi_h^e(x,t)$ is the local approximation of $\varphi(x,t)$ over $\bar{\Omega}_{xt}^{e}$ such that,

$$\varphi_h(x,t) = \bigcup_{e} \varphi_h^e(x,t) \tag{1.16}$$

From (1.15), for a sub-domain $\bar{\Omega}^e_{xt}$, we have,

$$B^e(v(x,t), \varphi^e_h(x,t)) = l^e(v(x,t)) \tag{1.17}$$

The approximation $\varphi^e_h(x,t)$ over $\bar{\Omega}^e_{xt}$ is constructed using

$$\varphi^e_h(x,t) = \sum_{i=1}^{n} N_i(x,t)\varphi^e_i = [N]\{\varphi^e\} \tag{1.18}$$

In which, $N_i(x,t)$ are space-time basis or local approximation functions and φ^e_i are nodal degrees of freedom.

When (1.18) is substituted in (1.17), integrated with respect to x, t and then assembled using (1.6), we obtain a system of algebraic equations (linear or non-linear depending upon the space-time operator A in (1.1)) in $\{\delta\}$, where $\{\delta\}$ are the nodal degrees of freedom for the entire space-time discretization Ω^T_{xt}. Thus,

$$\{\delta\} = \bigcup_e \{\varphi^e\} \tag{1.19}$$

A solution for $\{\delta\}$ from the algebraic system yield the numerical solution for the entire space-time discretization Ω^T_{xt}. We make following remarks :

(1) In this approach it is possible to mathematically classify all space-time differential operators A in (1.1) into: non-self adjoint and non-linear categories.

(2) Concepts of VC and VIC introduced by Surana et.al. [30]-[32] can be extended to STVC and STVIC for IVP and can be applied to the integral forms resulting from GM, GM/WF, PGM, WRM [chapter 2]. Similar to VC integral forms for BVP, STVC integral forms for IVP are expected to yield

unconditionally stable computational processes. The merits of these integral forms can be established clearly.

(3) In this approach, concurrent dependence of the solution space and time is preserved. This is in agreement with the physics of the evolution described by IVP (1.1).

(4) Due to not decoupling space and time, stability issues (when integral forms are STVC) and CFL number limitations are absent.

(5) Even though the treatment presented here is for $\bar{\Omega}_{xt}$, one could easily do the same over a space-time strip or slab over a single increment of time. (1)-(4) remain valid in this approach also. Benefits of using space-time strip (or slab) with time marching are discussed in chapter 2.

(6) For the IVP (1.1) one could also construct a space-time least squares method [44]-[45]. Details are given in the following

If $\varphi_h(x,t)$ is the approximation of $\varphi(x,t)$ in $\bar{\Omega}^T_{xt}$, then,

$$A\varphi_f - f = E \text{ in } \bar{\Omega}^T_{xt} \tag{1.20}$$

in which E is the residual. We construct a functional $I(\varphi_h)$,

$$I(\varphi_h(x,t)) = (E,E)_{\bar{\Omega}^T_{xt}} \tag{1.21}$$

$$\delta I(\varphi_h) = (E,\delta E)_{\bar{\Omega}^T_{xt}} = 0; \text{ necessary condition} \tag{1.22}$$

$$\delta^2 I(\varphi_h) \cong (\delta E,\delta E)_{\bar{\Omega}^T_{xt}} > 0; \text{ am extrema principle} \tag{1.23}$$

And a φ_h obtained from (1.22) minimizes $I(\varphi_h)$ in (1.21). Details of this approach for $\bar{\Omega}_{xt}^T = \bigcup_e \bar{\Omega}_{xt}^e$ are given in chapter 2.

(7) In summary, major benefit in space-time coupled approaches are:

(a) Possibility of developing a general mathematical and computational framework due to mathematical classification of space-time differential operators.

(b) Use of STVC or STVIC concept [chapter 2] to establish which space-time integral forms for which category of operators are STVC.

(c) From (a) and (b) we can easily establish the methodologies that can yield unconditionally stable computational processes.

A comprehensive literature review of various space-time methods, STGM/WF, STPGM and STLSP in references [44]-[56] can also be found in papers by Bell and Surana [57, 58].

1.2.6 Up-winding methods

In case of BVP, Surana et. al. [30]-[32] have shown that when the differential operators are non-self adjoint or non-linear, integral forms resulting from GM, PGM, WRM and GM/WF yield computational processes that are not unconditionally stable for all choices of computational parameters and the dimensionless parameters in the GDEs describing the BVP. This is due to the fact that these integral forms are VIC [30]-[32]. The numerical solutions from VIC integral forms may contain non-physical and spurious oscillations [51]-[52]. It has

been shown that when the integral forms are VIC, reasonable solutions are possible with extremely refined discretizations [33]. However, such discretizations for 2D and 3D BVP are impractical and computationally prohibitive. Thus, over last three decades the persisting philosophy has been, ”Is it possible to compute oscillation free solutions using coarser discretizations when the integral forms are VIC such as in GM/WF”. Thus has lead to the development of up-winding methods [33]-[35] such as SUPG, SUPG/DC, SUPG/DC/LS and their many variations. In such methods, addition of LS operator to GM/WF (for example) has been essential to stabilize computations. Surana et. al. [5] have shown that addition of LS functional to GM/WF is justified mathematically when the differential operator in the BVP is self-adjoint for which GM/WF is VC and hence precludes the necessity for stabilization and hence the addition of LS functional. Authors have shown that addition of LS functional in case of GM/WF when the differential operators are non-self adjoint or non-linear has no mathematical justification. Further, a more significant finding is that in all published work such as SUPG/LS, the addition of LS functional is done inappropriately [35] (such as use of spaces lower than minimally conforming, reduced integration etc.). Authors in references [30]-[32], have shown that integral forms from the LSP are always VC and that LSP constructed in the mathematically justified minimally conforming spaces are always stable. A closer examination of GM/WF/LSP shows that magnitude of the coefficients of the algebraic system from LSP is few orders larger than those from GM/WF and hence in GM/WF/LSP methods addition of the coefficient matrices resulting from GM/WF to those from LSP is of very little or no consequence. Up-winding methods

are essentially a means of adding diffusion in some form or the other which has no mathematical justification. Up-winded solutions are obviously not solutions of the original BVPs. The most disturbing feature of up-winding methods is that they are problem dependent and cannot be considered as general methodology in the development of mathematical and computational infrastructure for all BVPs.

The discussion presented above on up-winding methods for BVPs is significant due to the fact these methods developed for BVPs also form the basis for up-winding methods for IVPs. Authors in references [49]-[50] pointed out spurious and oscillation solutions for transient convection diffusion and Burgers equations when using space-time Galerkin method with weak form. In chapter 2 it shown that space-time differential operators are either non-self adjoint or non-linear and hence extension of the work presented by Surana et. al. [30]-[32] for IVPs (chapter 2) demonstrates need for up-winding in space as well as time. Many of the aspects of upwind methods discussed here for BVPs are directly applicable to IVPs and it is shown in chapter 2 that these methods for IVPs are also not justified mathematically for the space-time differential operators. Up-winded solutions of IVPs are never time accurate, another significant drawback.

1.2.7 Higher order smoothness or differentiability of approximations

Surana et. al. [30]-[32] have introduced the concept of k-version of finite element method for BVP. The authors have shown that k, the order of approximation spaces $H^{k,p}$ provides global differentiability of order $(k-1)$ of the approximations and that k is an independent parameter in all finite element

computations in addition to h and p and have introduced h, p, k processes as opposed to currently used h, p processes. This lead to the development of h, p, k mathematical and computational framework for BVPs [30]-[32]. The authors demonstrated the need for $k > 1$ based on the physics of BVPs intrinsic in the GDEs and the higher order global differentiability features of their theoretical solutions. Some published work [68]-[69] discusses use of C^1 basis functions for BVPs. But there never has been organized approach to recognize the importance of global differentiability of approximations for BVPs prior to references [30]-[32]. h, p, k mathematical and computational framework has been originated and used by Surana et. al. in many BVPs applications [30]-[32] in various areas of continuum mechanics.

Surana and Van Dyne [25]-[26] used solutions of class $C^{1,1}$ in space and time for gas dynamics application and showed remarkable improvement in the accuracy of evolutions for Riemann shock tube and impulsively driven piston problem. Just like in case of BVPs, the need for higher global differentiability approximations for IVPs also arises from the physics intrinsic in the GDEs describing the IVPs as well as the higher order global differentiability features of the theoretical solutions of the IVPs in space as well as time. In the following we present a short abstract discussion of such concepts that are elaborated in details in chapter 2.

Consider the IVP described by (1.1) in which the space-time differential operator is orders $2m_1$ in space and $2m_2$ in time (i.e., the highest orders of the derivatives in space and time). Let $\varphi_h(x,t)$ be an approximation of $\varphi(x,t)$ in $\bar{\Omega}^T_{xt}$

such that $\varphi_h(x,t) = \bigcup_e \varphi_h^e(x,t)$ in which $\varphi_h^e(x,t)$ is the local approximations of $\varphi_h(x,t)$ over $\bar{\Omega}_{xt}^e$, a space-time element e. Then :

(i) Admissibility of $\varphi_h(x,t)$ in (1.1) in point-wise sense requires that, $\varphi_h^e(x,t)$ be of class $C^{k_1}(\bar{\Omega}_{xt}^e)$; $k_1 \geq 2m_1$ in space and of class $C^{k_2}(\bar{\Omega}_{xt}^e)$; $k_2 \geq 2m_2$ in time.

(ii) $k_1 = 2m_1, k_2 = 2m_2$ correspond to minimally conforming approximation $\varphi_h(x,t)$ of $\varphi(x,t)$

(iii) If the theoretical solution $\varphi(x,t)$ of (1.1) over Ω_{xt} is of class $C^{L_1}(\Omega_{xt})$, $C^{L_2}(\Omega_{xt})$ in space and time in which $L_1, L_2 \to \infty$ is admissible, then we may consider $2m_1 \leq k_1 \leq L_1$, $2m_2 \leq k_2 \leq L_2$. The choice of k_1 and k_2 depends upon the desired global differentiability of $\varphi_h(x,t)$ in space and time.

(iv) Thus, if one wishes to design a mathematical framework for IVPs in which the approximation $\varphi_h(x,t)$ of $\varphi(x,t)$ over $\bar{\Omega}_{xt}^T$ has global differentiability of orders k_1 and k_2 ($2m_1 \leq k_1 \leq L_1$, $2m_2 \leq k_2 \leq L_2$) then $\varphi_h^e(x,t) \in H^{k,p}(\Omega_{xt}^e)$ in which $k = (k_1, k_2)$. The need for development of mathematical and computational framework for IVPs based on h, p, k is rather obvious and is one of the important aspects of the work presented here.

1.3 Scope of work

The main thrust of the work presented here is to demonstrate and establish the numerical computations of the solutions of BVPs and IVPs in viscous compress-

ible flows with actual transport properties (i.e, physical viscosity and conductivity) can be done accurately and efficiently without the use of up-winding methods or any other ad-hoc problem dependent treatments. Time dependent Burgers equation, 1-D Riemann shock tube are used as model problems for IVPs. The Carter's plate, and flow over a circular cylinder are used as model problems for two dimensional BVPs. An outline of the work in this thesis is described in the following :

(1) The mathematical models in all cases are based on Navier-Stokes equations incorporating physical viscosity, conductivity and other transport properties. Developments of the mathematical models is presented for temperature dependent transport properties i.e., μ, k_{ij} and c_v are function of temperature. The GDEs for the mathematical models are derived using conservation laws, equations of state for viscous compressible medium using variable transport properties in weak form (first order systems of PDEs) as well as strong form (containing only density, velocity and temperature as dependent variables).

(2) The mathematical framework for obtaining numerical solutions of the non-linear PDEs resulting from the mathematical models is based in h, p, k framework [5] in which h is the characteristic length of the discretization, p is the degree of local approximation and k is the order of the approximation space yielding global differentiability of order $(k-1)$ of the approximations. The method of approximations is based in LSP and STLSP in which the integral forms are VC and STVC when Newton's linear method is used for obtaining numerical solutions of the nonlinear algebraic systems. VC and

STVC integral forms ensure unconditionally stable computational processes regardless of the choices of h, p, k and dimensionless parameters in the mathematical models. The parameter k permits higher global differentiability local approximations in x and y for BVPs and x, y and t for initial value problems. This permits us to incorporate desired physics in the computational processes.

(3) To demonstrate the meritorious features of the mathematical models used and mathematical and computational framework employed, numerical studies are presented for a number of standard model problem that have been acknowledged as good benchmark tests.

(3a) Initial Value problems

(i) Time dependent Burgers equations: Numerical studies are presented for a number of different initial conditions and compared with published results such as $H(Div)$ approach. Studies are presented for low as well as very high Reynolds number to demonstrate the accuracy and versatility of the proposed methodology for high Re creating isolated high gradients of the solution. It is established that very accurate time evolution computations are possible for any Re with reasonable discretizations. In most cases, evolutions are continued till the stationary state is reached. The stationary states of the evolutions are compared with the solutions from the time independent form of the Burgers equation. It is shown that in the limit $Re \rightarrow \infty$ (high value), the

solutions of the inviscid form are approached. Evolutions are computed using space-time strip with time marching.

(ii) Numerical studies for 1-D Riemann shock tube are presented using ideal gas law as well as real gas laws. For ideal gas law, air is used as medium. For real gas law, FC70 is used as medium. In all numerical studies, we present shock evolution, shock structure resolution, shock propagation and shock reflections and interactions. For FC70 using real gas model (Van der Waals equation of state), studies are presented to investigate the possibility of rarefaction shocks and compression shocks for various choices of initial conditions. In all cases thermodynamic map of the "rate of production of entropy per unit volume" over the entire evolution is used to determine the onset, existence and propagation of shocks.

(iii) The numerical studies for 2-D compressible flow are aimed to demonstrate that the 2-D BVPs associated with viscous compressible flows can indeed be solved accurately using the mathematical and computational infrastructure presented here without any problem dependent and ad-hoc treatments such as various forms of up-winding method. This of course is contrary to what is currently believed and hence the reason for undertaking this work. The model problems used here consist of :

   (I) Carter's plate : We consider flow over a flat plate at Mach 1, 3 and 5. The medium is air and the transport properties at NTP are assumed constant with ideal gas law.

   (II) Flow past a circular cylinder

Chapter 2 contains details of finite element mathematical and computational framework based on h, p, k and VC or STVC integral forms. Derivation of mathematical models for viscous compressible flows with variable transport properties as well as associated finite element formulations for BVPs and IVPs are described in chapter 3. Chapter 4 contains numerical studies for 1-D transient Burgers equation. Numerical studies for 1-D Riemann shock tube are presented in chapter 5. 2-D compressible flow numerical studies for BVPs are given in chapter 5. Chapter 6 contains Summary and conclusions.

Chapter 2

Mathematical Framework and Computational Infrastructure for BVPs and IVPs

2.1 Introduction

In this chapter we present details of the mathematical framework and the computational infrastructure used for obtaining numerical solutions of 1-D and 2-D BVPs and IVPs in viscous compressible flows. The material is divided in two sections. Section 2.2 contains treatment for boundary value problems and section 2.3 describes the details for initial value problems. The mathematical framework and the computational infrastructure utilized for BVPs has been borrowed from the published work by Surana et.al [30]-[32], hence section 2.2 only contains the basic concepts. The details can be found in the references. The framework for IVPs has been part of the new developments undertaken during the course of this research and therefore will be described in detail in section 2.3.

2.2 Boundary value problems (BVPs)

Surana et.al. [30]-[32] have presented h, p, k mathematical and computational framework for BVPs regardless of their origin or field of application in which k, the order of the approximation space yielding global differentiability

of order $(k-1)$ is an independent parameter in addition to h, the characteristic length and p, the degree of local approximation. Thus, k-version of finite element method in addition to h-,p-versions used currently in finite element processes. The mathematical framework for BVPs introduced by Surana et.al. is based on h, p, k as independent computational parameters as apposed to just h and p used currently. Introduction of k, permits desired global differentiability in the design of the computational processes. This leads to better physics in the computations as well as reduced errors for fixed resources (degrees of freedom).

Another important aspect introduced by Surana et.al [30]-[32] is the concept of variational consistency of the integral forms. The authors showed that in order for an integral form to be variationally consistent it must conform to the requirements of the calculus of variations. There must exist a functional I such that $\delta I = 0$ yields the integral form (necessary condition) and $\delta^2 I$ yields a unique extremum principle or sufficient condition. The integral forms satisfying these three requirements were termed variationally consistent (VC) integral form and the others, variationally inconsistent (VIC) integral forms. The variationally consistent integral form yield symmetric and positive definite coefficient matrices in the algebraic systems with real basis and eigenvalues greater than zero and hence a unique solution of the algebraic system is always assured. The variationally inconsistent integral forms on the other hand, yield non-symmetric coefficient matrices in the algebraic systems that are not always ensured to be positive definite and may have partial or completely complex basis and may even totally degenerate in which case the computations may not even be possible.

In order to address the totality of all BVPs, authors in references [30]-[32] classified all differential operators appearing in all BVPs into three categories : self-adjoint, non-self adjoint and non-linear and established VC or VIC of the integral forms resulting from various methods of approximations. We summarize these in the following,

(i) The integral forms resulting from Galerkin method, Petrov-Galerkin method and Weighted Residual methods are always VIC for all three categories of the differential operators.

(ii) The integral forms resulting from the Galerkin method with weak form are VC only when this differential operators are self-adjoint and when the bilinear functional $B(.,.)$ is symmetric.

(iii) The integral forms resulting from the least squares method or process are always VC for all the three classes of differential operators.

Thus in the proposed work, for BVPs in viscous compressible flows where the differential operators are always non-linear, we utilize h, p, k mathematical framework in which the integral forms for finite element processes are constructed using least squares method and hence ensuring VC of the associated integral forms.

Details can be found in reference [32]. Another significant aspect pointed out by Surana et.al [70] is that the strong form of the governing differential equations in the mathematical models containing higher order derivatives of the dependent variables are meritorious in designing computational processes as

opposed to the GDEs containing only first order derivatives of the dependent and auxiliary variables (introduced by auxiliary equations) i.e., first order system (weak form of GDEs). In the present work we only consider mathematical models of viscous compressible flows in which the GDEs are in the strong form.

2.3 Initial Value Problems (IVPs)

In the following we present development of mathematical and computational infrastructure of IVPs. The developments are parallel to the h, p, k framework with VC integral forms presented by Surana et. al. [30]-[32] for BVPs but many of the aspects are new due to time as independent variable and hence are presented in detail.

2.3.1 General Considerations

Let

$$A\varphi - f = 0 \quad \text{in } \Omega_{xt} = \Omega_x \times \Omega_t = \Omega_x \times (0, \tau) \tag{2.1}$$

be an IVP (with some BC and IC) describing an evolution over a space time domain Ω_{xt}. Let $\varphi(x,t)$ be analytic over Ω_{xt}. Let $\bar{\Omega}^T_{xt}$ be a space time discretization of $\bar{\Omega}_{xt}$ such that,

$$\bar{\Omega}^T_{xt} = \bigcup_e \bar{\Omega}^e_{xt} \tag{2.2}$$

in which $\bar{\Omega}^e_{xt} = \Omega^e_{xt} \bigcup \Gamma^e$ is a space-time sub-domain of $\bar{\Omega}^T_{xt}$. Ω^e_{xt} is interior of $\bar{\Omega}^e_{xt}$ and Γ^e is the closed boundary of $\bar{\Omega}^e_{xt}$. Let $\varphi_h(x,t)$ and $\varphi^e_h(x,t)$ be approximations

of $\varphi(x,t)$ over $\bar{\Omega}_{xt}^{T}$ and $\bar{\Omega}_{xt}^{e}$. Then,

$$\varphi_h(x,t) = \bigcup_e \varphi_h^e(x,t) \tag{2.3}$$

and, the following must hold,

(1) Since $\varphi = \varphi(x,t)$ i.e., φ is simultaneously dependent on x,t, the approximation $\varphi_h(x,t)$ must also exhibit the same as it does. This requirement precludes space-time decoupled methods and necessitates the use of space-time coupled methods.

(2) φ_h must be admissible in the non-discretized form of (2.1) and furthermore,

   (a) Admissibility of $\varphi_h(x,t)$ in (2.1) must be in the pointwise sense i.e., $\forall (x,t) \in \bar{\Omega}_{xt}^{T}$.

   (b) If $E = A\varphi_h - f$ is the residual or error in $\bar{\Omega}_{xt}^{T}$, then $E \to 0$ when $\varphi_h \to \varphi$ in the pointwise sense.

   (c) When (b) holds, we also have $I = (E,E)_{\Omega_{xt}} \to 0$ i.e., convergence of I to zero implies pointwise convergence of E to zero in $\bar{\Omega}_{xt}^{T}$.

(3) If the space-time differential operator A in (2.1) is of order $2m_1$ in space and of order $2m_2$ in time (orders of highest derivatives in space and time), then (2) requires that $\varphi_h(x,t)$ at least be of class C^{2m_1} and C^{2m_2} in space and time. If the theoretical solution $\varphi(x,t)$ is of class C^{L_1}, C^{L_2} in space and time ($L_1 \geq 2m_1$, $L_2 \geq 2m_2$; $L_1, L_2 \to \infty$ admissible), then the approximation $\varphi_h(x,t)$ must be of class $C^{k_1}, C^{k_2}; 2m_1 \leq k_1 \leq L_1, 2m_2 \leq k_2 \leq L_2$ in space and

time. Choice of k_1 and k_2 depends upon the continuity of the highest orders of the derivatives in space and time desired in $\bar{\Omega}^T_{xt}$ in the computational process. Thus, approximation $\varphi_h(x,t)$ of $\varphi(x,t)$ over $\bar{\Omega}^T_{xt}$ must posses higher order global differentiability in space and time. $k_1 = 2m_1 + 1$ and $k_2 = 2m_2 + 1$ correspond to the minimally conforming global differentiability

(4) Based on (3), the independent parameters $h, p, k; k = (k_1, k_2)$ must form the basis of the mathematical framework.

(5) The mathematical framework must yield computational processes that remain unconditionally stable and non-degenerate.

(6) The mathematical and the computational framework must be applicable to all IVPs with the same rigor regardless of their origin or field of application without the use of problem dependent ad-hoc treatments such as upwinding methods.

2.3.2 Mathematical classification of space-time differential operators

In the development of a general mathematical framework for all IVP it is necessary to mathematically classify all space-time differential operators appearing in the IVPs. Let the discretization $\bar{\Omega}^T_{xt}$ of the space-time domain $\bar{\Omega}_{xt}$ consist of n space-time strips or slab (2.3.2) such that

$$\Omega^T_{xt} = \bigcup_n {}^n\bar{\Omega}^T_{xt} = \bigcup_n \left(\bigcup_e {}^n\bar{\Omega}^e_{xt} \right) \tag{2.4}$$

in which ${}^n\bar{\Omega}^T_{xt}$ is the n^{th} space-time strip or slab and ${}^n\bar{\Omega}^e_{xt}$ is a space-time sub-domain (element) 'e' of the n^{th} space-time strip. The space-time differential

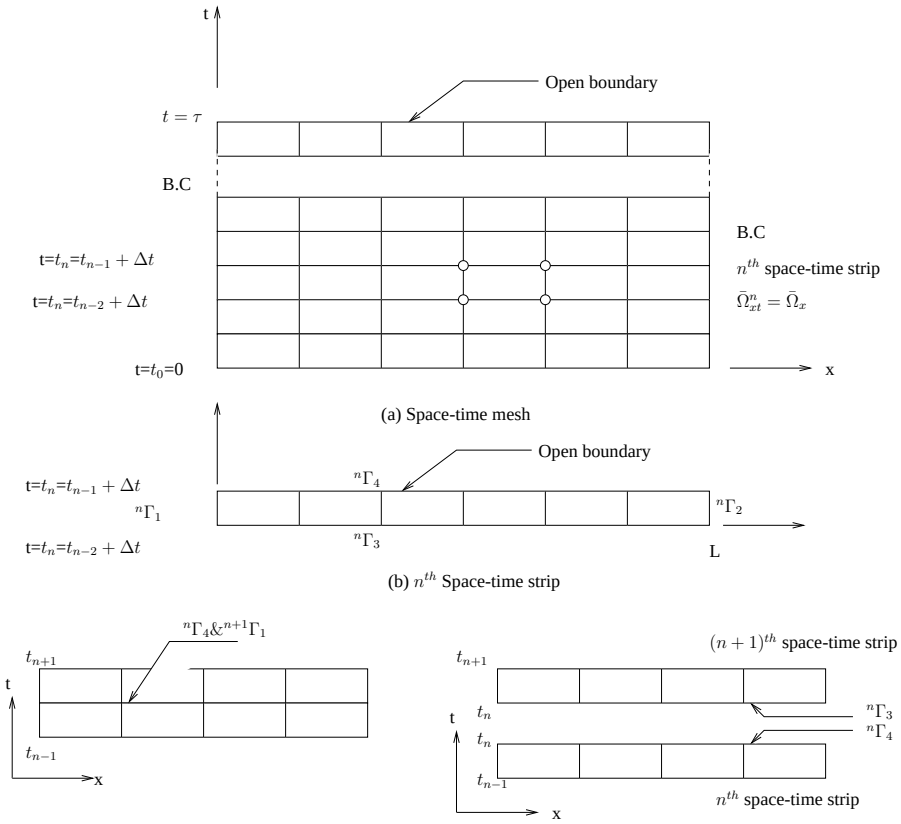

Figure 2.1: Space-time mesh and space-time strip or slab for an increment of time Δt

operators in IVPs can be mathematically classified either using $\bar{\Omega}_{xt}$ or ${}^n\bar{\Omega}_{xt}$ as their domain of definition (henceforth referred to as D_A). Using D_A as domain of the space-time operator A, the definitions of linearity, symmetry, self-adjoint, non-self adjoint and non-linear differential operators follows the usual definitions used for BVP [30]-[32, 71]. The definition of symmetry deserves special consideration.

Definition: A space-time differential operator A in D_A is symmetric if it is linear and if $\forall u, v \in V_A$ (a space of admissible functions defined over D_A) the following holds, $(Au, v) = (u, Av)$ ■

Consider D_A to be ${}^n\bar{\Omega}_{xt}$, space-time domain for n^{th} space-time strip or slab. Assume that on boundaries ${}^n\Gamma_1$ and ${}^n\Gamma_2$, boundary conditions (BC) are specified and on boundary ${}^n\Gamma_3$ initial conditions (IC) are known. On boundary ${}^n\Gamma_4$, neither solution nor its spaces and/or time derivatives are known. We refer to ${}^n\Gamma_4$ as open boundary. In determining symmetry of the space-time differential operator A, the linearity of A is straightforward and for symmetry we use integration by parts to obtain,

$$(Au, v) = (u, A^*v) + < Au, v >_{{}^n\Gamma} \tag{2.5}$$

where A^* is adjoint of A and $< Au, v >_{{}^n\Gamma}$ is called concomitant resulting as a consequence of transferring differentiation from u to v using integration by parts. Thus for A to be symmetric $A^* = A$ and $< Au, v >_{{}^n\Gamma} = 0$ must hold. We can write (2.5) as,

$$(Au, v) = (u, A^*v) + \sum_{i=1}^{3} < Au, v >_{{}^n\Gamma_i} + < Au, v >_{{}^n\Gamma_4} \tag{2.6}$$

Assume that $A^* = A$ (which is possible when the space-time differential operator has even order derivatives in space and time) and also assume that the concomitant becomes zero on ${}^n\Gamma_i; i = 1, 2, 3$ (may be possible due to BC and IC). Thus, if the conditions stated above hold, then (2.6) reduces to,

$$(Au, v) = (u, Av) + < Au, v >_{{}^n\Gamma_4} \tag{2.7}$$

Since ${}^n\Gamma_4$ is open boundary, $< Au, v >_{{}^n\Gamma_4}$ can never be zero, hence $(Au, v) \neq (u, Av)$.

Proposition 1: Let A be a linear space-time differential operator in IVP $A\varphi - f = 0$ in ${}^n\bar{\Omega}_{xt}$, then $\forall u, v \in V_A$, $(Au, v) \neq (u, Av)$, hence the differential operator A can never be symmetric.

Proposition 2: Let A be a linear space-time differential operator in IVP $A\varphi - f = 0$ in ${}^n\bar{\Omega}_{xt}$, then the space-time differential operator A is non-self adjoint.

Proposition 3: Let A be a non-linear space-time differential operator in the IVP $A\varphi - f = 0$ in ${}^n\bar{\Omega}_{xt}$, then, A is neither linear nor symmetric.

Thus the space-time differential operators in IVPs are either non-self adjoint or non-linear but not self-adjoint. A significant computational aspect of (2.7) is that since $< Au, v >_{{}^n\Gamma_4}$ contains unknown solution on the open boundary ${}^n\Gamma_4$, then it contributes to the coefficient matrix, thus, making the resultant coefficient matrix non-symmetric even if $A^* = A$.

2.3.3 Space-time Integral forms and space-time methods of approximation

In the methods of approximations that form the basis for space-time finite element processes for IVP, one constructs a space-time integral form using GDEs describing the IVP. This is possible based on fundamental lemma of the calculus of variations [29]-[64].

Lemma 1

If $\eta(x,t)$ *is continuous in* ${}^n\bar{\Omega}_{xt} = {}^n\Omega_{xt} \bigcup {}^n\gamma$, *and if* $\int_{{}^n\bar{\Omega}_{xt}} \eta(x,t)h(x,t)d\Omega_{xt} = 0$ $\forall\, h(x,t) \in H^1\,({}^n\bar{\Omega}_{xt})$ *such that* $h(x,t) = 0$ *on* γ^*, *a portion of* ${}^n\gamma$, *then* $\eta(x,t) = 0$ *every where in* ${}^n\Omega_{xt}$ ■

This lemma provides a means of constructing an integral form of the IVP defined by (2.1) in ${}^n\bar{\Omega}_{xt}$. If we consider (2.1) with $\varphi = \varphi_0$ on γ^*, a portion of the boundary ${}^n\gamma$ of ${}^n\bar{\Omega}_{xt}$, then if we choose a function $v(x,t)$ that is also continuous in ${}^n\bar{\Omega}_{xt}$ such that $v(x,t) = 0$ on γ^*, then,

$$\int_{{}^n\bar{\Omega}_{xt}} (A\varphi(x,t) - f(x,t))v(x,t)d\Omega_{xt} \;=\; (A\varphi(x,t) - f(x,t), v(x,t))_{{}^n\bar{\Omega}_{xt}} = 0 \quad (2.8)$$

is valid based on Lemma 1. Here $(\cdot,\cdot)$ denotes the scalar product of $A\varphi - f$ and v over space-time domain ${}^n\bar{\Omega}_{xt}$. Thus, in (2.8) we have an integral form of the initial value problem over the space-time domain ${}^n\bar{\Omega}_{xt}$. If $v = \delta\varphi$ (first variation of φ), then v is admissible in (2.8). v is referred to as the test function. If $\varphi(x,t)$ is analytic, then $(A\varphi - f)$ and $v = \delta\varphi$ are both continuous (provided f is smooth) and hence the integrand in (2.8) is continuous also.

In classical space-time methods of approximation (no discretization of ${}^n\bar{\Omega}_{xt}$) $\varphi(x,t)$ is approximated by ${}^n\varphi_h(x,t)$ over ${}^n\bar{\Omega}_{xt}$. In the following we consider

various space-time methods of approximation over the space-time strip or slab ${}^n\bar{\Omega}_{xt}$.

Space-Time Galerkin method (STGM) :

Let ${}^n\varphi_h(x,t)$ be an approximation of $\varphi(x,t)$ in ${}^n\bar{\Omega}_{xt}$ and $v = \delta({}^n\varphi_h)$, then based on fundamental Lemma and (2.8), we write,

$$\int_{{}^n\bar{\Omega}_{xt}} (A^n\varphi_h(x,t) - f(x,t))v(x,t)d\Omega_{xt} = (A^n\varphi_h(x,t) - f(x,t), v(x,t))_{{}^n\bar{\Omega}_{xt}} = 0 \tag{2.9}$$

$$\begin{array}{lrcl} \text{or} & B^g({}^n\varphi_h, v)_{{}^n\bar{\Omega}_{xt}} & = & l^g(v)_{{}^n\bar{\Omega}_{xt}} \\ \text{where} & B^g({}^n\varphi_h, v)_{{}^n\bar{\Omega}_{xt}} & = & (A^n\varphi_h, v)_{{}^n\bar{\Omega}_{xt}} \\ & l^g(v)_{{}^n\bar{\Omega}_{xt}} & = & (f, v)_{{}^n\bar{\Omega}_{xt}}. \end{array} \tag{2.10}$$

With approximation ${}^n\varphi_h$, the integral form (2.10) yields an algebraic system from which unknown constants in ${}^n\varphi_h(x,t)$ are determined. This method is known as space-time Galerkin method or classical STGM method due to the fact that space-time domain ${}^n\bar{\Omega}_{xt}$ is not discretized and there is no integration by parts to transfer differentiation from ${}^n\varphi_h(x,t)$ to the test function $v(x,t)$.

Space-Time Petrov Galerkin (STPGM) and Space-Time Weighted Residual Method (STWRM):

STPGM and STWRM are exactly the same as STGM except that in these methods $v \neq \delta({}^n\varphi_h)$ but $v = 0$ on γ^* where ${}^n\varphi_h = \varphi_0$

Space-Time Galerkin method with weak form (STGM/WF) :

Let ${}^n\varphi_h(x,t)$ be an approximation of $\varphi(x,t)$ in ${}^n\bar{\Omega}_{xt}$. In this method we begin with Galerkin method i.e., (2.9) and use integration by parts to transfer some differentiation from ${}^n\varphi_h(x,t)$ to $v(x,t)$ thereby weakening continuity requirements on ${}^n\varphi_h$ in the resulting integral form. Using boundary conditions, initial conditions and the conditions on v on the boundaries, the resulting boundary terms or the integrals are simplified and finally arranged in the following form.

$$B^{gw}({}^n\varphi_h(x,t), v(x,t))_{{}^n\bar{\Omega}_{xt}} = l^{gw}(v(x,t))_{{}^n\bar{\Gamma}};\ v = \delta({}^n\varphi_h) \tag{2.11}$$

This integral form is referred to as the weak form of (2.10). when the approximation ${}^n\varphi_h(x,t)$ is substituted in the integral form (or weak form) (2.11), we obtain an algebraic system, from which constants in ${}^n\varphi_h(x,t)$ are determined. This method is referred to as Galerkin method with weak form.

Space-Time Least Squares Method (STLSM) :

Let ${}^n\varphi_h(x,t)$ be an approximation of $\varphi(x,t)$ in ${}^n\bar{\Omega}_{xt}$, then, in space-time least squares method (or processes) we construct a space-time functional defined by,

$$I({}^n\varphi_h) = (E,E)_{{}^n\bar{\Omega}_{xt}};\ E = A^n\varphi_h - f \quad \forall\ (x,t) \in {}^n\bar{\Omega}_{xt} \tag{2.12}$$

E is called the residual or error functional over ${}^n\bar{\Omega}_{xt}$. The unknown constants in the approximation ${}^n\varphi_h(x,t)$ are determined using the algebraic equations resulting from,

$$\delta I({}^n\varphi_h) = 0 \tag{2.13}$$

(2.13) can also be written as,

$$B^{ls}({}^{n}\varphi_h(x,t), v(x,t))_{{}^{n}\bar{\Omega}_{xt}} = l^{ls}(v(x,t))_{{}^{n}\bar{\Omega}_{xt}} \tag{2.14}$$

Space-Time Finite Element Processes :

Using the integral forms described above, one could easily construct finite element processes by considering space-time discretization ${}^{n}\bar{\Omega}^{T}_{xt}$ of ${}^{n}\bar{\Omega}_{xt}$ containing space-time elements ${}^{n}\bar{\Omega}^{e}_{xt}$. From the methods of approximation described above, we obtain the following for the non-discretized space-time domain (a space-time strip or a space-time slab) ${}^{n}\bar{\Omega}_{xt}$.

$$B({}^{n}\varphi_h(x,t), v(x,t))_{{}^{n}\bar{\Omega}_{xt}} = l(v(x,t))_{{}^{n}\bar{\Omega}_{xt}} \tag{2.15}$$

For the discretization ${}^{n}\bar{\Omega}^{T}_{xt}$, (2.15) can be written as,

$$\sum_{e} B^{e}({}^{n}\varphi^{e}_h(x,t), v(x,t))_{{}^{n}\bar{\Omega}^{e}_{xt}} = \sum_{e} l^{e}(v(x,t))_{{}^{n}\bar{\Omega}^{e}_{xt}} \tag{2.16}$$

in which ${}^{n}\varphi^{e}_h(x,t)$ is the local approximation of $\varphi(x,t)$ over a space-time element ${}^{n}\bar{\Omega}^{e}_{xt}$.

If the integrands in (2.15) are continuous over ${}^{n}\bar{\Omega}_{xt}$, then (2.16) is valid in the strict sense of calculus (i.e., theory of continuous and differentiable functions). On the other hand, if the integrand in (2.15) exhibits pointwise discontinuities on sets of measure zero, as the case is if the continuity requirements are lowered on the integrand, then, (2.16) is only valid in the distributional sense. While the second approach has formed the basis of finite element method, there are significant merits in the first approach which obviously requires approximation ${}^{n}\varphi_h(x,t)$ to be of higher order global differentiability than of order zero.

Remarks

(1) It is significant to note that all of the methods discussed above yield necessary conditions $B(\cdot,\cdot) = l(v)$ which results in a set of algebraic equations from which the constants in the approximation ${}^{n}\varphi_h(x,t)$ are determined. However, these methods fail to establish the conditions under which the coefficient matrix in the algebraic system remains well conditioned or the computations remain stable. Lax-Milgrim theorem, Inf-Sup condition etc. are used on problem by problem basis to establish ranges of computational and dimensionless parameters (in GDEs) for which the algebraic systems remain stable. However, in many cases the resulting ranges of computational parameters may yield extremely refined and impractical discretizations. The necessity of computing with coarser discretizations due to resource limitations has led to the development of problem dependent upwinding methods [33]-[35]

(2) For an algebraic system to yield an unconditionally stable computational process a strict condition is that the coefficient matrix be positive definite with real and positive eigenvalues that are greater than zero.

(3) In a general mathematical and computational framework addressing all IVPs in a rigorous and consistent manner without problem dependent treatments, there needs to be a consistent mathematical methodology that automatically establishes the nature of the coefficient matrices resulting from the various space-time integral forms for the two classes of space-time differential

operators. The work presented by Surana et.al. [30]-[32] for BVPs and the concepts VC and VIC are extended here for IVPs to establish which integral forms yield unconditionally stable computational process for the two categories of space-time differential operators.

2.4 Higher order global differentiability approximation spaces

In section 1.2, the need for higher order global differentiability of the approximation in space and time has been established and discussed. Higher order global differentiability approximations obviously require higher order scalar product spaces. If ${}^n\varphi_h^e(x,t)$ is the local approximation of $\varphi(x,t)$ over a space-time sub-domain ${}^n\bar{\Omega}_{xt}^e$ then we require that,

$$
\begin{aligned}
&{}^n\varphi_h^e(x,t) \in V_h \subset H^{k,p}({}^n\bar{\Omega}_{xt}^e);\\
&\text{where } k=(k_1,k_2);\ p=(p_1,p_2), p_1 \geq 2k_1+1, p_2 \geq 2k_2+1
\end{aligned}
\tag{2.17}
$$

$H^{k,p}$ is the scalar product space containing approximation functions of global differentiability $(k-1)$ and degree p. k_1, k_2 are the orders of the approximation space in space and time and p_1, p_2 are the corresponding degrees of approximation. The approximation ${}^n\varphi_h(x,t)$ for the n^{th} space-time strip is given by,

$$
{}^n\varphi_h(x,t) = \bigcup_{e=1}^{M} {}^n\varphi_h^e(x,t) \tag{2.18}
$$

where M is the number of space-time elements in the n^{th} space-time strip. The global approximation $\varphi_h(x,t)$ for the entire space-time discretization $\bar{\Omega}_{xt}^T = \bigcup_{n=1}^{n^*} \bigcup_{e=1}^{M} {}^n\bar{\Omega}_{xt}^e$ is given by,

$$
\varphi_h(x,t) = \bigcup_{n=1}^{n^*} {}^n\varphi_h(x,t) \tag{2.19}
$$

(2.17-2.19) ensures ${}^n\varphi_h^e(x,t)$ and hence ${}^n\varphi_h(x,t)$ and $\varphi_h(x,t)$ are all of class C^{k_1-1} in space and of class C^{k_2-1} in time. If the space-time differential operator has highest derivatives of orders $2m_1$ and $2m_2$ in space and time then, $k_1 = 2m_1 + 1$ and $k_2 = 2m_2 + 1$ correspond to the minimally conforming space if the integrand in the space-time integral over ${}^n\bar{\Omega}_{xt}$ is to be continuous i.e, Riemann. If the theoretical solution $\varphi(x,t)$ is of class L_1 and L_2 in space and time ($L_1, L_2 \to \infty$ is admissible), then $2m_1+1 \leq k_1 \leq L_1$, $2m_2+1 \leq k_2 \leq L_2$. The choices of k_1 and k_2 depend upon the orders of global differentiability in space and time desired in the computational process.

2.5 Calculus of variations and space-time variational consistency (STVC) or variational inconsistency (STVIC) of the space-time integral forms

The concepts of STVC or STVIC are helpful in establishing which space-time integral forms yield algebraic system that are unconditionally stable and non-degenerate or only conditionally stable. This is done by establishing a correspondence between the integral forms resulting from the various methods of approximations for the two classes of space-time differential operators and the elements of the calculus of variations.

2.5.1 Elements of calculus of variations

Let ${}^n\varphi_h(x,t)$ be an approximation of $\varphi(x,t)$ over ${}^n\bar{\Omega}_{xt}$, then we have the following,

(a) Existence of a functional $I({}^n\varphi_h(x,t))$: Let there exist a functional $I({}^n\varphi_h(x,t))$ corresponding to the IVP (2.1). The existence is generally by construction. Extrema of $I({}^n\varphi_h(x,t))$ is of interest.

(b) Necessary condition : If $I({}^n\varphi_h(x,t))$ is differentiable in ${}^n\varphi_h(x,t)$ then $\delta I({}^n\varphi_h(x,t)) = 0$ (first variation of I set to zero) is a necessary condition for an extrema of $I({}^n\varphi_h(x,t))$ i.e., $\delta I({}^n\varphi_h(x,t)) = 0$ provides necessary conditions or equations for determining constants in ${}^n\varphi_h(x,t)$.

(c) Sufficient Condition or extremum principle : If $I({}^n\varphi_h)$ is differentiable twice in ${}^n\varphi_h$, then, second variation of $I({}^n\varphi_h)$ provides sufficient conditions or extremum principle and we have,

$$\delta^2 I = \begin{cases} < 0 & : \text{ maxima of } I \\ = 0 & : \text{ saddle point of } I \\ > 0 & : \text{ minima of } I \end{cases}$$

The existence of unique extremum principle ensures that a function ${}^n\varphi_h(x,t)$ obtained from $\delta I({}^n\varphi_h(x,t)) = 0$ indeed yields a unique extrema of $I({}^n\varphi_h(x,t))$ and establishes if $I({}^n\varphi_h(x,t))$ is minimized, maximized or we have its saddle point.

It can be shown that if the Euler's equation from $\delta I({}^n\varphi_h(x,t)) = 0$ is the IVP (2.1), then a function ${}^n\varphi_h(x,t)$ that yield unique extrema of $I({}^n\varphi_h(x,t))$ is also a unique solution of the IVP (2.1). Thus we have a correspondence between the solution of the IVP and the calculus of variations.

2.5.2 STVC or STVIC of space-time integral forms

STVC space-time integral forms (definition) : In finite element processes for IVPs, if one constructs a space-time integral form over ${}^n\bar{\Omega}_{xt}^T$ and then if one is able to show that there exists a functional $I({}^n\varphi_h(x,t))$ such that $\delta I({}^n\varphi_h(x,t)) = 0$ yields the space-time integral form and $\delta^2 I({}^n\varphi_h(x,t))$ yields a unique extremum principle then the space-time integral form conforms to the calculus of variations. Such integral forms are called STVC integral forms. ■

STVC space-time integral forms ensure unique solution ${}^n\varphi_h(x,t)$ from the integral form (i.e. $\delta I = 0$). This stems from the fact that STVC integral forms yield unique extremum principle which ensures that the coefficient matrices in the algebraic systems remain unconditionally positive definite and hence the resulting computational processes remain unconditionally stable.

STVIC space-time integral forms (Definition) : In space-time finite element processes in which either existence of $I({}^n\varphi_h(x,t))$ and/or existence of unique extremum principle is not possible, we are in violation with the principles of the calculus of variations. The space-time integral forms in such finite element processes are termed STVIC integral forms. ■

STVIC integral forms do not ensure a unique extrema and hence a unique solution of the IVP. Such integral forms yield algebraic systems in which the coefficient matrices are non-symmetric and are not ensured to be unconditionally positive definite and hence the resulting computational processes are not unconditionally stable. In STVIC integral forms one must use Lax-Milgrim theorem, Inf-Sup

condition etc., on problem by problem basis to establish ranges of computational and physical parameters for which the computational processes remain stable (as done currently in the finite element processes).

In the following we consider mathematical classification of the space-time differential operators (non-self adjoint and nonlinear) and various methods of approximation to establish which space-time integral forms are STVC or STVIC. In all cases we assume without loss of generality that there exists a functional $I({}^n\varphi_h(x,t))$ (though it may or may not be able to construct it) such that $\delta I({}^n\varphi_h(x,t)) = 0$ yields the desired integral forms. Then, it only remains to show whether a unique extremum principle exists or not. We state the results in the form of a series of theorems, proofs are straight forward and hence are omitted.

Theorem 1: Let $A\varphi - f = 0$ in ${}^n\bar{\Omega}_{xt}$ be an IVP in which A is space-time non-self adjoint differential operator and ${}^n\varphi_h(x,t)$ is an approximation of $\varphi(x,t)$ over ${}^n\bar{\Omega}_{xt}$. Let there exist a functional $I({}^n\varphi_h(x,t))$ such that $\delta I({}^n\varphi_h(x,t)) = 0$ yields the space-time integral form $\int\limits_{{}^n\bar{\Omega}_{xt}} (A^n\varphi_h(x,t) - f(x,t))v(x,t)d\Omega_{xt} = 0$ in which $v = \delta({}^n\varphi_h(x,t))$ or $v \neq \delta({}^n\varphi_h(x,t))$ are admissible with $v = 0$ on γ^* where ${}^n\varphi_h(x,t) = \varphi_0$, then this space-time integral form is STVIC i.e., $\delta^2 I({}^n\varphi_h(x,t))$ (first variation of the integral form) does not yield a unique extremum principle. ■

Based on this theorem it is straight forward to establish that space-time integral forms resulting from STGM, STPGM and STWRM are all space-time variationally inconsistent when the space-time differential operator is non-self adjoint.

Theorem 2: Let $A\varphi - f = 0$ in ${}^n\bar{\Omega}_{xt}$ be an IVP in which A is space-time non-linear differential operator and ${}^n\varphi_h(x,t)$ is an approximation of $\varphi(x,t)$ in ${}^n\bar{\Omega}_{xt}$. Let there exist a functional $I({}^n\varphi_h(x,t))$ such that $\delta I({}^n\varphi_h(x,t)) = 0$ yields the space-time integral form $\int\limits_{{}^n\bar{\Omega}_{xt}} (A^n\varphi_h(x,t) - f(x,t))v(x,t)d\Omega_{xt} = 0$ in which $v = \delta({}^n\varphi_h(x,t))$ or $v \neq \delta({}^n\varphi_h(x,t))$ are admissible with $v = 0$ on γ^* where ${}^n\varphi_h(x,t) = \varphi_0$, then this space-time integral form is STVIC i.e., $\delta^2 I({}^n\varphi_h(x,t))$ (first variation of the integral form) does not yield a unique extremum principle. ■

Based on this theorem it is straight forward to establish that space-time integral forms resulting from STGM, STPGM and STWRM are all space-time variationally inconsistent when the space-time differential operator is non-linear.

Theorem 3: Let $A\varphi - f = 0$ in ${}^n\bar{\Omega}_{xt}$ be an IVP in which A is space-time non-self adjoint differential operator and ${}^n\varphi_h(x,t)$ is an approximation of $\varphi(x,t)$ in ${}^n\bar{\Omega}_{xt}$. Let $B({}^n\varphi_h, v) = l(v)$; $v = \delta({}^n\varphi_h)$ represent all possible weak forms obtained from $\int\limits_{{}^n\bar{\Omega}_{xt}} (A^n\varphi_h(x,t) - f(x,t))v(x,t)d\Omega_{xt} = 0$. Let there exist a functional $I({}^n\varphi_h(x,t))$ such that $\delta I({}^n\varphi_h(x,t)) = 0$ yields all possible weak forms i.e, $\delta I({}^n\varphi_h(x,t)) = B({}^n\varphi_h, v) - l(v) = 0$. Then, all such weak forms are STVIC i.e., $\delta^2 I({}^n\varphi_h(x,t))$ (first variation of the weak form) does not yield a unique extremum principle. ■

Hence, the space-time integral forms resulting from STGM/WF are STVIC when the space-time differential operator is non-self adjoint.

Theorem 4: Let $A\varphi - f = 0$ in ${}^n\bar{\Omega}_{xt}$ be an IVP in which A is space-time non-linear differential operator and ${}^n\varphi_h(x,t)$ be an approximation of $\varphi(x,t)$

in ${}^n\bar{\Omega}_{xt}$. Let $B({}^n\varphi_h, v) = l(v)$; $v = \delta({}^n\varphi_h)$ represent all possible weak forms obtained from $\int\limits_{{}^n\bar{\Omega}_{xt}} (A^n\varphi_h(x,t) - f(x,t))v(x,t)d\Omega_{xt} = 0$. Let there exist a functional $I({}^n\varphi_h(x,t))$ such that $\delta I({}^n\varphi_h(x,t)) = 0$ yield all possible weak forms i.e, $\delta I({}^n\varphi_h(x,t)) = B({}^n\varphi_h, v) - l(v) = 0$. Then, all such weak forms are STVIC i.e., $\delta^2 I({}^n\varphi_h(x,t))$ (first variation of the weak form) does not yield a unique extremum principle. ■

Thus, the space-time integral forms resulting from STGM/WF are STVIC when the space-time differential operator is non-linear.

Theorem 5: Let $A\varphi - f = 0$ in ${}^n\bar{\Omega}_{xt}$ be an IVP in which A is space-time non-self adjoint differential operator and ${}^n\varphi_h(x,t)$ is an approximation of $\varphi(x,t)$ in ${}^n\bar{\Omega}_{xt}$. Let $E = A({}^n\varphi_h(x,t)) - f(x,t)$ represent residual or error in ${}^n\bar{\Omega}_{xt}$, then, the space-time least squares processes based on residual E are STVC and we have the following :

(a) *Existence of the functional* $I({}^n\varphi_h(x,t))$: $I({}^n\varphi_h(x,t)) = (E,E)_{{}^n\bar{\Omega}_{xt}}$

(b) *Necessary conditions* : $\delta I({}^n\varphi_h) = (E, \delta E)_{{}^n\bar{\Omega}_{xt}} = g = 0$

(c) *Sufficient condition or extremum principle* : $\delta^2 I({}^n\varphi_h) = (\delta E, \delta E)_{{}^n\bar{\Omega}_{xt}} > 0$ ■

Sufficient condition (c) implies that a ${}^n\varphi_h(x,t)$ obtained from (b) minimizes $I({}^n\varphi_h(x,t))$ in (a). Furthermore, minima of $I({}^n\varphi_h(x,t))$ is zero and when $I({}^n\varphi_h) \to 0$, $E \to 0 \forall (x,t) \in {}^n\bar{\Omega}_{xt}$ i.e., in the pointwise sense. Thus, convergence of the L_2-norm of E implies pointwise convergence of residual E which implies that $A^n\varphi_h - f \to 0 \ \ \forall (x,t) \in {}^n\bar{\Omega}_{xt}$.

Theorem 6: Let $A\varphi - f = 0$ in ${}^{n}\bar{\Omega}_{xt}$ be an IVP in which A is space-time non-linear differential operator and ${}^{n}\varphi_h(x,t)$ is an approximation of $\varphi(x,t)$ in ${}^{n}\bar{\Omega}_{xt}$. Let $E = A({}^{n}\varphi_h(x,t)) - f(x,t)$ represent residual or error in ${}^{n}\bar{\Omega}_{xt}$, then, the space-time least squares processes based on residual E are STVC provided the system of non-linear algebraic equations resulting from the necessary condition are solved using Newton's first order method and we have the following,

(a) *Existence of the functional* $I({}^{n}\varphi_h(x,t)) : I({}^{n}\varphi_h(x,t)) = (E,E)_{{}^{n}\bar{\Omega}_{xt}}$

(b) *Necessary conditions* : $\delta I({}^{n}\varphi_h(x,t)) = (E,\delta E)_{{}^{n}\bar{\Omega}_{xt}} = g({}^{n}\varphi_h) = 0$

(c) *Sufficient condition or extremum principle* : $\delta^2 I({}^{n}\varphi_h(x,t)) \cong (\delta E,\delta E)_{{}^{n}\bar{\Omega}_{xt}} > 0$ ■

The Newton's method with line search yields the following. ${}^{n}\varphi_h = {}^{n}\varphi_h^0 + \alpha\Delta({}^{n}\varphi_h)$ $\Delta({}^{n}\varphi_h) = -[\delta^2 I({}^{n}\varphi_h(x,t))]^{-1}_{{}^{n}\varphi_h^0}\{g({}^{n}\varphi_h^0)\}$. The scalar α is obtained such that $I({}^{n}\varphi_h) \leq I({}^{n}\varphi_h^0)$: line search. ${}^{n}\varphi_h^0$ is an assumed or starting solution in the Newton's method and ${}^{n}\varphi_h$ is the improved solution. Convergence of the iterative procedure is determined by the proximity of the each component of $g({}^{n}\varphi_h)$ to zero.

Remarks

(1) STGM, STPGM, STWRM, STGM/WF are always STVIC regardless of the nature of the space-time differential operator.

(2) STLSP are always STVC regardless of the nature of the space-time differential operator.

(3) Due to $\delta^2 I({}^n\varphi_h(x,t)) > 0$, the computational processes based on STLSP are unconditionally stable and non-degenerate during the entire evolution. The coefficient matrices in the algebraic systems are always symmetric (due to symmetry of $\delta^2 I({}^n\varphi_h(x,t))$) and positive definite and hence have a real basis with real eigenvalues greater than zero.

(4) In STVIC space-time integral forms the variations of the integral form i.e., $\delta^2 I({}^n\varphi_h(x,t))$ does not yield a unique extremum principle, hence a unique solution of the IVP is not ensured. The coefficient matrices in the algebraic systems are non-symmetric and hence, may have partial or completely complex basis. Such computational processes are not unconditionally stable for arbitrary choices of h, p, k and the dimensionless parameters of the problem and may even totally degenerate for some choices of the parameters in which case the computations cease.

2.6 Space-time mesh and space-time, time marching processes.

Since the IVPs describe evolutions, two space-time methodologies can be considered to simulate the time evolution : a space-time mesh in which the entire space-time domain $\bar{\Omega}_{xt}$ is discretized using space-time elements or a space-time time marching process in which one only considers a single space-time strip or a slab for an increment of time and then time marches to simulate the entire evolution for $t_0 \leq t \leq \tau$. In this section we consider and evaluate both approaches.

2.6.1 Space-time mesh :

Consider a space-time discretization $\bar{\Omega}_{xt}^{T}$ of the entire space-time domain $\bar{\Omega}_{xt}$ described in section 2.2 with global approximation $\varphi_h(x,t)\ \forall\ x,t \in \bar{\Omega}_{xt}^{T}$ given by (2.3). Let the local approximation be ${}^{n}\varphi_h^e(x,t)\ \forall\ x,t \in {}^{n}\bar{\Omega}_{xt}^{e}$, a space-time element 'e' belonging to n^{th} space-time strip in the discretization $\bar{\Omega}_{xt}^{T}$, then,

$$ {}^{n}\varphi_h^e(x,t) \in V_h \subset H^{k,p}({}^{n}\bar{\Omega}_{xt}^{e}); k=(k_1,k_2), p=(p_1,p_2) \tag{2.20} $$

such that $k_1 \geq 2m_1+1, k_2 \geq 2m_2+1$ and $p_1 \geq 2k_1-1, p_2 = 2k_2-1$. In (2.14) $k_1 = 2m_1+1$ and $k_2 = 2m_2+1$ corresponds to minimally conforming approximation space. If $\varphi(x,t)$ is of classes L_1 and L_2 in space and time $(L_1 > 2m_1+1, L_2 > 2m_2+1)$, then if we require converged (h,p,hp-adaptive processes) $\varphi_h(x,t)$ to approach $\varphi(x,t)$ in all aspects, then $k_1 = L_1+1$ and $k_2 = L_2+1$ is essential i.e., the approximation space must contain global smoothness higher than that given by the minimally conforming space. In space-time meshes, one increases k_1 and k_2 to achieve $\varphi_h(x,t)$ of desired smoothness. For fixed k_1 and k_2, p-levels in space and time can also be increased to achieve convergence. The space-time meshes obviously yield very large algebraic systems if the discretization length in time (i.e., time increment) is small and τ is large, hence, this approach may be computationally inefficient and may even become impractical.

2.6.2 Time marching using space-time strip or slab :

In such processes, one considers only one space-time strip or slab for an increment of time at a time and computes a converged solution for it. The computed

solution at the open boundary serves as initial condition for the next space-time strip or slab and this is continued until the evolution at $t = \tau$ is achieved. In the following we state two theorems and provide their proofs.

Theorem 7: *Let $A\varphi - f = 0$ in ${}^n\bar{\Omega}_{xt}$ be an IVP in which the space-time differential operator is of orders $2m_1$ and $2m_2$ in space and time. Let ${}^n\bar{\Omega}_{xt} = \bigcup_{e=1}^{M} {}^n\bar{\Omega}^e_{xt}$, ${}^n\bar{\Omega}^e_{xt} = {}^n\Omega^e_{xt} \bigcup {}^n\Gamma^e$, ${}^n\Gamma^e = \bigcup_{i=1}^{4} {}^n\Gamma^e_i$; be discretization of n^{th} space-time strip. Let ${}^n\varphi_h(x,t)\ \forall\ x,t \in {}^n\bar{\Omega}_{xt}$ be an approximation of $\varphi(x,t)$ such that ${}^n\varphi_h(x,t) = \bigcup_{e=1}^{M} {}^n\varphi^e_h(x,t)$ then, if ${}^n\varphi^e_h(x,t) \in H^{k,p}({}^n\bar{\Omega}^e_{xt})$; $k = (k_1,k_2)$, $p = (p_1,p_2)$ in which $k_1 \geq 2m_1 + 1, k_2 = 1, p_1 \geq 2k_1 - 1, p_2 \geq 2m_2$. Then ${}^n\varphi_h(x,t) \in H^{k,p}({}^n\bar{\Omega}_{xt})$; $k_1 \geq 2m_1 + 1$, $k_2 = p_2 + 1$.* ■

Proof: Let,

$$ {}^n\varphi_h = \bigcup_{e=1}^{M} {}^n\varphi^e_h(x,t); \forall x,t \in {}^n\bar{\Omega}_{xt} $$

where

${}^n\varphi^e_h(x,t) \in H^{k,p}({}^n\bar{\Omega}^e_{xt}); k_1 \geq 2m_1 + 1, k_2 = 1, p_1 \geq 2k_1 - 1$ and $p_2 \geq 2m_2$

and,

$$
\begin{aligned}
{}^n\bar{\Omega}_{xt} &= \bigcup_{e=1}^{M} {}^n\bar{\Omega}^e_{xt} \\
{}^n\hat{\Gamma}_{12} &= {}^n\Gamma^1_1 \bigcup_{e=1}^{M-1} ({}^n\Gamma^e_2 \bigcup {}^n\Gamma^{e+1}_1) \bigcup {}^n\Gamma^M_2 \\
{}^n\hat{\Gamma}_4 &= \bigcup_{e=1}^{M} {}^n\Gamma^e_4 \\
{}^n\hat{\Gamma}_3 &= \bigcup_{e=1}^{M} {}^n\Gamma^e_3
\end{aligned}
$$

Then, obviously,

$$ {}^{n}\bar{\Omega}_{xt} = (\bigcup_{e=1}^{M} \Omega_{xt}^{e}) {}^{n}\hat{\Gamma}_{12} \bigcup {}^{n}\hat{\Gamma}_{3} \bigcup {}^{n}\hat{\Gamma}_{4} $$

and, we have the following,

$$ \begin{array}{rcl} {}^{n}\varphi_h(x,t) & \in & H^{k,p}({}^{n}\Omega_{xt})\ ;\ k_1 = p_1 + 1, k_2 = p_2 + 1 \geq 2m_2 + 1 \\ {}^{n}\varphi_h(x,t) & \in & H^{k,p}({}^{n}\hat{\Gamma}_{12})\ ;\ k_1 \geq 2m_1 + 1, k_2 = p_2 + 1 \geq 2m_2 + 1 \\ {}^{n}\varphi_h(x,t) & \in & H^{k,p}({}^{n}\hat{\Gamma}_{3})\ ;\ k_1 \geq 2m_1 + 1, k_2 = p_2 + 1 \geq 2m_2 + 1 \\ {}^{n}\varphi_h(x,t) & \in & H^{k,p}({}^{n}\hat{\Gamma}_{4})\ ;\ k_1 \geq 2m_1 + 1, k_2 = p_2 + 1 \geq 2m_2 + 1 \end{array} \tag{2.21} $$

(2.21) imply the following,

${}^{n}\varphi_h(x,t) \in H^{k,p}({}^{n}\Omega_{xt}); k_1 \geq 2m_1 + 1, k_2 = p_2 + 1 \geq 2m_2 + 1$ ■

That is, the class or the order of global differentiability of the approximation ${}^{n}\varphi_h(x,t)$ in time for n^{th} space-time strip or slab is equal to p_2, the degree of local approximation in time in space-time time marching process when using a space-time strip or a slab.

Theorem 8: *Let $A\varphi - f = 0$ in ${}^{n}\bar{\Omega}_{xt}$ be an IVP and $\varphi_h(x,t)$ be an approximation of $\varphi(x,t)\ \forall x,t \in \bar{\Omega}_{xt}^{T} = \bigcup_{n=1}^{n^*} (\bigcup_{e=1}^{M} {}^{n}\bar{\Omega}_{xt}^{e})$, a space-time discretization of $\bar{\Omega}_{xt}$ containing n^* space-time strips or slabs. Let ${}^{n}\varphi_h^{e}(x,t) \in H^{k,p}({}^{n}\bar{\Omega}_{xt}^{e})$; $k_1 \geq 2m_1 + 1,\ k_2 \geq 2m_2 + 1,\ p_1 \geq 2k_1 - 1,\ p_2 \geq 2k_2 - 1$ be the local approximation, then in the space-time, time marching process based on a space-time strip or slab ${}^{n}\bar{\Omega}_{xt}$, the following holds,*

$\varphi_h(x,t) \in H^{k}(\bar{\Omega}_{xt}^{T}); k_1 \geq 2m_1 + 1, k_2 \geq 2m_2 + 1$ ■

Proof :

Consider two successive space-time strips ${}^{n}\bar{\Omega}_{xt}$ and ${}^{n+1}\bar{\Omega}_{xt}$, then based on theorem 7, the following holds,

$$\begin{array}{l} {}^{n}\varphi_h(x,t) \in H^{k,p}({}^{n}\bar{\Omega}_{xt}); k_1 \geq 2m_1+1, k_2 = p_2+1 \geq 2m_2+1 \\ {}^{n+1}\varphi_h(x,t) \in H^{k,p}({}^{n+1}\bar{\Omega}_{xt}); k_1 \geq 2m_1+1, k_2 = p_2+1 \geq 2m_2+1 \end{array} \tag{2.22}$$

But,

$${}^{n+1}\varphi_h({}^{n+1}\hat{\Gamma}_3) \equiv {}^{n}\varphi_h({}^{n}\hat{\Gamma}_4); \text{due to space-time, time marching} \tag{2.23}$$

However for,

$$({}^{n}\varphi_h(x,t) \bigcup {}^{n+1}\varphi_h(x,t)) \in H^{k,p}({}^{n}\bar{\Omega}_{xt} \bigcup {}^{n+1}\bar{\Omega}_{xt}) \tag{2.24}$$

only $k_1 \geq 2m_1+1, k_2 \geq 2m_2+1$ holds for $n = 1, \cdots, n^* - 1$. Hence, we have,

$$\varphi_h(x,t) = (\bigcup_{n=1}^{n^*} {}^{n}\varphi_h(x,t)) \in H^{k,p}(\bar{\Omega}^T_{xt}); k_1 \geq 2m_1+1, k_2 \geq 2m_2+1 \blacksquare$$

That is, even though the global differentiability of ${}^{n}\varphi_h(x,t)$ in time for a space-time strip is equal to p_2, the degree of local approximation in time, the global differentiability of $\varphi_h(x,t)$ for $\bar{\Omega}^T_{xt}$ remains of order $k_2 - 1$ where k_2 is the order of the local approximation in space and time.

Remarks

(1) In both space-time mesh approach as well as space-time strip time marching processes, the global differentiability in time of $\varphi_h(x,t)$ necessitates local approximations ${}^{n}\varphi^e_h(x,t)$ to be of the same class in time as $\varphi_h(x,t)$.

(2) In space-time time marching process local approximations of class C^0 in time but of degree p_2 yield global approximation ${}^{n}\varphi_h(x,t)$ of order p_2 in time.

A significant feature, through which local approximation over ${}^n\bar{\Omega}^e_{xt}$ can be maintained of class C^0, yet, global smoothness of ${}^n\varphi_h(x,t)$ can be increased by increasing p-level p_2 in time of local approximation ${}^n\varphi^e_h(x,t)$, however global smoothness of $\varphi_h(x,t)$ in $\bar{\Omega}^T_{xt}$ will be of class C^0 in time.

(3) Computational efficiency of space-time time marching processes is rather obvious and is well known. The space-time time marching processes are superior and meritorious to space-time meshes in all aspects.

2.7 Summary

The details of the h, p, k mathematical and computational framework with VC integral forms [30]-[32] for BVPs in 2D viscous compressible flows has been summarized.

A new mathematical and computational framework based on h, p and k and space-time coupled methodology with space-time variationally consistent space-time integral forms has been presented for initial value problems. In the following we present a summary.

(1) Space-time decoupled method with non-concurrent treatment in space and time are not in agreement with the physics of evolutions described by IVPs. In these approaches one can rarely use elements of the calculus of variations to establish the nature of the resulting coefficient matrices in the algebraic systems. These methods are limited in accuracy, have serious issues of stability that must be investigated on problem by problem basis and in general

rarely permit time accurate evolutions. Thus, these methods can not be considered as a general methodology for the development of a mathematical and computational framework for IVPs.

(2) The space-time coupled methods with concurrent treatment in space and time yielding simultaneous dependence of the dependent variables on space and time are in agreement with physics of evolution described by IVPs and hence are the preferred methodology for developing a general mathematical and computational framework for IVPs.

(3) The order $k = (k_1, k_2)$ of the approximation space is an independent parameter in the finite element computations in addition to h and p, hence, the development of the mathematical framework must be based on h, p and k permitting desired global smoothness of the approximations in space and time.

(4) It has been shown that space-time time marching process using a single space-time strip or slab is superior and meritorious in all aspects to space-time meshes. Space-time meshes require higher order global differentiability local approximation in space as well as time. Whereas, in space-time, time marching process the local approximations of class C^0 but of degree p_2 in time yield global differentiability or smoothness of order p_2 in time for a single space-time strip or a slab even though global approximation remains of class C^0 in time. The increased global differentiability in time for a space-time strip maybe beneficial.

(5) The space-time differential operators are classified mathematically over a space-time strip (or slab) and it is shown that all space-time differential operators are either non-self-adjoint (when linear) or non-linear but never self-adjoint.

(6) The concepts of space-time variational consistency (STVC) and space-time variational inconsistency (STVIC) are introduced and defined using space-time integral forms resulting from the GDEs describing IVPs and by applying the principles of calculus of variations. It is shown that STVC space-time integral form yield symmetric positive definite coefficient matrices with real eigenbasis and eigenvalues greater than zero. The computational processes based on STVC integral forms are unconditionally stable and non-degenerate and hence free of spurious solutions and stability issues. On the other hand STVIC space-time integral forms yield non-symmetric coefficient matrices that may have partial or completely complex basis. The computational processes based on such integral form may yield spurious solutions, may have stability issues and may even totally degenerate for some choices of h, p and k in which case the computations cease.

(7) STGM, STPGM, STWRM, STGM/WF and STLSP are presented as possible finite element computational strategies for IVPs. It is shown that STGM, STPGM, STWRM and STGM/WF are STVIC for non-self adjoint as well as non-linear space-time differential operators and hence should not be considered as general computational methodology for IVPs. STLSP

are STVC regardless of the nature of differential operator and hence are worthy of consideration in the development of a general mathematical and computational framework. STLSP for space-time strip with time marching permit strict control of solution error. One uses h, p, k refinements until the desired accuracy is achieved for the current space-time strip or slab before time marching is commenced. Thus, in this approach time accurate evolution is possible. When least squares space-time functional for a space-time strip approaches zero i.e., when $I = (E, E)_{{}^n\bar{\Omega}_{xt}} \rightarrow 0$, $E \rightarrow 0 \; \forall \; x, t \; \in {}^n\bar{\Omega}_{xt}$ i.e., GDEs are satisfied in the pointwise sense.

(8) In summary, STLSP in h, p, k framework with local approximation ${}^n\varphi_h^e \in H^{k,p}({}^n\bar{\Omega}_{xt}^e)$; $k_1 \geq 2m_1 + 1, \; k_2 \geq 2m_2 + 1, \; p_1 \geq 2k_1 - 1, \; p_2 \geq 2k_2 - 1$ yielding $\varphi_h(x, t) \; \forall \; x, t \in \bar{\Omega}_{xt}^T$ of class $k_1 \geq 2m_1 + 1, \; k_2 \geq 2m_2 + 1$ with space-time time marching is highly meritorious approach for all IVPs and hence worthy of consideration as a general mathematical and computational framework for IVPs.

Chapter 3

Mathematical Models and Finite Element Formulations

3.1 Introduction

In this chapter the mathematical models and the finite element formulations are described for the benchmark problems used in this work in order to avoid repetition of this material in the subsequent chapters containing numerical studies. We consider three benchmark problems : (I) Transient one dimensional viscous form of Burgers equation (IVP) (II) One dimensional Riemann shock tube with ideal and real gas models for equations of state (IVP) and (III) 2-D steady state compressible flow with ideal gas model for equation of state (BVP).

3.2 1-D Transient Viscous Burgers Equation

In this section, literature review, mathematical model details and the finite element formulation are presented for 1-D transient viscous form of Burgers equation. Numerical studies for the model problem are presented in chapter 4.

3.3 Literature Review

This model problem has been a subject of study for almost all new computational methodologies and hence, there is substantial published work. The material presented in the following is mainly related to non-linear hyperbolic and parabolic differential and partial differential equations. The idea of generalized solutions of the differential and partial differential equations was first proposed by S.L. Sobolev and constitutes the mathematics and thus the backbone of the finite element method. In an important paper Godunov [1] discussed the problem of generalized solutions of quasi-linear equations in gas dynamics. The author illustrated that for $\frac{\partial \varphi}{\partial t} + \varphi \frac{\partial \varphi}{\partial x} = 0$ (inviscid Burgers equation), the theory of generalized solutions leads to non-uniqueness. This situation can be corrected by imposing additional restriction on the weak form. For the Burgers equation (and its generalization to quasi-linear systems), this restriction leads to the law of conservation of entropy. Thus, in gas dynamics equations describing reversible processes, the law of conservation of entropy must hold in the theory of generalized solutions, whereas in irreversible processes there must be entropy production which in physical systems under adiabatic conditions is only possible through dissipative mechanisms. In other words, in the theory of generalized solutions of gas dynamics equations, the law of increase in entropy must be replaced by the law of dissipation of energy to ensure the uniqueness of generalized solutions. A rigorous mathematical exposition of the solutions of quasi-linear hyperbolic equations is presented by B.L. Rozhdestvenskii [2]. The findings are similar to those reported by Godunov and are summarized in reference [1]. The author shows

that systems of linear equations are always conservative, while the systems of non-linear equations, generally speaking, are conservative only for $n \leq 2$ (two conservation laws).

Solution of non-linear hyperbolic systems has also been reported by Grimm [3] and Smoller [9] and [72]. Grimm proposed an existence theorem and provided its proof. Smoller reported general characteristics of these solutions with specific details and discussion of the Riemann problem and contact discontinuities. Hopf [10] presented a mathematical proof of the convergence of weak solutions of quasi-linear equations of first order with artificial viscosity to strong solutions as viscosity approaches zero. Friedrich and Lax [11] discussed first order conservative systems of non-linear conservation laws which have as a consequence an additional conservation law. They show that if the additional conserved quantity is a convex function of the original ones, the original system can be put into symmetric hyperbolic form. They also derive an entropy inequality which has also been suggested by Kruzhkov [12] for discontinuous solutions of the given system of conservation laws. Existence of discrete shocks, genuine non-linearity and the use of fourth order dissipation in a single conservation law have been reported by Mock [13]-[14]. A thorough mathematical exposition with theorems and proofs for uniqueness of the solutions of hyperbolic conservation laws has been reported by DiPerna [15]. Existence and uniqueness of entropy solutions to the Riemann problem for hyperbolic systems of two conservation laws has been reported by Keyfitz and Kranzer [16]. The paper presents proofs of existence and uniqueness of the solutions in one space variable. Only strictly hyperbolic and genuinely non-

linear systems are investigated. Noh [17] reported an investigation of the errors introduced in the calculation of strong shocks using artificial viscosity of the type in reference [18] and artificial heat flux. An investigation of the errors introduced in the interaction of strong shocks due to the assumption of finite shock width has been reported by Menikoff [19].

There are many published works addressing numerical simulation of partial differential equations resulting from non-linear hyperbolic conservation laws. Here we primarily consider finite element approaches. Comprehensive literature review of published finite element approaches for convection-diffusion and Burgers equation can be found in references [20]-[21]. As pointed out in reference [2], for linear and non-linear hyperbolic systems based on one or two conservation laws it is possible to show the convergence of generalized solutions to strong solutions. However direct numerical computation of strong solutions is an exciting idea which may have benefits for systems in which the proof of the convergence of the generalized solutions to strong solutions may not be possible.

The one dimensional form of the time dependent momentum equation yields 1-D time dependent viscous form of the Burgers equation, which when non-dimensionalized, contains the dimensionless parameter, Reynolds number (Re). The viscosity of the medium is reflected in Re. For the viscous form of the Burgers equation the solutions are analytic with finite shock width dependent upon the Reynolds number (Re). For higher Re, the shock width is approximately $O(1/Re)$ and hence remains finite for a finite value of Re. The shock structure resolution in this case requires prudent mesh refinements in the shock zone to accommodate the

localized high gradients of the solution for high Re. The analytic solutions of the viscous form of the Burgers equation can be expressed as algebraic polynomials of infinite degree in space and time. Obviously, the best way to simulate such a solution is to use a single space-time element with p-levels in space and time approaching infinity, which of course is not possible. Thus, if we limit p-levels in space and time, then obviously discretization of the domain in space and time is necessary. For the converged numerical solutions to approach theoretical solutions (up to certain order derivatives), higher order global differentiability (smoothness) of local approximation in space and time becomes essential. Hence, h, p, k mathematical framework is essential for numerical simulation of such processes.

Inviscid form of the Burgers equation is a special case of the viscous form in which $Re = \infty$ (zero viscosity). In this case shock width $O(1/Re)$ becomes zero (hence requiring discretization length of zero for its accurate resolution) and we have a prefect shock i.e. jump with non-unique values of the solution at the shock. Such solutions are non-analytic and singular at the shock and therefore the solution derivatives are not defined at the shock. These solutions cannot be simulated in this precise form using finite element processes employing algebraic monomials as basis functions. As pointed out in reference [1] an attempt to compute solutions of inviscid Burgers equation would lead to non-uniqueness of the solution and hence obviously the lack of convergence of the associated functionals (for example residual functional in least squares processes). The solutions of the inviscid Burgers equation can only be approached as a limiting case. For example:

(i) Artificial viscosity approach [1] in which case one shows that as the artificial

viscosity approaches zero the solutions of the inviscid form are recoverable (but not possible to compute).

(ii) More recently $H(Div)$ least squares processes have been used in which the inviscid Burgers equation is recasted as a first order system of coupled partial differential equations using auxiliary variables [22]-[23]. The authors recognize the non-uniqueness of the solution and lack of existence of unique first derivative at the shock and introduce the Frêchet derivative to restore analyticity of the solution. Many theorems related to the convergence of the least squares functional, uniqueness of the solution of the reconstructed IVP and convergence of its weak solutions are presented. Some significant points are worth nothing: (a) As pointed out by Gudunov [1], the solutions of inviscid Burgers equation are non-unique and the uniqueness can only be restored by introducing some mechanism of viscosity (artificial or physical). (b) In the $H(Div)$ approach mesh dependent artificial viscosity is introduced in the inviscid form of the Burgers equation such that with progressively refined meshes in the spatial direction yield progressively decreasing viscous dissipation mechanism and hence it is possible to argue that in the limit the discretization length in space approaches zero, the solutions of the inviscid Burgers equation are possible to approach (but never possible to compute directly). (c) From (b) it is clear that in references [22]-[23] the authors only solve the viscous form of the Burgers equation in which the mechanism of viscous dissipation is artificial (non-physical) and not the inviscid form. (d) The viscous form of the Burgers equation resulting form the non-linear

conservation law already has a physical mechanism of viscous dissipation which in the dimensionless form of the GDE is intrinsic in the Reynolds number (Re). (e) In view of (a)-(d) it is quite clear that here we have two possible propositions. Should the solutions of the inviscid Burgers equation be approached using the artificial viscosity approach (let it be $H(Div)$ or any other) or should these be approached using viscous form of the GDE with progressively increasing Re thereby progressively diminishing viscosity. First we argue that the viscous form of the Burgers equation has a physical mechanism of viscosity and its solutions are always unique and that the computations using this form require no other artificial means. Secondly, we must show that the computations for the viscous form are possible with monotonic convergence of the least squares functional, accurate resolutions of the shock structure (depending upon Re) for discretizations that are no more refined than those employed in the artificial viscosity approaches (hence computationally competitive). For a given Re, the computed evolution is always time accurate and as Re is increased progressively the computed solutions indeed approach those of the inviscid form. (f) In reference [22] the solutions reported using $H(Div)$ approach for 16 x 16, 32 x 32, 64 x 64 and 256 x 256 space-time meshes show that these solutions correspond to progressively increasing Re, however, from this approach Re corresponding to these solutions can not be quantified.

Our view regarding $H(div)$ least squares methods and all others using artificial viscosity approaches is rather simple. If we are to diffuse the solutions

in some form or the other, then, we may as well use the viscous form of the Burgers equation in which the diffusion is physical due to viscosity of the medium and is reflected in the Reynolds number. In this approach if one could show that:

(a) The solutions remain unique and convergent for any finite Reynolds number.

(b) The associated least squares functional shows monotonic convergence and indeed approaches zero.

(c) For progressively increasing Re the progressively reduced shock width ($O(1/Re)$) for high Re is achieved and that the computations are always time accurate then, we indeed have a computational strategy in which the solutions of the inviscid Burgers equation can be visualized as a limiting case when the Reynolds approaches infinity. This approach is much more appealing because of the fact that viscous form of the Burgers equation is in agreement with the physics, and, that it requires no other treatments to regularize singular solutions of the inviscid Burgers equation, as they are naturally analytic due to the physics of the viscous medium.

3.3.1 Present Study

The theoretical solutions of the viscous form of the time dependent Burgers equation are of higher order global differentiability in space and time. It is shown that in h, p, k mathematical framework the solutions of the inviscid Burgers equation are approached with progressively increasing Reynolds number (Re) and order $k = (k_1, k_2)$; k_1 and k_2 being the orders of the approximation space in

space and time. Minimally conforming spaces in space and time are established and the need for spaces of orders higher than minimally conforming is clearly demonstrated. Theorems are presented to establish uniqueness of the numerical solutions from the space-time least squares processes in h, p, k framework when using strong form of the governing differential equations and Newton's linear method with line search for solving the resulting system of nonlinear algebraic equations. In the space-time least squares process non-linear GDEs are utilized without linearization or any other assumptions and that the least squares functional and its first variation correspond to the actual nonlinear GDEs. It is shown that least squares processes utilizing a system of first order GDEs by using auxiliary variables (including $H(Div)$-least squares finite element approaches) are prone to inconsistencies due to the fact that in the auxiliary equations a consistent choice of approximation spaces may or may not be possible. These inconsistencies are difficult (if not impossible) to eliminate. These inconsistencies may generate spurious numerical solutions when highly localized solution gradients exist as the case is for the Burgers equation for higher Re. Theorems are presented to establish that the space-time, time marching process is superior in all aspects to space-time meshes and that the space-time meshes can never compete with space-time marching processes in terms of accuracy, higher order global differentiability in time for each space time strip and computational efficiency. Numerical studies are presented to demonstrate all mathematical and computational features of the proposed framework and the numerical results are compared with the published work.

3.4 1-D Transient Burgers equation

3.4.1 Strong form of the GDE

The viscous form of the transient one-dimensional Burgers equation in the absence of sources and sinks is given by,

$$\frac{\partial \varphi}{\partial t} + \varphi \frac{\partial \varphi}{\partial x} - \frac{1}{Re} \frac{\partial^2 \varphi}{\partial x^2} = 0 \;\; \forall (x,t) \;\in\; \Omega_{xt} = \Omega_x \times \Omega_t = \Omega_x \times (0,\tau) \quad (3.1)$$

The boundary conditions and initial conditions will be discussed in context with specific numerical studies.

Equation (3.1) will be referred to as strong form of the GDE. It contains the highest order derivatives of the dependent variable. For a finite Re, the theoretical solution $\varphi(x,t)$ of (3.1) is analytic and hence can be expressed as an algebraic polynomial of degree p_1 and p_2 in space and time in which p_1 and p_2 may be infinity. Hence $\varphi(x,t)$ is class $C^{p_1,p_2}(\Omega_{xt})$; with $p_1, p_2 = \infty$ admissible. If $\varphi_h(x,t)$ is an approximation of $\varphi(x,t)$ in $\bar{\Omega}^T_{xt}$, then, based on equation (2.19) and section 2.4 we have the following (in space-time time marching process),

$$\begin{gathered} {}^n\varphi^e_h(x,t) \in \; H^{k,p}({}^n\bar{\Omega}^e_{xt}); \;\; k = (k_1,k_2); \;\; k_1 \geq 3 \;\text{ and }\; k_2 \geq 2 \\ p_1 \geq 2k_1 - 1 \;\text{ and }\; p_2 \geq 2k_2 - 1 \end{gathered} \quad (3.2)$$

In (3.2) $k_1 = 3$ and $k_2 = 2$ correspond to the minimally conforming space in space and time. If ${}^n\varphi_h(x,t)$ belongs to the space of orders lower than minimally conforming, then ${}^n\varphi^e_h(x,t)$ is not admissible in (3.1). The orders $k_1 > 3$ and $k_2 > 2$ are obviously essential if $\varphi_h(x,t)$ is to possess the global smoothness up to a desired order as necessitated by the nature of the theoretical solution $\varphi(x,t)$ and hence, the need for h, p, k framework is rather obvious. GDE (3.1) is suitable for computations

in the h, p, k framework using STLSP with space-time, time marching. Solutions $\varphi_h(x,t)$ are always non-spurious and ensured to be unique (chapter 2).

3.4.2 Weak form of the GDE

In a recent paper Surana et. al. [70] have presented an investigation of the strong and weak form of the GDEs in least squares processes for BVPs. Similar conclusions hold for IVPs as well. Here we present a short discussion of the weak form of the GDEs. Equation (3.1) can be recasted as a system of first order partial differential equations. This can be accomplished in more than one way. In the following we discuss two such approaches.

Approach 1: In this case we let $u = \frac{\partial \varphi}{\partial x}$ and substitute it in (3.1) for the purpose of converting (3.1) into a system of first order partial differential equation and we obtain,

$$\frac{\partial \varphi}{\partial t} + \varphi \frac{\partial \varphi}{\partial x} - \frac{1}{Re}\frac{\partial u}{\partial x} = 0 \tag{3.3}$$

$$u = \frac{\partial \varphi}{\partial x} \tag{3.4}$$

$\forall\, (x,t) \in \Omega_{xt}$

Approach 2: In this approach (3.1) is converted into a system of first order linear partial differential equations by using $u = \frac{\partial \varphi}{\partial x}$ and $\nu = \frac{1}{2}\varphi^2$ and we obtain the

following [22].

$$\frac{\partial \varphi}{\partial t} + \frac{\partial \nu}{\partial x} - \frac{1}{Re}\frac{\partial u}{\partial x} = 0 \tag{3.5}$$

$$u = \frac{\partial \varphi}{\partial x} \tag{3.6}$$

$$\nu = 1/2\, \varphi^2 \tag{3.7}$$

$\forall\, (x,t)\ \in\ \Omega_{xt}$

In this approach the GDE (3.1) is converted into (3.5-3.7), a first order linear differential equation and the non-linearity in (3.1) has been transferred to the algebraic equation (3.7) defining ν. The variables u and ν are called auxiliary variables and the corresponding equations are called auxiliary equations. We refer to both of these approaches as the approaches of obtaining "Weak form of the governing differential equations." The first question that arises is, are the numerical solutions $\varphi_h(x,t)$ from (3.3)-(3.4) and (3.5-3.7) the same as those from (3.1) ? Secondly, do these first order systems always yield unique solutions ? Thirdly, what are the other advantages or disadvantages of these types of approaches ?

Let us evaluate both of these approaches in context with STLSP. We first consider "Approach 1" (equations (3.3) and (3.4)). Let ${}^n\varphi_h^e(x,t)$ and ${}^n u_h^e(x,t)$ be approximations of $\varphi(x,t)$ and $u(x,t)$ over a space-time element ${}^n\bar{\Omega}_{xt}^e$ of n^{th} space-time strip. The using (3.3) and (3.4) we obtain the following residual equations for ${}^n\bar{\Omega}_{xt}^e$.

$${}^n E_1^e = \frac{\partial^n \varphi_h^e}{\partial t} + {}^n\varphi_h^e \frac{\partial^n \varphi_h^e}{\partial x} - \frac{1}{Re}\frac{\partial^n \varphi_h^e}{\partial x} \tag{3.8}$$

$${}^n E_2^e = {}^n u_h^e - \frac{\partial^e \varphi_h^n}{\partial x} \tag{3.9}$$

In which

$$ {}^{n}\varphi_h^e = [N_\varphi]\,{}^{n}\varphi^e \tag{3.10} $$

$$ {}^{n}u_h^e = [N_u]\,{}^{n}u^e \tag{3.11} $$

$\{{}^{n}\varphi^e\}$ and $\{{}^{n}u^e\}$ are nodal degrees of freedom for ${}^{n}\varphi_h^e$ and ${}^{n}u_h^e$ and $[N_\varphi]$ and $[N_u]$ are local approximation functions. In (3.8) and (3.9) ${}^{n}\varphi_h^e$ and ${}^{n}u_h^e$ are interpolated independently and $\{{}^{n}\varphi^e\}$ and $\{{}^{n}u^e\}$ are independent degrees of freedom in the computational process. From (3.4), we note that if we choose the approximation (3.10) for φ then the approximation for u is defined by (3.4) i.e., the degrees of freedom $\{{}^{n}u^e\}$ are dependent on $\{{}^{n}\varphi_h^e\}$ and should not be treated as independent degrees of freedom. Secondly, $[N_u]$ are generally chosen to be the same as $[N_\varphi]$ i.e., ${}^{n}\varphi_h^e$ and ${}^{n}u_h^e$ are interpolated over ${}^{n}\bar{\Omega}_{xt}^e$ using equal order equal degree interpolations. Thus, we note that local approximations (3.10) and (3.11) are inconsistent. Hence, each auxiliary equation in the first order system derived using auxiliary variables represents a source of inconsistency in the computational process. With this inconsistency, when the integrated sums of squares of the residuals are minimized i.e. forced to be zero, the computed solutions may become spurious. When the solution gradients are high and highly localized, this is almost sure to occur [27]. When the solutions $\varphi(x,t)$ are diffused, this approach may work satisfactorily i.e. the inconsistency in the auxiliary equations may not be able to cause enough visible or measurable damage to φ or u [70]. There are many model problems and practical applications with localized high solution gradient in which cases the approaches utilizing weak form of the GDEs are not always assured to

yield meaningful solutions due to inconsistencies in approximations caused by the auxiliary equations.

Approach 2 is similar to approach 1 except that in this case the inconsistency of local approximations exists in two auxiliary equations. The fact that (3.5) is a linear differential equation is of little or no consequence due to the fact that :

(i) STLSP is independent of the nature of non-linearities in the GDEs.

(ii) The resulting algebraic system remains non-linear in approach 2 as well as approach 1 and hence use of iterative solution methods is inevitable in both cases.

Use of auxiliary variables obviously increases the problem size in both approaches (more in the second approach). So from this point of view approach 1 is worse than strong form and approach 2 is worst of all three. Since in the work presented here the mathematical consistency is the main focus, we do not wish to emphasize the computational efficiency issue. The most damaging aspect of first order systems or other such approaches $(H(div))$ utilizing auxiliary equations is the inconsistency of local approximation in the auxiliary equations and its uncertain but surely adverse consequences that are problem and application dependent. In the present work we use only the strong form of the GDE (equation 3.1).

3.4.3 Space-time LSP in h, p, k framework

We consider STLSP for (3.1) over a space-time strip ${}^n\bar{\Omega}_{xt} = \bigcup_{e=1}^{M} {}^n\bar{\Omega}^e_{xt}$ in which ${}^n\bar{\Omega}^e_{xt}$ is a space-time element or sub-domain. Let ${}^n\varphi^e_h(x,t)$ be an approximation of $\varphi(x,t)$ over ${}^n\bar{\Omega}^e_{xt}$ and $V_h({}^n\bar{\Omega}^e_{xt})$ be the approximation space, then,

$$V_h({}^n\bar{\Omega}^e_{xt}) \subset H^{k,p}({}^n\Omega^e_{xt}); \;\; k=(k_1,k_2), \;\; p=(p_1,p_2) \;\; \forall \, {}^n\bar{\Omega}^e_{xt} \;\in\; {}^n\bar{\Omega}_{xt} \tag{3.12}$$

$$\begin{aligned} H^{(k_1,k_2),(p_1,p_2)}({}^n\bar{\Omega}^e_{xt}) = \{w : w|_{{}^n\bar{\Omega}^e_{xt}} \in C^{(k_1-1,k_2-1),(p_1,p_2)}({}^n\bar{\Omega}^e_{xt}), w|_{{}^n\bar{\Omega}^e_{xt}} \in \\ p^{p_1,p_2}({}^n\bar{\Omega}^e_{xt}); k_1 \geq 3, k_2 \geq 2, p_1 \geq 2k_1-1, p_2 \geq 2k_2-1 \forall {}^n\bar{\Omega}^e_{xt} \in {}^n\bar{\Omega}_{xt}\} \end{aligned} \tag{3.13}$$

${}^n\varphi^e_h(x,t) \;\in\; V_h({}^n\bar{\Omega}^e_{xt})$ can be defined using

$$\begin{gathered} {}^n\varphi^e_h(x,t) = [N^{(k_1-1,k_2-1),(p_1,p_2)}(x,t)]\{{}^n\varphi^e\} = \sum_{e=1}^{n} N_i(x,t) \; {}^n\varphi^e_i; \\ \forall \, (x,t) \;\in\; {}^n\bar{\Omega}^e_h(x,t) \end{gathered} \tag{3.14}$$

In which $\{{}^n\varphi^e\}$ are nodal degrees of freedom for the space-time element with domain ${}^n\bar{\Omega}^e_{xt}$ and $N^{(k_1-1,k_2-1),(p_1,p_2)}(x,t) \;\in\; V_h({}^n\bar{\Omega}^e_{xt})$ are the space-time local approximation functions [73]. With the local approximation ${}^n\varphi^e_h(x,t)$ defined by (3.14), the space-time least squares process can be described as follows. Find $\{{}^n\varphi\} = \bigcup_e \{{}^n\varphi^e\}$ such that,

$$\delta I({}^n\varphi_h) = \sum_{e=1}^{M} ({}^nE^e, \delta({}^nE^c)) = g({}^n\varphi_h) = 0$$

where

$$I({}^n\varphi_h) = \sum_{e=1}^{M} ({}^nE^e, {}^nE^e)_{{}^n\bar{\Omega}^e_{xt}}; \quad {}^nE^e = \frac{\partial({}^n\varphi^e_h)}{\partial t} + {}^n\varphi^e_h \frac{\partial({}^n\varphi^e_h)}{\partial x} - \frac{1}{Re}\frac{\partial^2({}^n\varphi^e_h)}{\partial x^2}$$

and

$$\delta^2 I({}^n\varphi_h) \approx \sum_{e=1}^{M} (\delta({}^nE^e, \delta({}^nE^e) > 0$$

in which

$$\delta({}^nE^e) = \frac{\partial v}{\partial t} + \nu \frac{\partial({}^n\varphi_h^e)}{\partial x} + {}^n\varphi_h^e \frac{\partial v}{\partial x} - \frac{1}{Re}\frac{\partial^2 v}{\partial x^2}$$

where

$$v = \delta({}^n\varphi_h^e) = N_j(x,t); \;\; j = 1, ...n$$

Using Newton's fist order method with line search to find ${}^n\varphi_h$ iteratively to satisfy $g({}^n\varphi_h) = 0$ yields,

$${}^n\varphi_h = ({}^n\varphi_h)_0 + \alpha \Delta {}^n\varphi_h$$

$$\Delta {}^n\varphi_h = -[\delta^2 I({}^n\varphi_h)]^{-1}_{({}^n\varphi_h)_0} \{g({}^n\varphi_h)\}_{({}^n\varphi_h)_0}$$

α is determined such that,

$$I({}^n\varphi_h) \leq I(({}^n\varphi_h)_0)$$

where $({}^n\varphi_h)_0$ is the assumed or starting solution in the Newton's first order method.

Remarks

(1) In the STLSP requiring construction of $I({}^n\varphi_h)$ and $\delta I({}^n\varphi_h) = 0$, the GDE is not linearized as done by the authors in references [23] and many others.

(2) The STLSP is STVC and hence ensures unique ${}^n\varphi_h$ and unconditionally non-degenerate computational process during time marching and thus the entire evolution.

(3) We note that in the STLSP, $I({}^n\varphi_h)$ is minimized by a ${}^n\varphi_h$ that satisfies $\delta I({}^n\varphi_h) = 0$ and that minima of $I({}^n\varphi_h)$ is zero. Hence, when $I({}^n\varphi_h) \rightarrow 0$ we have ${}^nE^e \rightarrow 0$ for $e = 1, ...M$ in the point-wise sense. That is convergence of ${}^nE^e$ in L_2-norm yields pointwise convergence of ${}^nE^e \; \forall \; (x,t) \; \in \; {}^n\bar{\Omega}_{xt}$.

(4) STLSP has the best approximation property in E-norm i.e. $\|{}^n\varphi_h\|_E = (\sum({}^nE^e, {}^nE^e)_{{}^n\bar{\Omega}^e_{xt}})^{1/2}$ is minimum is STLSP compared to any other processes.

3.5 Mathematical model for viscous conducting compressible flows with variable transport properties

The model problems discussed in section 3.6 and 3.7 require mathematical models i.e., GDEs for 1-D and 2-D compressible flows. Thus, it is fitting to present details of the development of the mathematical model in a separate section and then simply utilize these in subsequent sections for specific model problems. In this section the derivation of the GDEs for compressible flows of a viscous conducting medium with variable transport properties is presented using Eulerian description. The dimensionless form of the GDEs needed for computations are also derived. The quantities with the hat (ˆ) have dimension whereas those without the hat are dimensionless. In the following we use Einstein notations.

The conservation of mass leads to standard well known continuity equation (derivation is well known [74]),

$$\frac{\partial \hat{\rho}}{\partial \hat{t}} + \frac{\partial(\hat{\rho}\hat{v}_i)}{\partial \hat{x}_i} = 0 \tag{3.15}$$

Using Newton's second law for a volume of compressible matter, we can derive momentum equations [74]. In the absence of sources and sinks we obtain the following,

$$\hat{\rho}\frac{\partial \hat{v}_i}{\partial \hat{t}} + \hat{\rho}\hat{v}_j\frac{\partial \hat{v}_i}{\partial \hat{x}_j} - \frac{\partial \hat{\sigma}_{ij}}{\partial \hat{x}_j} = 0 \; ; \; i = 1, 2, 3 \tag{3.16}$$

where $i = 1, 2, 3$ corresponds to x, y and z directions. where $\hat{\sigma}_{ij}$ are total stresses (Cauchy).

The energy equation is a statement of conservation of energy and is derived using first law of thermodynamics [74],

$$\hat{\rho}\frac{D\hat{e}}{D\hat{t}} + \frac{\partial \hat{q}_i}{\partial \hat{x}_i} - \hat{\sigma}_{ij}\frac{\partial \hat{v}_i}{\partial \hat{x}_j} = 0 \tag{3.17}$$

in which $\hat{e}$ is the internal energy per unit mass and $\hat{q}_i$ are heat fluxes. Equation (3.15)-(3.17) are in the most fundamental form which result directly using conservation laws with minor simplifications in the momentum equations using continuity and some simplifications in energy equation using continuity and momentum equations.

Stokes hypothesis

The total stress $\hat{\sigma}_{ij}$ can be decomposed in terms of thermodynamics pressure $\hat{p}$ and viscous stresses $\hat{\tau}_{ij}$ and we have (considering compression to be positive for pressure). This is necessitated due to the fact that constitutive equations requires $\hat{\tau}_{ij}$, stress derivatives or viscous stresses in this case.

$$\hat{\sigma}_{ij} = -\hat{p}\delta_{ij} + \hat{\tau}_{ij} \tag{3.18}$$

The thermodynamic pressure is $\hat{p} = \hat{p}(\hat{\rho}, \hat{T})$ for compressible matter.

Constitutive Equation

For viscous compressible medium we can write [74],

$$\hat{\tau}_{ij} = 2\hat{\mu}\hat{D}_{ij} + \hat{\lambda}\delta_{ij}\hat{D}_{kk} \tag{3.19}$$

in which

$$\hat{D}_{ij} = \frac{1}{2}(\frac{\partial \hat{v}_i}{\partial \hat{x}_j} + \frac{\partial \hat{v}_j}{\partial \hat{x}_i}) \tag{3.20}$$

is the symmetric part of the velocity gradient tensor called strain rate tensor. We note that $\hat{\mu} = \hat{\mu}(\hat{T})$, $\hat{\lambda} = \hat{\lambda}(\hat{T})$ i.e., dependent on temperature. Furthermore, $\hat{\mu}$ can also be a function of the second invariant of $\hat{D}_{ij}$ if the medium is shear thinning or shear thickening.

Heat flux $\hat{q}_i$

Using Fourier law of heat conduction, we can write,

$$\hat{q}_i = -\hat{k}_{ij}\frac{\partial \hat{T}}{\partial \hat{x}_j} \tag{3.21}$$

in which $\hat{k}_{ij} = \hat{k}_{ij}(\hat{T})$ are thermal conductivities of the medium which can also be temperature dependent.

Specific internal energy $\hat{e}$

Since,

$$\hat{e} = \hat{e}(\hat{p}, \hat{\rho}, \hat{T}) = \hat{e}(\hat{\rho}, \hat{T}) \tag{3.22}$$

$\hat{e}$ can be considered as a function of $\hat{\rho}$ and $\hat{T}$ due to the fact that $\hat{p} = \hat{p}(\hat{\rho}, \hat{T})$. Consider,

$$\frac{\hat{D}\hat{e}}{\hat{D}\hat{t}} = \frac{\partial \hat{e}}{\partial \hat{t}} + \hat{v}_i\frac{\partial \hat{e}}{\partial \hat{x}_i} \tag{3.23}$$

But,

$$\frac{\partial \hat{e}}{\partial \hat{t}} = \frac{\partial \hat{e}}{\partial \hat{\rho}} \frac{\partial \hat{\rho}}{\partial \hat{t}} + \frac{\partial \hat{e}}{\partial \hat{T}} \frac{\partial \hat{T}}{\partial \hat{t}} \tag{3.24}$$

and

$$v_i(\frac{\partial \hat{e}}{\partial \hat{x}_i}) = v_i(\frac{\partial \hat{e}}{\partial \hat{\rho}} \frac{\partial \hat{\rho}}{\partial \hat{x}_i} + \frac{\partial \hat{e}}{\partial \hat{T}} \frac{\partial \hat{T}}{\partial \hat{x}_i}) \tag{3.25}$$

Further more, from continuity equation (3.15), we can write ,

$$\frac{\partial \hat{\rho}}{\partial \hat{t}} = -\frac{\partial}{\partial \hat{x}_i}(\hat{\rho}\hat{v}_i) = -\hat{\rho}\frac{\partial \hat{v}_i}{\partial \hat{x}_i} - \hat{v}_i \frac{\partial \hat{\rho}}{\partial \hat{x}_i} \tag{3.26}$$

Substituting (3.26) into (3.24) we obtain

$$\frac{\partial \hat{e}}{\partial \hat{t}} = \frac{\partial \hat{e}}{\partial \hat{\rho}}(-\hat{\rho}\frac{\partial \hat{v}_i}{\partial \hat{x}_i} - \hat{v}_i \frac{\partial \hat{\rho}}{\partial \hat{x}_i}) + \frac{\partial \hat{e}}{\partial \hat{T}} \frac{\partial \hat{T}}{\partial \hat{t}} \tag{3.27}$$

Substituting (3.25) and (3.27) into (3.24) and multiplying by $\hat{\rho}$ we obtain,

$$\hat{\rho}\frac{\hat{D}\hat{e}}{\hat{D}\hat{t}} = -\hat{\rho}^2 \frac{\partial \hat{e}}{\partial \hat{\rho}} \frac{\partial \hat{v}_i}{\partial \hat{x}_i} - \hat{\rho}\frac{\partial \hat{e}}{\partial \hat{\rho}} \hat{v}_i \frac{\partial \hat{\rho}}{\partial \hat{x}_i} + \hat{\rho}\frac{\partial \hat{e}}{\partial \hat{T}} \frac{\partial \hat{T}}{\partial \hat{t}} + \hat{\rho}\hat{v}_i \frac{\partial \hat{e}}{\partial \hat{\rho}} \frac{\partial \hat{e}}{\partial \hat{x}_i} + \hat{\rho}\hat{v}_i \frac{\partial \hat{e}}{\partial \hat{T}} \frac{\partial \hat{T}}{\partial \hat{x}_i} \tag{3.28}$$

and we finally have,

$$\hat{\rho}\frac{\hat{D}\hat{e}}{\hat{D}\hat{t}} = \hat{\rho}\frac{\partial \hat{e}}{\partial \hat{T}}(\frac{\partial \hat{T}}{\partial \hat{t}} + \hat{v}_i \frac{\partial \hat{T}}{\partial \hat{x}_i}) - \hat{\rho}^2 \frac{\partial \hat{e}}{\partial \hat{\rho}} \frac{\partial \hat{v}_i}{\partial \hat{x}_i} \tag{3.29}$$

Using viscous stresses $\hat{\tau}_{ij}$, fluxes $\hat{q}_i$ and (3.27), the continuity, momentum and energy equations can be expressed in various forms. The, two specific forms presented in the following two sections are meritorious from the point of view of finite element computational processes for compressible flows.

3.5.1 Weak form of GDEs

We refer to the weak form of GDEs to mean a system of partial differential equations containing only first order derivatives of the dependent variables. There is obviously more than one way to derive these equations. In the following we consider a form that naturally results from conservation laws, constitutive equations and Fourier heat conduction law.

Continuity equation (3.15) remains unaffected. In the momentum equations, we substitute $\hat{\sigma}_{ij}$ from Stokes hypothesis (i.e., 3.18). In the energy equation (3.17) we substitute (3.27) and $\hat{\sigma}_{ij}$ using Stokes hypothesis. The resulting equations (after some simplifications in the energy equation) are as follows.

$$\frac{\partial \hat{\rho}}{\partial \hat{t}} + \frac{\partial(\hat{\rho}\hat{v}_i)}{\partial \hat{x}_i} = 0 \tag{3.30}$$

$$\hat{\rho}\frac{\partial \hat{v}_i}{\partial \hat{t}} + \hat{\rho}\hat{v}_j\frac{\partial \hat{v}_i}{\partial \hat{x}_j} + \frac{\partial \hat{p}}{\partial \hat{x}_i} - \frac{\partial \hat{\tau}_{ij}}{\partial \hat{x}_j} = 0 \; ; \; i = 1, 2, 3 \tag{3.31}$$

$$\hat{\rho}\frac{\partial \hat{e}}{\partial \hat{T}}\left(\frac{\partial \hat{T}}{\partial \hat{t}} + \hat{v}_j\frac{\partial \hat{T}}{\partial \hat{x}_i}\right) + \frac{\partial \hat{q}_i}{\partial \hat{x}_i} - \left(\hat{p}(\hat{\rho}, \hat{T}) + \hat{\rho}^2\frac{\partial \hat{e}}{\partial \hat{\rho}}\right)\frac{\partial \hat{v}_i}{\partial \hat{x}_i} - \left(2\hat{\mu}(\hat{T})\hat{D}_{ij}\frac{\partial \hat{v}_i}{\partial \hat{x}_j} + \hat{\lambda}(\hat{T})(\hat{D}_{kk})^2\right) = 0 \tag{3.32}$$

where we have used $\delta_{ij}\hat{D}_{ij} = \hat{D}_{ii}$ and $\partial \hat{v}_i/\partial \hat{x}_i = \hat{D}_{ii}$

$$\hat{\tau}_{ij} = 2\hat{\mu}(\hat{T})\hat{D}_{ij} + \hat{\lambda}(T)\delta_{ij}\hat{D}_{kk} \; ; \; i = 1, 2, 3 \; and \; j = 1, 2, 3 \tag{3.33}$$

$$\hat{q}_i = -\hat{k}_{ij}(\hat{T})\frac{\partial \hat{T}}{\partial \hat{x}_j} \tag{3.34}$$

Remarks

1) In which $\hat{p} = \hat{p}(\hat{\rho}, \hat{T})$, needs to be defined using equations of state. $\hat{e}(\hat{\rho}, \hat{T})$ needs to be expressed more explicitly using thermodynamics and equations of state and hence is not a dependent variable.

2) Equation (3.30)-(3.34) is a system of fourteen first order partial differential equations in fourteen variables ($\hat{\rho}, \hat{u}, \hat{v}, \hat{w}, \hat{T}, \hat{\tau}_{ij}$,$\hat{q}_i$)

3) These equations in the form shown here are not suitable for computations due to the fact that the dependent variables may have diversely different magnitudes which would result in ill-conditioned algebraic systems during computations. To avoid this, these PDEs must be non-dimensionalized (see a later section).

3.5.2 Strong form of GDEs

In the system of PDEs given by (3.30)-(3.34), we observe that, it is possible to substitute $\hat{\tau}_{ij}$ from (3.33) into the momentum equations (3.31) and $\hat{q}_i$ from (3.34) into the energy equation, thereby eliminating them all together from the mathematical model. The resulting system of PDEs can be written as (continuity remains unchanged),

$$\frac{\partial \hat{\rho}}{\partial \hat{t}} + \frac{\partial (\hat{\rho}\hat{v}_i)}{\partial \hat{x}_i} = 0 \tag{3.35}$$

$$\hat{\rho}\frac{\partial \hat{v}_i}{\partial \hat{t}} + \hat{\rho}\hat{v}_j\frac{\partial \hat{v}_i}{\partial \hat{x}_j} + \frac{\partial \hat{p}(\hat{\rho},\hat{T})}{\partial \hat{x}_i} - 2\frac{\partial}{\partial \hat{x}_j}(\hat{\mu}(\hat{T})\hat{D}_{ij}) - \frac{\partial}{\partial \hat{x}_j}(\hat{\lambda}(\hat{T})\delta_{ij}\hat{D}_{kk}) = 0\ ;\ i = 1,2,3 \quad (3.36)$$

$$\hat{\rho}\frac{\partial \hat{e}}{\partial \hat{T}}\left(\frac{\partial \hat{T}}{\partial \hat{t}} + \hat{v}_i\frac{\partial \hat{T}}{\partial \hat{x}_i}\right) - \frac{\partial}{\partial \hat{x}_i}(\hat{k}_{ij}(\hat{T})\frac{\partial \hat{T}}{\partial \hat{x}_j}) - \left(\hat{p}(\hat{\rho},\hat{T}) + \hat{\rho}^2\frac{\partial \hat{e}}{\partial \hat{\rho}}\right)\frac{\partial \hat{v}_i}{\partial \hat{x}_i} - 2\hat{\mu}(\hat{T})\hat{D}_{ij}\frac{\partial \hat{v}_i}{\partial \hat{x}_j} - \hat{\lambda}(\hat{T})(\hat{D}_{kk})^2 = 0 \quad (3.37)$$

Remarks

1) Equations (3.35)-(3.37) are a system of five equations in five dependent variables ($\hat{\rho}, \hat{u}, \hat{v}, \hat{w}, \hat{T}$)

2) Unlike the weak form of GDEs, these contain up to second order derivatives of velocities and temperature.

3) These also need to be non-dimensionalized before using them in a finite element computational process.

3.5.3 Dimensionless form of the GDEs for compressible flow

Let us define the following dimensionless variables,

$$\begin{aligned} L &= \frac{\hat{L}}{L_0}, v_i = \frac{\hat{v}_i}{u_0}, \rho = \frac{\hat{\rho}}{\rho_0}, \mu = \frac{\hat{\mu}}{\mu_0}, \\ \lambda &= \frac{\hat{\lambda}}{\mu_0}, \tau_{ij} = \frac{\hat{\tau}_{ij}}{\tau_0}, T = \frac{\hat{T}}{T_0}, k_{ij} = \frac{\hat{k_{ij}}}{k_0}, \\ e &= \frac{\hat{e}}{e_0}, p = \frac{\hat{p}}{p_0}, t = \frac{\hat{t}}{t_0}, t = \frac{L_0}{u_0}, \end{aligned} \quad (3.38)$$

where the quantities with the subscript zero are reference quantities and let,

$$\begin{aligned} Re &= u_0\rho_0 L_0/\mu_0 \quad \text{; Reynolds number} \\ Br &= \mu_0 u_0^2/k_0 T_0 \quad \text{; Brinkman number} \\ Ec &= u_0^2/c_{v0} T_0 \quad \text{; Eckerts number} \end{aligned} \tag{3.39}$$

Using these dimensionless variables and Re, Br, Ec we obtain the following weak form of GDEs and strong form of GDEs :

3.5.4 Dimensionless form of GDEs (Weak form)

Using (3.30)-(3.34) and substituting for quantities with hat(ˆ), we obtain. Continuity Equation :

$$\frac{\partial \rho}{\partial t} + \frac{\partial(\rho v_i)}{\partial x_i} = 0 \tag{3.40}$$

Momentum Equation :

$$\rho\frac{\partial v_i}{\partial t} + \rho v_j \frac{\partial v_i}{\partial x_j} + \left(\frac{p_0}{\rho_0 u_0^2}\right)\frac{\partial p}{\partial x_i} - \left(\frac{\tau_0}{\rho_0 u_0^2}\right)\frac{\partial \tau_{ij}}{\partial x_j} = 0 \; ; \quad i = 1, 2, 3 \tag{3.41}$$

substituting for quantities into hat (ˆ) into energy equation and dividing throughout by $\rho_0 u_0^3/L_0$ we obtain, the following for the energy equation,

$$\frac{e_0}{u_0^2}\rho\frac{\partial e}{\partial T}\left(\frac{\partial T}{\partial t} + v_i\frac{\partial T}{\partial x_i}\right) + \frac{1}{ReBr}\frac{\partial q_i}{\partial x_i} - \left(\frac{p_0}{\rho_0 u_0^2}p + \frac{e_0}{u_0^2}\rho^2\frac{\partial e}{\partial \rho}\right)\frac{\partial v_i}{\partial x_i} - \frac{1}{Re}\left(2\mu(T)D_{ij}\frac{\partial v_i}{\partial x_j} + \lambda(T)(D_{kk})^2\right) = 0 \tag{3.42}$$

Constitutive Equations :

$$\tau_{ij} = \frac{\mu_0 u_0}{L_0 \tau_0}\left(2\mu(T)D_{ij} + \lambda(T)\delta_{ij}D_{kk}\right) \tag{3.43}$$

Heat conduction law :

$$q_i = -k_{ij}(T)\frac{\partial T}{\partial x_j}\ ;\ i = 1, 2, 3 \tag{3.44}$$

where we have chosen $q_0 = k_0 T_0 / L_0$.

Remarks

(1) With specific choices of p_0 and τ_0 we can obtain more familiar form of the constants. This will be done at a later stage after defining e, the specific internal energy.

(2) We remark that different choices of p_0 and τ_0 are essential in the dimensionless form of the GDEs in order for us to perform computation at critical pressure in which case the choice of $p_0 = \tau_0$ may not be good.

3.5.5 Dimensionless form of GDEs (Strong form)

Using (3.35)-(3.37) and substituting for quantities with hat ($\hat{}$), we obtain the following. The momentum equation has been divided by $\rho_0 u_0^2 / L_0$ and energy equation by $\rho_0 u_0^3 / L_0$.

Continuity Equation :

$$\frac{\partial \rho}{\partial t} + \frac{\partial (\rho v_i)}{\partial x_i} = 0 \tag{3.45}$$

Momentum Equation :

$$\rho\frac{\partial v_i}{\partial t}+\rho v_j\frac{\partial v_i}{\partial x_j}+\left(\frac{p_0}{\rho_0 u_0^2}\right)\frac{\partial p}{\partial x_i}-\frac{1}{Re}\frac{\partial}{\partial x_j}\left(2\mu(T)D_{ij}+\lambda(T)\delta_{ij}D_{kk}\right)=0;$$
$$i=1,2,3 \quad (3.46)$$

Energy Equation :

$$\frac{e_0}{u_0^2}\rho\frac{\partial e}{\partial T}\left(\frac{\partial T}{\partial t}+v_i\frac{\partial T}{\partial x_i}\right)-\frac{1}{ReBr}\frac{\partial}{\partial x_i}(k_{ij}(T)\frac{\partial T}{\partial x_j})-\left(\frac{p_0}{\rho_0 u_0^2}p+\frac{e_0}{u_0^2}\rho^2\frac{\partial e}{\partial \rho}\right)\frac{\partial v_i}{\partial x_i}-\frac{1}{Re}\left(2\mu(T)D_{ij}\frac{\partial v_i}{\partial x_j}+\lambda(T)(D_{kk})^2\right)=0 \quad (3.47)$$

The remarks in section 3.5.4, hold here as well.

3.5.6 General remark on the mathematical models : GDEs in weak and strong form

(i) The mathematical models both in strong and weak form of GDEs have closure i.e., in both cases we have as many equations as the number of dependent variables.

(ii) Additional information needed for these GDEs to be functional in computations are :

(a) $p = p(\rho, T)$; Thermodynamic pressure expressed in terms of ρ and T i.e., the equation of state.

(b) The specific internal energy e need to be expressed in terms of thermodynamics of the compressible matter.

We present these developments in the following.

3.5.7 Equation of state : $p = p(\rho, T)$

The equation of state [75] provides the relationship between thermodynamic pressure p in terms of density ρ, temperature T and thermodynamic properties of the medium. A specific choice of the equation of state is of course dependent on the medium and the ranges of p, ρ and T.

3.5.7.1 Perfect gas or ideal gas

For all common gases the relationship between p, ρ and T can be described with reasonable accuracy in some finite range of p, ρ and T by perfect or ideal gas law, which holds for thermally and calorically perfect gases.

$$\hat{p} = \hat{R}\hat{\rho}\hat{T} \tag{3.48}$$

or in dimensionless form,

$$p = \left(\frac{R_0\rho_0 T_0}{p_0}\right) R\rho T \tag{3.49}$$

where R is the gas constant, defined by the ratio of the Boltzmann's constant k to the mass of a single molecule i.e,

$$R = \frac{k}{m} \tag{3.50}$$

Some useful relations relating $\hat{R}$ to $\hat{C}_p(\hat{T})$, $\hat{C}_v(\hat{T})$ (specific heats at constant pressure and constant volume respectively) are,

$$\hat{C}_p(\hat{T}) = \hat{C}_p(\hat{T}) + \hat{R} = \frac{\gamma(\hat{T})\hat{R}}{\gamma(\hat{T}) - 1} \tag{3.51}$$

$$\hat{C}_v(\hat{T}) = \frac{\hat{R}}{\gamma(\hat{T}) - 1} \tag{3.52}$$

where $\gamma(T) = \frac{\hat{C}_p(\hat{T})}{\hat{C}_v(\hat{T})}$.

3.5.7.2 Thermal equations of state for real gases or real gas models

In the high temperature region, vibrational excitation, electronic excitations, molecular dissociation and ionization come into play. On an equilibrium basis many of these effects can be accounted reasonably by introducing several free parameters into the thermal equations of state. These models describing a relationship between p, ρ and T are known as real gas models. We describe some commonly used in the following,

Van der Waals Equation of state :

$$\hat{p}(\hat{\rho}, \hat{T}) = \frac{\hat{\rho}\hat{R}\hat{T}}{1 - \hat{b}\hat{\rho}} - \hat{a}\hat{\rho}^2 \tag{3.53}$$

or in dimensionless form,

$$p(\rho, T) = \left(\frac{\rho_0 R_0 T_0}{p_0}\right) \frac{\rho R T}{1 - b\rho} - a\rho^2 \tag{3.54}$$

where $b = \hat{b}\rho_0$, $a = \frac{\hat{a}\rho_0^2}{p_0}$; $\hat{a}$ and $\hat{b}$ are constants of Van der Waals model.

Redlich-Kwang Equation of state :

$$\hat{p}(\hat{\rho}, \hat{T}) = \frac{\hat{\rho}\hat{R}\hat{T}}{1 - \hat{b}\hat{\rho}} - \frac{\hat{a}\hat{\rho}^2}{1 + \hat{b}\hat{\rho}}\hat{T}^{-1/2} \tag{3.55}$$

or in dimensionless form,

$$p(\rho, T) = \left(\frac{\rho_0 R_0 T_0}{p_0}\right) \frac{\rho R T}{1 - b\rho} - \frac{a\rho^2}{1 + b\rho}T^{-1/2} \tag{3.56}$$

where $b = \hat{b}\rho_0$, $a = \frac{\hat{a}\rho_0^2 T_0^{-1/2}}{p_0}$; $\hat{a}$ and $\hat{b}$ are constants of Redlich-Kwang model.

Beattie-Bridgeman Equation of state :

$$\hat{p}(\hat{\rho},\hat{T}) = \hat{\rho}^2\hat{R}\hat{T}\left(1-\frac{\hat{c}\hat{\rho}}{\hat{T}^3}\right)\left(\frac{1}{\hat{\rho}}+\hat{B}_0(1-\hat{b}\hat{\rho})\right)-\hat{\rho}^2\hat{A}_0(1-\hat{a}\hat{\rho}) \qquad (3.57)$$

or in dimensionless form,

$$p(\rho,T) = \left(\frac{\rho_0 R_0 T_0}{p_0}\right)\rho^2 RT\left(1-\frac{c\rho}{T^3}\right)\left(\frac{1}{\rho}+B_0(1-b\rho)\right)-\rho^2 A_0(1-a\rho) \quad (3.58)$$

where $c = \frac{\hat{c}\rho_0}{T_0^3}$, $B_0 = \hat{B}_0\rho_0$, $b = \hat{b}\rho_0$, $A_0 = \frac{\hat{A}_0\rho_0^2}{p_0}$, $a = \hat{a}\rho_0$; $\hat{c}$, $\hat{B}_0$, $\hat{b}$, $\hat{A}_0$ and $\hat{a}$ are constants of the model.

Benedict-Webb-Rubin equation of state :

$$\hat{p}(\hat{\rho},\hat{T}) = \hat{\rho}\hat{R}\hat{T}+\hat{\rho}^2\left(\hat{B}_0\hat{R}\hat{T}-\hat{A}_0-\frac{\hat{C}_0}{\hat{T}^2}\right)+\hat{\rho}^3(\hat{b}\hat{R}\hat{T}-\hat{a})+\hat{a}\hat{\alpha}\hat{\rho}^6+\frac{\hat{\rho}\hat{c}(1+\hat{\gamma}\hat{\rho}^2)}{\hat{T}^2}e^{-\hat{\nu}\hat{\rho}^2} \qquad (3.59)$$

or in dimensionless form,

$$p(\rho,T) = \left(\frac{\rho_0\hat{R}_0\hat{T}_0}{p_0}\right)\rho RT+\rho^2\left(B_0RT-A_0-\frac{\hat{C}_0}{T^2}\right)+\rho^3(bRT-a)+a\alpha\rho^6 + \frac{\rho c(1+\gamma\rho^2)}{T^2}e^{-\nu\rho^2} \quad (3.60)$$

where $B_0 = \frac{\rho_0^2\hat{B}_0R_0T_0}{p_0}$, $A_0 = \frac{\hat{A}_0\rho_0^2}{p_0}$, $C_0 = \frac{\hat{C}_0\rho_0^2}{T_0^2p_0}$, $b = \frac{\rho_0^3\hat{b}R_0T_0}{p_0}$, $a = \frac{\rho_0^3\hat{a}}{p_0}$, $\alpha = \rho_0^3\hat{\alpha}$, $c = \frac{\rho_0^3\hat{c}}{T_0^2p_0}$, $\gamma = \hat{\gamma}\rho_0^2$, $\nu = \hat{\nu}\rho_0^2$; $\hat{B}_0, \hat{A}_0, \hat{c}_0, \hat{b}, \hat{a}, \hat{\alpha}, \hat{c}, \hat{\gamma}, \hat{\nu}$ are constants of the model.

3.5.8 Specific internal energy $\hat{e}$ and other transport properties :

In this section we present details of specific internal energy $\hat{e} = \hat{e}(\hat{p},\hat{\rho},\hat{T})$. Since $\hat{p} = \hat{p}(\hat{\rho},\hat{T})$ (equation of state), we have $\hat{e} = \hat{e}(\hat{\rho},\hat{T})$. For a compressible

matter with temperature dependent specific heat, we can write the following for $\hat{e}$ [76].

$$\hat{e} = \int_{\hat{T}_0}^{\hat{T}} \hat{C}_v d\hat{T} - \int_{\hat{\rho}_0}^{\hat{\rho}} \frac{1}{\hat{\rho}^2} \left((\hat{T} \frac{\partial \hat{P}}{\partial \hat{T}})_{\hat{\rho}} - \hat{p} \right) d\hat{\rho} \tag{3.61}$$

with $\hat{C}_v = \hat{C}_v(\hat{T})$, we have,

$$\hat{C}_v = \hat{C}_v^* - \hat{T} \int_{\hat{\rho}_0}^{\hat{\rho}} \frac{1}{\hat{\rho}^2} \left(\frac{\partial^2 \hat{p}}{\partial \hat{T}^2} \right)_{\hat{\rho}} d\hat{\rho} \tag{3.62}$$

$$\hat{C}_v^* = \sum_{j=0}^{m} \hat{C}_j \hat{T}^j \tag{3.63}$$

$\hat{C}_j$ are constants of the medium.

Limits of integration are not important, as we only need the derivative $\hat{e}$ with respect to temperature and density in the energy equation. Equations (3.61)-(3.63) can be non-dimensionalized using the reference quantities and the corresponding dimensionless quantities,

$$e = \int_{T_0}^{T} C_v dT - Ec \int_{\rho_0}^{\rho} \frac{1}{\rho^2} \left((T \frac{\partial P}{\partial T})_{\rho} - p \right) d\rho \tag{3.64}$$

$$C_v = C_v^* - E_c T \int_{\rho_0}^{\rho} \frac{1}{\rho^2} \left(\frac{\partial^2 p}{\partial T^2} \right)_{\rho} d\rho \tag{3.65}$$

$$C_v^* = \sum_{j=0}^{m} C_j T^j \tag{3.66}$$

in which $C_j = (\frac{\hat{C}_j T_0^j}{C_{v0}})$, $e = \hat{e}/e_0$; $e_0 = C_{v0} T_0$

Remarks

(1) Using $p = p(\rho, T)$ from equations of state, we can obtain explicit expressions for $e = e(\rho, T)$ for any derived equation of state and hence $\partial e/\partial T$ and $\partial e/\partial \rho$ needed in the energy equation are defined explicitly.

(2) Since $e_0 = c_{v0}T_0$, we can now substitute this in the dimensionless form of the energy equation to obtain more specific forms for e_0/u_0^2 i.e., $e_0/u_0^2 = C_{v0}T_0/u_0^2 = 1/E_c$. Henceforth, we use the energy equation with this substitution.

3.5.9 Specific choices of p_0, τ_0 :

In this section we consider the specific choices of p_0, τ_0 which help in simplifying the constants to familiar dimensionless parameters commonly used in the GDEs for compressible flow. After making the substitution for e_0(remarks 1 and 2), we have the following,

3.5.9.1 Weak form of GDEs (dimensionless) :

$$\frac{\partial \rho}{\partial t} + \frac{\partial(\rho v_i)}{\partial x_i} = 0 \tag{3.67}$$

$$\rho\frac{\partial v_i}{\partial t} + \rho v_j\frac{\partial v_i}{\partial x_j} + \left(\frac{p_0}{\rho_0 u_0^2}\right)\frac{\partial p}{\partial x_i} - \left(\frac{\tau_0}{\rho_0 u_0^2}\right)\frac{\partial \tau_{ij}}{\partial x_j} = 0\ ;\ i = 1, 2, 3 \tag{3.68}$$

$$\frac{\rho}{Ec}\frac{\partial e}{\partial T}\left(\frac{\partial T}{\partial t}+v_i\frac{\partial T}{\partial x_i}\right)-\frac{1}{ReBr}\frac{\partial q_i}{\partial x_i}-\left(\frac{p_0}{\rho_0 u_0^2}p+\frac{\rho^2}{Ec}\frac{\partial e}{\partial \rho}\right)\frac{\partial v_i}{\partial x_i} - \frac{1}{Re}\left(2\mu(T)D_{ij}\frac{\partial v_i}{\partial x_j}+\lambda(T)(D_{kk})^2\right)=0 \quad (3.69)$$

$$\tau_{ij} = \frac{\mu_0 u_0}{L_0\tau_0}(2\mu(T)D_{ij}+\lambda(T)\delta_{ij}(D_{kk}))\ ;\ i=1,2,3; j=i,..,3 \quad (3.70)$$

$$q_i = k_{ij}(T)\frac{\partial T}{\partial x_j}\ ;\ i=1,2,3 \quad (3.71)$$

3.5.9.2 Strong form of GDEs (dimensionless) :

$$\frac{\partial \rho}{\partial t}+\frac{\partial(\rho v_i)}{\partial x_i}=0 \quad (3.72)$$

$$\rho\frac{\partial v_i}{\partial t}+\rho v_j\frac{\partial v_i}{\partial x_j}+\left(\frac{p_0}{\rho_0 u_0^2}\right)\frac{\partial p}{\partial x_i}-\frac{1}{Re}\frac{\partial}{\partial x_j}\Big(2\mu(T)D_{ij} + \lambda(T)\delta_{ij}D_{kk}\Big)=0\ ;\ i=1,2,3 \quad (3.73)$$

$$\frac{\rho}{Ec}\frac{\partial e}{\partial T}\left(\frac{\partial T}{\partial t}+v_i\frac{\partial T}{\partial x_i}\right)-\frac{1}{ReBr}\frac{\partial}{\partial x_i}(k_{ij}(T)\frac{\partial T}{\partial x_j})-\left(\frac{p_0}{\rho_0 u_0^2}p+\frac{\rho^2}{Ec}\frac{\partial e}{\partial \rho}\right)\frac{\partial v_i}{\partial x_i} - \frac{1}{Re}\left(2\mu(T)D_{ij}\frac{\partial v_i}{\partial x_j}+\lambda(T)(D_{kk})^2\right)=0 \quad (3.74)$$

Remarks

(1) If we choose $p_0=\tau_0=\rho_0 u_0^2$ (characteristic kinetic energy), then

$$(\frac{p_0}{\rho_0 u_0^2}=1), \frac{\mu_0 u_0}{L_0 T_0}=\frac{1}{Re}$$

(2) If we choose $p_0 = \tau_0 = \frac{\mu_0 u_0}{L_0}$ (characteristic viscous stress), then

$$(\frac{p_0}{\rho_0 u_0^2} = \frac{1}{Re}), \frac{\tau_0}{\rho_0 u_0^2} = \frac{1}{Re}, \frac{\mu_0 u_0}{L_0 \tau_0} = 1$$

3.6 1-D Riemann shock tube (IVP)

In this section we consider 1-D single diaphragm Riemann shock tube with ideal and real gas laws. The medium is viscous and conducting with physical transport properties. The importance of this work to demonstrate evolution of shock, shock propagation as well as resolution of shock structure with actual viscosity and conductivity of the medium.

This model problem has been a subject of study for a long time using finite difference and finite volume methods. Most reported computations employ mathematical models based on Euler's equations with upwinding methods. Such solutions though may yield correct shock relations but fail to resolve shock structure. Secondly, in this approach evolutions are never time accurate (due to artificial diffusion) [77]. Many finite element computational strategies based in Galerkin method with weak form employing space-time coupled or decoupled method suffer from some of the same problems due to the fact that VIC integral form require upwinding methods to stabilize computations.

Recently Surana et.al. [25] presented solutions of class $C^{1,1}$ for 1-D single diaphragm Riemann shock tube for air with actual transport properties and ideal gas equation of state. The transport properties were assumed constant. The authors utilized space-time coupled least squares finite element formulation with strong

form of GDEs. They reported time accurate evolutions of shock structure, shock speeds and shock width. The solutions of higher classes for the same problem have also been reported by Surana et.al.[27]. Further discussion on these is provided in the section on numerical studies. In this section we only consider details of the mathematical model as well as the finite element formulation.

3.6.1 Mathematical models

We assume the physics to be purely one dimensional. Let x be the direction along the length of the shock tube, then the Riemann shock tube problem reduces that of 1-D normal shocks. In the following we present dimensionless form of the GDEs for this problem in the weak form (i.e., a first order system) as well as strong form.

3.6.2 Weak form of GDEs : 1-D Riemann shock tube

Using the system of PDEs in section 3.5.9.1 and letting $i = 1$, $v_1 = u$ and $x_1 = x$ and $q_1 = q_x$, we can write the following for 1-D Riemann shock tube.

$$\frac{\partial \rho}{\partial t} + \frac{\partial (\rho u)}{\partial x} = 0 \tag{3.75}$$

$$\rho \frac{\partial u}{\partial t} + \rho u \frac{\partial u}{\partial x} + \left(\frac{p_0}{\rho_0 u_0^2} \right) \frac{\partial p}{\partial x} - \left(\frac{\tau_0}{\rho_0 u_0^2} \right) \frac{\partial \tau_{xx}}{\partial x} = 0 \tag{3.76}$$

$$\frac{\rho}{Ec} \frac{\partial e}{\partial T} \left(\frac{\partial T}{\partial t} + u \frac{\partial T}{\partial x} \right) - \frac{1}{ReBr} \frac{\partial q_{xx}}{\partial x} - \left(\frac{p_0}{\rho_0 u_0^2} p + \frac{\rho^2}{Ec} \frac{\partial e}{\partial \rho} \right) \frac{\partial u}{\partial x} - \frac{1}{Re} \left(2\mu(T) (\frac{\partial u}{\partial x})^2 + \lambda(T) (\frac{\partial u}{\partial x})^2 \right) = 0 \tag{3.77}$$

$$\tau_{xx} = \frac{\mu_0 u_0}{L_0 \tau_0}\left(2\mu(T)\frac{\partial u}{\partial x} + \lambda(T)\frac{\partial u}{\partial x}\right) \tag{3.78}$$

$$q_x = -k_x(x)\frac{\partial T}{\partial x} \tag{3.79}$$

$\forall (x,t) \in \Omega_{xt}$

This is a system of five first order partial differential equations in ρ, u, T, τ_{xx} and q_x. The stress and the flux equations ((3.78)and(3.79)) are called auxiliary equations and τ_{xx}, q_x are called auxiliary variables. Let

$$\{\varphi\} = [\rho, u, T, \tau_{xx}, q_x]^t \tag{3.80}$$

be the vector of dependent variables. Consider a space-time element 'e' of domain ${}^n\bar{\Omega}^e_{xt}$ of the n^{th} space-time strip. Let $\{{}^n\varphi^e_h\}$ be the approximation of $\{\varphi\}$ over ${}^n\bar{\Omega}^e_{xt}$,

$${}^n\varphi^e_h = {}^n\{\varphi\}^e_h = [{}^n\rho^e_h, {}^nu^e_h, {}^nT^e_h, {}^n(\tau_{xx})^e_h, {}^n(q_x)^e_h]^t \tag{3.81}$$

In general we can write the following for local approximations.

$$\begin{array}{lcl} {}^n\rho^e_h & = & [N_\rho^{(k_1-1,k_2-1),(p_1,p_2)}]\{{}^n\rho^e\} \\ {}^nu^e_h & = & [N_u^{(k_1-1,k_2-1),(p_1,p_2)}]\{{}^nu^e\} \\ {}^nT^e_h & = & [N_T^{(k_1-1,k_2-1),(p_1,p_2)}]\{{}^nT^e\} \\ {}^n(\tau_{xx})^e_h & = & [N_{\tau_{xx}}^{(k_1-1,k_2-1),(p_1,p_2)}]\{{}^n(\tau_{xx})^e\} \\ {}^n(q_x)^e_h & = & [N_{q_x}^{(k_1-1,k_2-1),(p_1,p_2)}]\{{}^n(q_x)^e\} \end{array} \tag{3.82}$$

By substituting $\{{}^n\varphi^e_h\}$ in (3.75)-(3.79) yields the residual equations ${}^nE^e_i$; $i = 1, ..., 5$ for $\forall x, t \in {}^n\bar{\Omega}^e_{xt}$. Equal order equal degree local approximations for $\{{}^n\varphi^e_h\}$ over ${}^n\bar{\Omega}^e_{xt}$ are valid too.

$N_\varphi^{(k_1-1,k_2-1),(p_1,p_2)}$ are the local approximation functions for $\rho, u, T, \tau_{xx}, q_x$. These

are of continuity $(k_1-1),(k_2-1)$ and degrees p_1 and p_2 in space and time. $\{{}^n\rho^e\}$, $\{{}^nu^e\}$, $\{{}^nT^e\}$, $\{{}^n\tau^e_{xx}\}$, $\{{}^nq^e_x\}$ are degrees of freedom for ${}^n\rho^e_h$, ${}^nu^e_h$, ${}^nT^e_h$, ${}^n(\tau_{xx})^e_h$, ${}^n(q_x)^e_h$. k_1, k_2, p_1 and p_2 can be different for each variable. Let $V_h({}^n\bar{\Omega}^e_{xt})$ be the approximation space, then

$$V_h({}^n\bar{\Omega}^e_{xt}) \subset H^{k,p}({}^n\bar{\Omega}^e_{xt}); k=(k_1,k_2)\ \forall\ {}^n\bar{\Omega}^e_{xt} \subset \bar{\Omega}^T_{xt} \tag{3.83}$$

$$\begin{aligned} H^{(k_1,k_2),(p_1,p_2)}({}^n\bar{\Omega}^e_{xt}) = \{&w : w|_{{}^n\bar{\Omega}^e_{xt}} \in C^{(k_1-1,k_2-1),(p_1,p_2)}({}^n\bar{\Omega}^e_{xt}),\\ &w : w|_{{}^n\bar{\Omega}^e_{xt}} \in P^{p_1,p_2}({}^n\bar{\Omega}^e_{xt}); p_1 \geq 2k_1-1, p_2 \geq 2k_2-1 \forall {}^n\bar{\Omega}^e_{xt} \subset \bar{\Omega}^T_{xt}\} \end{aligned} \tag{3.84}$$

- We note that for $k_2 \geq 2$, $k_2 \geq 2$, the integrals in the entire finite element processes are Riemann in space and time.
- When $k_1 = k_2 = 1$, the local approximations are of class C^0 and the integrals are Lebesgue in space and time.
- We clearly see that if $N_i^{(k_1-1,k_2-1),(p_1,p_2)}({}^n\bar{\Omega}^e_{xt}) \in V_h({}^n\bar{\Omega}^e_{xt})$ then $\{\varphi^e_h\} \in V_h({}^n\bar{\Omega}^e_{xt})$
- The system of PDEs (3.75)-(3.79) are non-linear, hence only space-time least square processes yield STVC integral forms. Using residuals ${}^nE^e_i, i = 1, ..., 5$, the details of the space-time least squares finite element processes can be obtained.

Let ${}^n\bar{\Omega}^T_{xt} = \bigcup_e {}^n\bar{\Omega}^e_{xt}$ be the discretization of an n^{th} space-time strip in which ${}^n\bar{\Omega}^e_{xt}$ is a typical space-time element e. Then, ${}^n\varphi_h = \bigcup_e {}^n\varphi^e_h$ is the approximation ${}^n\bar{\Omega}^T_{xt}$. We

construct space-time least squares functional $I({}^n\varphi_h)$ for the discretization ${}^n\bar{\Omega}^T_{xt}$, the existence of $I({}^n\varphi_h)$.

$$I({}^n\varphi_h) = \sum_{i=1}^{5}({}^nE({}^n\varphi_h), {}^nE({}^n\varphi_h)) = \sum_{i=1}^{M}\sum_{i=1}^{5}({}^nE^e({}^n\varphi^e_h), {}^nE^e({}^n\varphi^e_h)) \quad (3.85)$$

$\delta I({}^n\varphi_h) = 0$ gives necessary condition,

$$\delta I({}^n\varphi_h) = \sum_{i=1}^{5}({}^nE_i({}^n\varphi_h), {}^nE_i({}^n\varphi_h)) = g({}^n\varphi_h) = 0 \quad (3.86)$$

or

$$\delta I({}^n\varphi_h) = \sum_{e=1}^{M}\sum_{i=1}^{5}({}^nE^e_i({}^n\varphi^e_h), {}^nE^e_i({}^n\varphi^e_h)) = g^e({}^n\varphi^e_h) = g({}^n\varphi_h) = 0 \quad (3.87)$$

Sufficient condition or extremum principle is given by,

$$\delta^2 I({}^n\varphi_h) \cong \sum_{e=1}^{M}\sum_{i=1}^{5}(\delta({}^nE^e_i({}^n\varphi^e_h)), \delta({}^nE^e_i({}^n\varphi^e_h))) > 0 \quad (3.88)$$

A solution ${}^n\varphi_h$ is obtained using Newton's first order method with line search,

$$\begin{aligned} {}^n\varphi_h &= ({}^n\varphi_h)_0 + \alpha\Delta({}^n\varphi_h) && (3.89)\\ \Delta({}^n\varphi_h) &= -[\delta^2 I({}^n\varphi_h)]^{-1}_{({}^n\varphi_h)_0} g(({}^n\varphi_h)_0) && (3.90) \end{aligned}$$

Where α is determined such that $I({}^n\varphi_h) \leq I(({}^n\varphi_h)_0)$

Convergence of the iterative method is determined by checking $\|g({}^n\varphi_h)\| \leq \Delta_1$, a preset tolerance for zero. $({}^n\varphi_h)_0$ is a starting solution for the Newton's linear method. Remarks in section 3.2.5 are valid here as well and are not repeated for the sake of brevity.

3.6.3 Strong form of GDEs : 1-D Riemann shock tube

Using the system of PDEs in section 3.5.9.2 and letting $i = 1, x_i = x, v_1 = u$ and $q_1 = q_x$, we can write the following system of PDEs for 1-D Riemann shock tube.

$$\frac{\partial \rho}{\partial t} + \frac{\partial (\rho u)}{\partial x} = 0 \tag{3.91}$$

Momentum Equation :

$$\rho \frac{\partial u}{\partial t} + \rho u \frac{\partial u}{\partial x} + \left(\frac{p_0}{\rho_0 u_0^2} \right) \frac{\partial p}{\partial x} - \frac{1}{Re} \left(2 \frac{\partial}{\partial x} (\mu(T) \frac{\partial u}{\partial x}) + \frac{\partial}{\partial x} (\lambda(T) \frac{\partial u}{\partial x}) \right) = 0 \tag{3.92}$$

Energy Equation :

$$\frac{\rho}{Ec} \frac{\partial e}{\partial T} \left(\frac{\partial T}{\partial t} + u \frac{\partial T}{\partial x} \right) - \frac{1}{ReBr} \frac{\partial}{\partial x} (k_x(T) \frac{\partial T}{\partial x}) - \left(\frac{p_0}{\rho_0 u_0^2} p + \frac{\rho^2}{Ec} \frac{\partial e}{\partial \rho} \right) \frac{\partial u}{\partial x} - \frac{1}{Re} \left(2\mu(T) (\frac{\partial u}{\partial x})^2 + \lambda(T) (\frac{\partial u}{\partial x})^2 \right) = 0 \tag{3.93}$$

Equations (3.91)-(3.93) are a system of nonlinear PDEs in dependent variables ρ, u and T. These contain only first order derivatives of ρ but up to second order derivatives u and T in x but only first order derivatives of u and T in time t.

Let,

$$\varphi = \{\varphi\} = [\rho, u, T]^t \tag{3.94}$$

Consider a space-time element 'e' of domain ${}^n\bar{\Omega}^e_{xt}$ of the n^{th} space-time strip. Let ${}^n\varphi^e_h$ be the approximation of φ over ${}^n\bar{\Omega}^e_h$,

$${}^n\varphi^e_h = \{{}^n\varphi^e_h\} = [{}^n\rho^e_h, {}^nu^e_h, {}^nT^e_h]^t \tag{3.95}$$

The local approximations ${}^n\rho_h^e, {}^nu_h^e, {}^nT_h^e$ over ${}^n\bar{\Omega}_{xt}^e$ can be written as,

$$
\begin{aligned}
{}^n\rho_h^e &= [N_\rho^{(k_1^\rho-1,k_2^\rho-1),(p_1^\rho,p_2^\rho)}({}^n\bar{\Omega}_{xt}^e)]\{{}^n\rho^e\} && (3.96)\\
{}^nu_h^e &= [N_u^{(k_1^u-1,k_2^u-1),(p_1^u,p_2^u)}({}^n\bar{\Omega}_{xt}^e)]\{{}^nu^e\} && (3.97)\\
{}^nT_h^e &= [N_T^{(k_1^T-1,k_2^T-1),(p_1^T,p_2^T)}({}^n\bar{\Omega}_{xt}^e)]\{{}^nT^e\} && (3.98)
\end{aligned}
$$

In which $\{{}^n\rho^e\}$, $\{{}^nu^e\}$, $\{{}^nT^e\}$ are nodal degrees of freedom for ${}^n\rho_h^e, {}^nu_h^e, {}^nT_h^e$ and $N_\rho^{(k_1^\rho-1,k_2^\rho-1),(p_1^\rho,p_2^\rho)}$, $N_u^{(k_1^u-1,k_2^u-1),(p_1^u,p_2^u)}$, $N_T^{(k_1^T-1,k_2^T-1),(p_1^T,p_2^T)}$ are local approximation functions in which k_1^ρ, k_2^ρ,k_1^u, k_2^u,k_1^T, k_2^T are the orders of the approximation space and p_1^ρ, p_2^ρ,p_1^u, p_2^u,p_1^T, p_2^T are the degrees of approximation in space and time. Since the PDEs have only first order derivatives of ρ, u, T in time, first order derivative of ρ with respect to x, and up to second order derivatives of u and T with respect to x, we consider the following,

(i) $k_1^\rho \geq 2$, $k_2^\rho \geq 2$ for ${}^n\rho_h^e$ and $k_1^u = k_1^T \geq 3$, $k_2^u = k_2^T \geq 2$ for ${}^nu_h^e$ and ${}^nT_h^e$ are necessary for the space-time integrals to be Riemann in the finite element processes using STLSP. Equality defines minimally conforming spaces.

(ii) If we choose $k_1^\rho = 1$, $k_2^\rho = 1$ for ${}^n\rho_h^e$ and $k_1^u = k_1^T = 2$, $k_2^u = k_2^T = 1$ for ${}^nu_h^e$ and ${}^nT_h^e$ then the integrals in the STLSP are in Lebesgue sense.

(iii) If we wish the space-time integrals to be Riemann in STLSP then for the sake of convenience one could also choose the following $k_1 \geq 3$, $k_1 \geq 2$ for ${}^n\rho_h^e$, ${}^nu_h^e$ and ${}^nT_h^e$ i.e., same order of global differentiability for all variables.

Benefits of Riemann integrals over Lebesgue has been discussed by Surana et.al.[78] in STLSP and finite element processes in general.

Let $V_h({}^n\bar{\Omega}^e_{xt})$ be the approximation space. Then,

$$V_h({}^n\bar{\Omega}^e_{xt}) \subset H^{k,p}({}^n\bar{\Omega}^e_{xt}); k = (k_1, k_2), p = (p_1, p_2) \forall {}^n\bar{\Omega}^e_{xt} \subset \bar{\Omega}^T_{xt} \tag{3.99}$$

$$\begin{aligned} H^{(k_1,k_2),(p_1,p_2)}({}^n\bar{\Omega}^e_{xt}) = \{w : w|_{{}^n\bar{\Omega}^e_{xt}} \in C^{(k_1-1,k_2-1),(p_1,p_2)}({}^n\bar{\Omega}^e_{xt}), \\ w : w|_{{}^n\bar{\Omega}^e_{xt}} \in P^{p_1,p_2}({}^n\bar{\Omega}^e_{xt}); p_1 \geq 2k_1 - 1, p_2 \geq 2k_2 - 1 \forall {}^n\bar{\Omega}^e_{xt} \subset \bar{\Omega}^T_{xt}\} \end{aligned} \tag{3.100}$$

Choices of k_1, k_2 for ${}^n\rho^e_h$, ${}^nu^e_h$ and ${}^nT^e_h$ have already been discussed. If we substitute local approximations (3.95)-(3.97) in the GDEs (3.91)-(3.93), then we obtain the residuals,

$${}^nE^e_i({}^n\varphi^e_h); i = 1, 2, 3 \; \forall \; x, t \in {}^n\bar{\Omega}^e_{xt} \tag{3.101}$$

Since the GDEs are nonlinear PDEs, only space-time least squares finite element method yields integral forms that are STVC. Details of the STLSP are identical to those for weak form of GDEs (section 3.4.1.1) except that in this case we only have three residual equations as opposed to five residual equations for the weak form of GDEs, and hence, are not repeated here.

3.7 2-D Compressible flow : BVPs

In this section we present specific forms of the GDEs (weak form and strong form) for 2-D steady compressible flow applicable to BVPs. The least squares finite element formulation of these GDEs will be constructed and utilized in simulating Carter's plate and flow over a circular cylinder in chapter 6.

3.7.1 Mathematical models (2-D BVPs) :

3.7.1.1 Weak form of GDEs

In this section we present weak form of GDEs for 2-D time independent compressible flows. Using the PDEs in section 3.5.9.1 and setting : time derivatives zero, $x_1, x_2 \rightarrow x, y$, $v_1, v_2 \rightarrow u, v, \tau_{11}, \tau_{12}, \tau_{22} \rightarrow \tau_{xx}, \tau_{xy}, \tau_{yy}$ and $q_1, q_2 \rightarrow q_x, q_y$, we obtain the following system of GDEs.

$$\frac{\partial(\rho u)}{\partial x} + \frac{\partial(\rho v)}{\partial y} = 0 \tag{3.102}$$

$$\rho u \frac{\partial u}{\partial x} + \rho v \frac{\partial u}{\partial y} + \left(\frac{p_0}{\rho_0 u_0^2}\right) \frac{\partial p}{\partial x} - \frac{\tau_0}{\rho_0 u_0^2} \left(\frac{\partial \tau_{xx}}{\partial x} + \frac{\partial \tau_{xy}}{\partial y}\right) = 0 \tag{3.103}$$

$$\rho u \frac{\partial v}{\partial x} + \rho v \frac{\partial v}{\partial y} + \left(\frac{p_0}{\rho_0 u_0^2}\right) \frac{\partial p}{\partial y} - \frac{\tau_0}{\rho_0 u_0^2} \left(\frac{\partial \tau_{xy}}{\partial x} + \frac{\partial \tau_{yy}}{\partial y}\right) = 0 \tag{3.104}$$

$$\begin{aligned} &\frac{\rho}{Ec} \frac{\partial e}{\partial T} \left(u \frac{\partial T}{\partial x} + v \frac{\partial T}{\partial y}\right) - \frac{1}{ReBr} \left(\frac{\partial q_x}{\partial x} + \frac{\partial q_y}{\partial y}\right) - \left(\frac{p_0}{\rho_0 u_0^2} p + \frac{\rho^2}{Ec} \frac{\partial e}{\partial \rho}\right) \\ &\left(\frac{\partial u}{\partial x} + \frac{\partial v}{\partial y}\right) - \frac{1}{Re} \left(2\mu(T) \left((\frac{\partial u}{\partial x})^2 + (\frac{\partial v}{\partial y})^2 + (\frac{\partial u}{\partial y} + \frac{\partial v}{\partial x})^2\right)\right. \\ &\left. + \lambda(T) \left((\frac{\partial u}{\partial x} + \frac{\partial v}{\partial y})^2\right)\right) = 0 \end{aligned} \tag{3.105}$$

$$\tau_{xx} = \frac{\mu_0 u_0}{L_0 \tau_0}\left(2\mu(T)\frac{\partial u}{\partial x} + \lambda(T)(\frac{\partial u}{\partial x} + \frac{\partial v}{\partial y})\right) \tag{3.106}$$

$$\tau_{xy} = \frac{\mu_0 u_0}{L_0 \tau_0}\left(\mu(T)(\frac{\partial u}{\partial y} + \frac{\partial v}{\partial x})\right) \tag{3.107}$$

$$\tau_{yy} = \frac{\mu_0 u_0}{L_0 \tau_0}\left(2\mu(T)\frac{\partial v}{\partial y} + \lambda(T)(\frac{\partial u}{\partial x} + \frac{\partial v}{\partial y})\right) \tag{3.108}$$

$$q_x = -\left(k_{xx}(T)\frac{\partial T}{\partial x} + k_{xy}(T)\frac{\partial T}{\partial y}\right) \tag{3.109}$$

$$q_y = -\left(k_{yx}(T)\frac{\partial T}{\partial x} + k_{yy}(T)\frac{\partial T}{\partial y}\right) \tag{3.110}$$

Equations (3.102)-(3.110) are a system of nine first order nonlinear partial differential equations in nine dependent variables, $\rho, u, v, T, \tau_{xx}, \tau_{xy}, \tau_{yy}, q_x$ and q_y in independent variables x and y. Let

$$\varphi = \{\varphi\} = [\rho, u, v, T, \tau_{xx}, \tau_{xy}, \tau_{yy}, q_x, q_y]^t \tag{3.111}$$

and $\bar{\Omega}_{xy}$ be the domain of definition. Let $\bar{\Omega}^T_{xy} = \bigcup_e \bar{\Omega}^e_{xy}$ be a discretization of $\bar{\Omega}_{xy}$ in which $\bar{\Omega}^e_{xy}$ is the domain of an element $'e'$. We approximate φ by φ^e_h over an element $\bar{\Omega}^e_{xy}$.

$$\varphi^e_h = \{\varphi^e_h\} = [\rho^e_h, u^e_h, v^e_h, T^e_h, (\tau_{xx})^e_h, (\tau_{xy})^e_h, (\tau_{yy})^e_h, (q_x)^e_h, (q_y])^e_h]^t \tag{3.112}$$

The local approximations $\rho^e_h, u^e_h, v^e_h, T^e_h, (\tau_{xx})^e_h, (\tau_{xy})^e_h, (\tau_{yy})^e_h, (q_x)^e_h$ and $(q_y)^e_h$ can be expressed using the approximation functions $[N^{(k_1-1),p}_\rho(\bar{\Omega}^e_{xy})]$, $[N^{(k_1-1),p}_u(\bar{\Omega}^e_{xy})]$, $[N^{(k_1-1),p}_v(\bar{\Omega}^e_{xy})]$, $[N^{(k_1-1),p}_{\tau_{xx}}(\bar{\Omega}^e_{xy})]$, $[N^{(k_1-1),p}_{\tau_{xy}}(\bar{\Omega}^e_{xy})]$, $[N^{(k_1-1),p}_{\tau_{yy}}(\bar{\Omega}^e_{xy})]$, $[N^{(k_1-1),p}_{q_x}(\bar{\Omega}^e_{xy})]$, $[N^{(k_1-1),p}_{q_y}(\bar{\Omega}^e_{xy})]$ and the nodal degrees of freedom $\{\rho^e\}$, $\{u^e\}$, $\{v^e\}$, $\{T^e\}$, $\{(\tau_{xx})^e\}$,$\{(\tau_{xy})^e\}$, $\{(\tau_{yy})^e\}$, $\{(q_x)^e\}$, $\{(q_y)^e\}$ as done in earlier sections. Since the PDEs are non-linear only least squares finite element method yields variationally

consistent integral form. The choices of k the order of the approximation space in x and y (assumed same here, but could be different) is important. We discuss this here,

- If $k \geq 2$ then obviously all integrals in the LSP are Riemann and $k = 2$ corresponds to the minimally conforming approximation space.
- If $k = 1$, then the local approximations over $\bar{\Omega}^e_{xy}$ are of class C^{00} in x and y and the integrals in LSP are labesgue.

More on the choice of Lebesgue or Riemann integrals, their merits or drawbacks [78] will be discussed in the subsequent chapter containing numerical studies.
Let,

$$V_h(\bar{\Omega}^e_{xy}) \subset H^{k,p}(\bar{\Omega}^e_{xy}); p \geq 2k-1 \; \forall \; \bar{\Omega}^e_{xy} \subset \bar{\Omega}^T_{xy} \tag{3.113}$$

$$H^{k,p}(\bar{\Omega}^e_{xy}) = \{w : w|_{\bar{\Omega}^e_{xy}} \in C^{(k-1,k-1),p}(\bar{\Omega}^e_{xy}), \\ w : w|_{\bar{\Omega}^e_{xy}} \in P^p(\bar{\Omega}^e_{xy}); p \geq 2k-1 \; \forall \; \bar{\Omega}^e_{xy} \in \bar{\Omega}^T_{xy} \tag{3.114}$$

If we substitute the local approximations in the PDEs we obtain residuals,

$$E^e_i(\varphi^e_h); i = 1, ..., 9 \; \forall \; x, y \in \bar{\Omega}^e_{xy} \tag{3.115}$$

Since, the PDEs are non-linear, only least squares finite element process yields VC integral form. Details of LSP follow standard details discussed for STLSP, except that in this case the integrals are over $\bar{\Omega}^e_{xy}$ as opposed to space-time element.

3.7.1.2 Strong form of GDEs

The strong form of GDEs can be easily obtained by setting time derivatives terms to zero in the GDEs for corresponding IVPs. If we choose $x_1, x_2 \rightarrow x, y$; $v_1, v_2 \rightarrow u, v$ and $\tau_{11}, \tau_{12}, \tau_{22} \rightarrow \tau_{xx}, \tau_{xy}, \tau_{yy}$, then we obtain the following system of PDEs,

$$\frac{\partial(\rho u)}{\partial x} + \frac{\partial(\rho v)}{\partial x} = 0 \tag{3.116}$$

$$\rho u\frac{\partial u}{\partial x} + \rho v\frac{\partial u}{\partial y} + \left(\frac{p_0}{\rho_0 u_0^2}\right)\frac{\partial p}{\partial x} - \frac{1}{Re}\left(2\frac{\partial}{\partial x}\left(\mu(T)\frac{\partial u}{\partial x}\right) - \frac{\partial}{\partial x}\left(\lambda(T)(\frac{\partial u}{\partial x} + \frac{\partial v}{\partial y})\right) - \frac{\partial}{\partial y}\left(\mu(T)(\frac{\partial u}{\partial y} + \frac{\partial v}{\partial x})\right)\right) = 0 \tag{3.117}$$

$$\rho u\frac{\partial v}{\partial x} + \rho v\frac{\partial v}{\partial y} + \left(\frac{p_0}{\rho_0 u_0^2}\right)\frac{\partial p}{\partial x} - \frac{1}{Re}\left(2\frac{\partial}{\partial x}\left(\mu(T)\frac{\partial u}{\partial x}\right) - \frac{\partial}{\partial x}\left(\lambda(T)(\frac{\partial u}{\partial x} + \frac{\partial v}{\partial y})\right) - \frac{\partial}{\partial y}(\mu(T)(\frac{\partial u}{\partial y} + \frac{\partial v}{\partial x}))\right) = 0 \tag{3.118}$$

$$\frac{\rho}{Ec}\frac{\partial e}{\partial T}\left(u\frac{\partial T}{\partial x} + v\frac{\partial T}{\partial y}\right) - \frac{1}{ReBr}\left(\frac{\partial}{\partial x}\left(k_{xx}(T)\frac{\partial T}{\partial x} - k_{xy}(T)\frac{\partial T}{\partial y}\right) - \frac{\partial}{\partial y}\left(k_{yx}(T)\frac{\partial T}{\partial x} - k_{yy}(T)\frac{\partial T}{\partial y}\right)\right) - \left(\frac{p_0}{\rho_0 u_0^2}p + \frac{\rho^2}{Ec}\frac{\partial e}{\partial \rho}\right)(\frac{\partial u}{\partial x} + \frac{\partial v}{\partial y}) - \frac{1}{Re}\left(2\mu(T)(\frac{\partial u}{\partial x})^2 - 2\mu(T)(\frac{\partial v}{\partial y})^2 - \mu(T)(\frac{\partial u}{\partial y} + \frac{\partial v}{\partial x})^2 - \lambda(T)(\frac{\partial u}{\partial x} + \frac{\partial v}{\partial y})^2\right) = 0 \tag{3.119}$$

Equations (3.116)-(3.119) are a system of four non-linear PDEs in four variables, ρ, u, v and T.

Let $\varphi = \{\varphi\} = [\rho, u, v, T]^t$ and $\bar{\Omega}^T_{xy} = \bigcup_e \bar{\Omega}^e_{xy}$ be a discretization of $\bar{\Omega}_{xy}$ in which $\bar{\Omega}^e_{xy}$ is an element $'e'$. We approximate φ by φ^e_h over $\bar{\Omega}^e_{xy}$

$$\varphi^e_h = \{\varphi^e_h\} = [\rho^e_h, u^e_h, v^e_h, T^e_h]^t \tag{3.120}$$

The approximations $\rho^e_h, u^e_h, v^e_h, T^e_h$ can be expressed in terms of local approximation functions and nodal degrees of freedom.

$$\begin{array}{rcl} \rho^e_h &=& [N^{k^\rho,p^\rho}_\rho(\bar{\Omega}^e_{xy})]\{\rho^e\} \\ u^e_h &=& [N^{k^u,p^u}_u(\bar{\Omega}^e_{xy})]\{u^e\} \\ v^e_h &=& [N^{k^v,p^v}_v(\bar{\Omega}^e_{xy})]\{v^e\} \\ T^e_h &=& [N^{k^T,p^T}_T(\bar{\Omega}^e_{xy})]\{T^e\} \end{array} \tag{3.121}$$

We have assumed equal order equal degree local approximation in x and y, however these could be different. For each dependent variable the choices of k and p can be different as well. In the following we discuss choices of approximation spaces.

(1) If $k^\rho \geq 2$, $k^u = k^v = k^T \geq 3$, Then the integrals in LSFE processes are Riemann. Equality yields minimally conforming spaces.

(2) If $k^\rho = 1$, $k^u = k^v = k^T = 2$ then the integrals in the LSFE processes are in Lebesgue sense.

(3) Obviously u^e_h, v^e_h and T^e_h of class $C^{00}(\bar{\Omega}^e_{xy})$ are not admissible.

(4) We remark that $k^\rho = k^u = k^v = k^T \geq 3$ are also admissible in the LSFE processes. The integrals in this case obviously remain Riemann.

Let $V_h(\bar{\Omega}^e_{xy})$ be the approximation space, then,

$$V_h(\bar{\Omega}^e_{xy}) \subset H^{k,p}(\bar{\Omega}^e_{xy}) \tag{3.122}$$

$$H^{k,p}(\bar{\Omega}^e_{xy}) = \{w : w\|_{\bar{\Omega}^e_{xy}} \in C^{(k-1,k-1),(p,p)}(\bar{\Omega}^e_{xy}), w : w\|_{\bar{\Omega}^e_{xy}} \in P^{(p,p)}(\bar{\Omega}^e_{xy});$$
$$p \geq 2k-1 \forall \bar{\Omega}^e_{xy} \in \bar{\Omega}^T_{xy} \quad (3.123)$$

Upon substituting local approximations in the GDEs (3.112)-(3.115) we obtain residual equations,

$$E^e_i(\varphi^e_h); i = 1, ..., 4 \quad (3.124)$$

Since the PDEs are non-linear , only least squares finite element processes are variationally consistent and hence are used in the present work

3.7.2 Summary

In this chapter mathematical models based on conservation laws, costitutive equations and equations of state are presented for the model problems : 1-D transient Burgers equation, 1-D Riemann shock tube with ideal and real gas models and 2-D steady state compressible flow. For each mathematical model details of the least squares finite element formulations and space-time least squares finite element formulations are also presented. We summarize these in the following.

(1) The governing differential equations are presented in the weak forms (a system of first order partial differential equations) as well as in the strong forms containing higher than first order derivatives of the dependent variables.

(2) The GDEs in (1) are non-dimensionalized so that the resulting mathematical models be suitable for least squares and space-time least squares processes.

(3) Both ideal and real gas models are presented for the equation of state $\hat{p} = \hat{p}(\hat{\rho}, \hat{T})$. These are also non-dimensionalized using the same reference quantities as in (2).

(4) For each model problem least squares or space-time least squares finite element formulation is presented for both types of mathematical models (weak form and strong form).

(5) The approximation spaces are discussed for each finite element formulation. Minimally conforming spaces are established. How the choices of approximation spaces influence the integral in the finite element processes (Riemann or Lebesgue) is demonstrated.

(6) In case of 1-D transient Burgers equation, literature riview is also presented. Some of these works are applicable to 1-D Riemann shock tube as well. The literature review for 2-D steady compressible flow is presented in the chapter containing numerical studies.

Chapter 4

Numerical Studies : 1-D Transient Viscous Burgers Equation

4.1 Introduction

In this chapter the h, p, k mathematical and computational framework and STVC integral forms presented in chapter 2 are utilized for 1-D transient viscous form of Burgers equation (1-D nonlinear conservation law) to demonstrate applicability, robustness, accuracy and unconditional stability of the methodology. The model problem with various boundary conditions and initial conditions based on published work are considered and the results are compared.

4.2 Numerical Studies

In this section we present a number of numerical studies to demonstrate the importance of space-time variational consistency of the space-time integral forms and that of the higher order spaces in simulating numerical solutions of the transient viscous Burgers equation under various initial and boundary conditions. The significance of this study is to demonstrate that accurate time evolutions of viscous Burgers equation are possible for any Re in the present framework. In the limit $Re \rightarrow \infty$, the solution of the inviscid form is approached. The numerical

studies are divided into three sections and the model problems used are the same as those used in the published work [22], so that our computed results can be compared with those in reference [22]. In all of our computations, viscous form of the Burgers equation is used and hence, the numerical studies are for specific values of Reynolds numbers (given with the numerical results). We consider the following three cases for the viscous form of the Burgers equation.

(i) Evolutions and stationary states of a single shock for $Re = 100, 1000$ and 10000

(ii) Evolution and stationary state of a double shock for $Re = 1000$

(iii) Evolution of a transonic shock at $Re = 1000$

In all numerical studies evolution details as well as the details of the stationary states of the evolutions are presented. For the strong form of the GDE for the Burgers equation, $k_1 = 3$ and $k_2 = 2$ correspond to the minimally conforming spaces. Actual values of k_1 and k_2 as well as p_1 and p_2 used in the computations are given with the numerical results.

4.2.1 Evolution and stationary states of a single shock

The space-time domain $\Omega_{xt} = [0, 1] \times [0, 1]$ is considered in this study with the following initial conditions (ICs) and boundary conditions (BCs).

$$\begin{aligned} IC : \varphi(x, 0) &= 0.5;\ 0 \leq x \leq 1 \\ BC : \varphi(0, t) &= \begin{cases} 0.5 & ; \quad t \leq 0.0 \\ 1.0 & ; \quad t > 0.0 \end{cases} \end{aligned}$$

4.2.1.1 Mathematical representation of step boundary condition and rationale for comparison between theoretical and numerical solutions.

From the description of the BC we note that at $t = 0.0$ φ changes from 0.5 to 1.0 (i.e., step function) as shown in figure(4.1.

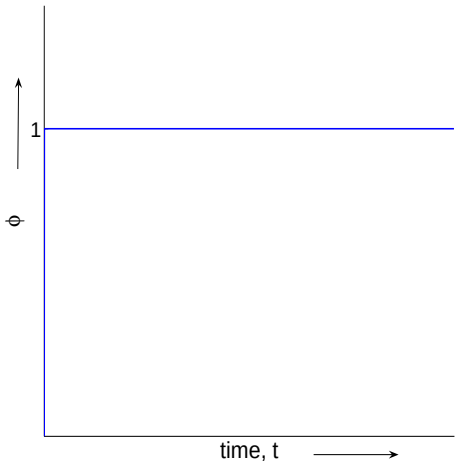

Figure 4.1: BC at x=0 i.e., $\varphi(0,t)$

From figure 4.1 we clearly observe the non-analytic nature of $\varphi(x,t)$ at $t = 0.0$. Let ${}^{n}\varphi^{e}(x,t) \in H^{k,p}(\bar{\Omega}^{e}_{xt})$; $k = (k_1, k_2)$ in which k_2 is the order of the approximation in time. If we assume φ changes from 0.5 to 1.0 over an increment of time Δt in a continuous and differentiable fashion based on the interpolants in the approximation spaces $H^{k,p}(\bar{\Omega}^{e}_{xt})$, then for progressively increasing k_2 the behavior of $\varphi_h(0,t)$ over Δt figure 4.2 clearly demonstrates that as k_2 increases, the distribution of $\varphi_h(0,t)$ becomes progressively steeper and in the limiting case $(k_2 \rightarrow \infty)$ approaches the step function at $t = \Delta t/2$. Another way to visualize this is that the distribution shown in figure 4.2 for various values of k_2 are infact

the properties of the distributions shown in figure 4.1 in the spaces of progressively higher order global differentiability in time. From figure 4.2 we clearly see that when $k_2 \rightarrow \infty$, φ_h remains 0.5 for $0 \leq t < \Delta t/2$ and only attains a value of 1.0 for $t = \Delta t/2$ and there after maintains a value of 1.0. Thus if the theoretical solutions of this model problem were available for BC shown in figure 4.1, then when comparing with numerical solutions, one must observe the following.

$$\varphi(x,t)\|_{t=\Delta t/2} = \varphi_h(x,t)\|_{t=\Delta t}$$

and

$$\varphi(x,t)\|_{t=\Delta t/2+n\Delta t} = \varphi_h(x,t)\|_{t=\Delta t+n\Delta t} \; for \; n = 1, 2, ...$$

Remarks

(1) As $k_2 \rightarrow \infty$ we do achieve impulsive (step change) changes in $\varphi_h(0,t)$ but with a time lag of $\Delta t/2$ (assuming φ_h changes for 0.5 to 1.0 over Δt). This time lag must be taken into account when comparing with theoretical solutions.

(2) Impulsive theoretical nature of $\varphi(0,t)$ at $t = 0$ is only realized at high values of k_2 i.e., order of the approximation space in time in the computation at $t = \Delta t/2$ but not at $t = 0$.

(3) Figure 4.2 clearly shows the meritorious nature of ${}^n\varphi_h^e(x,t)$ in $H^{k,p}({}^n\bar{\Omega}_{xt}^e)$ spaces in achieving the desired behavior of $\varphi(0,t)$, at $t = 0$. The descriptions of $\varphi(0,t)$ in figure 4.1 becomes analytic in $H^{k,p}({}^n\bar{\Omega}_{xt}^e)$ spaces. The representations shown in figure 4.2 are based on interpolants.

(4) Due to (3) the theoretical solutions of the numerically posed problem in various order spaces in time remain analytic. This aspects permits meaningful numerical simulation in which we can derive benefits from the weak convergence of the approximations.

(5) In all numerical studies a step change is applied over an increment of time Δt with features similar to those shown in figure 4.2.

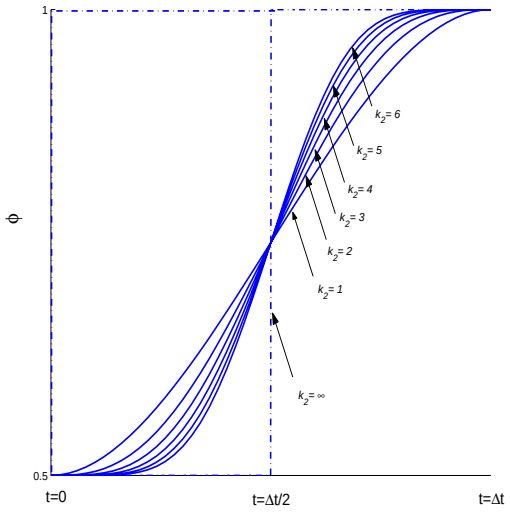

Figure 4.2: Descriptions of impulsive $\varphi(0,t)$ for $0 \leq t \leq \Delta t$ in spaces of progressively higher order global differentiability in time obtained using interpolants

The BC (figure(4.2)) imposed over Δt evolves into a steady propagating front (shock wave). The speed of the steady front in this case is given by $(\varphi(0,0)+\varphi(0,\Delta t))/2$ which for $\varphi(0,0)$ of 0.5 and $\varphi(0,\Delta t)$ of 1.0 is 3/4.

4.2.1.2 Evolution and its stationary state for Re = 100.

Here we consider a single shock at $Re = 100$ over $\Omega_{xt} = (0, 1) \times (0, 1.6)$. The spatial discretization consists of a 50 element uniform mesh over $\bar{\Omega}_x = [0, 1]$. The solution is time marched with $\Delta t = 0.02$. Since the numerically posed problem (based on section 4.2.1.1) has smooth solution, we expect weak convergence of the solutions of lower classes. We consider solutions of class $C^{1,1}({}^n\bar{\Omega}^e_{xt})$ i.e., of class C^1 in space as well as time. In this choice the order of the approximation space in x is one order lower than minimally conforming space. We consider $p_1 = p_2 = 11$ (i.e., uniform p-level in space and time). For these choices of h (i.e, $h_t = \Delta t, h_x = \Delta x$), p and k, the computed values of g ($= \delta I$) and the least squares functional I are $O(10^{-6})$ and $O(10^{-8})$ respectively and the Newton's method with line search converges in less than 10 iterations. Low values of I indicate good accuracy of the computed evolution for each space-time strip. With shock speed of 1.5, the disturbance reaches $x = 1$ (end of the spatial domain) at $t = 1.33$ but we continue the evolution till the stationary state is achieved. Figure 4.3(a) and 4.3(b) show contours and profiles of φ_h in $x - t$ space. From figure 4.3(a) we observe that due to low Reynolds number (and hence significant physical diffusion) the contours progressively diffuse for progressively increasing values of x and t. Near vertical lines at $x = 1.0$ correspond to the stationary state of the evolution. Profiles of φ_h in figure 4.3(b) are smooth and oscillation free. By examining L_2-norms of $\partial\varphi_h/\partial x$ and $\partial\varphi_h/\partial t$ as a function of time for each space-time strip during evolution, a clear assessment of the accuracy of the stationary state of the evolution can be made. Figures 4.4(a) and 4.4(b) show plots of L_2-norms of $\partial\varphi_h/\partial x$ and $\partial\varphi_h/\partial t$

as a function of time. At or near $t = 1.6$, $\| \partial\varphi_h/\partial x \|_{L_2}$ ceases to changes and $\| \partial\varphi_h/\partial t \|_{L_2}$ becomes zero confirming that the evolution has reached stationary state.

4.2.1.3 Evolution and its stationary state for Re = 1000.

At $Re = 1000$ the shock width is obviously much smaller compared to $Re = 100$. This of course requires a different discretization. Choice of Δt and k_2 depend upon how closely we want to approximate non-analytic nature of $\varphi(0, t)$ at $t = 0$. These choices influence initial stages of evolution significantly, however $\varphi_h(x, t)$ during the later stages of evolution is not effected due to self correcting nature of the evolution inherent due to non-linear GDEs. In this study also we consider solutions of class $C^{1,1}({}^n\bar{\Omega}^e_{xt})$ with $k_1 = k_2 = 2$, $h_x = \Delta x = 0.01$, $p_1 = p_2 = 11$ and $h_t = \Delta t = 0.01$. Accuracy of g and I similar to those for $Re = 100$ (section 4.2.1.2) is achieved in this case also and the Newton's method with line search also has similar performance. Figures 4.5(a) and 4.5(b) show contours and profiles of φ_h in $x - t$ space. From figure 4.5(b) we observe that due to higher value of Reynolds number (and hence diminished physical diffusion), the contours do not diffuse significantly for progressively increasing values of x and t. Near vertical lines at $x = 1.0$ indicate that the evolution has reached stationary state. Smooth and oscillation free profiles φ_h with higher solution gradients (compared to $Re = 100$) can be clearly observed in figure 4.5(b). Stationary value of $\| \partial\varphi_h/\partial x \|_{L_2}$ and near zero value of $\| \partial\varphi_h/\partial t \|_{L_2}$ for $t > 1.4$ in the graphs shown in Figures 4.6(a) and 4.6(b) confirm accurate stationary state of the evolution for $t > 1.4$.

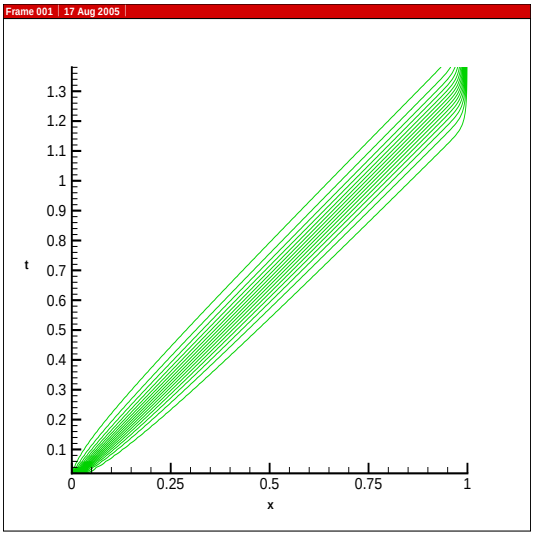

(a) Contours of φ_h in x-t domain

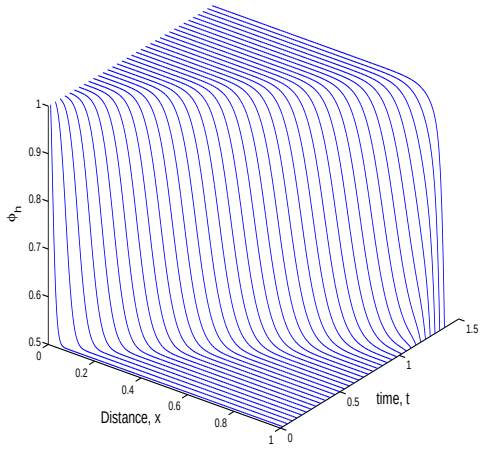

(b) Profiles of φ_h in x-t domain

Figure 4.3: Contours and profiles of φ_h in x-t domain for a single shock at $Re = 100$

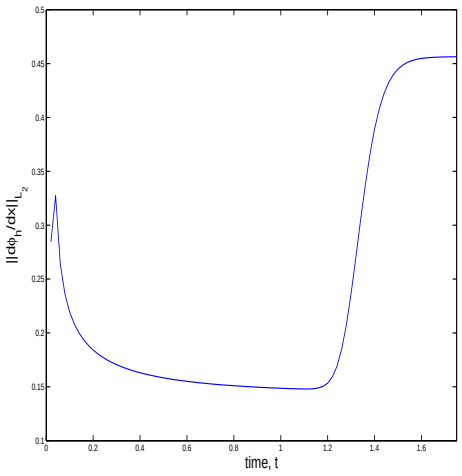

(a) L_2-norm of $\partial\varphi_h/\partial x$ versus time

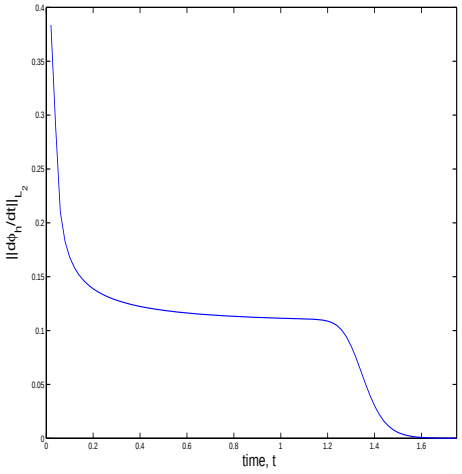

(b) L_2-norm of $\partial\varphi_h/\partial t$ versus time

Figure 4.4: L_2-norms of the $\partial\varphi_h/\partial x$ and $\partial\varphi_h/\partial t$ versus time for a single shock at Re=100 using space-time strip with time marching

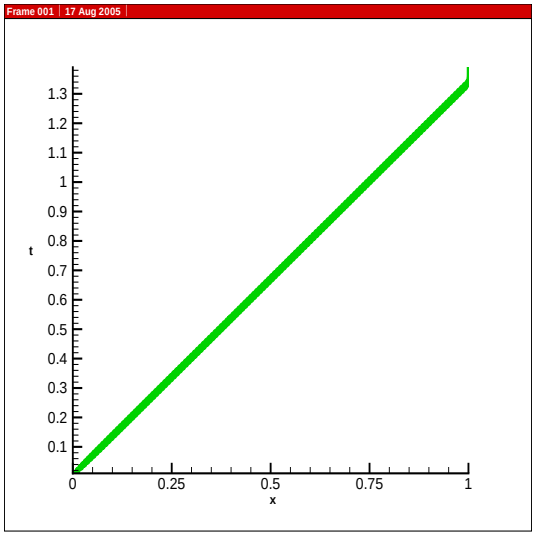

(a) Contours of φ_h in x-t domain

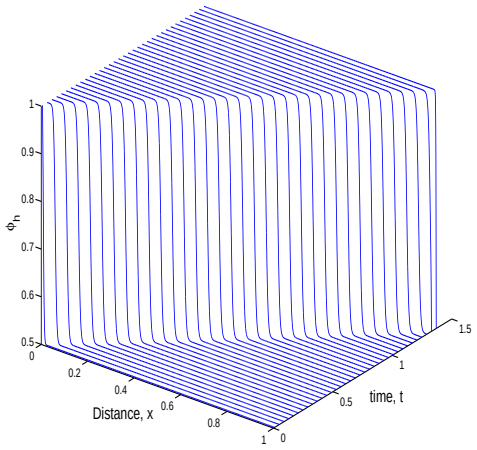

(b) Profiles of φ_h in x-t domain

Figure 4.5: Contours and profiles of φ_h in x-t domain for a single shock at $Re = 1000$

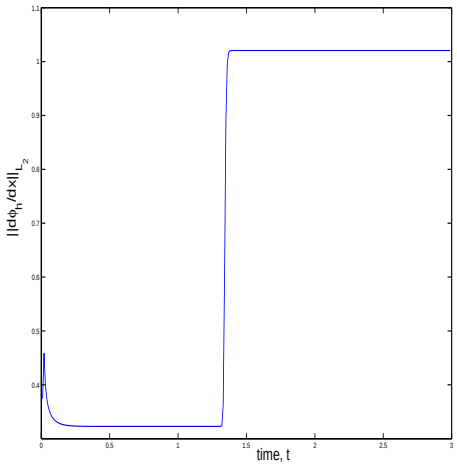

(a) L_2-norm of $\partial\varphi_h/\partial x$ versus time

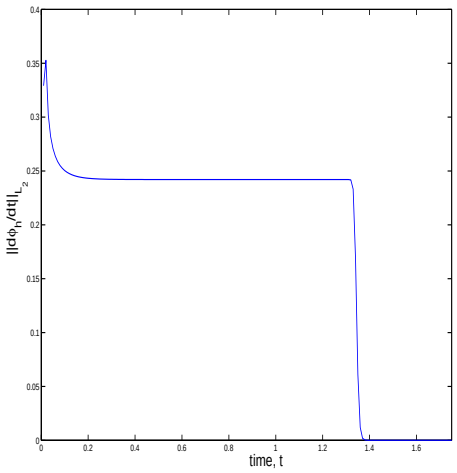

(b) L_2-norm of $\partial\varphi_h/\partial t$ versus time

Figure 4.6: L_2-norms of the $\partial\varphi_h/\partial x$ and $\partial\varphi_h/\partial t$ versus time for a single shock at Re=1000 using space-time strip with time marching

4.2.1.4 Evolution and its stationary state for Re = 10000

At this Reynolds number the shock width is even smaller than that for $Re = 1000$ (section 4.2.1.3). In this study we choose $h_x = \Delta x = 0.00125$ and $h_t = \Delta t = 0.001$, $k_1 = k_2 = 2$ (i.e., solutions of class $C^{1,1}({}^n\bar{\Omega}^e_{xt})$) and $p_1 = p_2 = 9$. The evolution is obtained by time marching the solution. Accuracy of g and I similar to those in section 4.2.1.2 are achieved here as well and the Newton's method with line search also performs similarly. Figures 4.7(a) and 4.7(b) show plots of the contours of φ_h and profiles of φ_h in $x - t$ domain. From figure 4.7(a) we clearly note the consequence of significantly reduced physical diffusion at this Reynolds number resulting in much narrower width of the contours in $x-t$ domain. This is obviously due to much isolated and higher solution gradients that are quite clear in figure 4.7(b). Profiles of φ_h in figure 4.7(b) are smooth and oscillation free. Behaviors of the L_2-norms of $\partial\varphi_h/\partial x$ and $\partial\varphi_h/\partial t$ versus time similar to those presented in sections 4.2.1.2 and 4.2.1.3 are also observed here (not shown for sake of brevity) confirming the accuracy of the stationary state of the evolution.

4.2.2 Evolution and stationary state of a double shock at $Re = 1000$

In this section we consider evolution and stationary state of a double shock over $\Omega_{xt} = (0, 2) \times (0, 1.6)$ for $Re = 1000$ we consider the following IC and BC.

$$IC : \varphi(x, 0) \;=\; \begin{cases} 1.5 & ; \quad 0 \le x < 0.5 \\ 0.5 & ; \quad 0.5 \le x \le 2 \end{cases}$$

$$BC : \varphi(0, t) \;=\; \begin{cases} 1.5 & ; \quad t < 0 \\ 2.5 & ; \quad t \ge 0 \end{cases}$$

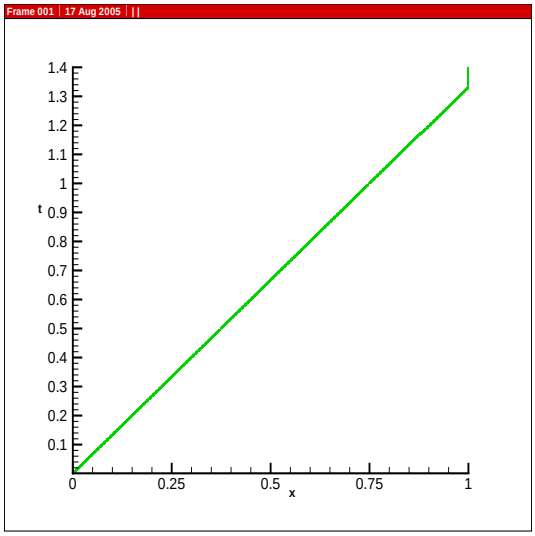

(a) Contours of φ_h in x-t domain

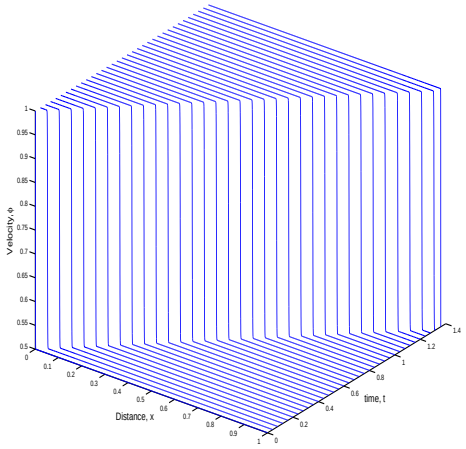

(b) Profiles of φ_h in x-t domain

Figure 4.7: Contours and profiles of φ_h in x-t domain for a single shock at $Re = 10000$

Figures 4.8(a) and 4.8(b) show graphs of IC and BC.

We note that initial condition at $t = 0$ is non-analytic due to step change in φ at $x = 0.5$ and the boundary conditions at $x = 0.0$ is also non-analytic due to step change in φ. In the numerical solutions such behaviors in $H^{k,p}({}^n\bar{\Omega}^e_{xt})$ spaces are represented using interpolants (similar to figure 4.2). These representations of 4.8(a) and 4.8(b) are analytic (similar to figure 4.2) and as we increase k_1 and k_2, the representations in the respective spaces approach the desired behaviors but always remain analytic and hence the theoretical solutions of the numerically posed double shock IVP always remains analytic as well. This significant feature permits us to lower the order of approximation spaces below minimally conforming due to the fact that weak convergence of the lower class solutions to higher class is possible. In this study we consider solutions of class $C^{1,1}({}^n\bar{\Omega}^e_{xt})$ and $C^{2,1}({}^n\bar{\Omega}^e_{xt})$ to demonstrate the importance of higher order global differentiability in space x. The BC and IC shown in figures 4.8(a)-4.8(b) create two disturbances, both of which propagate from left to right but at different speeds and evolve into two shocks. Since the shock due to BC (figure 4.8(b)) is traveling at faster speed than the one due to IC (figure 4.8(a)), the two shocks interact and form a single shock that eventually reaches the end of the domain and evolves into stationary state.

In the numerical study presented here we choose $h_x = \Delta x = 0.01$, $p_1 = p_2 = 11$ and $h_t = \Delta t = 0.005$ at $Re = 1000$. First we consider solutions of class $C^{1,1}({}^n\bar{\Omega}^e_{xt})$. Figures 4.9(a) and 4.9(b) show contours and profiles of φ_h in $x - t$ domain. From figure 4.9(a) shock formations, interactions and subsequent propagation of the resulting shock are clearly observed. Profiles of φ_h in 4.9(b)

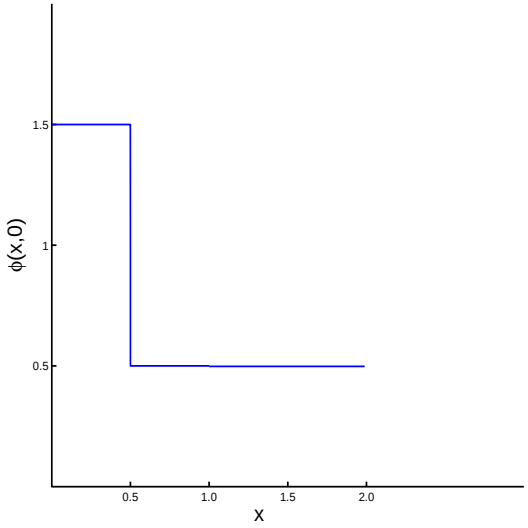

(a) Initial conditions

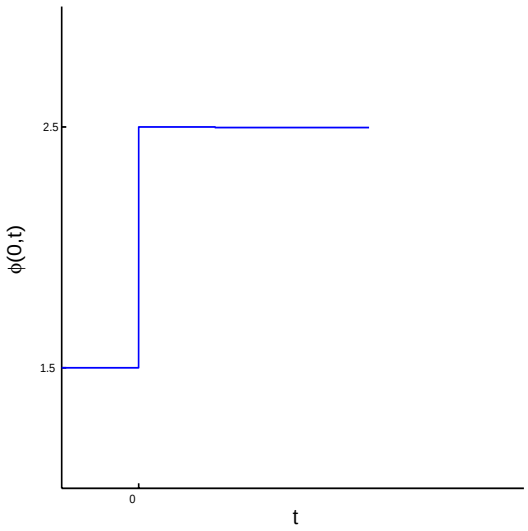

(b) Boundary conditions

Figure 4.8: IC and BC for double shock at $Re = 1000$

remain smooth, oscillation free and clearly show high solution gradients and their accurate resolution. Solutions of class $C^{2,1}({}^n\bar{\Omega}^e_{xt})$ were also computed using the same discretization and p-levels as used for solutions of class $C^{1,1}({}^n\bar{\Omega}^e_{xt})$. Figures 4.10(a) and 4.10(b) show plots of L_2-norms of $\partial\varphi_h/\partial x$ and $\partial\varphi_h/\partial t$ versus time t for solutions of class $C^{1,1}$ and $C^{2,1}$ obtained by using space-time time marching processes. We make the following remarks :

(a) In general, solutions of both classes show good agreement.

(b) In case of solutions of class $C^{1,1}$, $\parallel \partial\varphi_h/\partial t \parallel_{L_2}$ becomes constant when evolution ceases but has a finite non-zero value. For local approximations of class $C^{2,1}$, $\parallel \partial\varphi_h/\partial t \parallel_{L_2}$ is very close to zero indicating better accuracy of the stationary state achieved when the local approximations are of class $C^{2,1}$.

(c) Different values of $\parallel \partial\varphi_h/\partial x \parallel_{L_2}$ for the two classes of solution for $t > 1.2$ is clearly seen as well.

(d) Exploded views in Figures 4.10(a) and 4.10(b) show oscillatory behaviors of both L_2-norms when the local approximations are of class $C^{1,1}$ but free of oscillations for solutions of class $C^{2,1}$.

(e) Solutions of class $C^{2,1}({}^n\bar{\Omega}^e_{xy})$ correspond to $k_1 = 3$ and $k_2 = 2$ which is the minimally conforming space for the model problem. Superiority of the solutions of classes $C^{2,1}$ over $C^{1,1}$ is clearly observed.

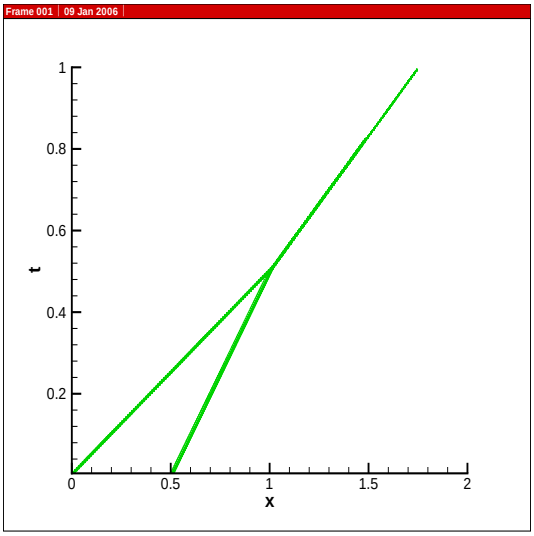

(a) Contours of φ_h in x-t domain

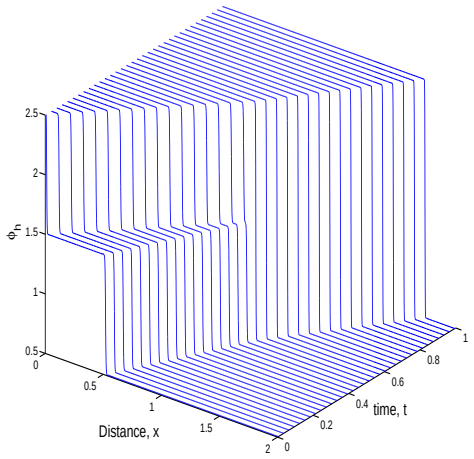

(b) Profiles of φ_h in x-t domain

Figure 4.9: Contours and profiles of φ_h in x-t domain for a double shock at $Re = 1000$

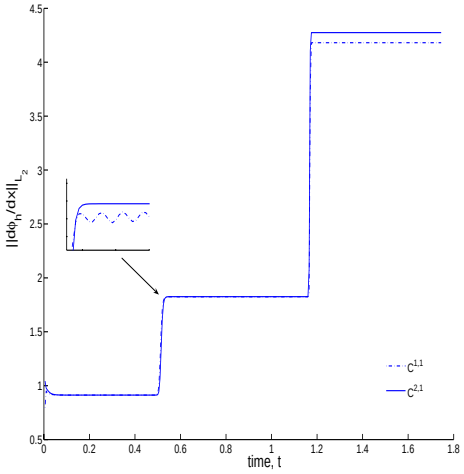

(a) L_2-norm of $\partial\varphi_h/\partial x$ versus time

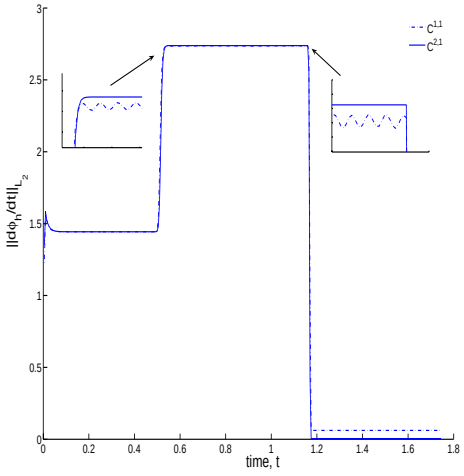

(b) L_2-norm of $\partial\varphi_h/\partial t$ versus time

Figure 4.10: L_2-norms of the $\partial\varphi_h/\partial x$ and $\partial\varphi_h/\partial t$ for solutions of class $C^{1,1}$ and $C^{2,1}$ for double shock at $Re = 1000$

4.2.3 Evolution of transonic shock at $Re = 1000$

In this section we consider a transonic shock problem described by the following initial and boundary conditions.

$$IC : \varphi(x,0) \quad = \begin{cases} -0.5 & ; \quad -1 \leq x < 0 \\ 2.5 & ; \quad 0 < x \leq 1.5 \end{cases}$$

$$BC : \varphi(0,t) \quad = \quad -0.5 \; ; \; \forall t \in [0,\tau]$$

In this case we note that BC data do not have discontinuity but the IC data shown in figure 4.11(a) are non-analytic. As in the previous model problem, here also we regularize IC using interpolants over $h_x = \Delta x$. The domain of definitions $\Omega_{xt} = (-1, 1.5) \times (0, 3.0)$ is discretized using $h_x = \Delta x = 0.0125$ and $h_t = \Delta t = 0.005$. We consider local approximations of class $C^{1,1}({}^n\bar{\Omega}^e_{xy})$ corresponding to $k_1 = k_2 = 2$ and we choose $p_1 = p_2 = 9$. The evolution is time marched using space-time strip. The values of g and $I({}^n\varphi_h)$ remain $O(10^{-6})$ and $O(10^{-8})$ during the entire evolution indicating convergence of Newton's method with line search and good accuracy of the evolution.

Figure 4.12(a) and 4.12(b) show contours and profiles of φ_h in $x - t$ domain. Evolutions are oscillation free and smooth. Evolution of rarefaction is simulated quite well as time elapses. Profiles of φ_h shown in figure 4.12(b) indicate that gradients of φ_h are preserved and solutions are oscillation free as well. Due to rarefaction (i.e., diffusion) the stationary state of the evolution will require a much larger value of time. This is quite obvious from the graphs of L_2-norms of $\partial\varphi_h/\partial x$ and $\partial\varphi_h/\partial t$ versus time t shown in figure 4.13(a). Even at $t = 3.0$ L_2-norm of the

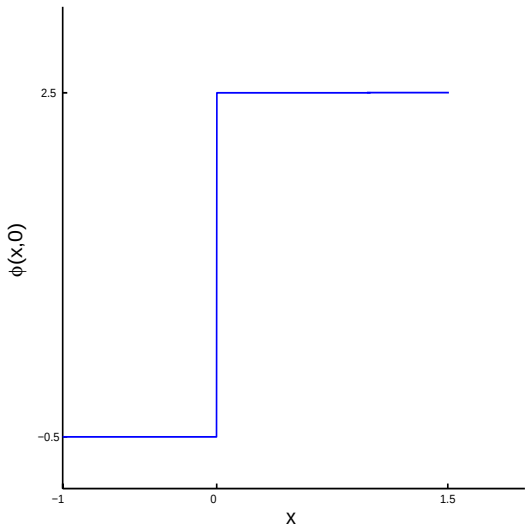

(a) Initial Conditions

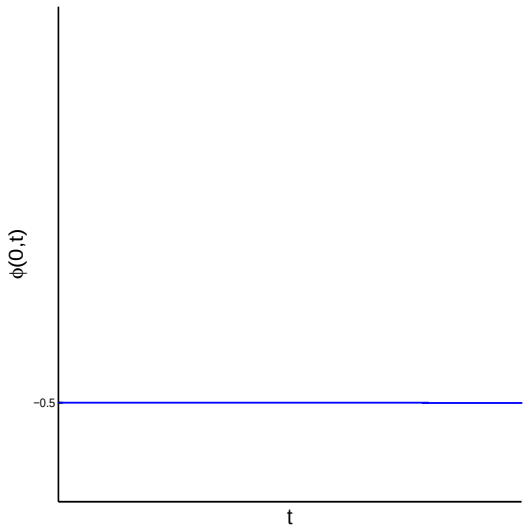

(b) Boundary Conditions

Figure 4.11: IC and BC for transonic shock at $Re = 1000$

$\partial\varphi_h/\partial x$ has not reached a steady value and L_2-norm of the $\partial\varphi_h/\partial t$ continues to decrease but has not reached zero (numerically computed) value.

4.2.4 Evolutions for progressively increasing CFL numbers : unconditional non-degeneracy and stability of STLSP

Numerical studies are presented in this section: (i) To demonstrate the STLSP are unconditionally non-degenerate i.e., computations are possible for any choices of h, p and k (ii) To show that even though the CFL number does influence accuracy but STLSP are unconditionally stable (iii) To show that good accuracy of evolution is achievable for very high CFL numbers. We consider the model problem with a single shock at $Re = 1000$ (section 4.2.1.3). Numerical studies were conducted using space-time strip with time marching for 200, 400 and 800 element uniform discretizations in spatial domain using $h_t = \Delta t = 0.01$ which correspond to CFL numbers of 2, 4 and 8. $k_1 = k_2 = 2$ and $p_1 = p_2 = 9$ were chosen. For these values of the computational parameters g and $I({}^n\varphi_h)$ were of $O(10^{-10})$ and $O(10^{-7})$ for all space-time strips for three values of the CFL numbers. Figures 4.14(a) and 4.14(b) show that L_2-norms of $\partial\varphi_h/\partial x$ and $\partial\varphi_h/\partial t$ versus time are indistinguishable from each other for all three values of CFL numbers.

4.3 Summary

The mathematical and computation aspects as well as numerical studies in h, p, k framework are presented for time dependent partial differential equation resulting from a single non-linear conservation law. Viscous form of the Burgers

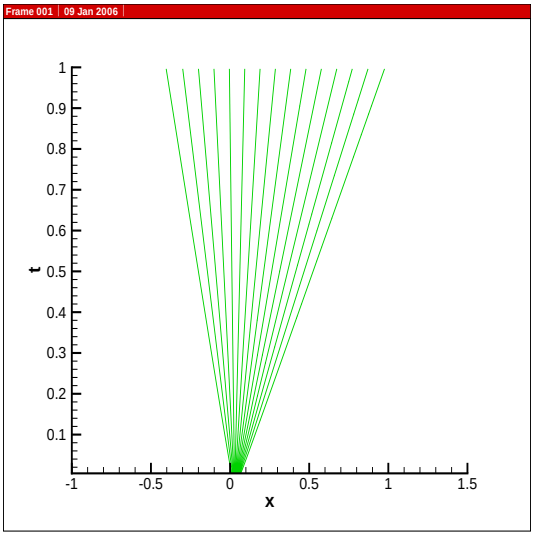

(a) Contours of φ_h in x-t domain

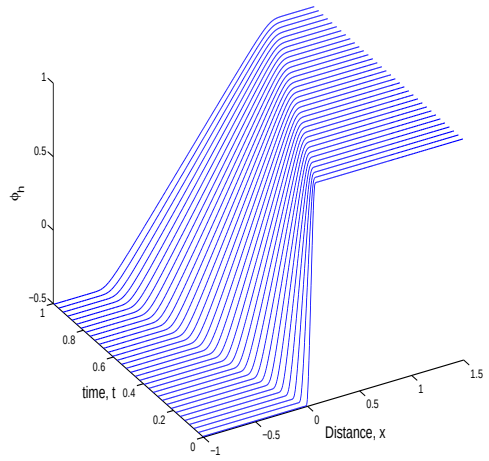

(b) Profiles of φ_h in x-t domain

Figure 4.12: Contours and profiles of φ_h in x-t domain for a transonic shock at $Re = 1000$

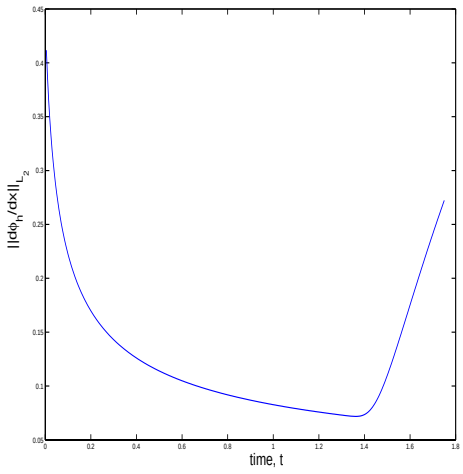

(a) L_2-norm of $\partial\varphi_h/\partial x$ versus time

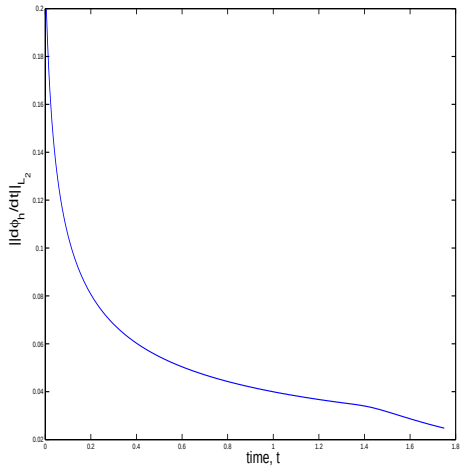

(b) L_2-norm of $\partial\varphi_h/\partial t$ versus time

Figure 4.13: L_2-norms of the $\partial\varphi_h/\partial x$ and $\partial\varphi_h/\partial t$ for transonic shock problem at Re=1000

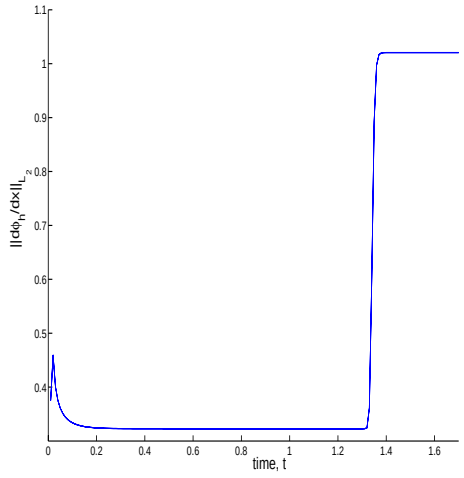

(a) L_2-norm of $\partial\varphi_h/\partial x$ versus time

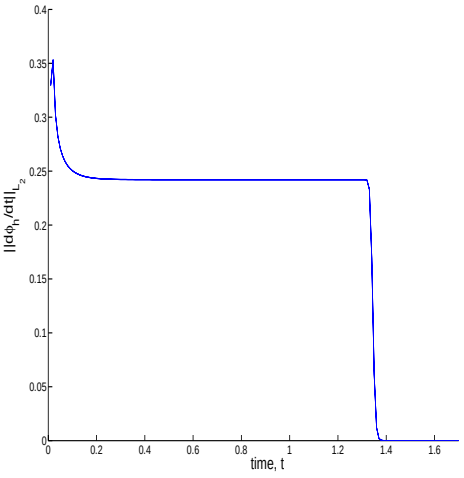

(b) L_2-norm of $\partial\varphi_h/\partial t$ versus time

Figure 4.14: L_2-norms of the $\partial\varphi_h/\partial x$ and $\partial\varphi_h/\partial t$ for meshes of 200, 400, 800 elements in space with $h_t = \Delta t = 0.01$ and $Re = 1000$

equation is used as a specific model problems. A summary of the work and the conclusions are given in the following.

(1) Strong form of the Burgers equation is used in the space-time least squares formulation and in the numerical studies as opposed to the weak form of the GDEs consisting of a system of first order equations obtained using auxiliary variables and the corresponding auxiliary equations. Merits of the approach can be found in reference [70].

(2) GDEs are not linearized prior to constructing the least squares functional as done in reference [22]. This is significant departure from the published work. The merits of this approach are :(a) The least squares functional and its first variation correspond to the precise non-linear mathematical model. (b) In this simple model problem, the linearization of GDE may be obvious but in the case of more complex physics (such as Navier Stokes equations) this may not be the case. (c) Newton's method with line search (linearization) is only employed while solving the non-linear algebraic equations resulting from the first variation of least squares functional set to zero. (d) This approach is free of assumptions, approximations and is applicable to all non-linear partial differential equations.

(3) The space-time local approximations are in higher order space $H^{k,p}(\bar{\Omega}^e_{xt})$ which permit higher order global differentiability of the approximations in space as well as time. The order k of the approximation space is an independent parameter in addition to h and p. Use of higher order spaces

permit use of GDE with higher order derivatives of dependent variables in the integral forms as well as allow us to incorporate the desired solution behavior in the design of the computational process.

(4) For the specific model problems (IVPs) considered here (same as those used in reference [22]), the space-time strip with time marching is utilized as opposed to space-time meshes [22]. This is computationally very efficient. In all numerical studies, viscous form of the Burgers equation is used.

(5) In case of a single shock (section 4.2.1), numerical studies for progressively increasing Reynolds numbers demonstrate : (a) smooth evolutions (b) accurate stationary state (c) and progressively reduced shock width. As $Re \rightarrow \infty$, the solution of the inviscid form of the Burgers equation are approached. Similar features exist for the double shock also (section 4.2.2), even though the numerical study in the paper is only for $Re = 1000$. Simulation of transonic shock at $Re = 1000$ (section 4.2.3) presents no difficulties. Evolution is smooth and oscillation free. Significantly low values of least squares functional $I = O(10^{-8})$ or lower for all space-time strips indicate that GDE is satisfied accurately during the entire evolution and hence all evolutions presented here are time-accurate. Space-time least squares functional converges monotonically and remains bounded for all choices of h, p, k.

(6) It is worth reiterating that solutions of inviscid Burgers equation are singular, hence non-analytic and thus cannot be computed directly [1]. As pointed out

in reference [1], the theory of generalized solutions leads to non-uniqueness when applied to the inviscid Burgers equation and that the only means of restoring uniqueness is to incorporate viscous mechanism. Thus all approaches and methodologies dealing with numerical solutions of inviscid Burgers equation are based on addition of artificial diffusion in the inviscid form and then demonstrating its vanishing nature in some limiting process. Secondly, the viscous mechanism in these approaches may not be in the agreement with the physics of diffusion present in the viscous form of Burgers equation. Thus the numerical solutions obtained from artificial viscosity approach may or may not correspond to that of the viscous form with a specific value of Re. This obviously raises the question of time accuracy of the evolutions in artificial diffusion approaches.

(7) In the approach presented here using viscous form of the Burgers equation the time accurate evolutions and their stationary state can be established precisely for any specific Re and as $Re \rightarrow \infty$ the vanishing nature of the shock width is quite clear from the numerical studies presented here. In this approach the solution remain analytic, associated functionals exhibit monotonic convergence and the computational processes remain unconditionally stable and non-degenerate. The space-time least squares process for Burgers equation is constructed in a straight forward manner without any assumption or approximations. Upwinding methods or any other ad-hoc treatments are neither needed nor used in the work presented here.

Chapter 5

Numerical Studies : 1-D Riemann Shock tube with Viscous and Conducting medium using ideal and real gas models for equation of state

5.1 Introduction

The mathematical models for 1-D time dependent compressible flow in Riemann shock tube (1-D compressible flow) based on conservation laws have been presented in chapter 3. Constitutive equations (Stokes 1845-1852) relating viscous stresses and thermodynamic pressure to Cauchy stress for viscous compressible medium have also been presented in chapter 3. The equation of state describing thermodynamic pressure $p = p(\rho, T)$ using ideal gas laws and real gas models, specific internal energy e, and transport properties (c_v, μ, λ) dependent on temperature have also been discussed in details. The dimensionless forms of the mathematical models (weak form of GDEs and strong form of GDEs) ; constitutive equations, equations of state, e, c_v etc. have also been derived using p_0 and τ_0 as reference pressure and reference stress amongst others. Since the GDEs are non-linear PDEs in space and time, only space-time least squares finite element processes yield integral forms that are space-time variationally consistent when Newton's linear method is used for solving non-linear algebraic equations iteratively and hence, will be used in presenting numerical studies in this chapter using strong form of GDEs

[70] in dependent variables ρ, u and T. Space-time strip with time marching [44]-[45] is utilized for determining time evolution. The following numerical studies are considered.

I. Ideal gas law. medium : air at NTP (initial conditions)

   (a) Shock evolution, shock structure resolution, propagation, reflection : density ratios of 20.

   (b) Repeated shock reflections, interaction and propagation : density ratios of 20.

II. Real gas law with constant transport properties :

   Shock evolution and propagation

   - Van der Waals equation of state
   - Media (FC70)
     - near critical point
     - away from critical point

   The numerical studies are aimed to determine existence of shock, shock evolution and shock structure resolution

5.2 Riemann shock tube : Ideal gas Law

The Riemann shock tube problem using solution of class $C^{11}(\bar{\Omega}^e_{xt})$ was first studied by Surana et.al [60]. The authors showed that: (i) The strong form of

GDEs and space-time local approximation of class C^{11} were essential in obtaining oscillation free solution and low values of the L_2 norm of the residuals. (ii) Accurate shock resolution as well as shock evolution were possible. The authors presented graphs of the evolution of ρ, u and T for various density ratios using ideal gas law for air. Subsequently Surana, Allu et.al. [27] presented solutions of higher classes in space and time that demonstrated the meritorious features of these solutions and also showed that weak form of GDEs resulted in failure and the progressively increased global differentiability local approximation in space and time yielded progressively deteriorated solutions and earlier onset of the failure of computations. The problems associated with the weak form of GDEs in LSP and STLSP have been discussed by Surana et.al. [70]. In the works by Surana, Allu et.al. [27] evolutions of ρ, u and T were reported.

While the works in references [27], amply demonstrate qualitatively the formation of shock and its propagation, these works donot provide a thermodynamic map of the evolution, which could have served as a quantitative measure to ensure without doubts as to when the shocks are fully formed and if indeed they propagate without diffusion. In the studies presented here, this is the main trust.

5.2.1 Definition of shock

We define a sustained wave that does not disperse or diffuse anymore during further evolution as a shock. In case of Riemann shock tube upon rupture of the diaphragm, compression waves with progressively increased speed pile up in the low density region. These processes results in steepening of the front or traveling

wave. On the other hand the mechanism of dispersion comes into play due to viscosity of the medium which results in elongation of the base of the wave or the front. If the steepening process is stronger than the base elongation process, then the wave begins to steepen as evolution proceeds and eventually we reach a time during evolution when both processes equilibrate. At this value of time we have a wave or a front that would neither steepen nor disperse during further evolutions. We refer to this wave or front as 'shock'. This process can be quantified by examining the increase in entropy per unit volume for each space-time strip. The basic mechanism of entropy production in shocks is due to conversion of mechanical energy into heat through viscous dissipation and conduction. Thus if S_r is the rate of entropy production per unit volume then,

$$\hat{S}_r = \frac{1}{\hat{T}}(\hat{\Phi} + \frac{1}{\hat{T}}\hat{q}.\hat{\nabla}\hat{T}) \tag{5.1}$$

where, $\hat{\Phi} = 2\hat{\mu}(\hat{T})\hat{D}_{ij}\frac{\partial \hat{v}_i}{\partial \hat{x}_j} + \hat{\lambda}(\hat{T})(\hat{D}_{kk})^2$

This can be non-dimensionalized using the reference quantities and dimensionless variables in chapter 3. For this specific case of 1-D Riemann shock tube we obtain dimensionless expression for $\hat{S}_r$ i.e., S_r given by,

$$S_r = \frac{1}{T}\left(\frac{1}{Re}\Phi + \frac{1}{BrRe}\frac{k}{\hat{T}}(\frac{\partial T}{\partial x})^2\right) \tag{5.2}$$

where, $\Phi = 2\mu(T)D_{ij}\frac{\partial v_i}{\partial x_j} + \lambda(T)(D_{kk})^2$

We note from the definition of a shock, that S_r must be constant for a fully developed shock to exist during further evolution. Thus presence of S_r alone is not an evidence of a shock. Thus S_r provides a thermodynamic map that quantitatively

establishes when shocks are formed for the first time as well as their existence upon further evolution. Secondly, most numerical process suffer from numerical dispersion in which case the presence of shock may be possible to establish but the shock structure would be in error. Surana et.al. [79] have shown that the LSP and STLSP can be completely free of numerical dispersion with proper choices of h, p and k. In the present work we demonstrate this feature by sustained shock propagation and repeated shock reflections without any deterioration in S_r.

This work for the first time establishes a computational infrastructure in which shocked viscous flow can be treated with utmost accuracy without special and problem dependent treatments.

5.2.1.1 Numerical Studies : Ideal gas Law

In this section we present numerical studies for shock evolution, shock structure resolution and propagation including reflection. We consider the medium to be air with the following properties at room temperature (NTP).

$$\hat{\rho} = 1.225 \ \mathrm{Kg/m^3}, \hat{\mu} = 0.198 \times 10^{-4} \ \mathrm{Pa-s}, \hat{\mathrm{k}} = 0.028859 \ \mathrm{N/s/K}$$

$$\hat{R} = 286.99 \ \mathrm{J/kg/K}, \hat{\mathrm{c}}_{\mathrm{v}} = 410.52 \ \mathrm{J/kg/K}$$

We choose the following reference values,

$$L_0 = 0.156 \times 10^{-5} \ \mathrm{m}, \rho_0 = \hat{\rho}, \mu_0 = \hat{\mu}, \mathrm{k}_0 = \hat{\mathrm{k}}, \mathrm{c_{v0}} = \hat{\mathrm{c}}_{\mathrm{v}}$$

$$u_0 = 343.25 \ \mathrm{m/s}, \mathrm{T}_0 = 410.52 \ \mathrm{K}, \mathrm{R}_0 = 286.99 \ \mathrm{J/kg/K}$$

$$\tau_0 = p_0 = \rho_0 u_0^2 = 0.14438 \times 10^6 \ \mathrm{Kg/m/s^2}$$

With this choice of reference values, we have the following dimensionless properties and the dimensionless parameters,

$$\rho = 1.0, \mu = 1.0, k = 1.0, c_v = 1.0, R = 1.0$$

$$Re = 31.891, Br = 0.19724, Ec = 0.40027$$

We consider the tube length $L = 2$. The diaphragm separating the high density medium on the right from the low density medium on the left is located at the center of the tube (Figure 5.1). The boundaries A and B are impermeable and non-conducting ($u = 0, \partial T \partial x = 0$) for all values of time. We consider a density ratio $\rho_h \rho_l = 20$ with $\rho_l = 1$. The space-time domain ${}^n\bar{\Omega}_{xt}$ is descretized using 101 element uniform mesh in the x-direction with only one element in the t direction. This gives $\Delta x = h_x^e = 0.0198$. We choose $\Delta t = 0.02$. A continuous and differentiable distribution of density from ρ_h to ρ_l is applied over Δx for element 51 located symmetrically at the center of the tube. This gives rise to the following initial conditions for ρ,

$$\rho(x, 0) = 20; 0 \leq x \leq 1 - \frac{\Delta x}{2}$$

$$\rho(x, 0) = 1; 1 + \frac{\Delta x}{2} \leq x \leq 2$$

Other initial conditions used are ,

$$u(x, 0) = 0 \ ; \ 0 \leq x \leq 2$$

$$T(x, 0) = 1 \ ; \ 0 \leq x \leq 2$$

Boundary conditions at A and B are,

$$u(0, t) = 0$$

$$\frac{\partial T}{\partial x}(0, t) = 0$$

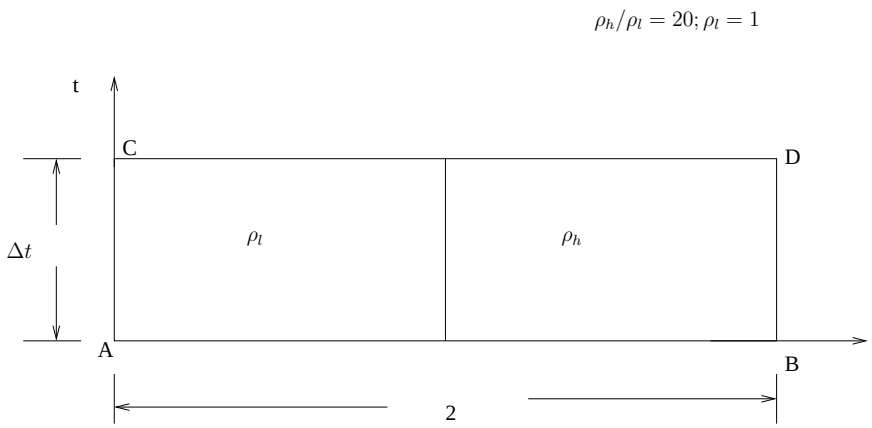

Figure 5.1: Schematic of Riemann shock tube for an increment of time Δt

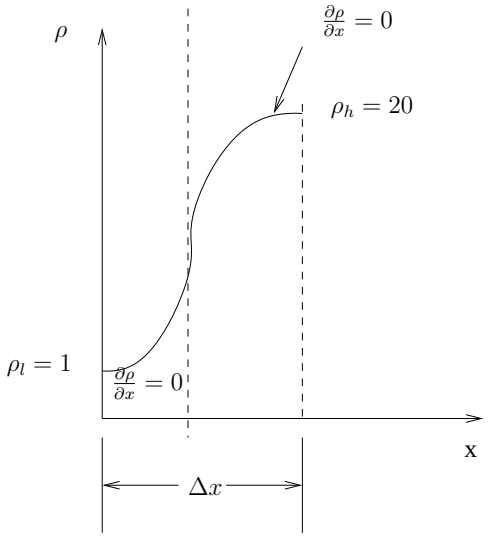

Figure 5.2: Distribution of density over an element at the diaphragm

First, we consider solutions of class $C^{11}({}^n\bar{\Omega}^e_{xt})$ with $p = 11$ in space and time. At time $t = 0$ the diaphragm is assumed to rupture. The time evolution is computed using STLSP for the first space-time strip containing 101 space-time elements and then time marched to obtain entire evolution history of ρ, u, T and S_r for 30 time steps. $|g_i|$ of $O(10^{-6})$ or lower during each time step of the evolution confirms that non-linear algebraic equations are solved accurately using Newton's linear method with line search. The least squares functional I remain $O(10^{-8})$ or lower during entire evolution ensuring that the numerically computed solution satisfies GDEs accurately and that evolution is indeed close to time accurate. Results are shown in figures 5.3-5.5.

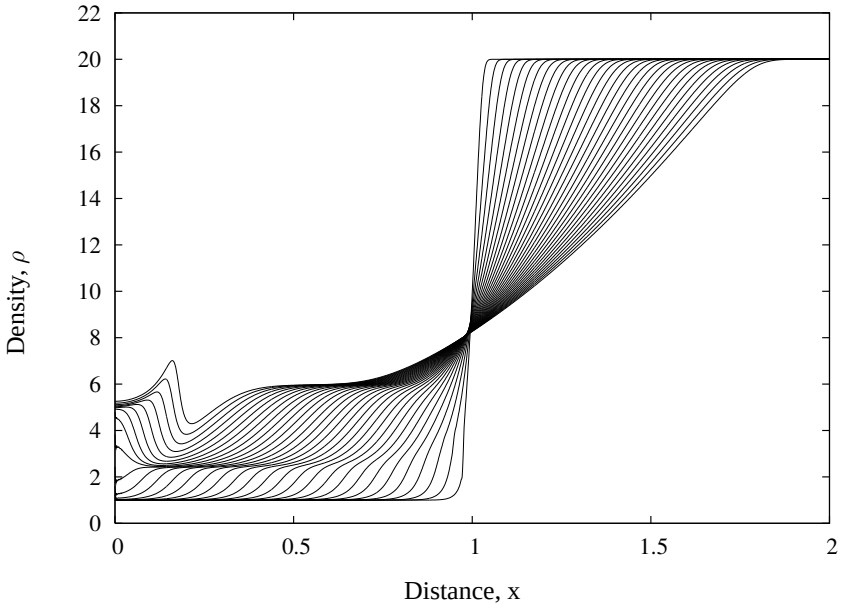

Figure 5.3: Evolution of density ρ : $\rho_h/\rho_l = 20$; $\varphi^e_h \in C^{11}({}^n\bar{\Omega}^e_{xt}), p = 11$

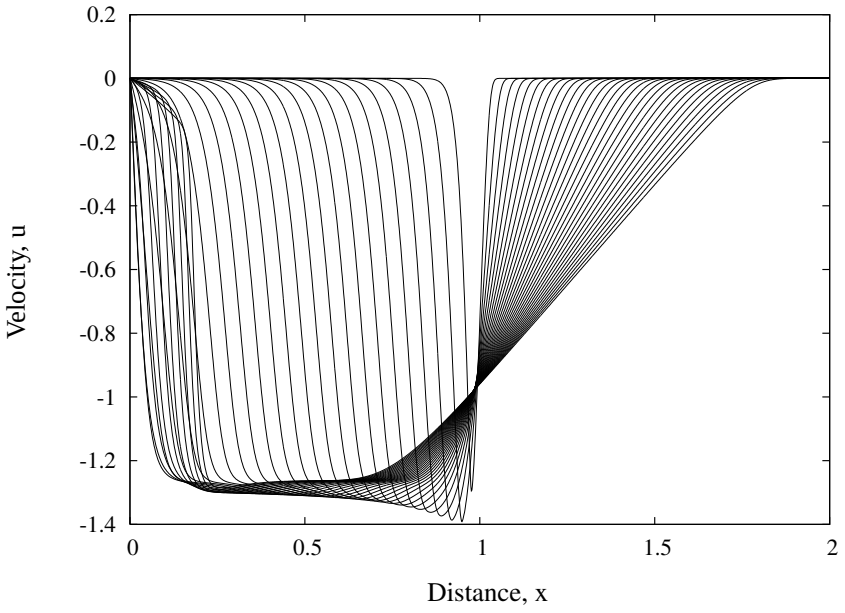

Figure 5.4: Evolution of velocity u : $\rho_h/\rho_l = 20$; $\varphi_h^e \in C^{11}({}^n\bar{\Omega}_{xt}^e), p = 11$

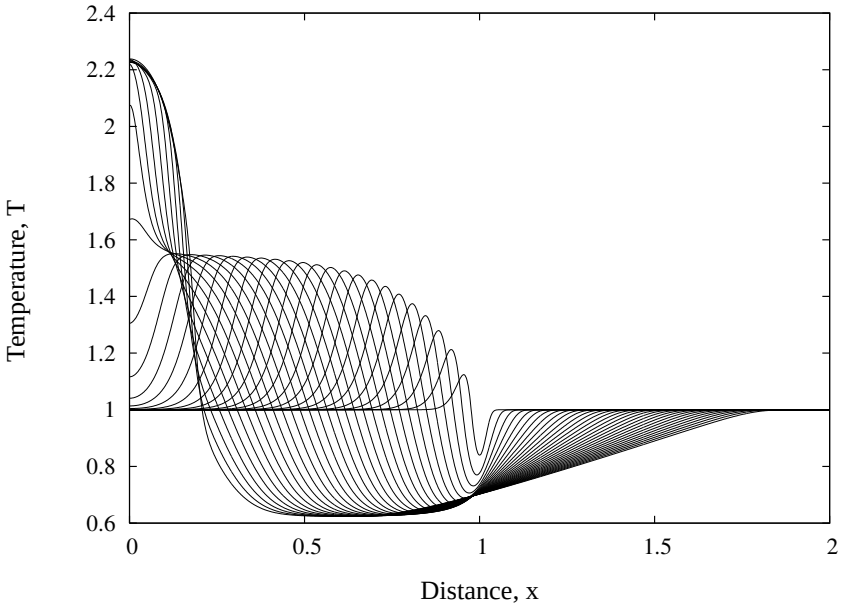

Figure 5.5: Evolution of temperature T : $\rho_h/\rho_l = 20$; $\varphi_h^e \in C^{11}({}^n\bar{\Omega}_{xt}^e), p = 11$

Discussion of results:

From figure 5.3, we note after about the first 10 time steps, the shock structure appear to be steady which then propagates upon further evolution leaving behind a constant density plug. Upon reaching the impermeable and non-conducting boundary, the shock reflection occurs which interacts with the constant density plug. The rise in temperature during shock reflection is clearly demonstrated in figure 5.5. The velocity evolution follows the normal pattern of propagating wave and its reflection. The rarefaction in the high density region is as expected (continuous dispersion of the wave). Here we note that shock detection process is rather visual i.e, when we don't observe any perceivable dispersion of the front, we call it a shock.

In figure 5.6 the space-time plot of S_r quantifies the shock formation process. We note that what starts out as a sharp front in the low density region (left) disperses upon until $(x, t) = (0.75, 0.1)$ and then remains steady during the remainder of the evolution including the reflection and thereafter, indicating that for $x < 0.75$ and $t > 0.1$ S_r is constant for the evolution. This undoubtedly confirms a sustained front i.e., a shock. The corresponding space-time plot of velocity confirm constant velocity of moving front with constant S_r. Space-time plot of density show similar features as shown in figure 5.3. Space-time plot of temperature evolution clearly indicates that highest temperature occur upon reflection as evident in figure 5.5. Out of all of the graphical presentations of results, perhaps the most important one is that of space-time plot of S_r that undoubtedly confirms :(1) evolution of a shock and its propagation and (2) based on ref [34], the true shock structure. An

exploded view of the space-time plot of S_r for a few initial time steps is shown in figure 5.6b. We note that maximum S_r occurs in the rarefaction region during initial stages of the evolution, but the dispersion of the waves in this region during evolution quickly diffuses this. Whereas, the compression waves in the low density region are able to generate sustained S_r essential for the existence and propagation of a shock.

Remarks

(1) An important point to note here is that, since the strong form of GDEs contain second order derivatives of u and T, the minimally conforming space for these would be $k_1 = 3$, i.e., u_h^e and T_h^e of class C^2 in space. But the solution presented here are of class C^{11}, thus, the integrals in the STLSP are not Riemann but Lebesgue. Smoothness of the solution allows us to do so.

(2) Based on (1), it is essential to either show a convergence study or present solutions that correspond to minimally conforming spaces (C^{21} solutions) so that the integrals in STLSP become Riemann and demonstrate that the solution of class C^{11} and C^{21} are identical, thus confirming the convergence of C^{11} to C^{21} in the weak sense.

Solutions of class $C^{21}({}^n\bar{\Omega}^e_{xt})$

A study similar to that for the solutions of class $C^{11}({}^n\bar{\Omega}^e_{xt})$ has also been conducted for conditions identical to these used for solutions of class C^{11}. Here, we use only a 41 element uniform dicretization for $L = 2$ and the density distribution

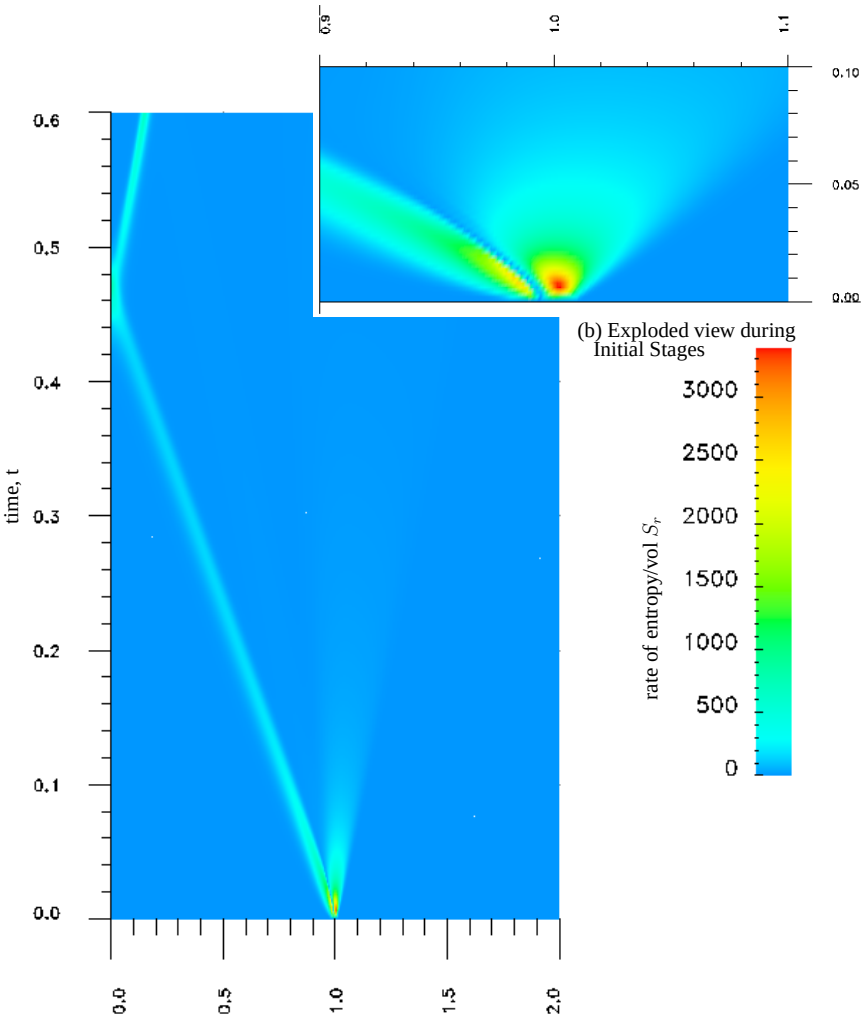

(a) Full Evolution

Figure 5.6: Space-time plot of evolution of S_r

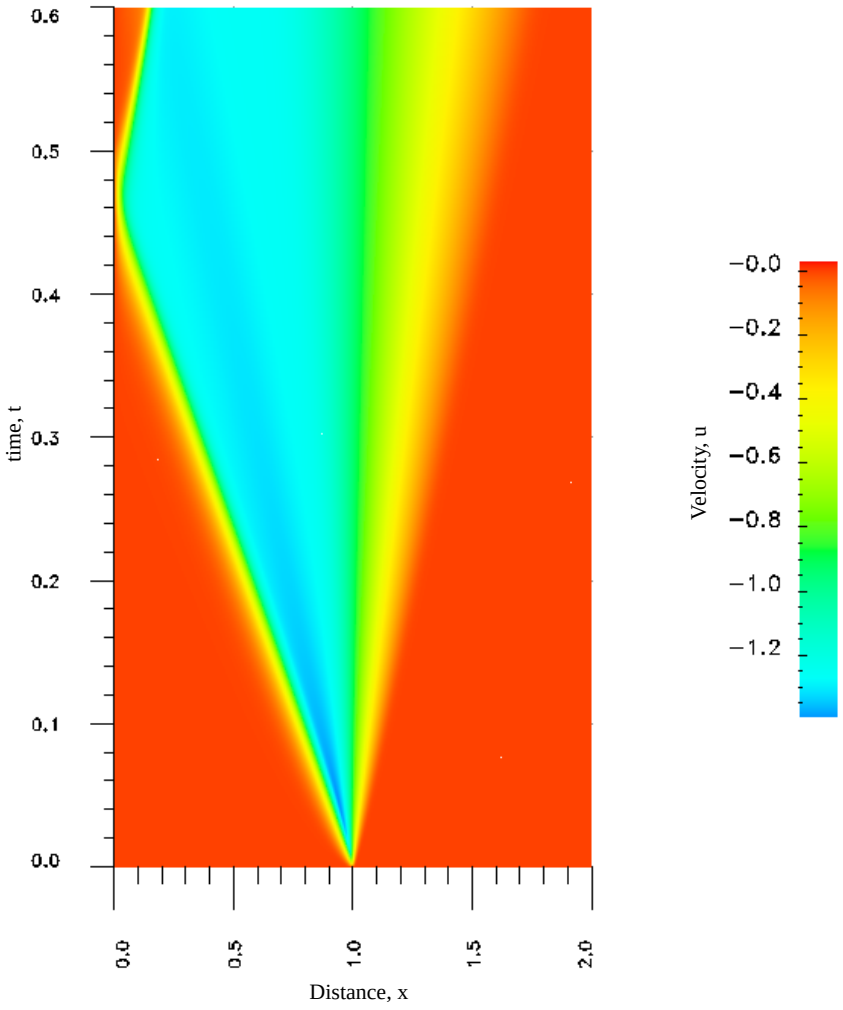

Figure 5.7: Space-time plot of evolution of velocity, u

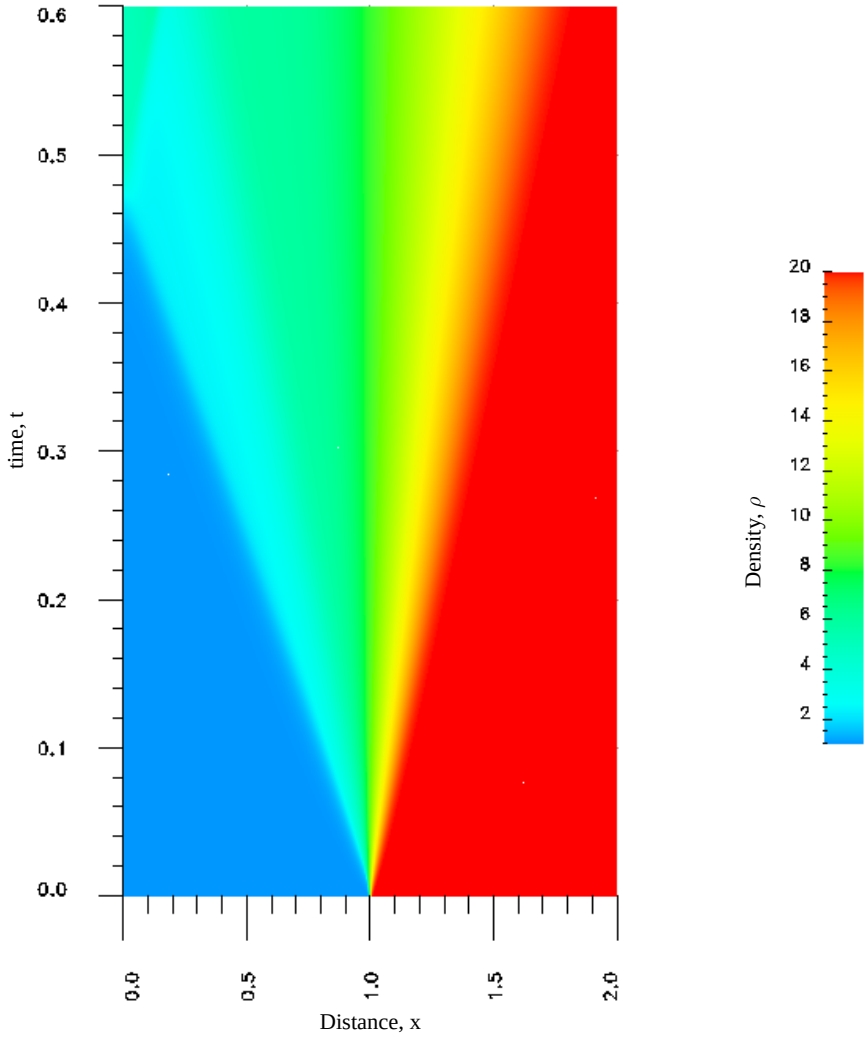

Figure 5.8: Space-time plot of evolution of density, ρ

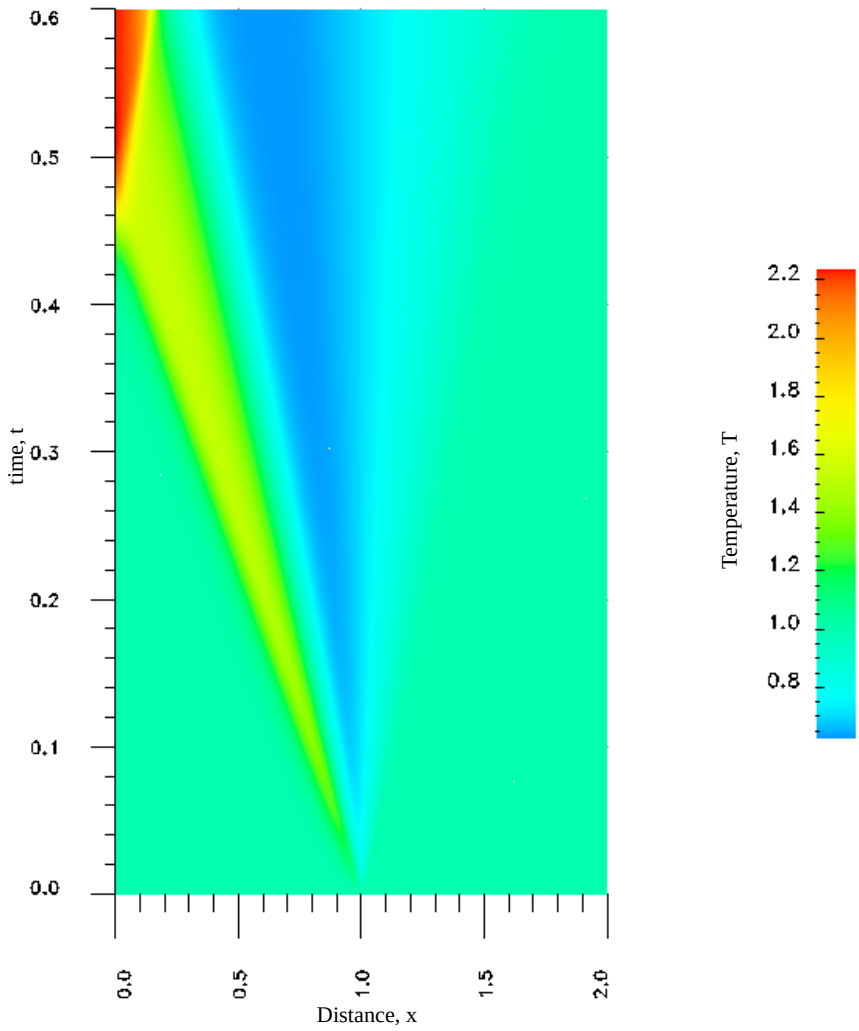

Figure 5.9: Space-time plot of evolution of temperature, T

from 20 to 1 applied over element '21' located symmetrically to the diaphragm. $p = 11$ is used in space and time to compute the evolution for 25 time steps. Evolution of density, velocity and temperature along the length is shown in figure 5.10-5.12. Figures 5.13-5.16 show space-time evolution of S_r, ρ, u and T.

In this case also g_i of order $O(10^{-6})$ or lower confirms the accuracy of the solution of non-linear algebraic equations obtained using Newton's linear method with line search. During the entire evolution, the least squares functional I remains $O(10^{-8})$ or lower ensuring that the computed solutions for each space-time strip satisfy the GDEs accurately. A comparison of these results with those reported for solutions of class $C^{11}({}^n\bar{\Omega}^e_{xt})$ in figures 5.6-5.9 confirms the accuracy of the solutions of class $C^{11}({}^n\bar{\Omega}^e_{xt})$.

Thus, in all future studies we shall only consider solutions of class $C^{11}({}^n\bar{\Omega}^e_{xt})$ keeping in mind $|g_i|$ and I are the measures of the accuracy of the evolution for each space-time strip.

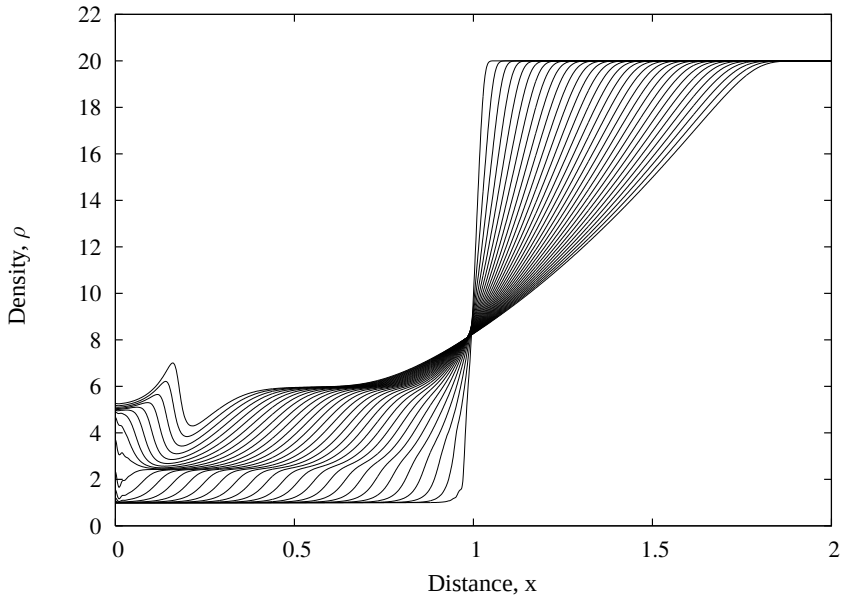

Figure 5.10: Evolution of density ρ : $\rho_h/\rho_l = 20$; $\varphi_h^e \in C^{21}({}^n\bar{\Omega}_{xt}^e), p = 5$

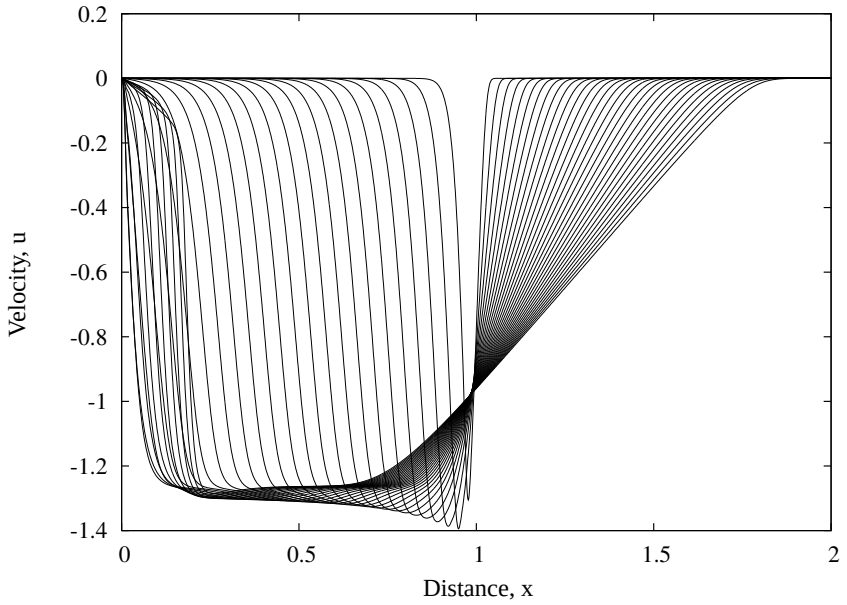

Figure 5.11: Evolution of velocity u : $\rho_h/\rho_l = 20$; $\varphi_h^e \in C^{21}({}^n\bar{\Omega}_{xt}^e), p = 5$

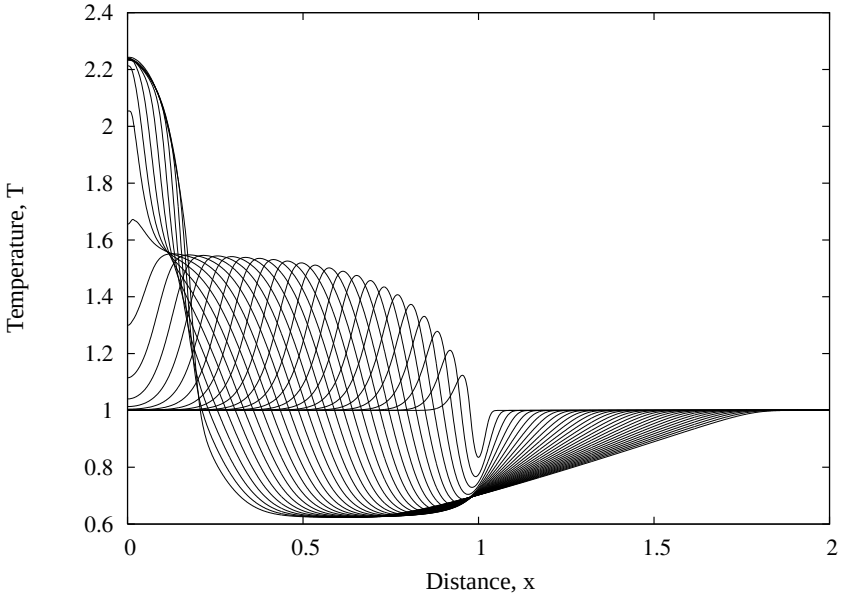

Figure 5.12: Evolution of temperature T : $\rho_h/\rho_l = 20$; $\varphi_h^e \in C^{21}({}^n\bar{\Omega}_{xt}^e), p = 5$

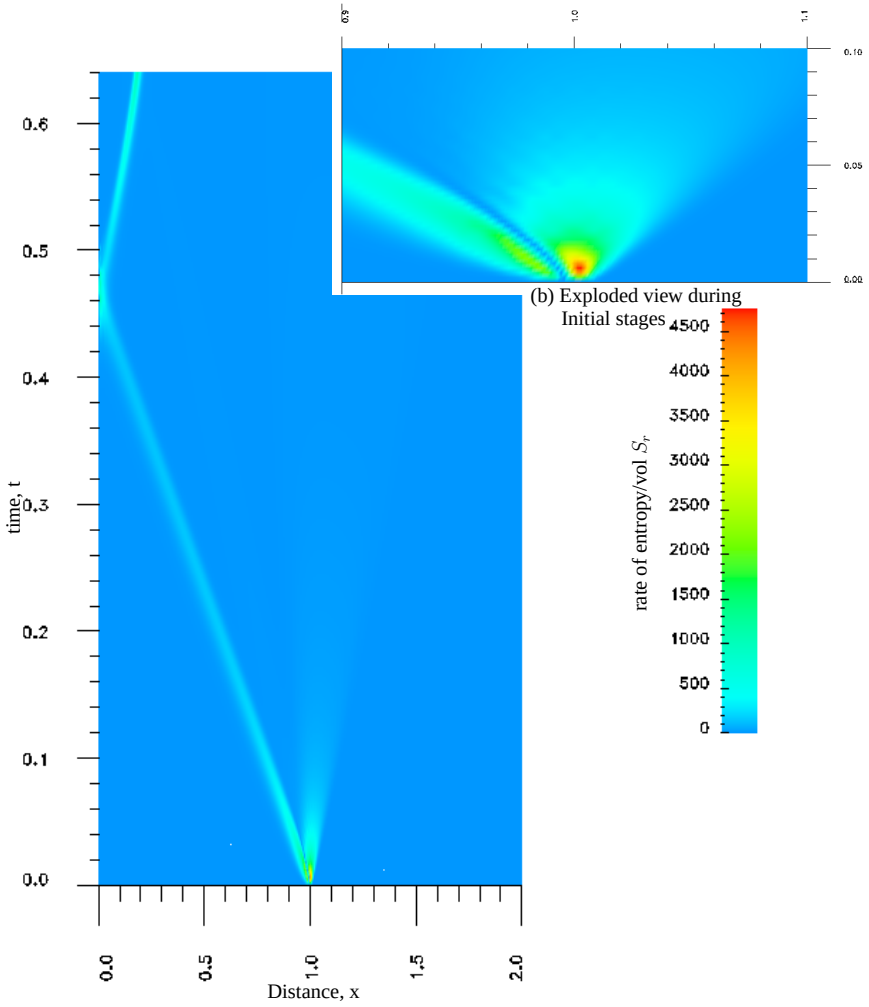

(a) Full Evolution

(b) Exploded view during Initial stages

Figure 5.13: Space-time plot of evolution of S_r

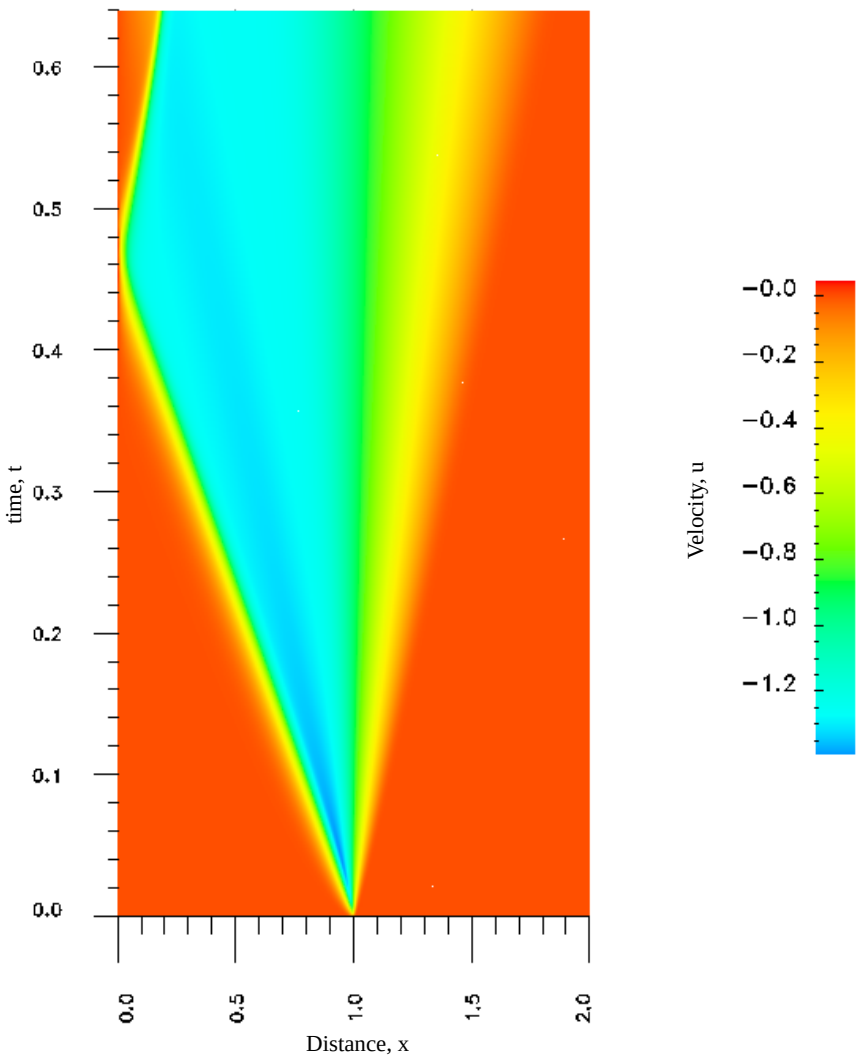

Figure 5.14: Space-time plot of evolution of velocity, u

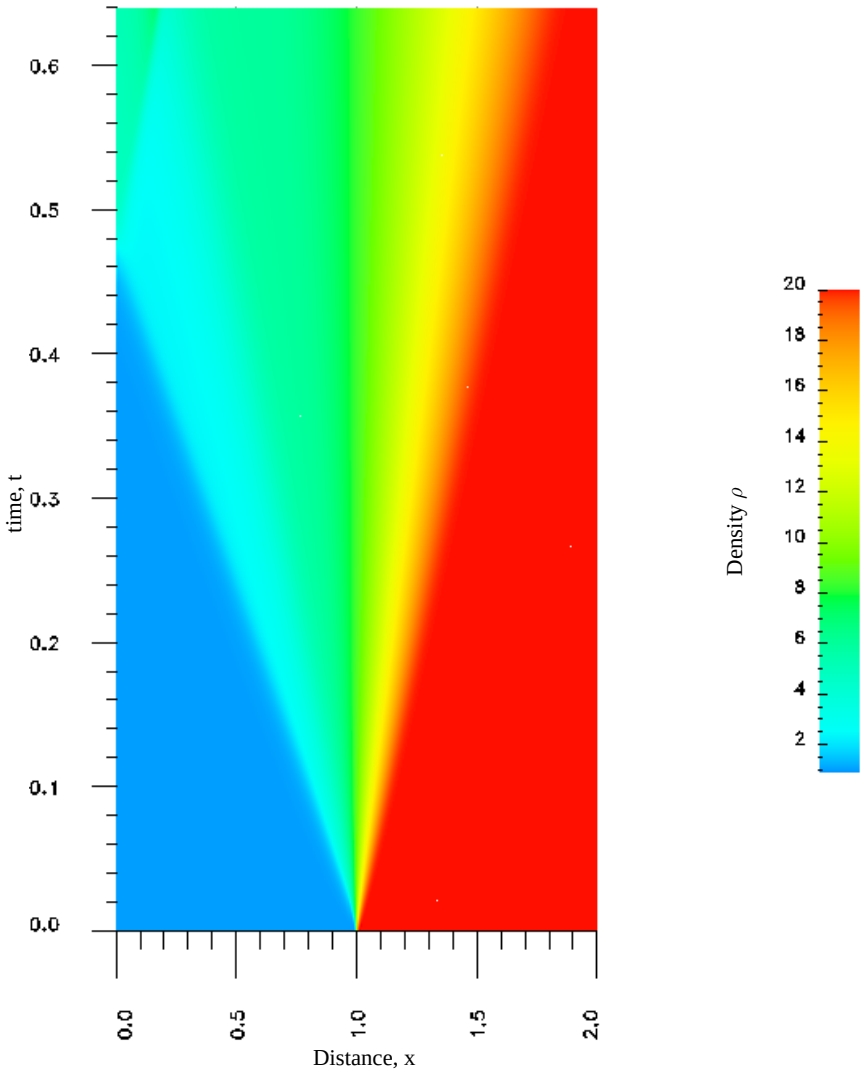

Figure 5.15: Space-time plot of evolution of density, ρ

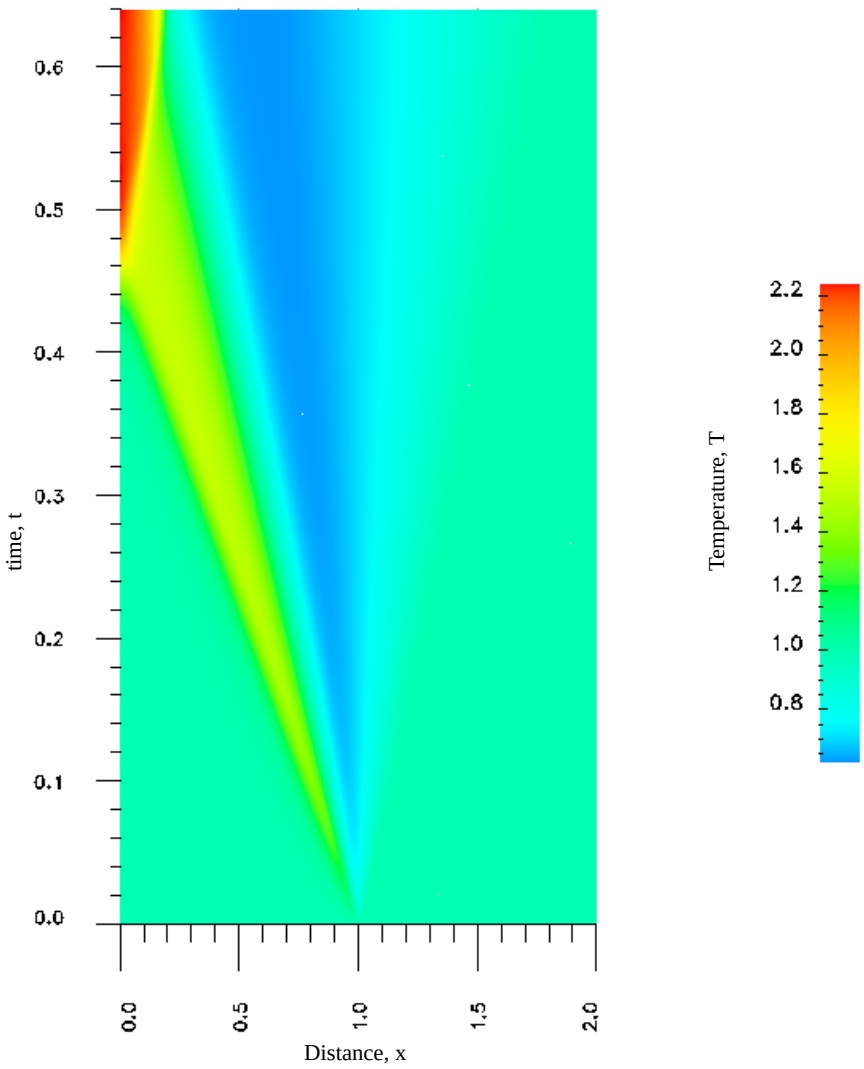

Figure 5.16: Space-time plot of evolution of temperature, T

Case(b) Repeated shock reflections, interactions and propagation

In this section we consider the same Riemann shock tube problem as in (a) with identical boundary conditions, initial conditions, p-levels and $L = 2$ to study repeated shock reflections from the impermeable and non-conducting boundaries A and B (figure 5.1). The evolution is computed for 250 time steps (with $\Delta t = 0.02$ giving a total dimensionless time of 5 units (0.02189μs)). For each space-time step $|g_i| \leq O(10^{-6})$ and $I \leq O(10^{-8})$ are maintained for time accuracy of the evolution. Figures 5.17-5.20 show space-time evolutions of S_r, u, ρ and T.

Consider evolution of S_r in figure 5.17. The paths $a - b$ shows evolution and steady propagation of shock. At b shock reflection occurs from boundary A. The reflected shock interacts with the constant density plug and eventually enters the rarefaction region ($x > 1$). Upon further evolution the shock is reflected at the boundary B. This reflected shock propagates along $c - d$. At d, it reaches boundary A again where upon reflection it propagates along $d - e$. We observe that the straight path $a - b$ indicates pure propagation without any interaction. Along $b - c$ and $c - d$ the curved nature of the S_r path shows interaction of the shock with existing disturbance along its path. Sustained S_r during entire process confirms (i) that the shock is maintained i.e., remains intact (ii) and that the computational process is free of any major numerical dispersion that could influence the rate of entropy production per unit volume S_r during the evolution.

Space-time evolution of velocity in figure 5.18 is synchronous with evolution of S_r i.e., points a, b, c, d and e correspond to various instances of reflection and interaction in figures 5.17 and 5.18. The entire velocity profile in figure 5.18 in the

shock zone corresponds to the S_r profile in figure 5.17. We note positive u velocity in the significant portion of zone bcd in figure 5.18. Repeated shock reflections lower the maximum velocity in the domain as seen in figure 5.18.

Space-time evolution of density in figure 5.19, also shows distinct variations with reflections and interactions at locations a, b, c, d and e. As evolution proceeds the maximum density progressively falls below 20 as seen by diminishing intensity of red zones for higher values of time.

In the space-time evolution of temperature shown in figure 5.20 we note the highest temperature occurs at boundary A upon first reflection which conducts during evolution (red zone). The shock path $a - b - c - d - e$ is clearly observed here as well. As evolution proceeds the maximum temperature in the tube domain decreases as expected.

This study clearly demonstrates the high accuracy and unconditional stability of the computational process in h, p, k framework for viscous shock flows. The sustained value of S_r during entire evolution with three reflections and complex interactions demonstrate that viscous shock flows in conducting medium can indeed be simulated accurately with physical transport properties and without any problem dependent special treatments and that the computational process is free of any appreciable numerical dispersion. Very low values of $|g_i|$ and I during entire evolution ensure good time accuracy of the evolution.

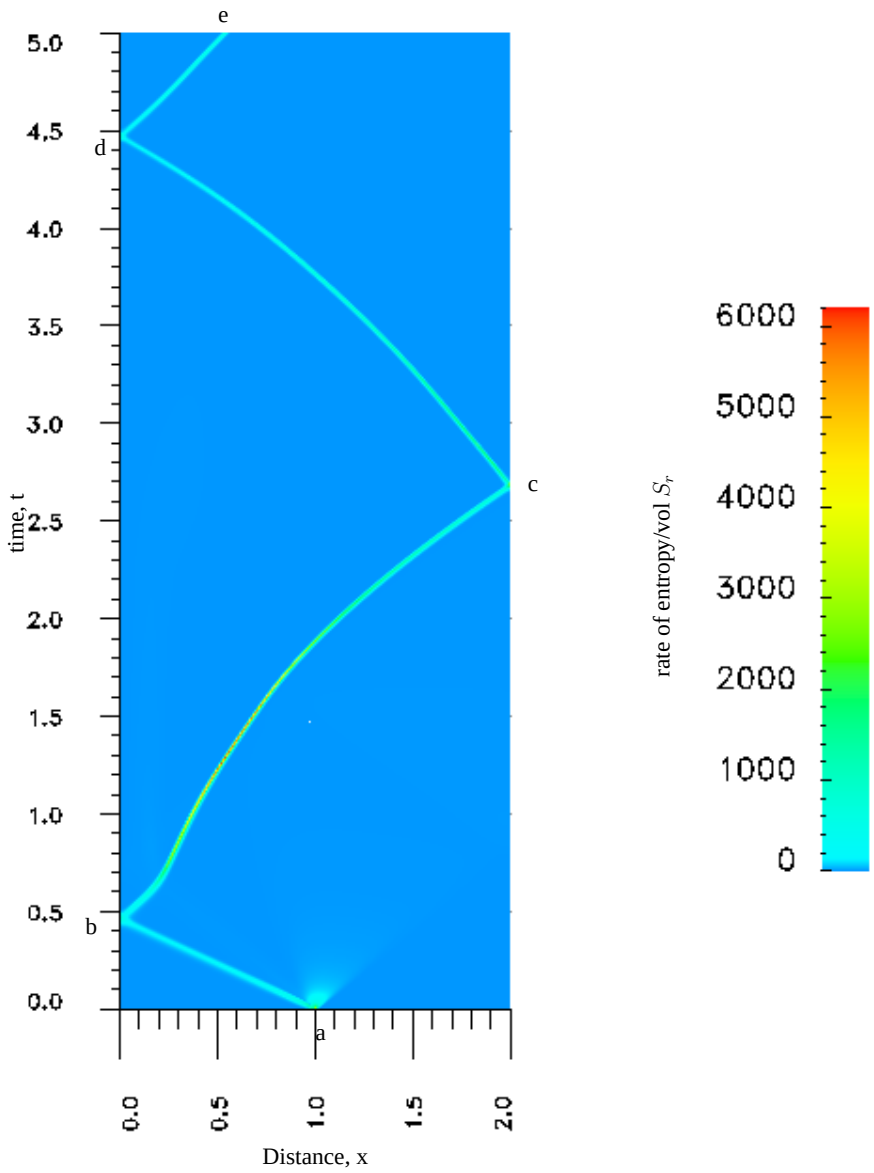

Figure 5.17: Space-time plot of evolution of S_r

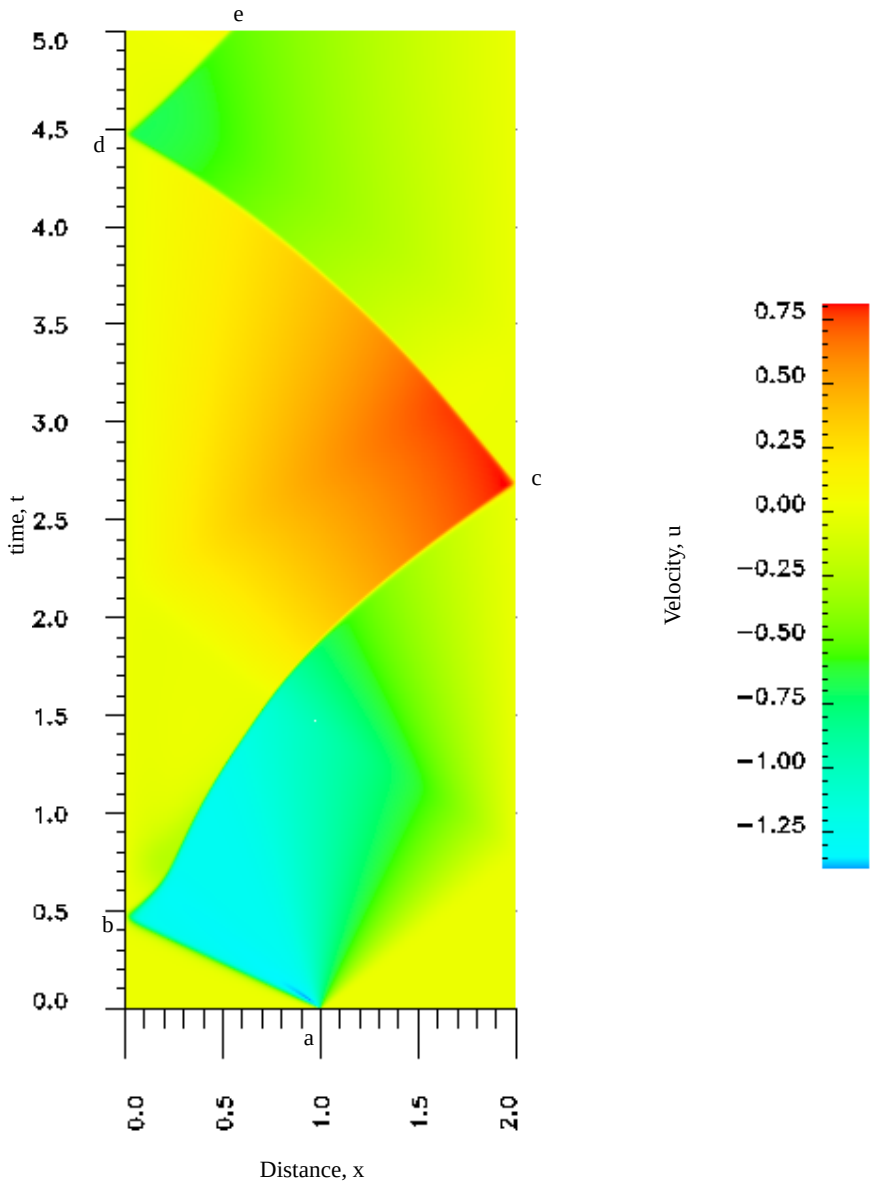

Figure 5.18: Space-time plot of evolution of velocity, u

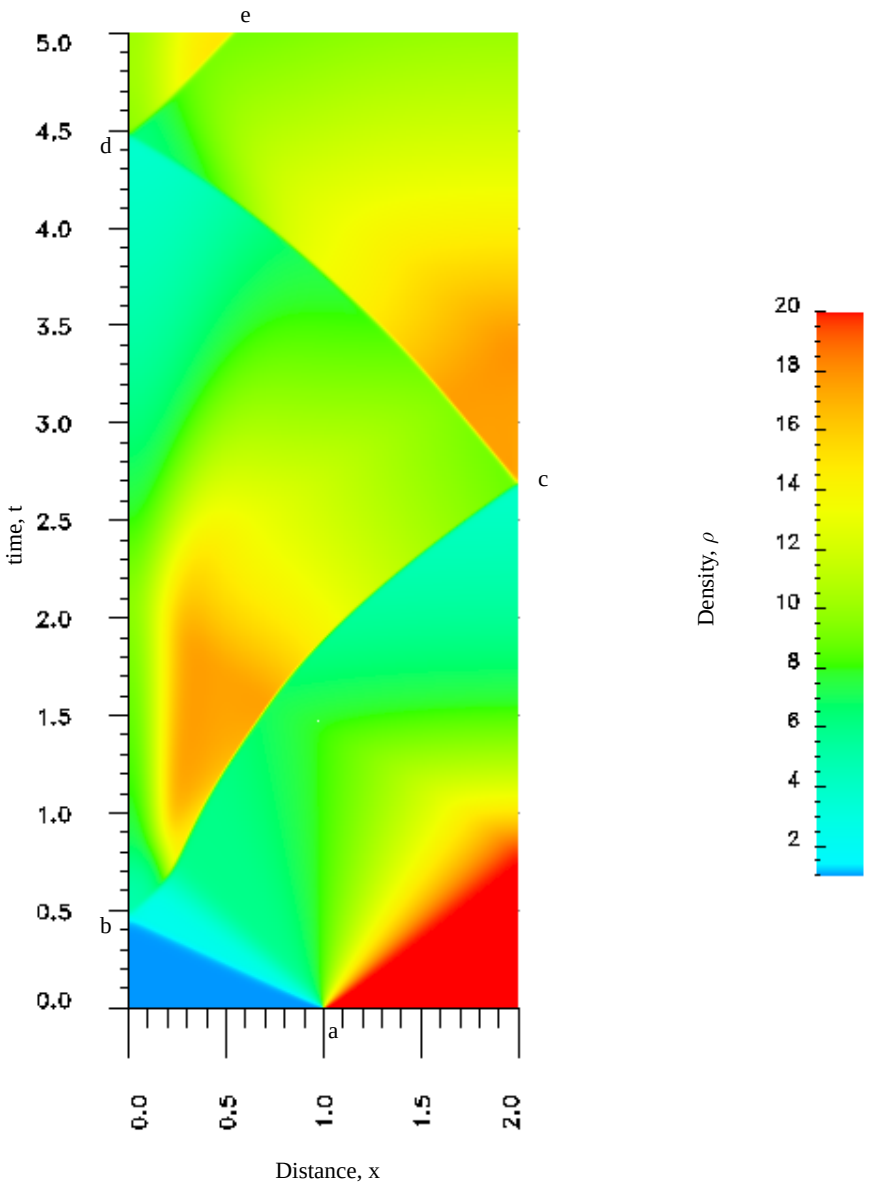

Figure 5.19: Space-time plot of evolution of density, ρ

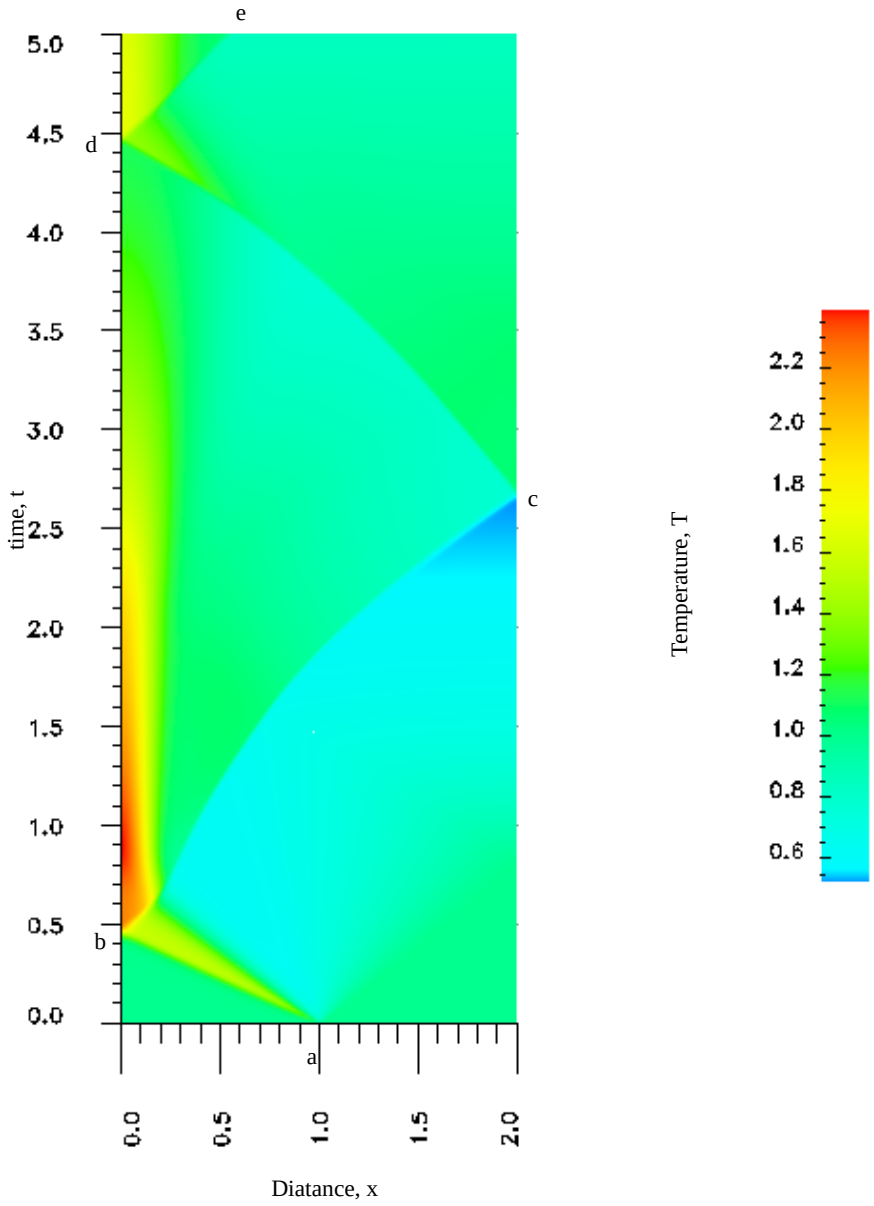

Figure 5.20: Space-time plot of evolution of temperature, T

5.3 Riemann shock tube : Real gas Laws

5.3.1 Real gas behavior and possibility of rarefaction shocks

Though ideal gas equation of state predicts the behavior of gases reasonably in the normal temperature and pressure ranges, there are large deviations from ideal gas behavior at or near the critical point. For the heavy molecular weight gases at high density values, the molecular interactions are large and intermolecular attractive forces must be accounted. The Van der Waals equation of state is a second order approximation that considers the size of molecules and correction of pressure due to intermolecular forces. Other real gas models exhibit behaviors similar to Van der Waals equation of state. All real gas models exhibit inflection point on $p - v$ diagram near the critical point.

Anomalous behaviors of the heavy molecular weight gases have been reported near the gas-liquid critical point. Long before the critical point is reached the gaseous isotherms show an inflection. For a fluid with sufficiently high specific heat and the specific heat ratio close to unity, the isentropes and isotherms do not differ appreciably from each other. We can therefore expect that the isentropes will have an inflection outside the two-phase region where the second derivative will have negative sign. Figure 5.21 (taken from Zeldovich [80]) shows a saturation curve which is the two-phase region and a second curve which is the locus of the points of the inflection of the isentropes $(\partial^2 p/\partial V^2)_s = 0$. When the second derivative $\partial^2 p/\partial V^2$ is negative over some part of the isentropic curve, then the shock waves may be expected to exhibit some unusual behavior. We consider a gas with thermodynamic properties such that $\partial^2 P/\partial V^2$ is negative at least over some

part of the isentropic curve.

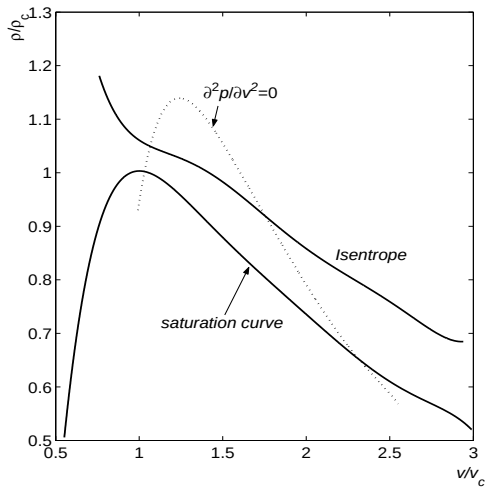

Figure 5.21: Isentrope with anomalous convexity in Van der Waals equation of state

A review of published work on the theory of formation of single phase rarefaction shock wave and numerical computations of such behaviors is presented in the following. The first authors to suggest existence of dense gases by demonstrating thermodynamic regions referred to as negative non-linearity were Beth [81] and Zeldovich [80]. In 1971, Thompson [82] showed that the change in sign of fundamental derivative ($\Gamma = -\frac{v}{2}(\frac{\partial^2 p}{\partial v^2})_s/(\frac{\partial p}{\partial v})_s$) governs nonlinear dynamics of gases. In perfect gas regime, $\Gamma > 0$ is said to exhibit positive nonlinearity. In dense gases where specific heat ratios are higher, the isentropes have inflection near critical point regions, which results in $\Gamma < 0$ and hence the negative nonlinearity. These fluids where negative nonlinearity occurs above the saturation curve are referred to as Bethe-Zeldovich-Thompson (BZT) fluids by Cramer, M.S. [83]. Thompson and Lambrakis [84] analytically showed specific

examples of existing fluids where negative nonlinearity may be observed. Cramer, M.S. [85] reported few commercially available fluorocarbons fluids with negative Γ. Thompson & Carafano [86] also experimentally observed non-classical flow phenomena including expansion shocks in multi-phase flows. Cramer & Kluwick [87] and Cramer [88] examined dissipative structure of weak shocks in the dense gas regime analytically. Fergason & Argrow [28] presented numerical simulation of single phase one-dimensional shock-tube flows. In this paper the authors present an approach for generating initial conditions required to produce a triple discontinuity wave in shock tube, where one discontinuity is addressed as rarefaction shock wave. In this work Rankine-Hugoniot relations are used to generate various states across the waves by the choice of three parameters. Using these three parameters for Van Der Waals gas, the initial conditions for triple-discontinuity solutions are produced. Brown & Argrow [89] presented the extension of their previous work by studying flow of dense gases with obstacles in two-dimensional shock tube. There are many published works showing the behavior of transport properties of dense gases near critical region. Many flow characteristics are studied for dense gases in internal and external flows. Kluwick [90] points out that the transonic flows of dense gases around turbine blade cascades may lead to increase of the lower critical Mach number regime resulting in narrowing the loses due to shocks. Monaco & Cramer [91] also observed that these flows can result in significant reduction in adverse pressure gradients associated with the collision of compression waves neighboring turbine blades.

The purpose of the study undertaken in the research for the heavy molecular

weight gases discussed above is multifold.

(1) Simulations for time evolutions with actual transport properties

   (a) near critical point such that a part of the initial conditions or all of the initial conditions are in the critical zone for

      (i) isothermal initial conditions

      (ii) non-isothermal initial conditions

   (b) Initial conditions away from the critical point

(2) To determine from these simulations the nature of the waves in low density and high density regions, and to establish if and when shocks exist and propagate in rarefaction and low density regions

The determination of the existence of shocks and their propagation requires quantification over and beyond graphical presentation and observation of the nature of the waves. The material presented here (in parallel to the definition of shock presented earlier in the section of ideal gas law) is aimed towards establishing a quantitative criterion that ensures the formation of shocks and their propagation. As in case of ideal gas, here we use S_r for this purpose.

Figure 5.22 shows schematic of a shock tube with high density (ρ_h) region separated from the low density region (ρ_l) by a diaphragm. Upon rupture of the diaphragm the waves AB and CD initiate in the high density and low density region. We note the following :

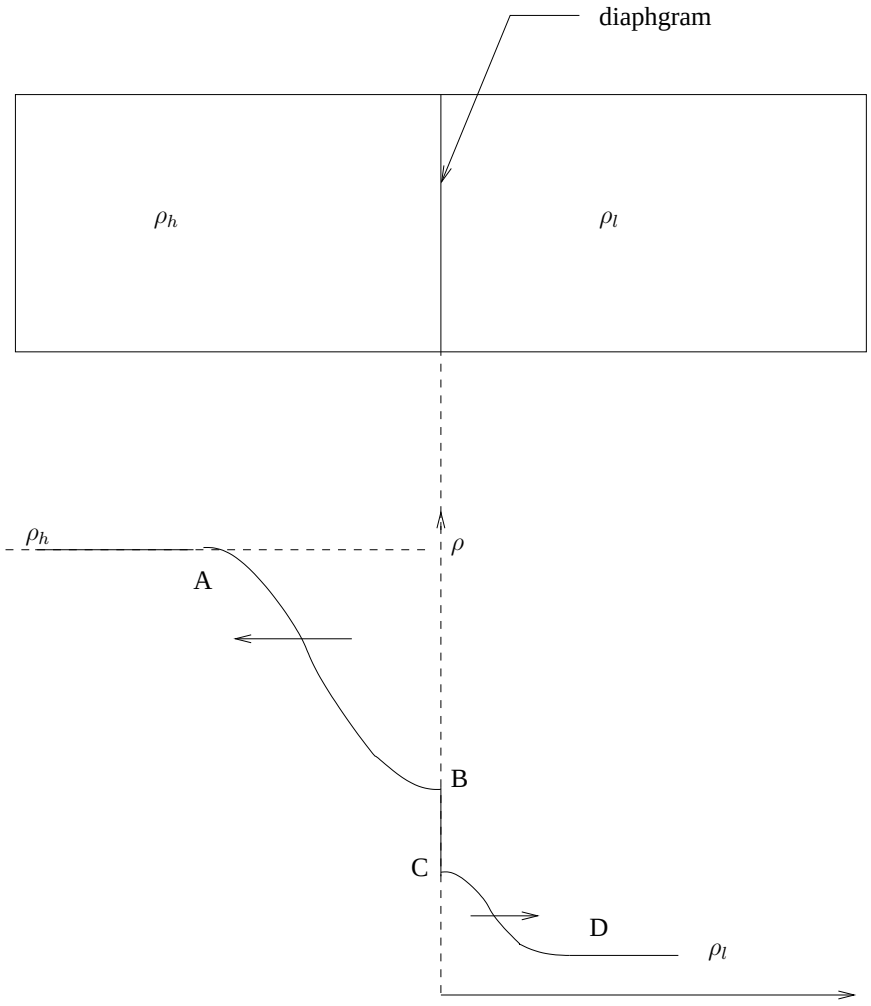

Figure 5.22: 1D-Riemann shock tube with density distribution for some value ot time

(I) A shock formation in the low density region requires the movement of the end C of the wave at a higher speed than D. This would result in progressive compression waves of higher and higher speeds piling on each other and eventually becoming steady at which stages the steepening of waves due to compression is in equilibrium with the dispersion process and we have a shock which will sustain and propagate as long as this equilibrium is maintained. On the other hand if the dispersion of wave is dominated over the steepening due to the compression, the wave will disperse and there will be no shock formation.

(II) Exactly same arguments as in (I) hold in the rarefaction region except that in this case the dispersion of the wave due to rarefaction is quite significant and thus for a shock to form and propagate in the rarefaction region, the velocity of point B of the wave must be greater than that of A but more importantly the steepening process must overcome the dispersion of the wave.

(III) We observe that upon the rupture of the diaphragm if we monitor the rate of entropy production per unit volume (S_r) then there is S_r in rarefaction region (left of diaphragm) as well as in low density region (right of diaphragm). In all cases studied during this research including ideal gas, we find that maximum S_r for the first several time steps (immediately upon the rupture of the diaphragm) occurs in the rarefaction region. This of course, does not mean that there is a shock in the rarefaction region. During time evolution we monitor S_r to see when S_r becomes stationary first, so this marks the

possibility of appearance of a shock. Upon further evolution, if this stationary value of S_r persists, then we have a propagating shock.

(IV) Thus space-time evolution of S_r is critical in detecting shocks and their propagation. Value of S_r is a measure of the strength of the shock. In the numerical studies presented here for real gas models we use this criterion to show existence of the shocks or their absence.

5.3.2 Numerical Studies : Real gas model ; Van der Waals equation of state

In this section numerical studies are presented for 1D Riemann shock tube using FC70 [28] as a medium. The properties of FC70 given in the following.

$$\hat{\rho} = 621.19\ \mathrm{Kg/m^3}, \hat{\mu} = 0.8324 \times 10^{-4}\ \mathrm{Pa-s}, \hat{\mathrm{k}} = 0.0001636\ \mathrm{N/s/K}$$

$$\hat{R} = 286.99\ \mathrm{J/kg/k}, \hat{\mathrm{c}}_{\mathrm{v}} = 1202.036\ \mathrm{J/kg/k}$$

$$\hat{a} = 11.15216\ \mathrm{Pa-m^6/Kg^2}, \hat{\mathrm{b}} = 0.0005362\ \mathrm{m^3/Kg}(\text{VW model constants})$$

$$\hat{R} = 10.26\ \mathrm{J/Kg/K}$$

We use the following reference quantities,

$$L_0 = 8.62 \times 10^{-8}\ \mathrm{m}, \rho_0 = \hat{\rho}, \mu_0 = \hat{\mu}, \mathrm{k}_0 = 0.000163, \mathrm{c_{v0}} = 10.126$$

$$u_0 = \sqrt{R_0/T_0} = 78.474\ \mathrm{m/s}, \mathrm{T}_0 = 608.15\ \mathrm{K}, \mathrm{R}_0 = \hat{\mathrm{R}}, \tau_0 = \rho_0 \mathrm{u}_0^2 = 0.38254 \times 10^7$$

$$p_0 = 1.033 \times 10^6\ \mathrm{Pa}$$

We note that p_0 and k_0 are chosen at the critical point. With these reference values we have the following values of the dimensionless parameters.

$$Re = 50.481, Br = 5.1521, Ec = 1.000, c_v = 118.71, k = 0.99633, R = 1.000$$

The ratio $\hat{c}_v/\hat{R} = 118 >> 20$, which is considered to be threshold for the possibility of the shocks in the rarefaction region. The numerical studies are divided into the following groups.

(a) Initial conditions (partly or completely) in the critical zone (isothermal)

(b) Initial conditions (partly or completely) in the critical zone (non-isothermal)

(c) Initial conditions far away from the critical zone (isothermal)

(d) Initial conditions (partly or completely) in the critical zone (non-isothermal) with reduced viscosity

Case (a) Initial conditions partly inside the critical zone (Isothermal)

We consider a density ratio $\rho_h\rho_l = 0.8333/0.3846$ with $u = 0$ and isothermal initial conditions of $T = 1$ and $L = 4$. The two ends of the shock tube are assumed impermeable and non-conducting. The diaphragm is located at the center of the domain. The left of the diaphragm is high density region and the right of it is low density zone. The spatial discretization consists of 801 uniform mesh using space-time $C^{ij}({}^n\bar{\Omega}^e_{xt})$ p-version elements with nine nodes. The density distribution of 0.8333 to 0.3846 is applied in a continuous and differentiable manner over an element symmetrically located about the diaphragm. The element characteristic length in the spatial direction is $h_x = \Delta x = 0.00499$. We consider $\Delta t = 0.005$ for a space-time strip and consider local approximations of class $C^{11}({}^n\bar{\Omega}^e_{xt})$ at $p = 7$ in space and time.

Figure 5.23 shows a $p - v$ diagram with initial conditions. Clearly we observe that a portion of the initial conditions is in the critical zone for ICs as well as during the entire evolution; a requirement for the rarefaction shocks to exist. The evolution is computed for 200 time steps using a space-time strip with time marching. $|g| \leq O(10^{-6})$ and $I = O(10^{-6})$ or lower for each space-time strip ensure good accuracy of the computed solution. Plots of $p - v$ during the entire evolution shown in figure 5.23 confirm that some portion of $p - v$ curve remains in the critical zone during the entire evolution. Figures 5.24-5.26 show evolutions of ρ, u and T over the spatial domain during the entire evolution. Only the results for the first time increment, 10^{th} and then every 10^{th} time increment up to 200^{th} time increment are shown in these figures. From the density evolution in figure 5.24, it appears that fronts in rarefaction as well as low density zone are dispersing, however, during the later stages of the evolution this cannot be ascertained conclusively. Figures 5.27-5.30 show space-time evolution of S_r, u, ρ and T. The exploded view of S_r in figure 5.27b confirm the maximum S_r in rarefaction region. Both sides of the diaphragm show S_r which disperses from 14.0 to 0.4 and continues to do so as evolution proceeds, indicating the lack of formation of a shock in the rarefaction as well as low density regions. Velocity evolution shows waves of similar speeds in either sides of the diaphragm. Compression waves in the low density region increase density where as in the rarefaction region it continues to decrease. Initial isothermal conditions show same temperature upon commencement of the evolution, a temperature rise in low density region due to compression waves and likewise a decrease in temperature in the rarefaction region.

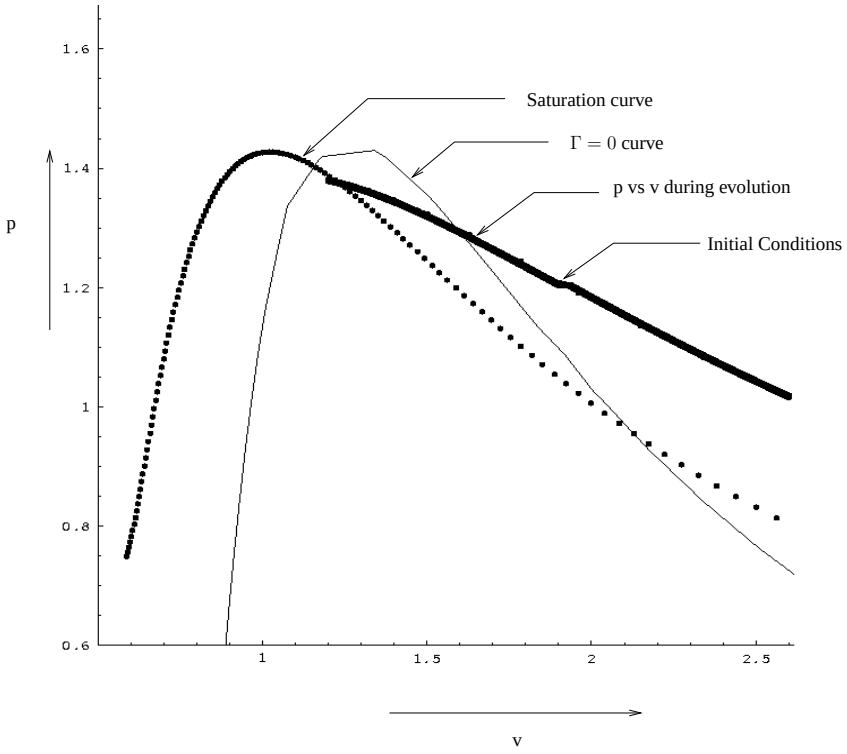

Figure 5.23: p versus v for case(a) : Isothermal ; Initial Conditions inside the critical zone

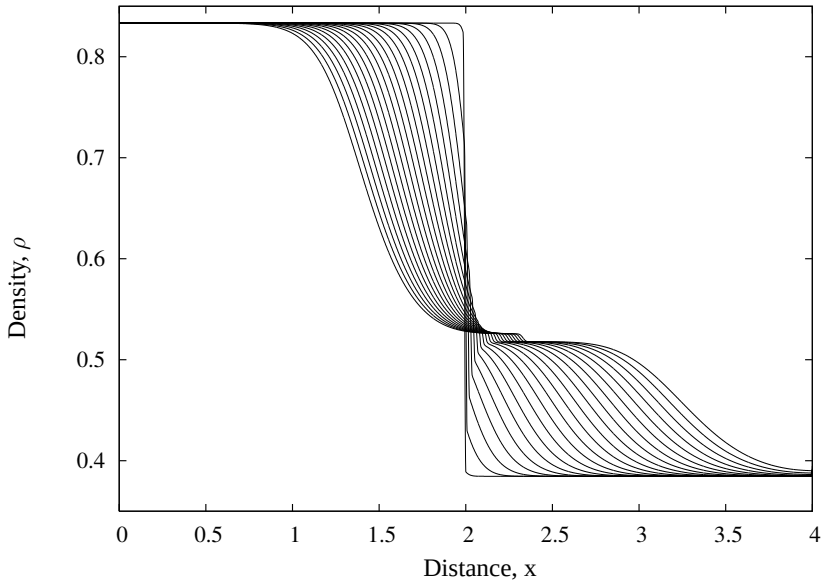

Figure 5.24: Evolution of Density for case(a) : Isothermal ; Initial Conditions inside the critical zone

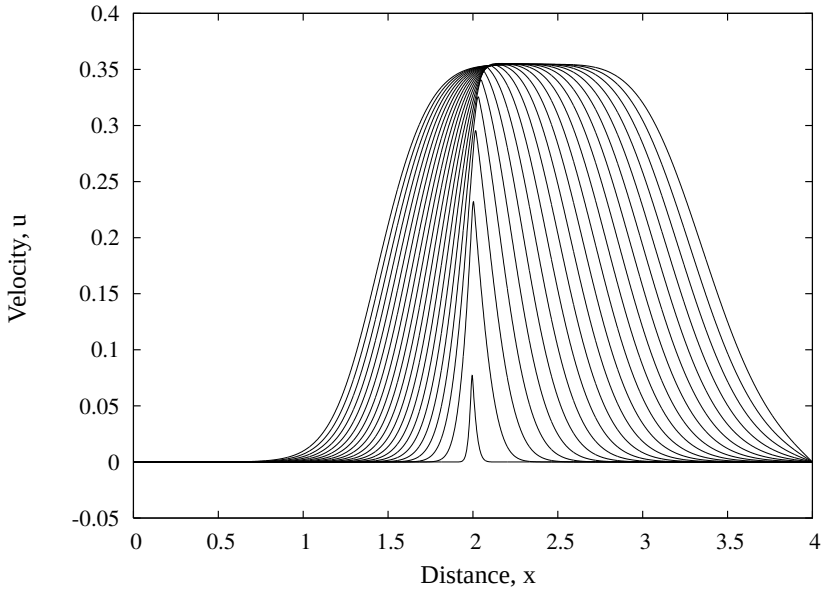

Figure 5.25: Evolution of Velocity for case(a) : Isothermal ; Initial Conditions inside the critical zone

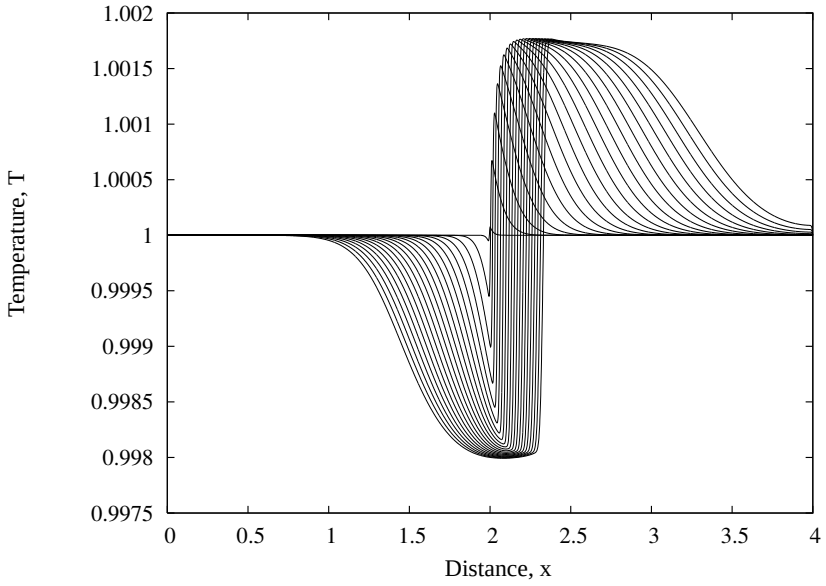

Figure 5.26: Evolution of Temperature for case(a) : Isothermal ; Initial Conditions inside the critical zone

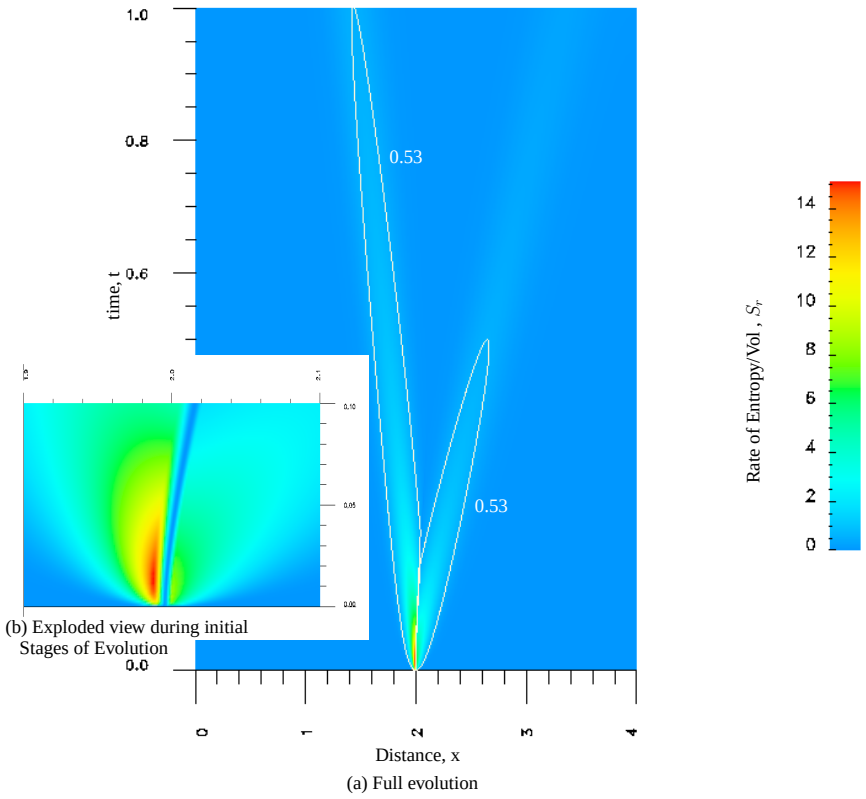

Figure 5.27: Space-time plot of evolution of S_r ; case(a) : Isothermal , Initial Conditions inside the critical zone

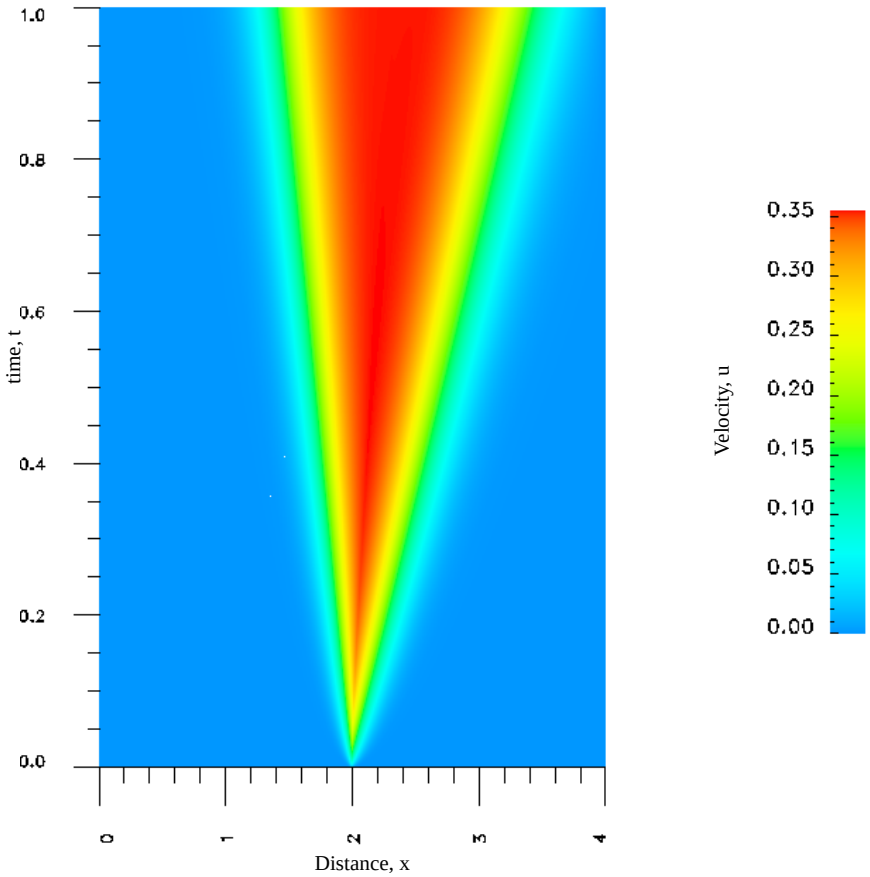

Figure 5.28: Space-time plot of evolution of velocity, u ; case(a) : Isothermal , Initial Conditions inside the critical zone

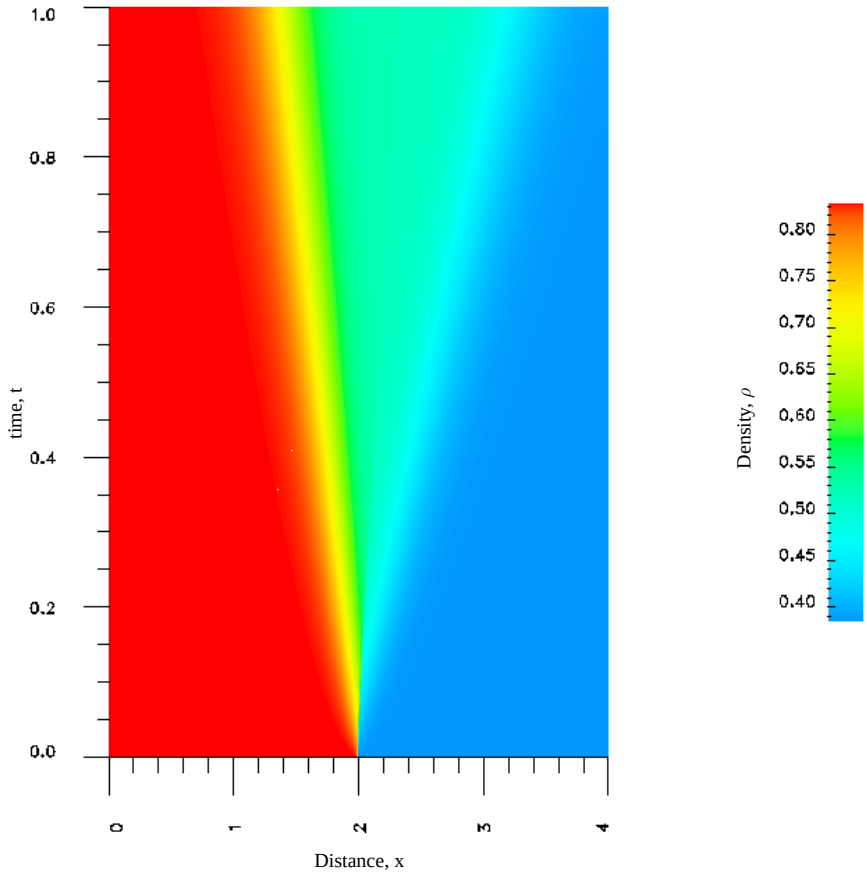

Figure 5.29: Space-time plot of evolution of density, ρ ; case(a) : Isothermal , Initial Conditions inside the critical zone

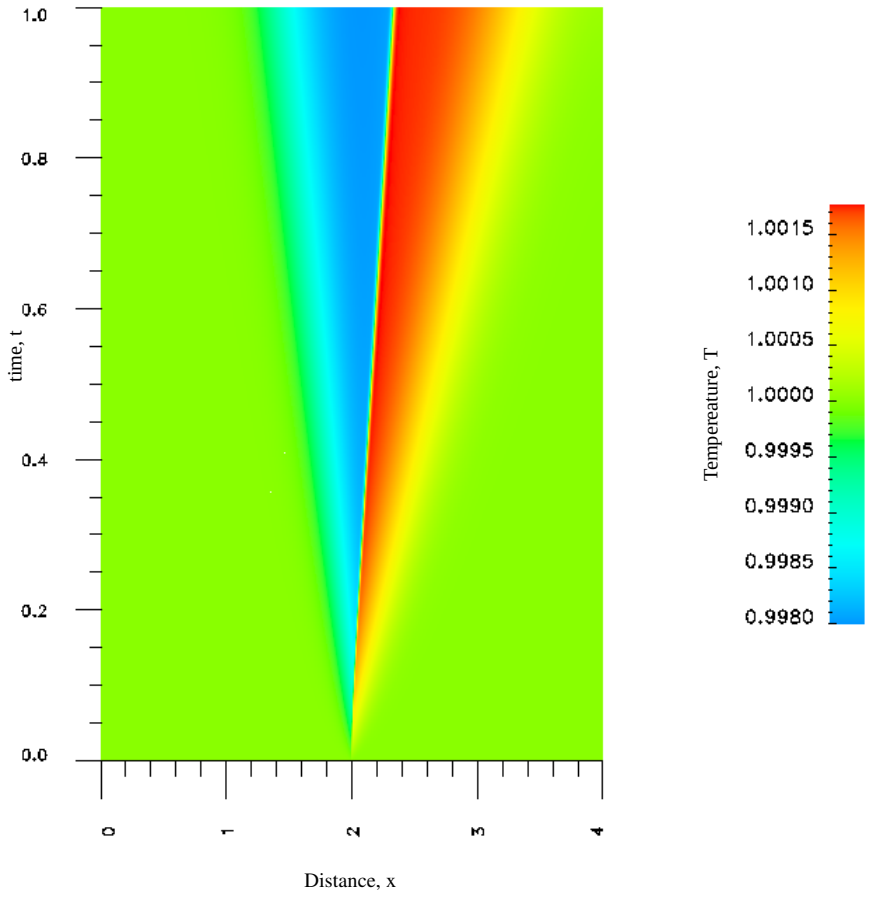

Figure 5.30: Space-time plot of evolution of temperature, T ; case(a) : Isothermal , Initial Conditions inside the critical zone

Case (b) Initial conditions partly inside the critical zone (Non-isothermal)

In this study all conditions, discretizations, number of time steps, $|g_i|$, I, solution class, p-levels and initial conditions remain the same as in case (a) except the initial conditions for the temperature are not isothermal. The high density region (left of diaphragm) is at T=1.0 at t=0 where as the low density region (right of diaphragm) is at $T = 1.05$ for t=0. The temperature distribution from $T = 1.0$ to $T = 1.05$ is applied over an element centered symmetrically to the diaphragm in a continuous and differentiable fashion. Evolution is computed for 200 time steps using solutions of class $C^{11}({}^n\bar{\Omega}^e_{xt})$ with p-level of 7 in space and time.

Figure 5.29 confirms that the initial condition (partially) and $p - v$ curve during entire evolution remains partially in the critical zone. Figures 5.32-5.34 show evolution of ρ, u and T over the spatial domain for the entire evolution. From figure 5.32, we observe a constant density zone in the lower density region followed by a constant density plug behind the traveling waves. The waves in the rarefaction are smooth and disperse quickly during initial stages. The continuously dispersing waves in the low density region are rather obvious indicating the lack of shock formation. In the rarefaction zone a clear assessment of the nature of waves specially during later stages of the evolution is rather difficult. Velocity evolution is smooth and clearly indicates faster moving fronts in the low density zone compared to high density zone. Temperature distribution show sharp change at the interface.

Figures 5.35-5.38 show space-time evolutions of S_r, u, ρ and T. From figure 5.35 we note that maximum S_r occurs in the rarefaction region (figure 5.35b). Upon evolution S_r disperses in rarefaction region as well as low density region

establishing the lack of shocks in either regions. The evolutions of u and ρ follow the usual patterns as in case (a). It is interesting to note that the contact zones keep the high temperatures isolated in the low density zone.

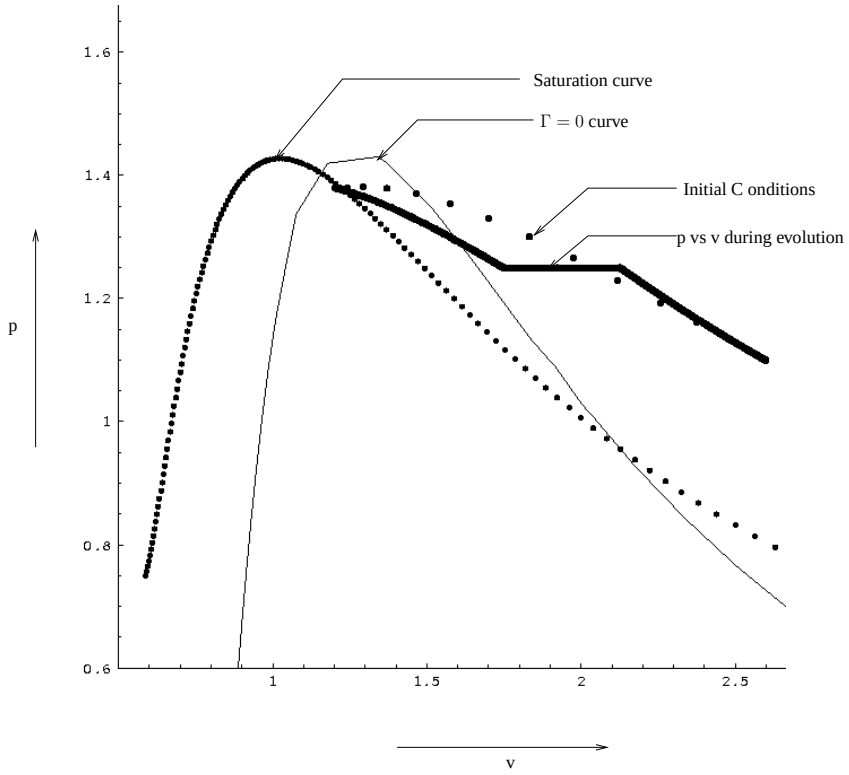

Figure 5.31: p versus v for case(b) : Non-isothermal ; Initial Conditions inside the critical zone

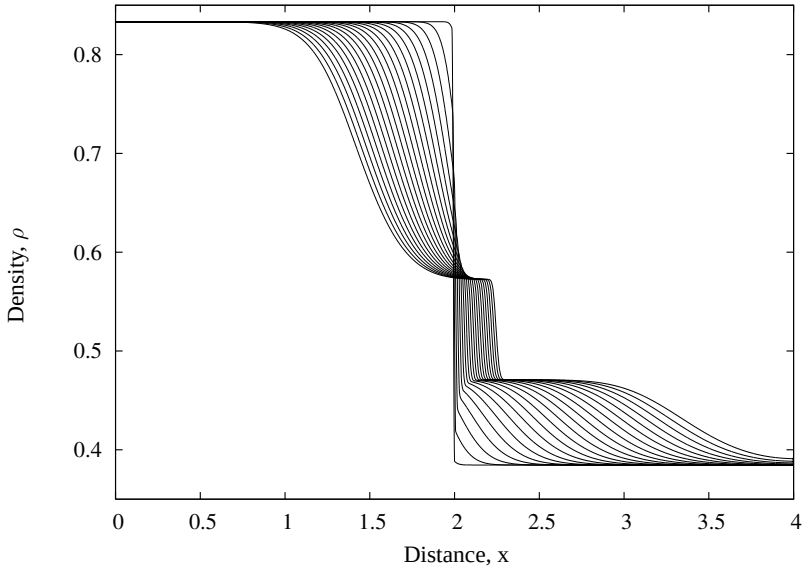

Figure 5.32: Evolution of Density for case(b) : Non-isothermal ; Initial Conditions inside the critical zone

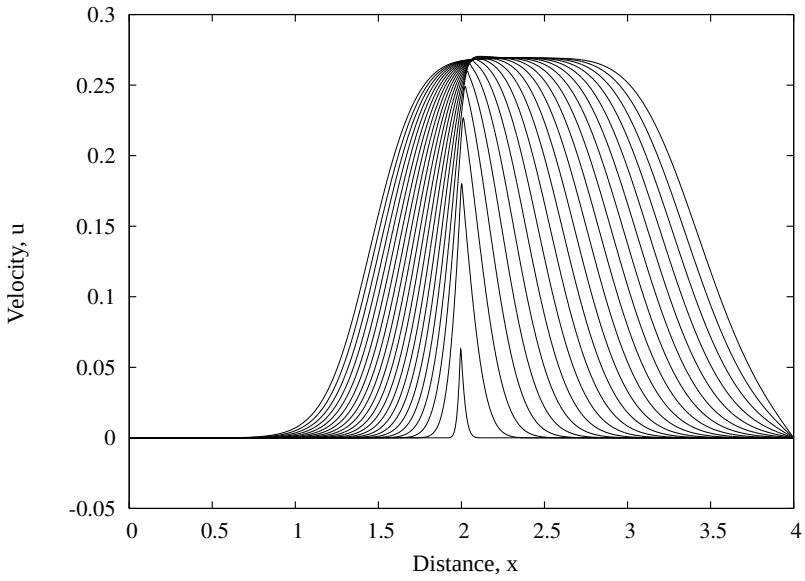

Figure 5.33: Evolution of Velocity for case(b) : Non-isothermal ; Initial Conditions inside the critical zone

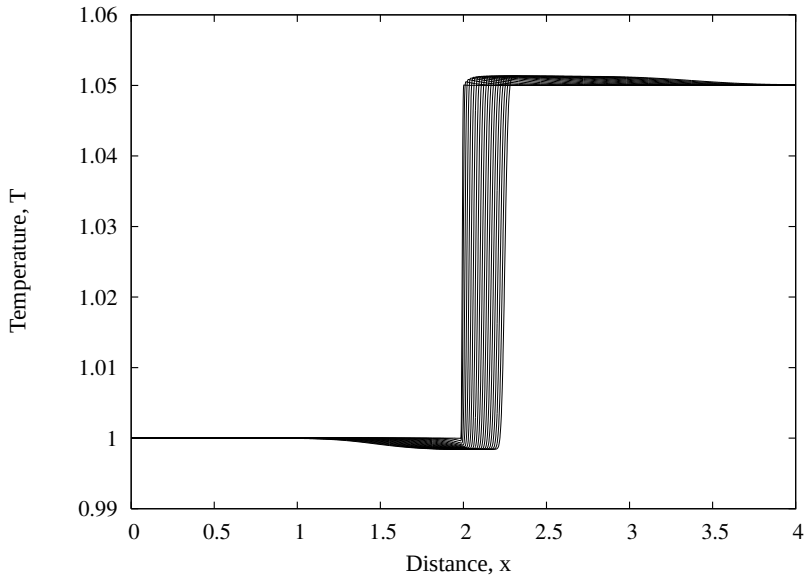

Figure 5.34: Evolution of Temperature for case(b) : Non-isothermal ; Initial Conditions inside the critical zone

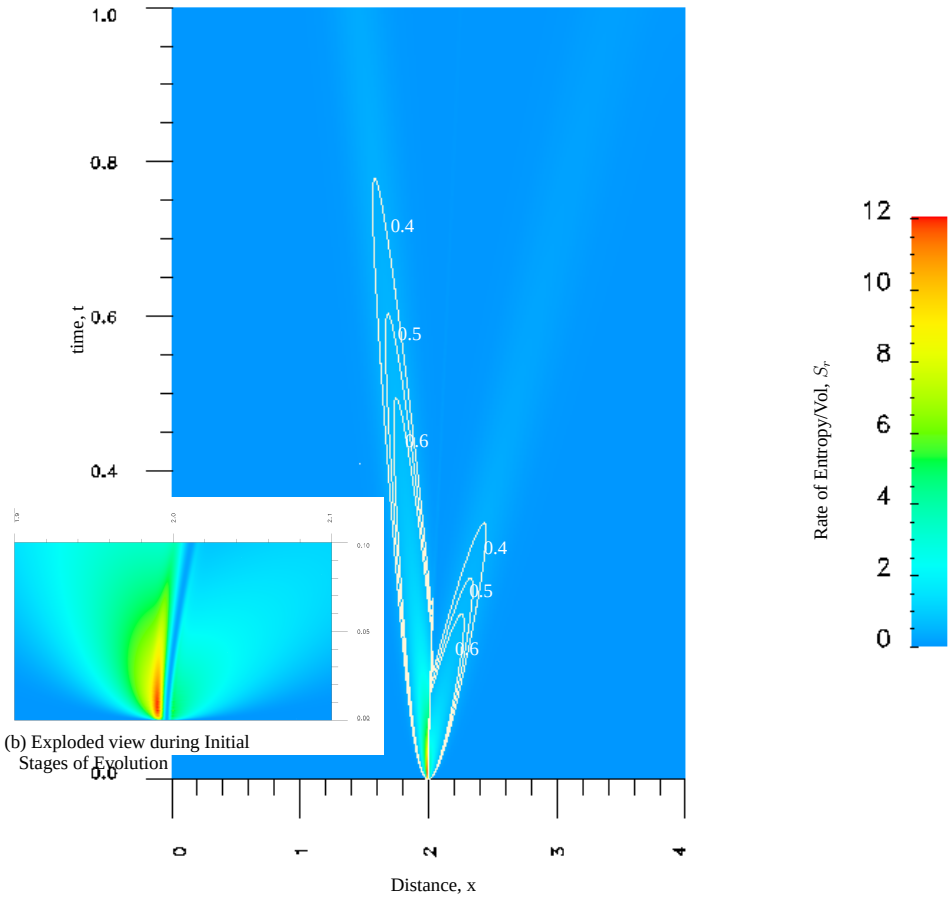

(b) Exploded view during Initial Stages of Evolution

(a) Full Evolution

Figure 5.35: Space-time plot of evolution of S_r ; case(b) : Non-isothermal , Initial Conditions inside the critical zone

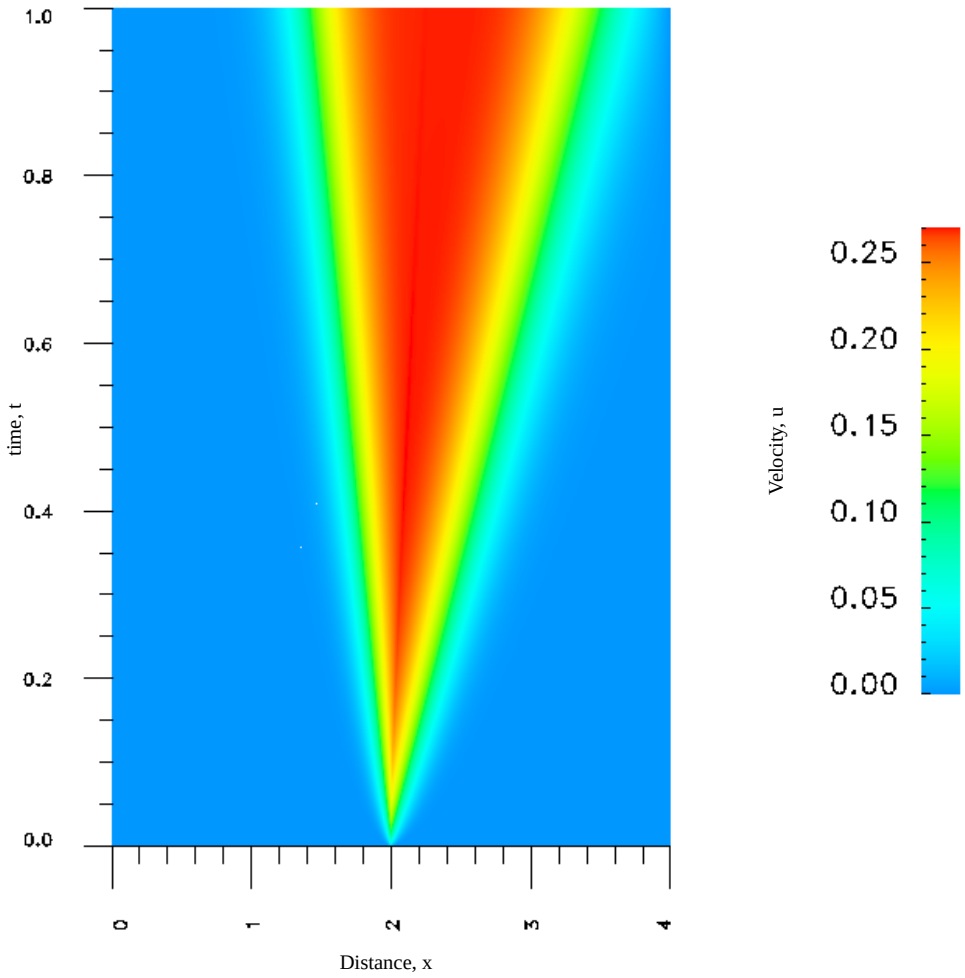

Figure 5.36: Space-time plot of evolution of velocity, u ; case(b) : Non-isothermal , Initial Conditions inside the critical zone

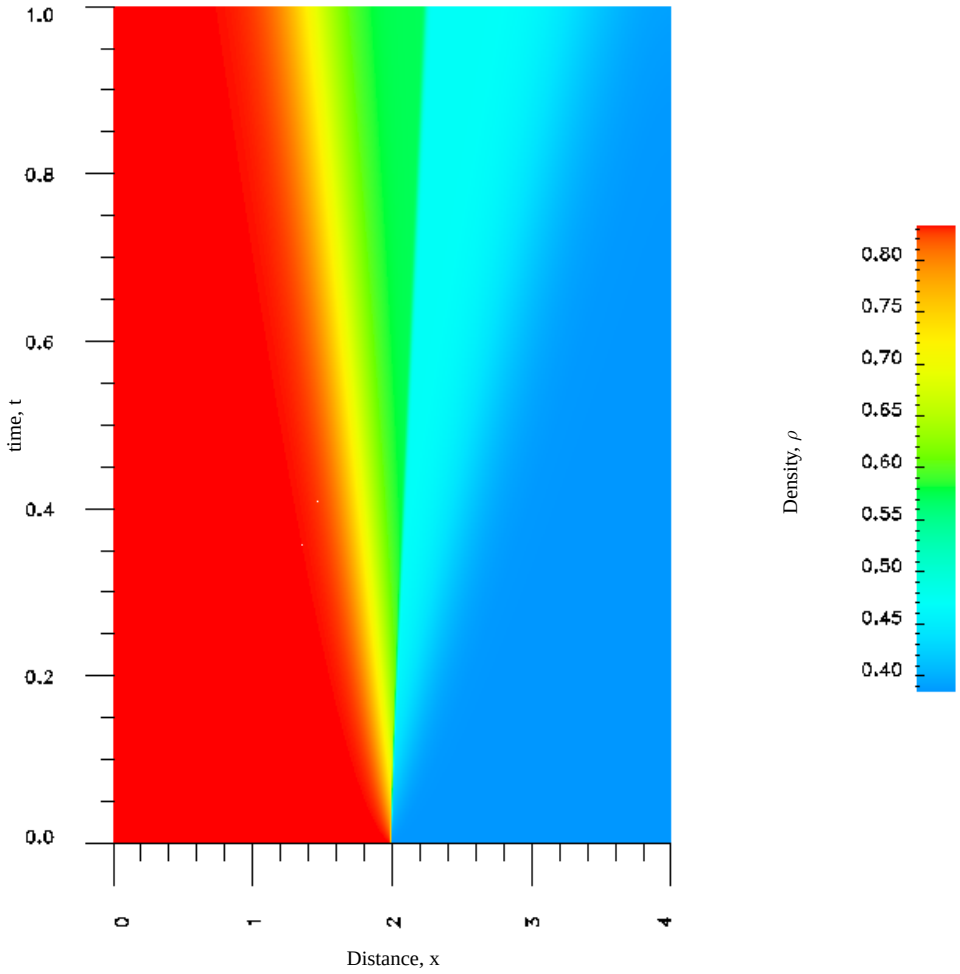

Figure 5.37: Space-time plot of evolution of density, ρ ; case(b) : Non-isothermal , Initial Conditions inside the critical zone

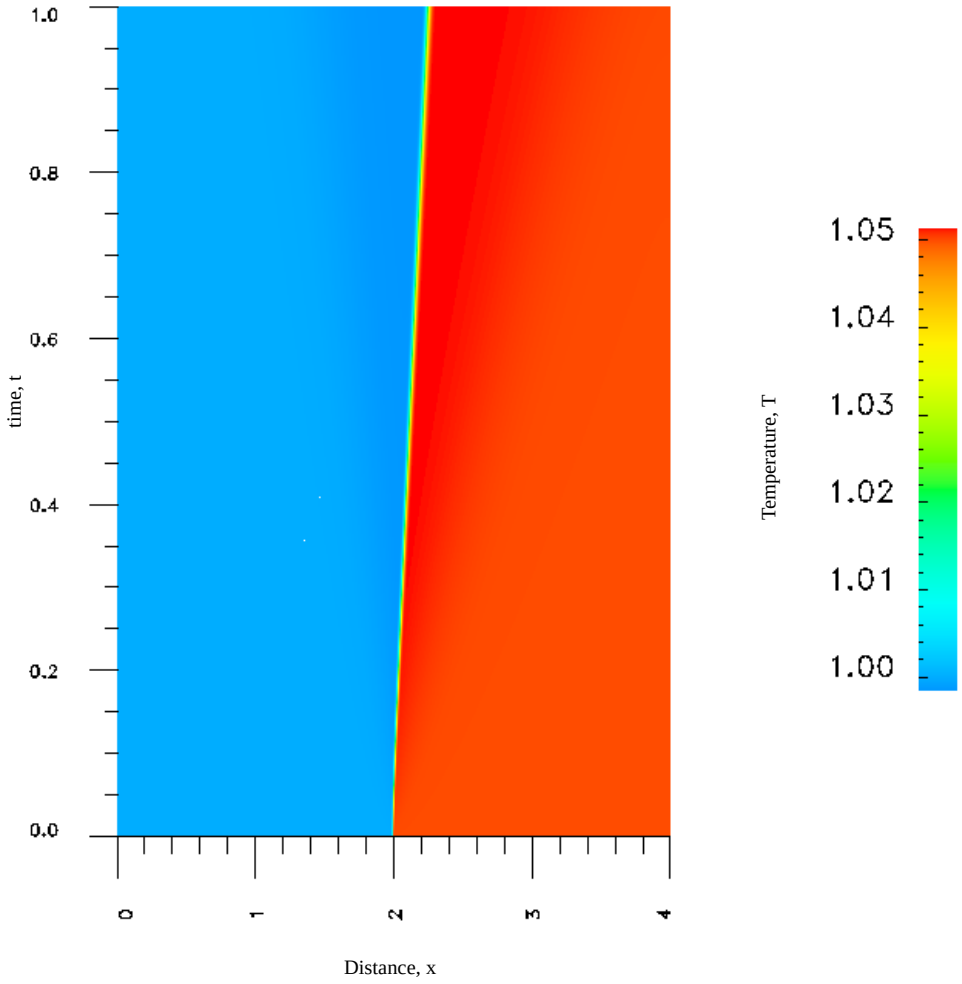

Figure 5.38: Space-time plot of evolution of temperature, T ; case(b) : Non-isothermal , Initial Conditions inside the critical zone

Case (c) Initial conditions far away from the critical zone (Isothermal)

We consider $\rho_h/\rho_l = 0.25/0.1$ with initial temperature value of $T = 1.4$ at t=0 (initial condition). All other details remain the same as in case(a). Evolution is computed for 100 time steps with same accuracy of $|g_i|$ and I as in case(a). Figure 5.39 clearly show that $p-v$ curve during entire evolution including initial conditions is well outside the critical zone. Plots of the evolution of ρ, u and T along the spatial domain are shown in figures 5.40-5.42. All fronts are smooth and diffused. Figures 5.43-5.46 show space-time evolutions of S_r, u, ρ and T. Exploded view in figure 5.43b confirms the largest values of S_r in the rarefaction region. Continously diminishing S_r in rarefaction as well as low density region is obvious, confirming the lack of formation of shocks in both regions. Space-time evolutions of u, ρ and T need no special discussion.

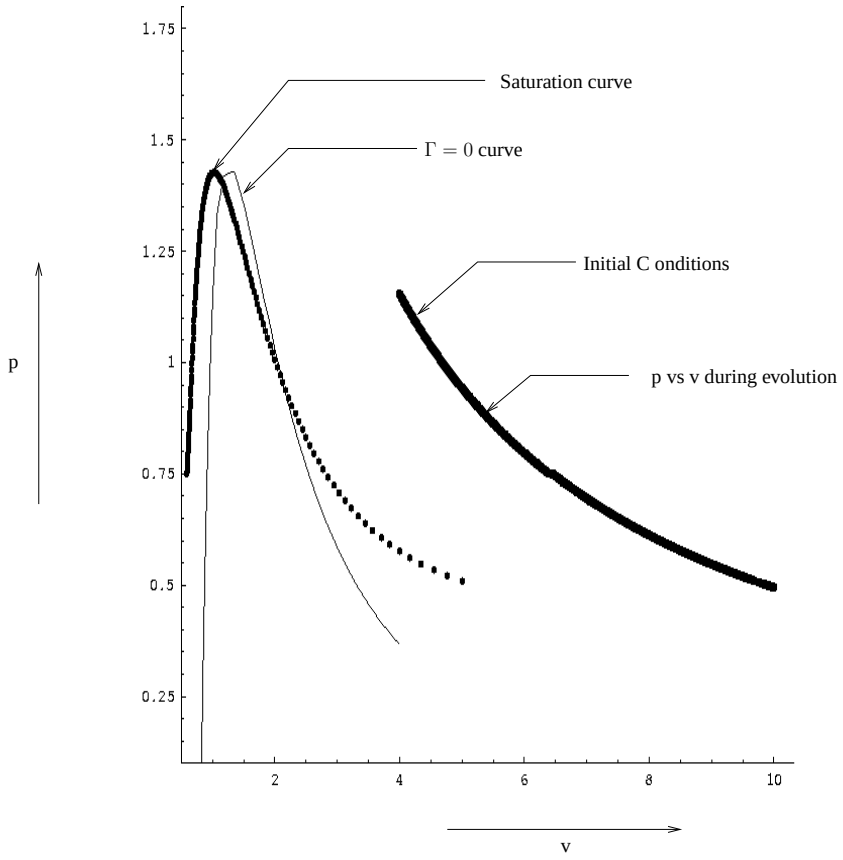

Figure 5.39: p versus v for case(c) : Isothermal ; Initial Conditions outside the critical zone

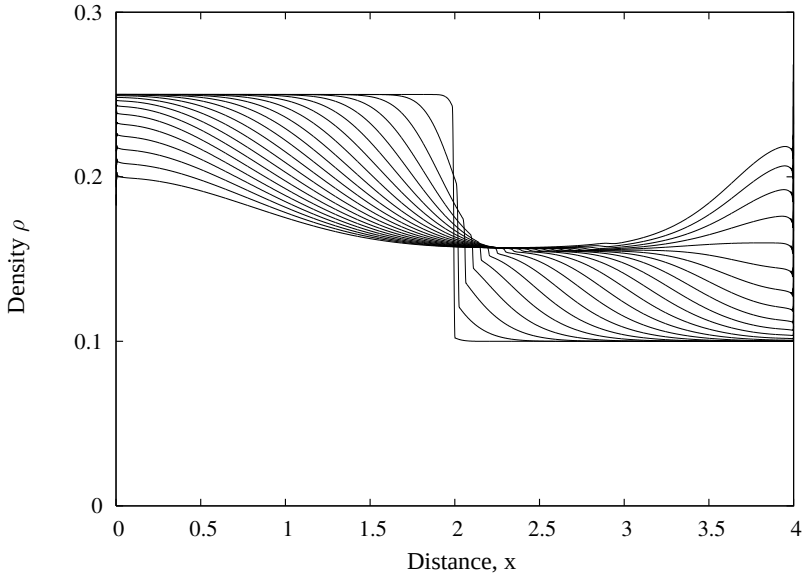

Figure 5.40: Evolution of Density for case(c) : Isothermal ; Initial Conditions outside the critical zone

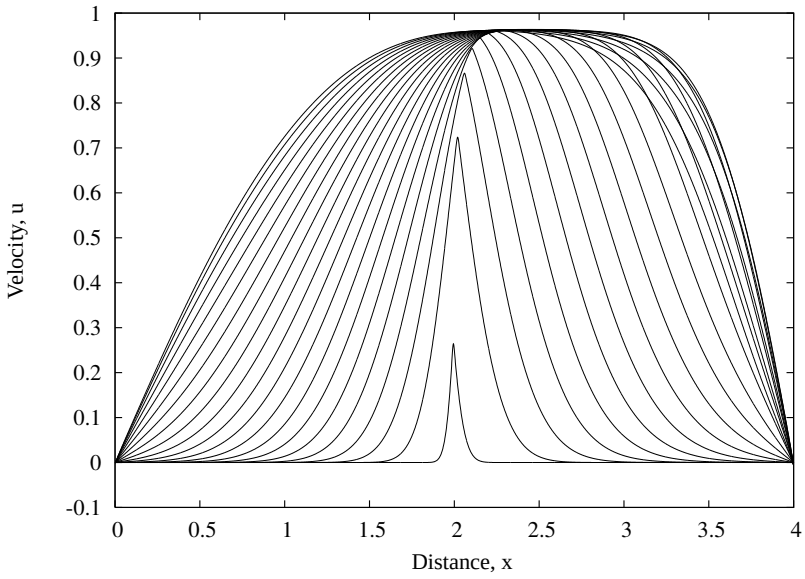

Figure 5.41: Evolution of Velocity for case(c) : Isothermal ; Initial Conditions outside the critical zone

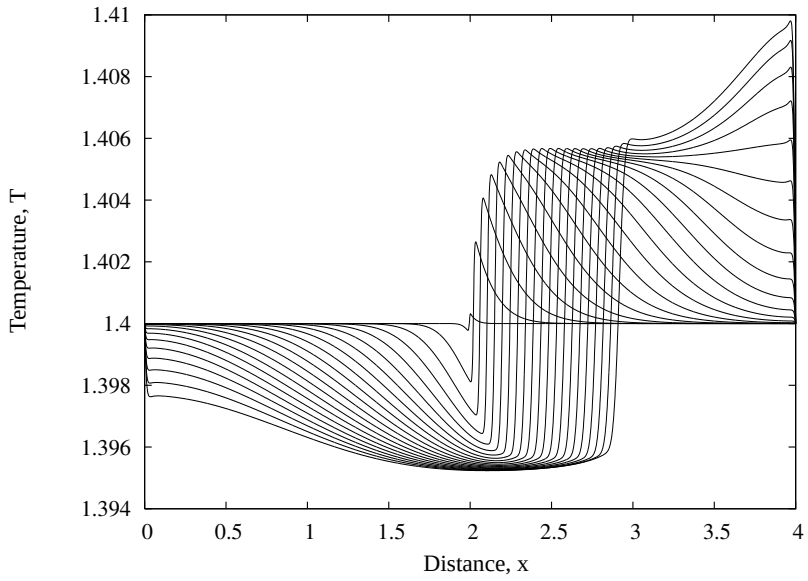

Figure 5.42: Evolution of Temperature for case(c) : Isothermal ; Initial Conditions outside the critical zone

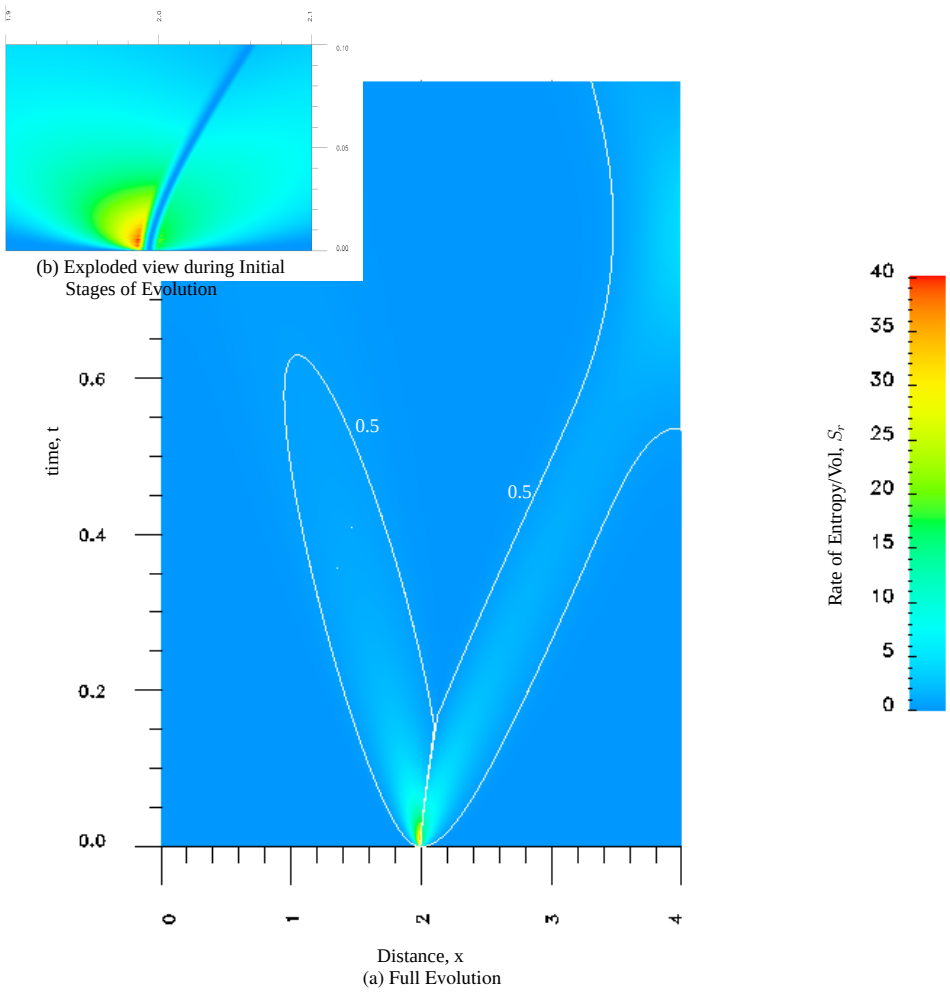

Figure 5.43: Space-time plot of evolution of S_r ; case(c) : Isothermal , Initial Conditions outside the critical zone

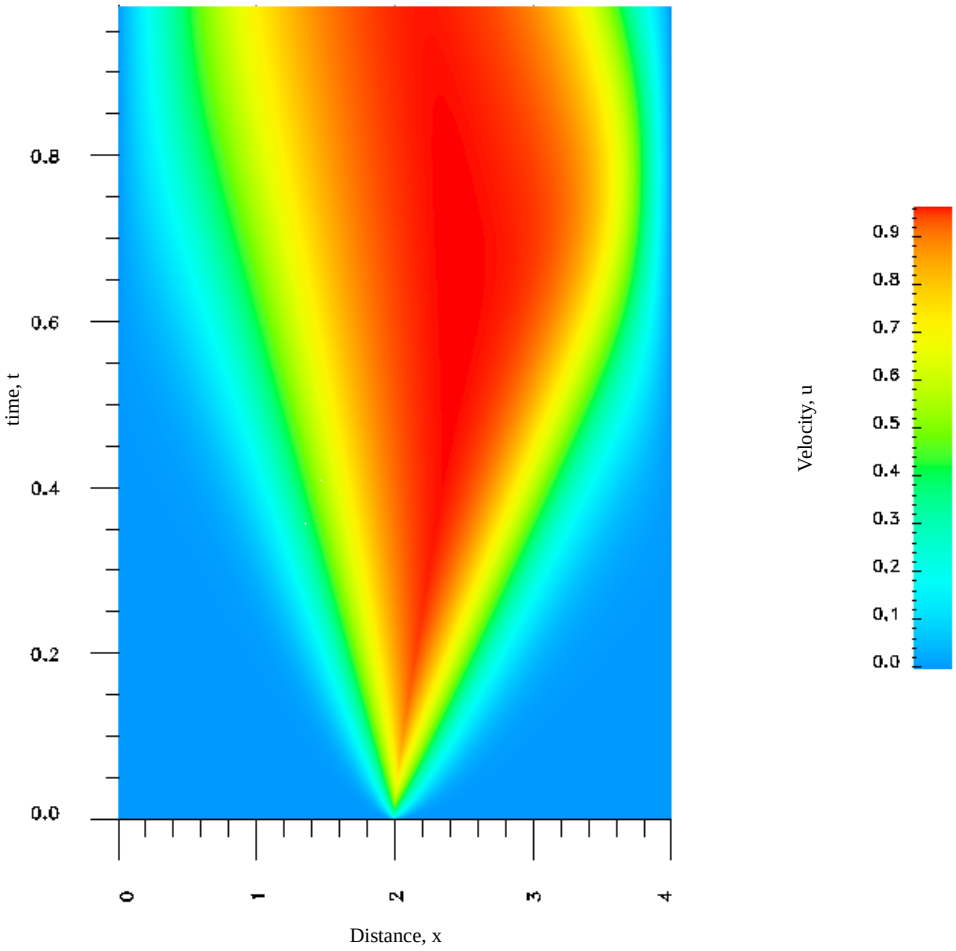

Figure 5.44: Space-time plot of evolution of velocity, u ; case(c) : Isothermal , Initial Conditions outside the critical zone

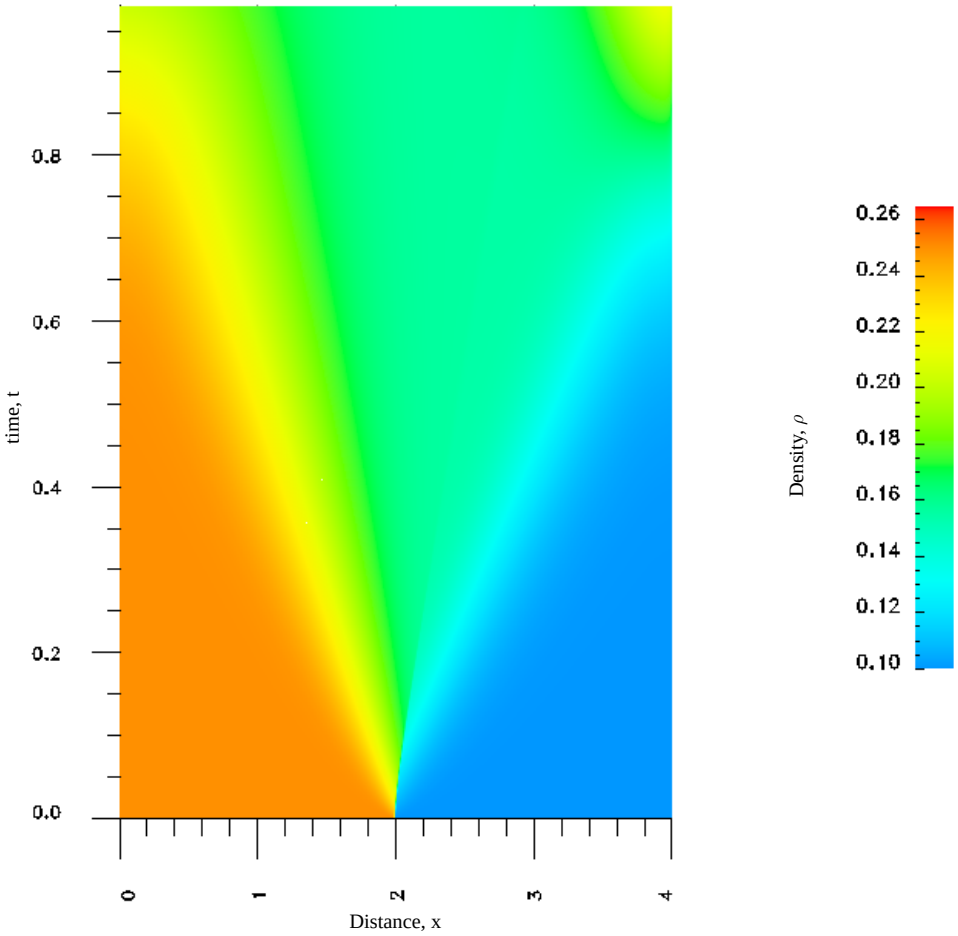

Figure 5.45: Space-time plot of evolution of density, ρ ; case(c) : Isothermal , Initial Conditions outside the critical zone

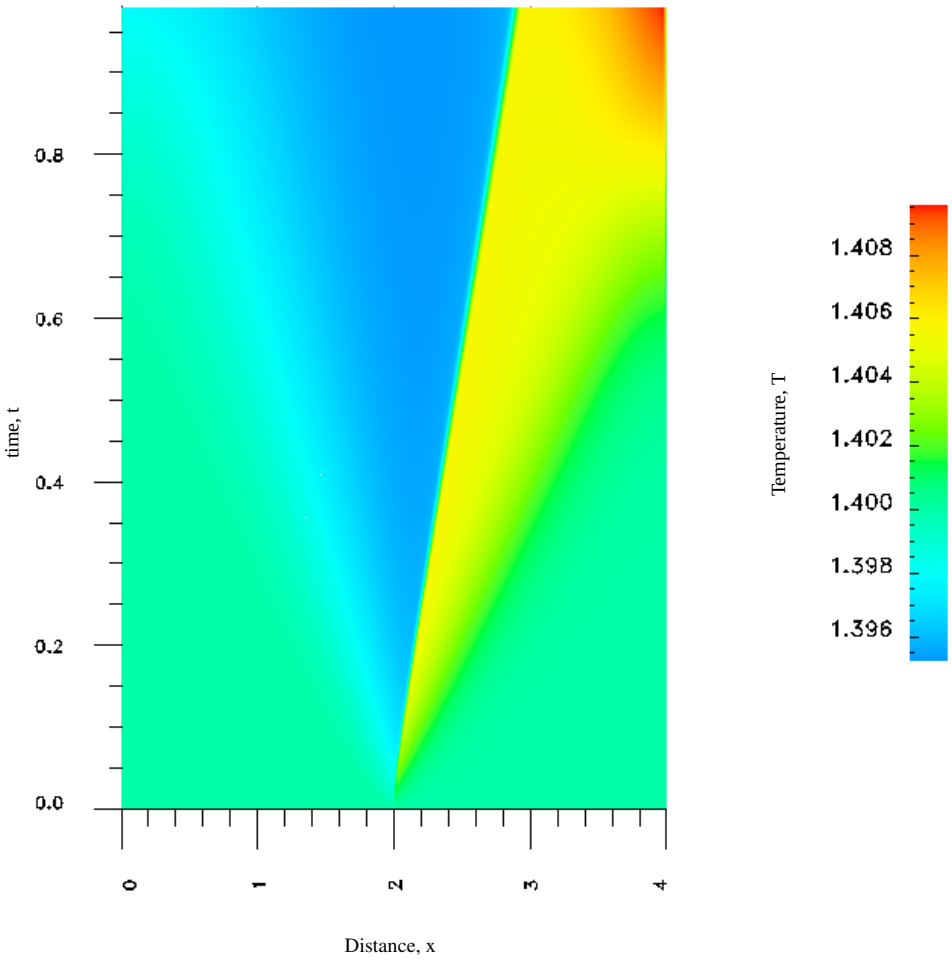

Figure 5.46: Space-time plot of evolution of temperature, T ; case(c) : Isothermal , Initial Conditions outside the critical zone

Case (d) Initial conditions partly inside the critical zone (Non-isothermal) with reduced viscosity

The theories of the existence of shocks in the rarefaction region for gases with $\hat{c}_v/\hat{R} > 20$ when initial conditions are in the critical zone are all based on Euler's equations and Rankine-Hugoniot relations. Euler's equations have zero viscosity and conductivity. Thus, it is perhaps fitting and interacting to conduct some studies with reduced viscosity (all other transport properties remaining same) just to explore if there is a possibility of rarefaction shocks.

We consider exactly same conditions and details as for case (b) but choose a reduced value of viscosity. First, we consider the viscosity of medium to be $\hat{\mu}/10$ i.e., one tenth of the critical viscosity of FC70 and compute the evolution for 200 time steps. Figure 5.47 confirms that initial condition as well as $p - v$ curve partially remain in the critical zone for the entire evolution. Figures 5.48-5.50 show details of the evolution of ρ, u and T in the spatial direction. From figure 5.48 we observe considerable steepening of waves in rarefaction as well as low density region compared to case (b) (with actual viscosity $\hat{\mu}$, all other conditions remaining identical), contact zone is clear and distinct. Wave appears to be sharp and non-dispersive in both region specially during later part of the evolution but not quantitative to claim shock formation. Space-time evolution of S_r, u, ρ and T are shown in figures 5.51-5.54. From figures 5.54b we confirm the largest S_r in the rarefaction region. In figure 5.51a we note dispersion of S_r values from 35 at the onset of the evolution to 0.4 in 20 time increments and then almost remain constant during next 180 increments of time in the rarefaction region indicating

the formation and sustained propagation of a rarefaction shock. In the low density region S_r disperses quickly indicating lack of formation of a shock. This study demonstrates that for FC70 rarefaction shocks do exist if we consider the viscosity of the medium to be $1/10^{th}$ of actual viscosity of FC70. But, when the viscosity is the actual viscosity of FC70(case(b)) rarefaction shocks are not possible. In view of this study it is quite clear why the theories based on Euler's equations (zero viscosity) conclude the existence of rarefaction shocks. Our view is that there is perhaps a threshold value of $\hat{\mu}^* < \hat{\mu}$ for which rarefaction shocks will exist in FC70. $\hat{\mu}^*$ of course is nonphysical and so are the rarefaction shocks corresponding to $\hat{\mu}^*$.

5.4 Summary

Numerical studies are presented for 1-D Riemann shock tube for ideal gas law as well as real gas law using Van der Waals equation of state. Air and FC70 are used as medium for ideal and real gas models respectively. A brief summary is presented in the following :

(1) In all numerical studies, S_r, the rate of approximation of entropy per unit volume, is used to detect the formation, propagation reflection and interaction of shocks. A constant value of S_r during evolution confirms a constant propagating shock.

(2) In case of ideal gas law with air as medium :

   (a) Compression shock evolution and propagation is demonstrated.

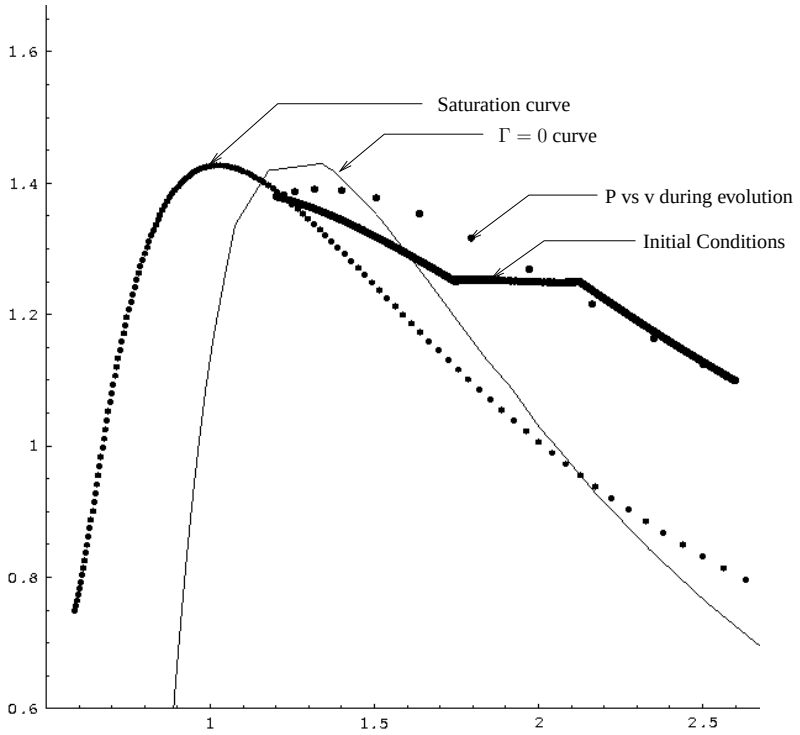

Figure 5.47: p vs v for case(d) : Non-isothermal ; Initial Conditions inside the critical zone

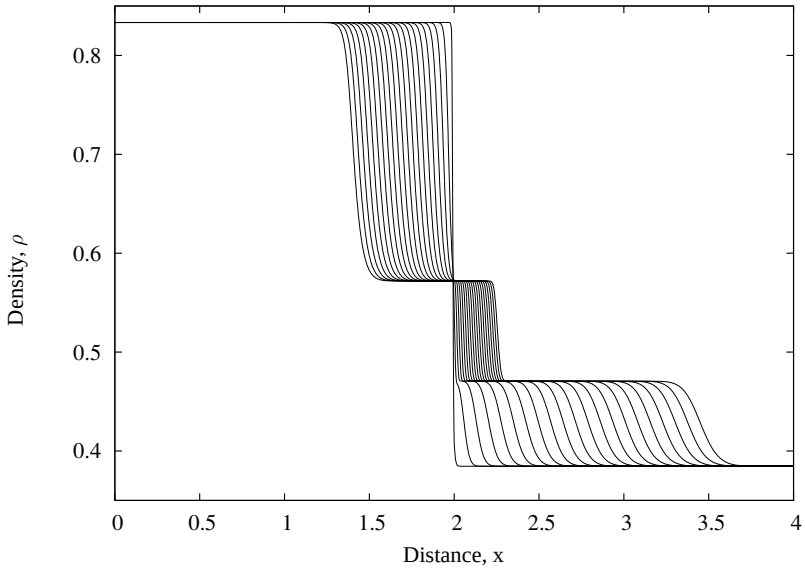

Figure 5.48: Evolution of Density for case(d) : Non-isothermal ; Initial Conditions inside the critical zone

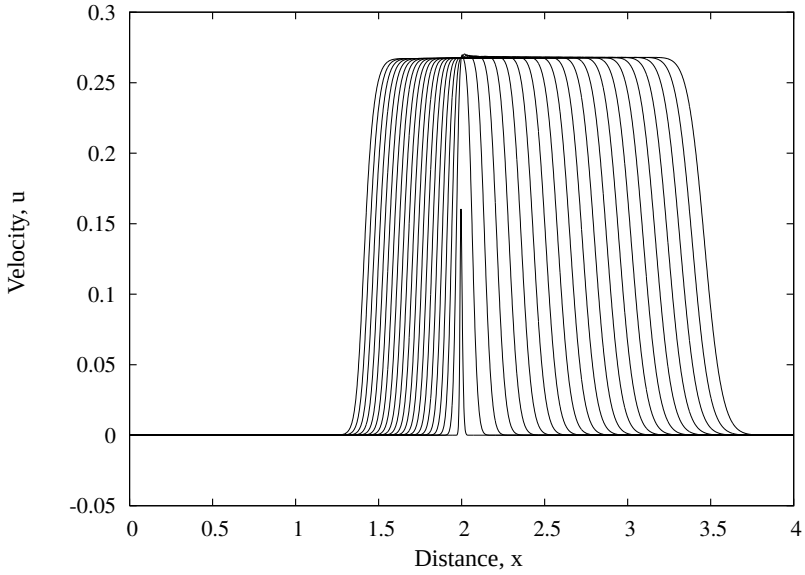

Figure 5.49: Evolution of Velocity for case(d) : Isothermal ; Initial Conditions inside the critical zone

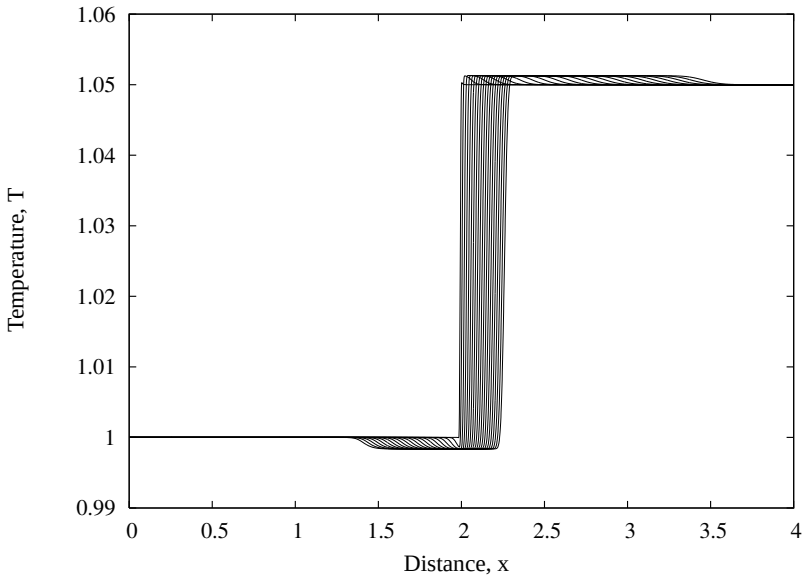

Figure 5.50: Evolution of Temperature for case(d) : Non-isothermal ; Initial Conditions inside the critical zone

(b) Repeated reflections of the compression shock, interactions and propagation is shown.

(3) For real gas model using Van der Waals equation of state and FC70 as medium, the shock tube behavior is investigated :

(a) When the initial conditions are near critical point and partially in the zone of interest in the $p - v$ diagram. During evolution a portion of the $p - v$ curve remains in the zone of interest also. Numerical studies have been presented for isothermal as well as non-isothermal initial conditions.

(b) When the initial conditions are far away from the critical zone and the

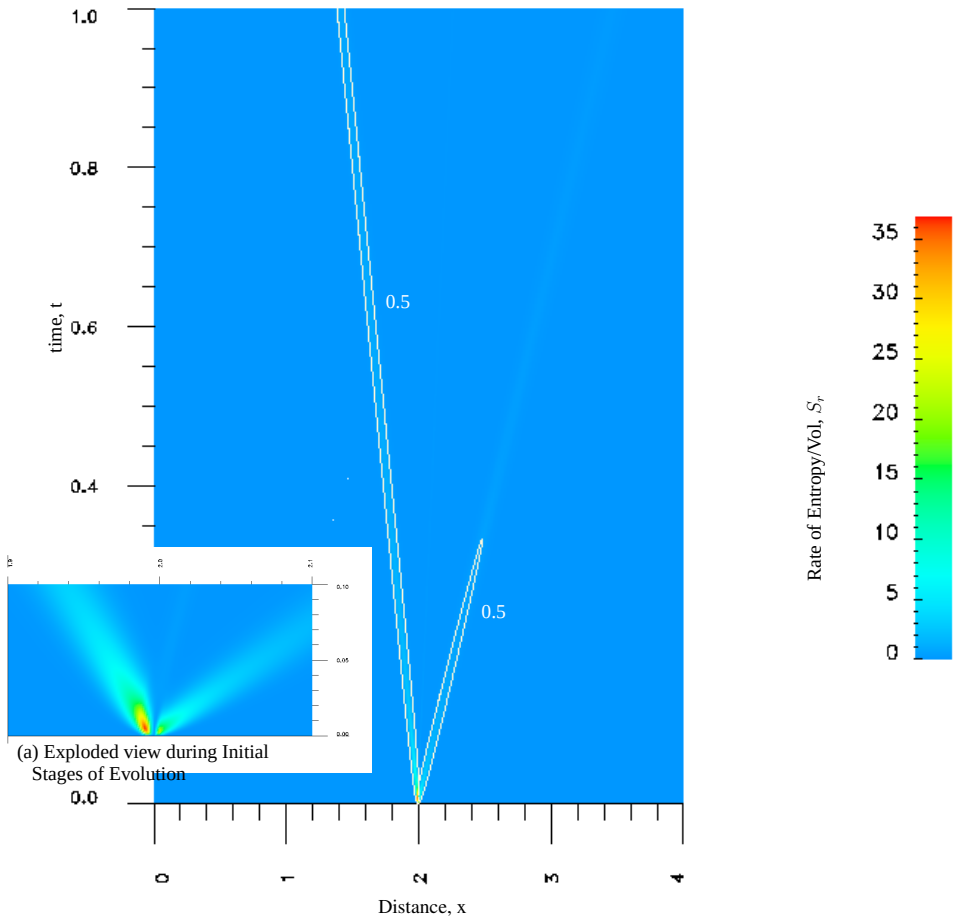

(a) Exploded view during Initial Stages of Evolution

(a) Full Evolution

Figure 5.51: Space-time plot of evolution of S_r ; case(d) : Non-isothermal , Initial Conditions inside the critical zone

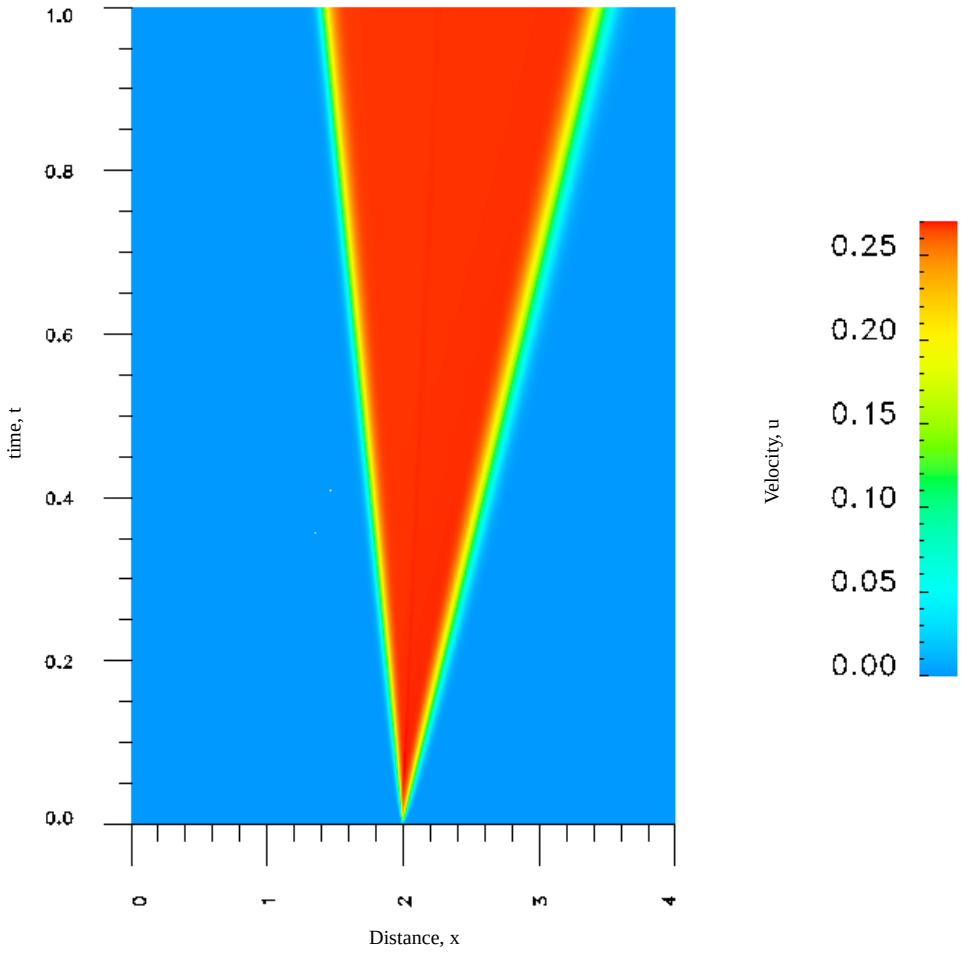

Figure 5.52: Space-time plot of evolution of velocity, u ; case(d) : Non-isothermal , Initial Conditions inside the critical zone

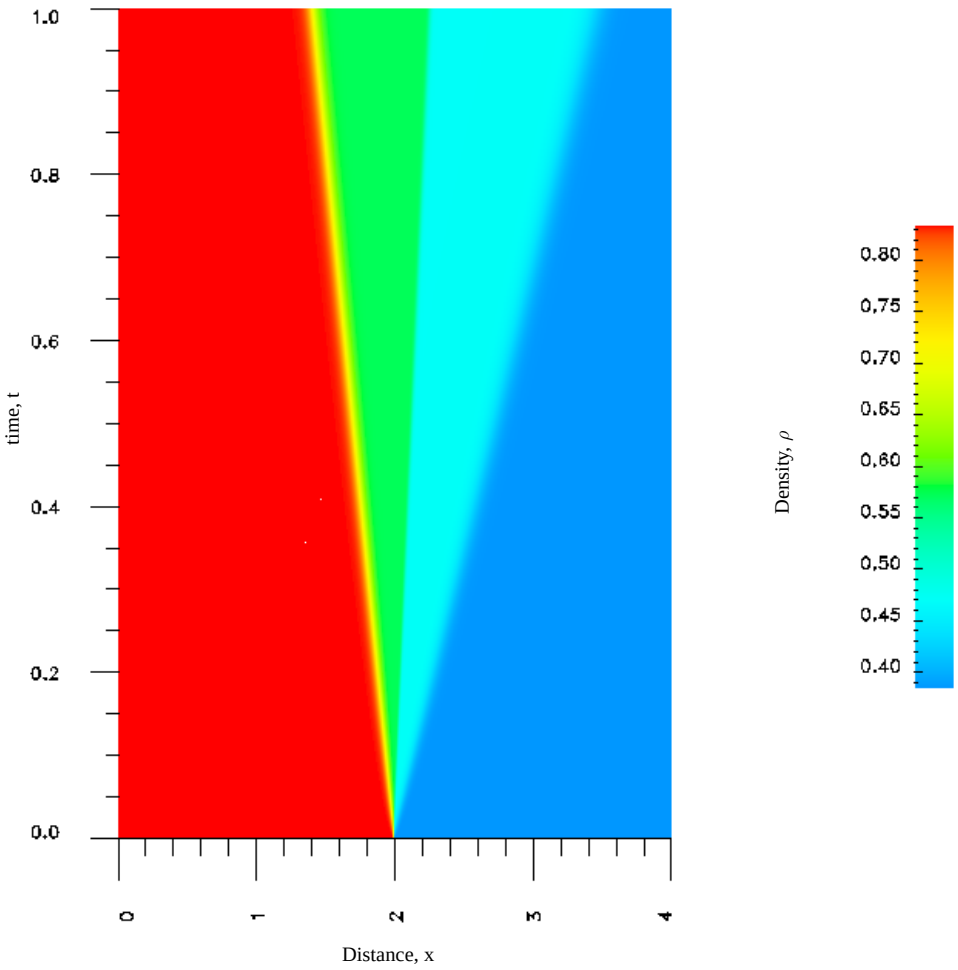

Figure 5.53: Space-time plot of evolution of density, ρ ; case(d) : Non-isothermal , Initial Conditions inside the critical zone

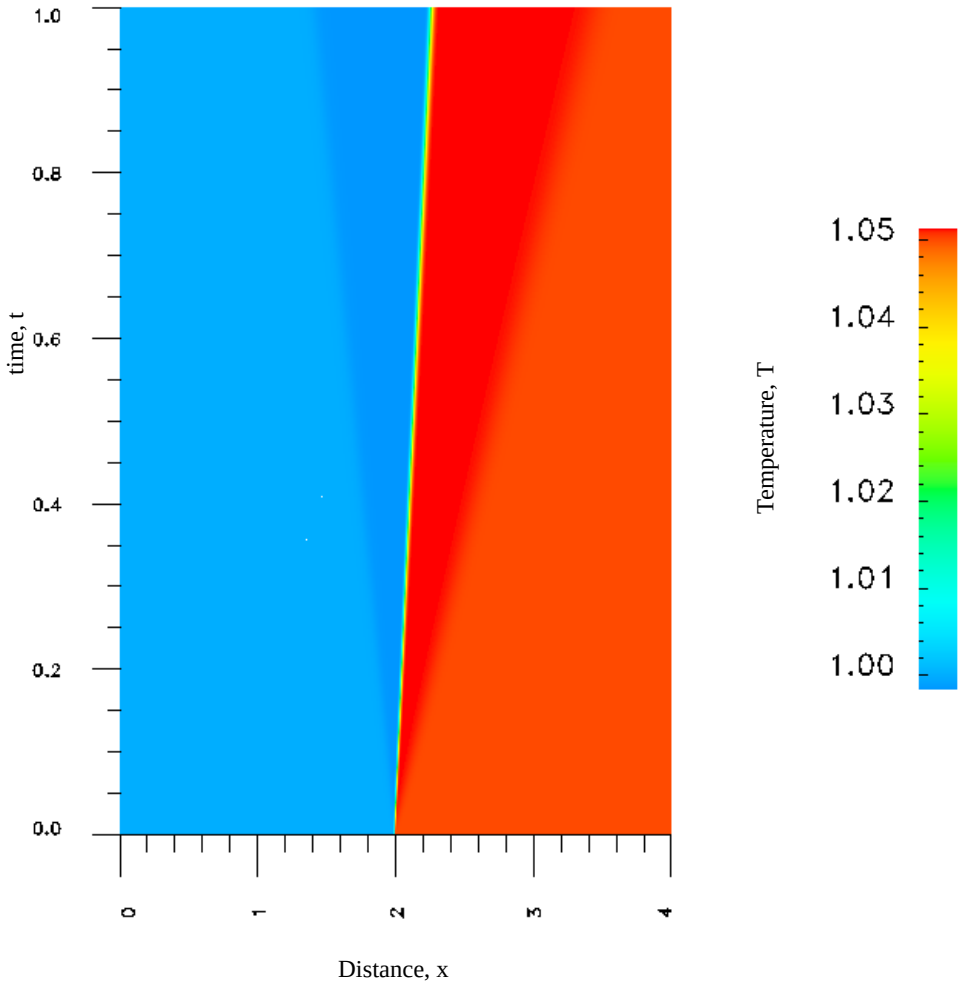

Figure 5.54: Space-time plot of evolution of temperature, T ; case(d) : Non-isothermal , Initial Conditions inside the critical zone

$p - v$ curve remains outside the critical zone during entire evolution. Isothermal initial conditions were used in thus study.

(c) When the non-isothermal initial conditions are partially in the critical zone and some portion of $p - v$ curve remains in the critical zone during entire evolution but the viscosity of the medium is reduced by a factor of ten from the actual viscosity of FC70.

The findings from these studies are summarized in the following :

(i) With actual properties of FC70 (specially viscosity) the formation of rarefaction shocks has not been observed regardless of the choice of initial conditions.

(ii) In all numerical studies compression shocks in the low density region were never observed either. However, with sufficiently high initial density ratio, the compression shocks are possible.

(iii) With reduced viscosity (one tenth of actual viscosity of FC70) formation and steady propagation of rarefaction shock is observed. This of course is non physical (due to non-physical value of viscosity) but proves an important point i.e., Euler's equations (zero viscosity) are used to study the possibility of rarefaction shocks then undoubtedly rarefaction shocks will be observed. This conclusion based on Euler's equations is obviously false due to the fact that essential physics due to viscosity is absent in the Euler's equations. This is also substantiated by the study with reduced viscosity in which case we do observe rarefaction shock.

(4) In all published work except those reported by Surana et. al. [25, 26, 27, 60, 61], evolution of shock is never reported. The studies in published literature on FC70 are based on Euler's equations in which calculated shock relations from Rankine-Hugoniot equations are used as initial conditions to show shock generation and their propagation. In the work presented here we present evolution of shock (or lack of it) , its propagation, interaction and reflections. S_r quantities without doubt whether waves evolve into a shock or not as well as their sustained propagation, reflections etc. During entire evolution for all studies, care is taken to ensure low values of $|g_i|$ and I to ensure that the numerical results infact satisfy the GDEs accurately.

Chapter 6

Numerical Studies for 2-D viscous compressible flows : BVPs

6.1 Introduction

In this chapter we consider numerical studies for BVPs describing 2D viscous compressible flows in conducting medium. The mathematical models for 2D IVPs have been presented in chapter 3. The mathematical models for 2D BVPs can be easily obtained by discarding time derivative terms in the GDEs for IVPs. The constitutive equations and equations of state for both ideal and real gas models have been presented in chapter 3 and these remain the same for IVPs and BVPs. The dimensionless forms of the GDEs were derived using p_0 and τ_0 as reference pressure and reference stress value so that numerical studies could be performed near critical pressure for the shock tube.

In the numerical studies considered here we use strong form of GDEs in x and y independent coordinates with ρ, u, v and T as dependent variables. These are a system of four non-linear PDEs and hence LSP with Newton's linear method is ideally suited for constructing a finite element formulation as it is the only method of approximation that yields variationally consistent integral form. Details are given in chapters 2 and 3.

The main motivating factor for the numerical studies presented here is to demonstrate robustness of the formulation process and the computational infrastructure for compressible viscous flows. As discussed in chapter 1, high Reynolds number compressible flows associated with high Mach numbers invariably are turbulent and hence, it becomes necessary to treat such processes as evolutions. The solutions of the corresponding BVPs obviously are laminar and hence do not contain the realistic flow feature that are present in the physical systems. In the published works it is generally accepted that solutions of BVPs for compressible flows are difficult to compute and most methods of approximation such as finite volume, finite difference and finite element methods using Galerkin method with weak form fail in simulating them. In the studies presented here we shed some light on the causes of failure of these methods and propose as well as demonstrate that the infrastructure used here is quite robust in obtaining numerical solutions of BVPs describing viscous compressible flows in conducting media. In the following we present some significant aspects of the proposed methodology as well as discussion of some requirements for an infrastructure to address numerical solutions of such problem. This will perhaps help us in understanding the reason of the failure of currently used approaches and strength of the proposed approach that helps us in simulating the solutions of BVPs describing compressible flows.

Remarks

(1) The GDEs for these BVPs are highly non-linear and they require a framework free of linearizations before formulation. In context with finite element

method it means no linearization before or during the construction of the integral forms.

(2) The strong form of GDEs contains up to second order derivatives of velocity and temperature in spatial coordinates. Hence, the local approximations must at least be of class $C^1(\bar{\Omega}^e_{xy})$, but preferably of class $C^2(\bar{\Omega}^e_{xy})$ to ensure that all integrals in the entire computational process are Riemann, but more importantly to incorporate the desired physics.

(3) In the solutions of the non-linear system of algebraic equations the coefficient matrix must always remain positive definite. This is assured in the present work due to variational consistency of the integral form resulting from the LSP and Newton's linear method.

(4) Newton's linear method for non-linear algebraic systems has quadratic convergence but only if the starting or initially assumed solution is in a sufficiently small neighborhood of the solution sought. This presents a major difficulty due to the fact that Stokes flow as a starting solution fails to meet this requirement. Thus, in order to be able to obtain numerical solutions of algebraic systems for high Reynolds number flows, we must device a scheme that provides a good starting solution that is in a sufficiently small neighborhood of the solution sought.

(5) In view of (4), one could possibly use low Reynolds number solutions of the compressible flow BVPs as a starting solution for higher Reynolds numbers

and then continue this process (continuation in Reynolds number) until the desired Reynolds number is reached.

(6) Our initial attempts in using (5) suggest that even the solutions of the BVPs describing compressible flow for very low Reynolds numbers experience difficulty and the Newton's method often leads to spurious and non-physical solutions. We find that a good approximation for the "velocity field features" is critical in a starting solution. ρ and T could be set to their values based on NTP or initial conditions.

(7) Our work in BVPs and IVPs for incompressible flows suggests that solution of BVPs in incompressible flows is rather straight forward and easier to obtain using LSP with Newton's linear method. Such solutions for higher Reynolds numbers (but significantly lower than those in compressible flows) may provide good first approximation of the feature of velocity field for the initial solutions of the compressible flow BVPs. We use water and its properties at NTP to obtain a velocity field by solving the associated BVP (with same domain and realistic BCs). The velocity field obtained serves as a starting or initial solution for the compressible flow BVPs. Specific details of this procedure are given in the following sections with each of the model problems.

(8) What we have described in (7) is not as straightforward as it might appear. The success or lack of it is highly dependent on the complexity of the flow features in compressible flow BVPs. In other words if the flow is simple such

as Carter's plate (model problem 1), then the procedure described in (7) will work or may not even be required at all specially for low Mach number flows.

(9) Another significant point to note is that the procedure described in (7) is not necessary for the solution of compressible flow BVPs for every Reynolds number. Instead, we may use (7) to obtain the compressible flow BVPs solution for a low Reynolds number and then may use this solution of compressible flow BVP as a starting solution for higher Reynolds number i.e., continuation in Reynolds number. Our experience in working with compressible flow BVPs shows this approach to be quite good and hence is adopted in the present work.

Model Problems

We consider two model problems

(a) Carter's plate : Flow over a flat plate at Mach 1, 3 and 5 are considered. The medium is air and the transport properties at NTP are assumed constant with ideal gas law.

(b) Circular cylinder : Flow over a cylinder with varying trailing lengths are considered. Medium is air with constant properties at NTP and ideal gas law.

For both model problems we consider solution of class $C^1(\bar{\Omega}^e_{xy})$ as well as of class $C^2(\bar{\Omega}^e_{xy})$ at p-levels described in the following sections.

6.2 Carter's plate

We consider a BVP describing flow over a flat plate at Mach numbers 1, 2, 3 and 5.

The following properties are used in the computations (air at NTP)

$$\rho_0 = 1.12254\ \mathrm{Kg/m^3}\ ;\ \mu_0 = 0.1983 \times 10^{-4}\ \mathrm{Pa-s}\ ;\ \mathrm{T}_0 = 410.52\ \mathrm{K}$$

$$c_{v0} = 717.0\ \mathrm{J/Kg/K}\ ;\ \hat{\mathrm{R}} = 286.9965\ \mathrm{J/kg/K}\ ;\ \mathrm{k}_0 = 0.028854\ \mathrm{N/Kg/K}$$

we choose the following values for the reference quantities,

$$L_0 = 1.0\ \mathrm{m}, \rho_0 = \hat{\rho}, \mu_0 = \hat{\mu}, \mathrm{k}_0 = \hat{\mathrm{k}}, \mathrm{c_{v0}} = \hat{\mathrm{c}}_\mathrm{v}$$

$$u_0 = 343.25\ \mathrm{m/s}, \mathrm{T}_0 = 410.52\ \mathrm{K}, \mathrm{R}_0 = 286.99\ \mathrm{J/Kg/K}$$

$$\tau_0 = p_0 = \rho_0 u_0^2 = 0.14438 \times 10^6\ \mathrm{Kg/m/s^2}$$

With these reference quantities we have the following dimensionless quantities and the dimensional parameters,

$$\rho = 1.0, \mu = 1.0, k = 1.0, c_v = 1.0, R = 1.0, \gamma = 1.4$$

$$Re = 0.212 \times 10^6, Br = 0.19724, Ec = 0.40027$$

We choose L=2 ($\hat{L}$ = 2 meters) and h=0.01($\hat{h}$=0.01 meters). Figure 6.1 shows a schematic of the plate. Figure 6.2 shows the domain ABCD $(L \times h)$ to be modeled and boundary conditions on various boundaries.

The description of dependent variables on the boundaries is crucial to ensure that the BVP is well posed but not overly constrained. That is, we only define what is permissible based on physics and that too only basic quantities and thus avoiding redundant descriptions of BCs.

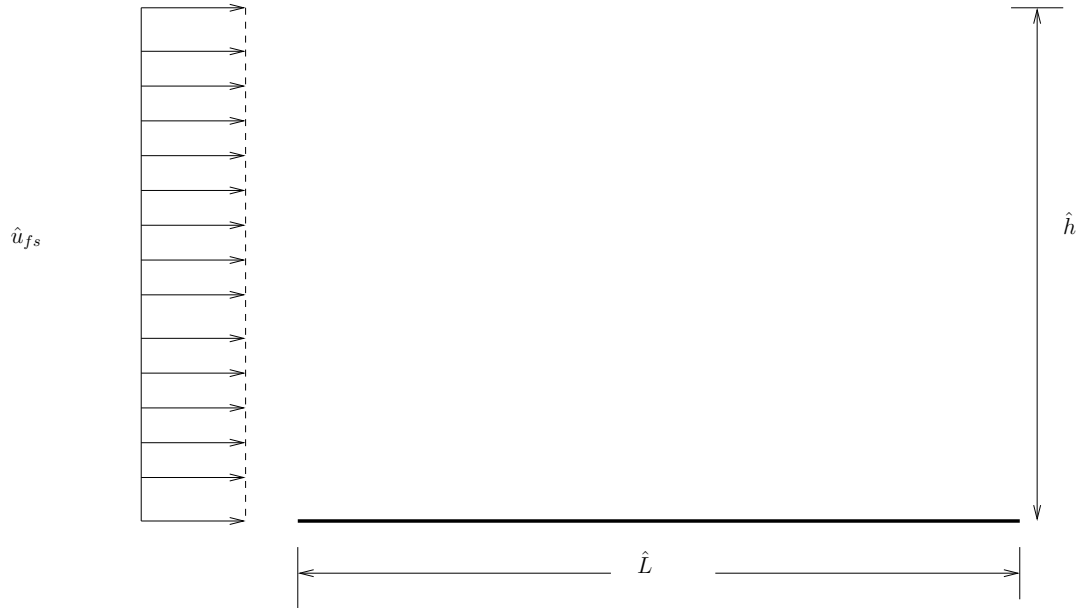

Figure 6.1: Schematic of Carter's plate

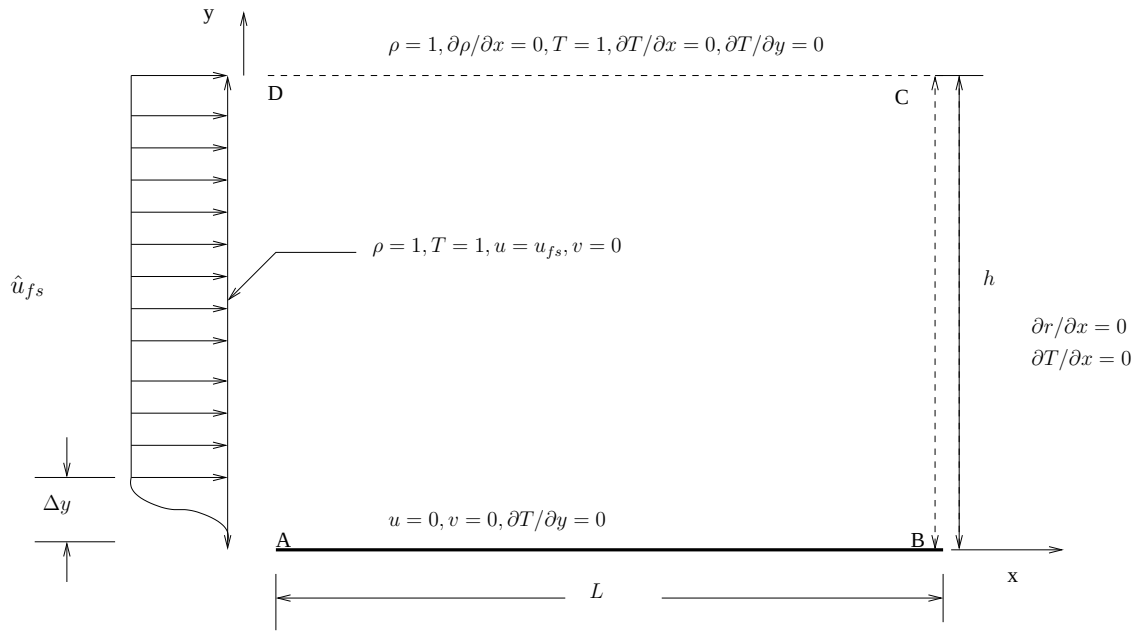

Figure 6.2: Carter's plate Boundary conditions

At the Inlet :

$\rho = 1, T = 1$ which implies : $\partial T/\partial y = 0$. $\partial T/\partial x = 0 \Rightarrow$ no heat transfer across inlet AD.

At the Plate :

$u = 0, v = 0, \partial T/\partial y = 0$ (no heat transfer normal to the plate)

At the top boundary CD :

$\rho = 1 \Rightarrow \partial \rho/\partial x = 0$

$T = 1 \Rightarrow \partial T/\partial x = 0$

$\partial T/\partial y = 0$ (no heat transfer normal to the boundary CD)

At the outflow boundary BC :

$\partial T/\partial x$ no heat transfer across the boundary BC.

We remark that fully developed conditions on BC are dangerous to use if L is not sufficient. To avoid over specification of BCs on CD, we avoid defining u and v and/or their gradients. We present numerical studies for free stream velocity $\hat{u}_{fs}$ of Mach 1, 2, 3 and 5. The domain (2×0.01) is discretized using a (70×30) graded mesh in which the element size at the lower left corner is 10^{-5}. Let u_s =speed of sound. Solutions for all Mach numbers are of class C^{11} at $p = 3$ in space and time.

6.2.1 Mach 1 flow :

If we choose $u_0 = u_s$ then, $u_{fs} = 1$. The other reference quantities are chosen as shown above. This choice of u_0 gives rise to $(Re)_{M1}$, $(Ec)_{M1}$, $(Br)_{M1}$ i.e., Re, Ec and Br at Mach 1.

The choice of initial solutions is critical as well. We choose $\rho = 1$, $T = 1$, $v = 0$ and $u = 1$ as initial solution. At the leading edge, the velocity distribution of 0 to u_{fs} is applied over a distance of Δy in the element located at the leading edge in a continuous and differentiable manner (shown in figure 6.2). Newton's linear method with line search converged in 35 iterations with $|g_i|_{max} = 0.862 \times 10^{-6}$ and $I = 0.325 \times 10^{-2}$. The largest value of I is from the element located at the leading edge.

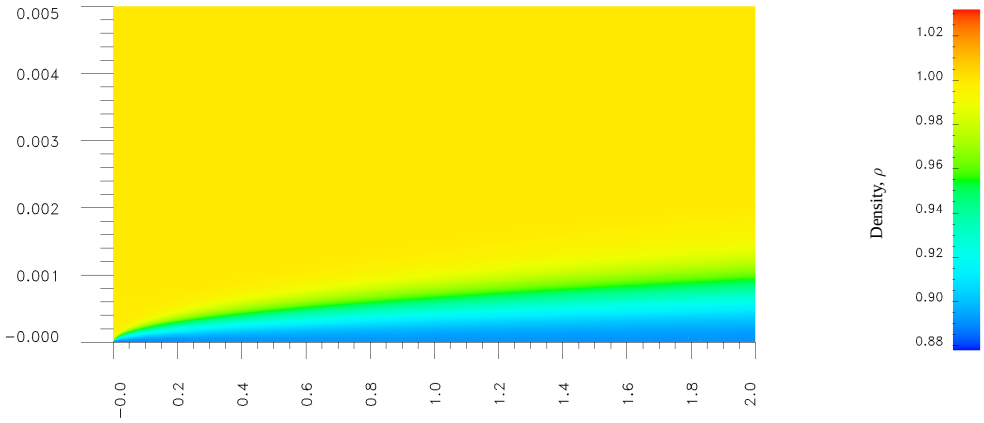

Figure 6.3: Contour of the Density, ρ for Mach 1.0 flow

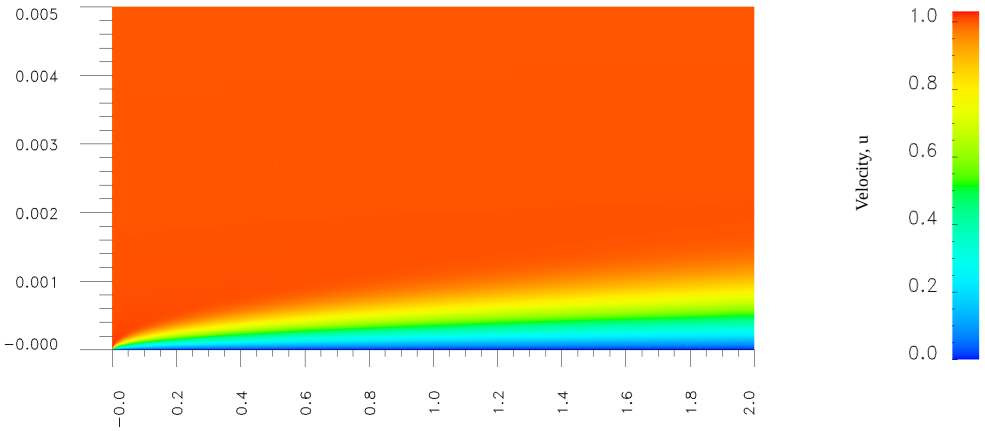

Figure 6.4: Contour of the Velocity, u for Mach 1.0 flow

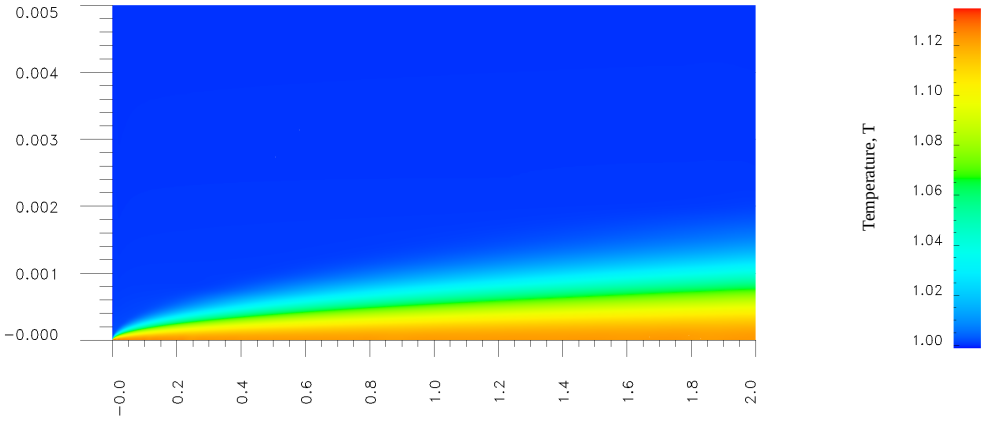

Figure 6.5: Contour of the Temperature, T for Mach 1.0 flow

Figures 6.3-6.5 show contour plots of density, velocity and temperature over (x, y) domain of $(0, 2)\times(0, 0.005)$. From the figures we observe that boundary layer may not be fully developed, hence the reason for not imposing fully developed flow conditions at the outflow. Progressive development of the boundary layer is clearly observed. Temperature rise due to viscous dissipation at the plate with progressively higher values for increasing x are clearly seen in 6.5.

6.2.2 General consideration for higher Mach number flows :

For calculating flow at Mach 2, 3 and 5 a direct calculation similar to that described for Mach 1 resulted in lack of convergence of the iterative solution method for solving non-linear algebraic equations. This is largely due to inadequate starting or initial solution method for solving non-linear algebraic equations i.e., the choice of free stream values as initial solution (as used for Mach 1 flow) is not in close proximity of the solution sought for Newton's linear method to converge.

Thus a continuation process becomes essential to use. For example we could use Mach 1 solution as a starting or initial solution for Mach 2. For illustration purposes consider Mach 2 flow. For Mach 2 flow, $u_0 = 2u_s$ gives $u_{fs} = 1$ (same as in case of Mach 1). But $(Re)_{M2}$, $(Ec)_{M2}$, $(Br)_{M2}$ will be different compared to Mach 1 flow. With this choice, the boundary and free stream values of u, ρ, T and v in Mach 1 solution are same as those for Mach 2 flow but new Re, Br and Ec for Mach 2 flow are characteristic dimensionless parameters of the flow at Mach 2.
Thus we can proceed as follows :

Mach 2 flow :

Starting solution for Mach 1, $u_0 = 2u_s$; (all other reference values same as those for Mach 1), $u_{fs} = 1$

Mach 3 flow :

$u_0 = 3u_s, u_{fs} = 1$

(a) Starting solution for Mach 1 flow

(b) Starting solution for Mach 2 flow

Mach 5 flow :

$u_0 = 5u_s, u_{fs} = 1$

(a) Starting solution for Mach 1 flow

(b) Starting solution for Mach 2 flow

(c) Starting solution for Mach 3 flow

6.2.3 Mach 2 flow

Using the continuation from Mach 1 described above with $u_0 = 2u_s$, $u_{fs} = 1$ (same as Mach 1 flow), the Newton's linear method converges in 17 iteration with $|g_i|_{max} = 0.883 \times 10^{-6}$ and $I = 0.105 \times 10^{-2}$. The contour plots of ρ, u, T are shown in figures 6.6-6.8 over the same (x, y) domain as used for Mach 1 flow. Thinner boundary layer and increased temperature values at the plate are clearly observed compared to Mach 1 flow.

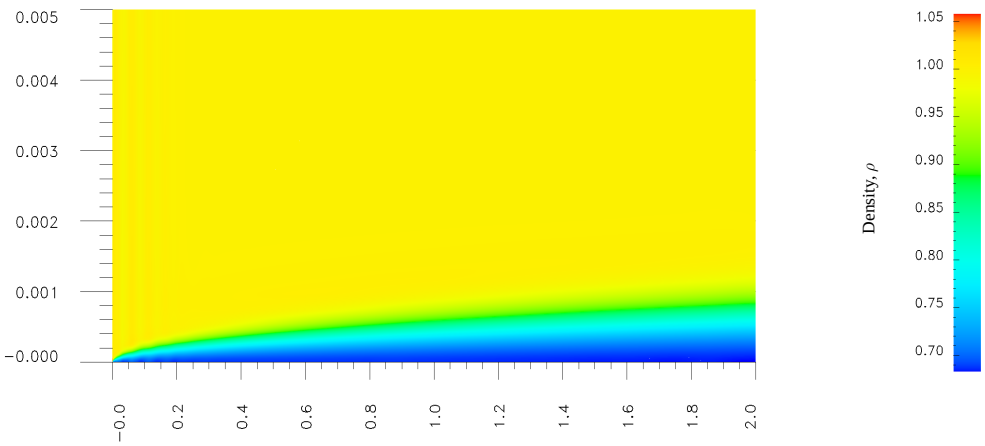

Figure 6.6: Contour of the Density, ρ for Mach 2.0 flow

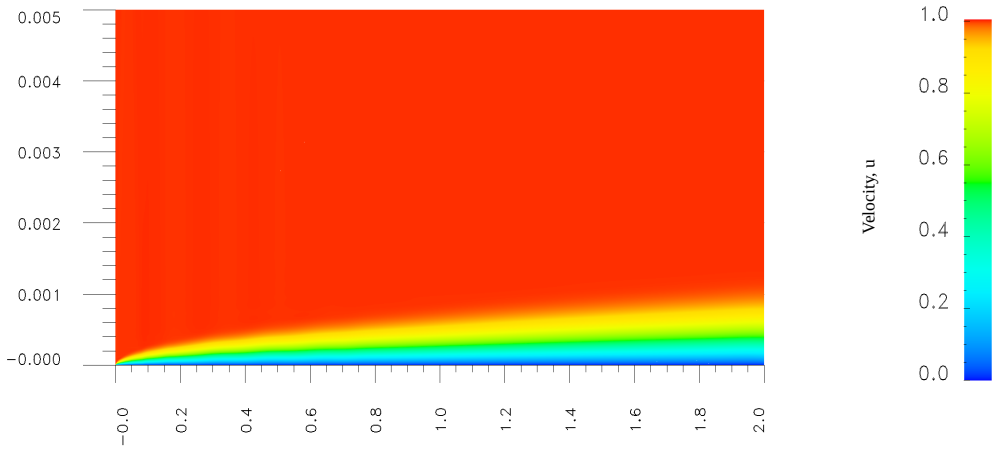

Figure 6.7: Contour of the Velocity, u for Mach 2.0 flow

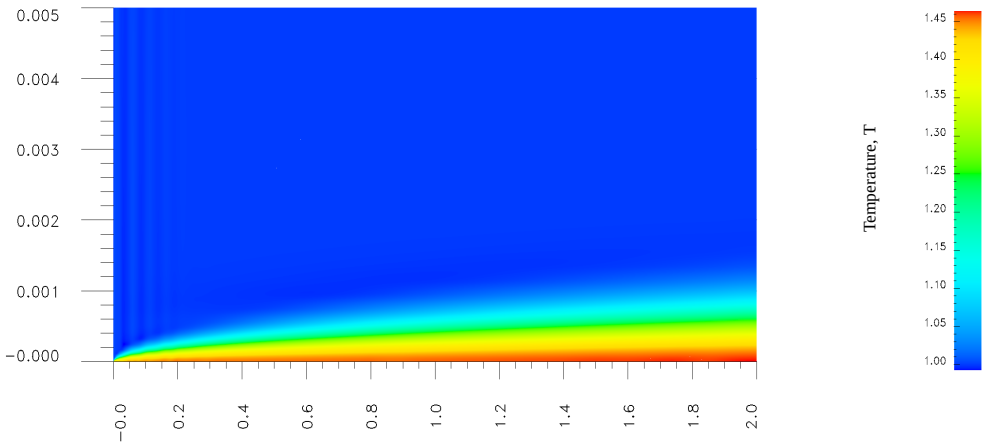

Figure 6.8: Contour of the Temperature, T for Mach 2.0 flow

6.2.4 Mach 3 flow

In this case Mach 1 solution as well as Mach 2 solutions were used as starting or initial solutions in two separate studies. The final converged solutions at Mach 3 were identical from either of these two as initial solutions. Using Mach 1 solution as initial solutions, Newton's linear method converges in 17 iterations with $|g_i|_{max} = 0.254 \times 10^{-6}$ and $I = 0.716 \times 10^{-3}$. Contour plots of ρ, u, T are shown in figures 6.9-6.11. Thinner boundary layer and increased temperature compared to Mach 2 flow are quite clear.

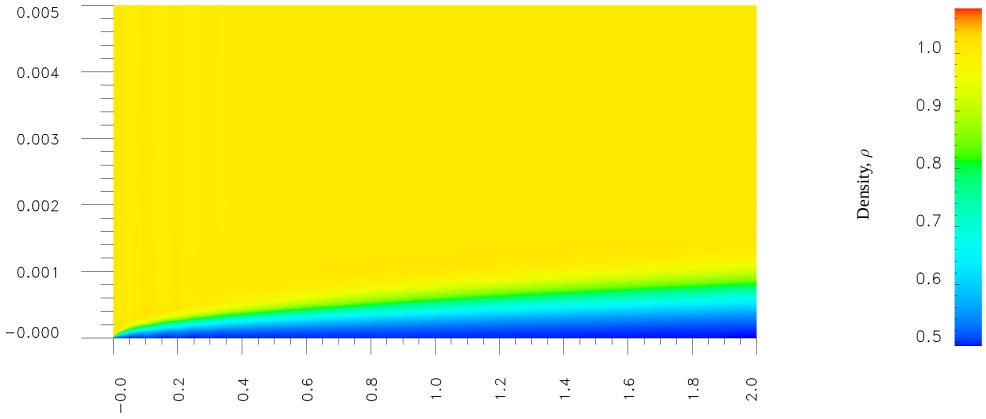

Figure 6.9: Contour of the Density, ρ for Mach 3.0 flow

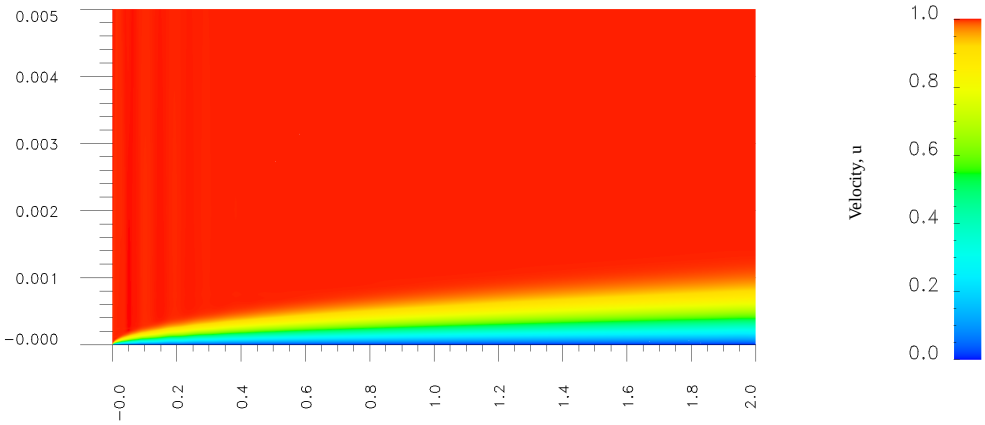

Figure 6.10: Contour of the Velocity, u for Mach 3.0 flow

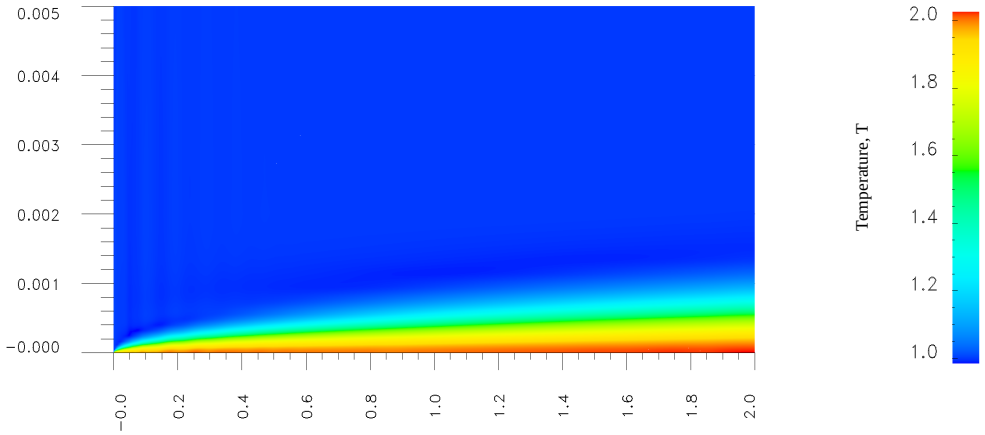

Figure 6.11: Contour of the Temperature, T for Mach 3.0 flow

6.2.5 Mach 5 flow

For Mach 5 flow, the initial or starting solutions were used from Mach 1, 2 and 3 for three different studies (with $u_0 = 5u_s$ and $u_{fs} = 1$). They all converged to the identically same solution. We present results obtained using Mach 1 solution as a starting or initial solution.

The Newton's linear method converges in 29 iterations with $|g_i|_{max} = 0.473 \times 10^{-6}$ and $I = 0.425 \times 10^{-3}$. Contour plots of ρ, u, T are shown in figures 6.12-6.14. We observe similar trend of diminishing boundary layer thickness with increasing temperature values at the plate.

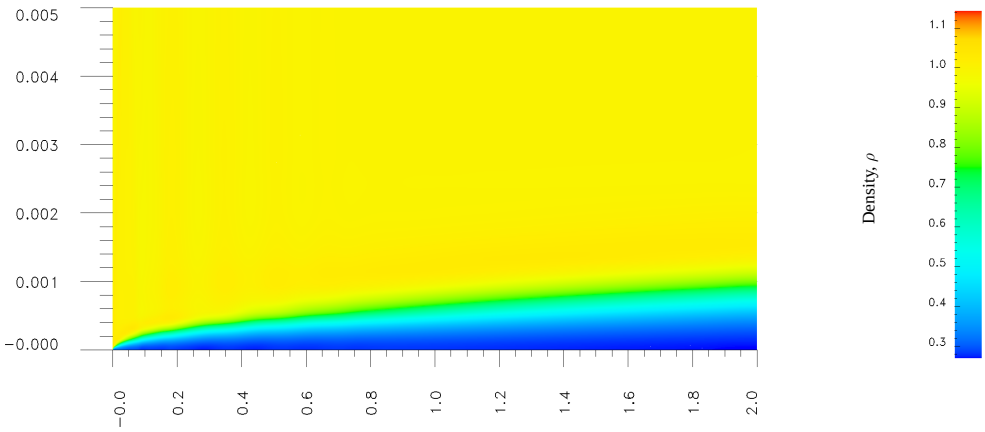

Figure 6.12: Contour of the Density, ρ for Mach 5.0 flow

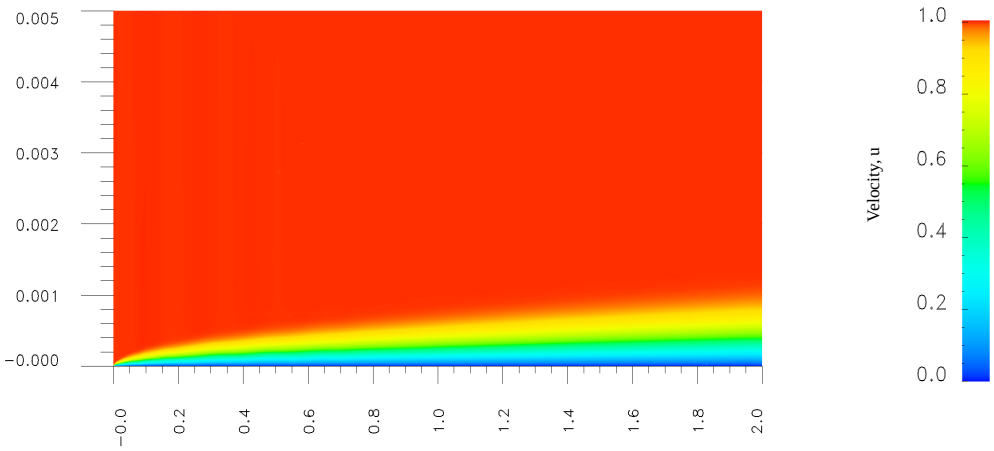

Figure 6.13: Contour of the Velocity, u for Mach 5.0 flow

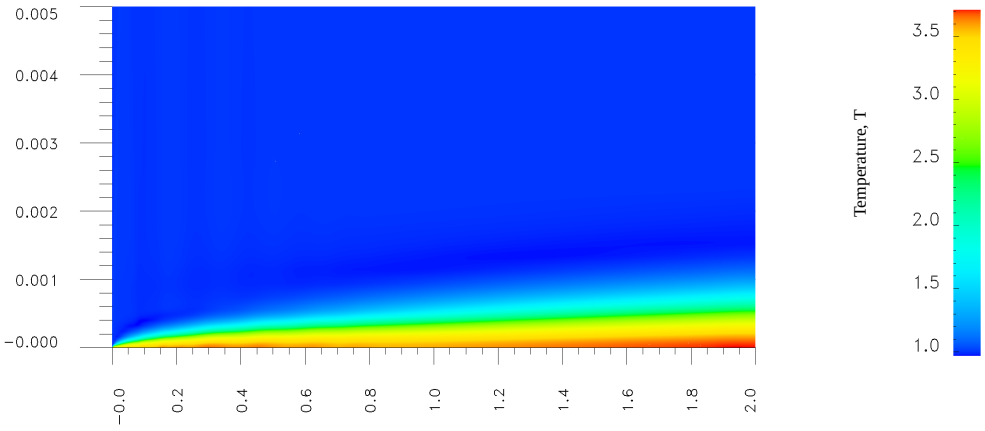

Figure 6.14: Contour of the Temperature, T for Mach 5.0 flow

6.2.6 Comparison of results for Mach 1, 2, 3 and 5 flows

Figures 6.15 shows plots of velocity u at the outflow boundary for Mach 1, 2, 3 and 5 flows. An exploded view of these is also shown in figure 6.16. We clearly see thinning boundary layer for increasing Mach numbers. Free stream value of $u = u_{fs} = 1$ for $y > 0.004$ for all Mach numbers shows that h-value of 0.01 chosen in numerical studies is sufficiently large. Plots of ρ, T and v at the outflow for Mach 1, 2, 3 and 5 are shown in figures 6.17-6.19. Progressively decreasing density at the plate for progressively increasing Mach number flows is clearly observed. Free stream density of one is clearly seen for $y > 0.004$, conforming adequate choice of h. From figure 6.18 we observe progressively increasing temperature values at the plate for progressively increasing Mach number flows and a free stream temperature of 1 for $y > 0.004$. Plots of v at the outflow boundary confirm that v of the order of 10^{-5} implies very close to fully developed flow.

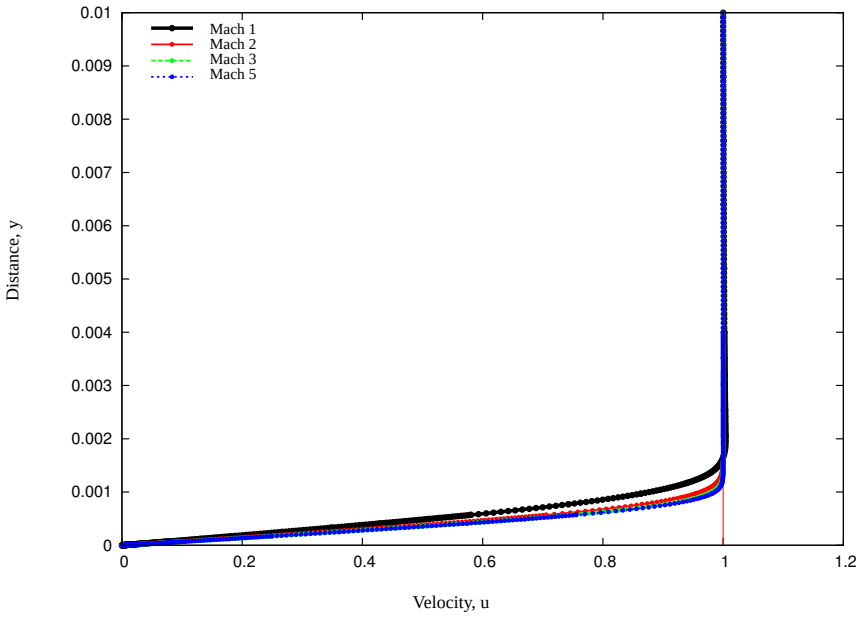

Figure 6.15: Velocity u at the outflow for Mach 1, 2, 3 and 5 flows

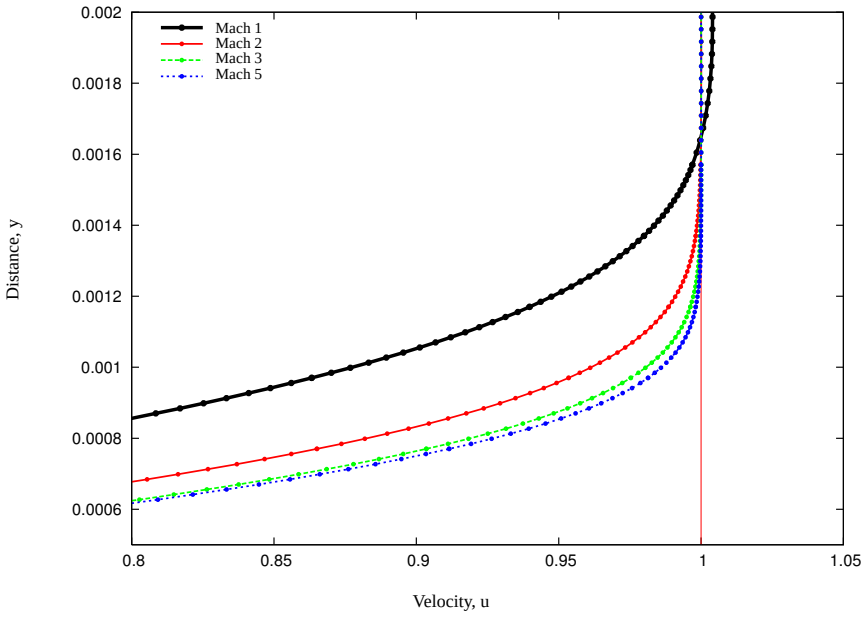

Figure 6.16: Exploded View of Velocity u for Mach 1, 2, 3 and 5 flows

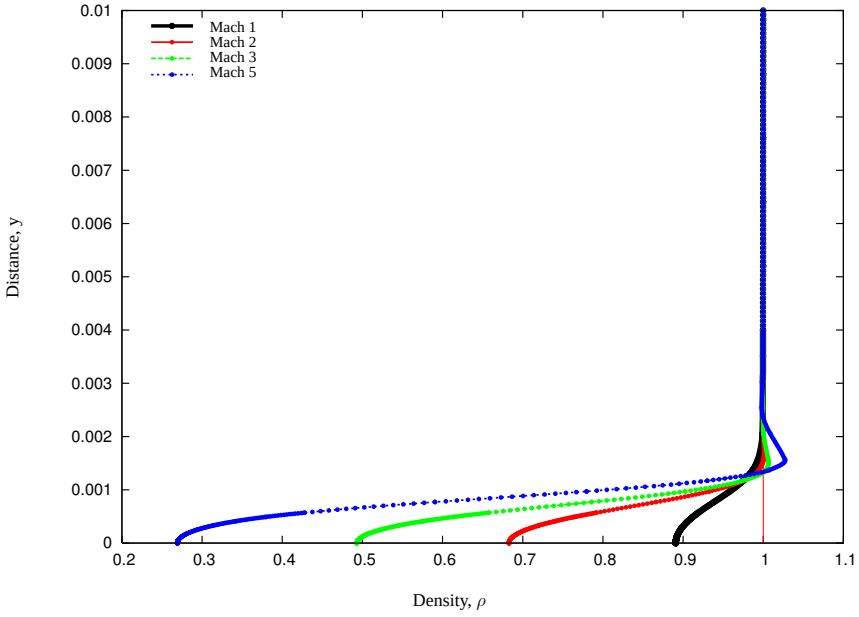

Figure 6.17: Density ρ at the outflow for Mach 1, 2, 3 and 5 flows

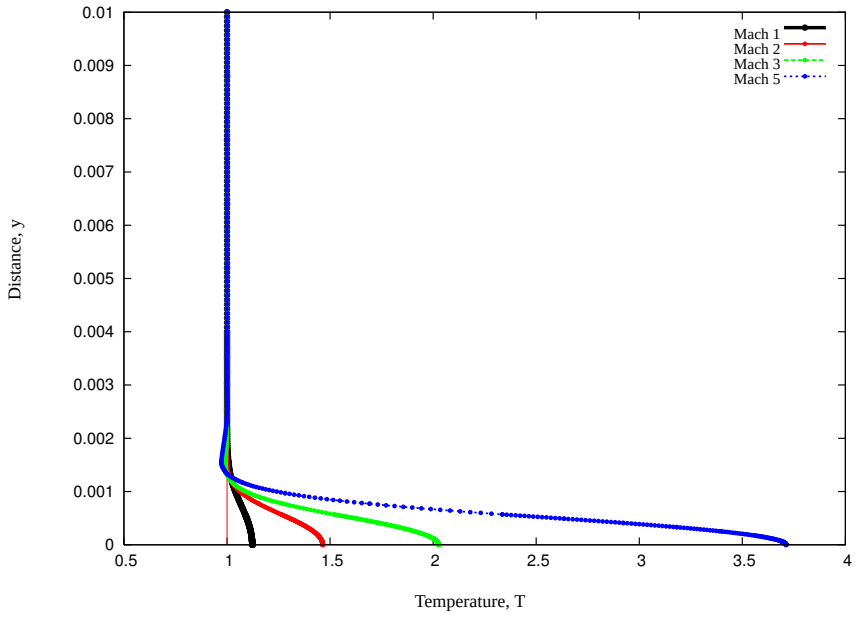

Figure 6.18: Temperature T at the outflow for Mach 1, 2, 3 and 5 flows

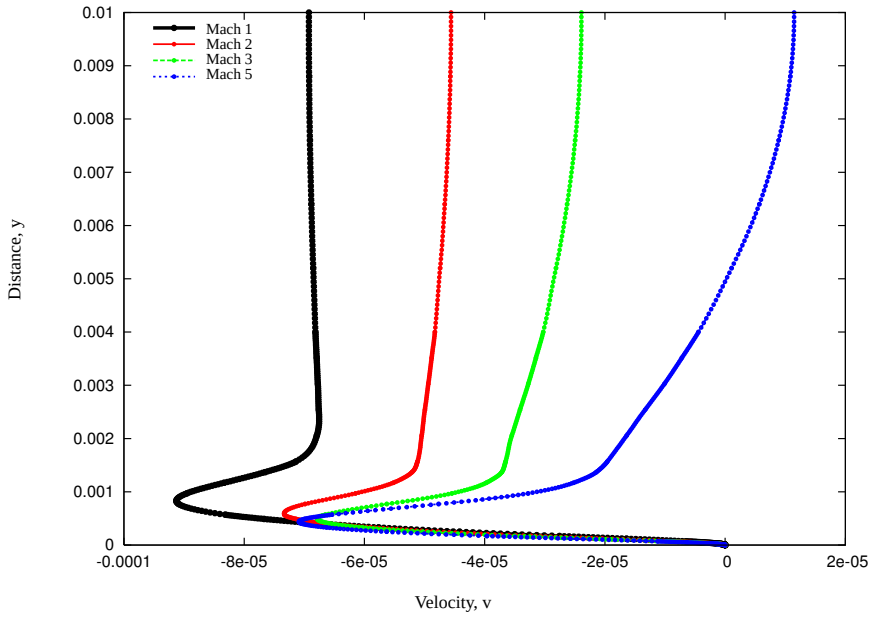

Figure 6.19: Velocity v at the outflow for Mach 1, 2, 3 and 5 flows

6.3 Flow past a circular cylinder

The purpose of this study is to demonstrate that the solutions of BVPs for fairly complex physics can be computed using the methodology presented here. For the Reynolds number considered, the flow is undoubtedly turbulent, and the h, p used in the simulations as well as the length past the cylinder are not adequate (for the BCs used at the outflow) for the flow physics. Nonetheless we present a strategy that allows us to compute solutions of the 'Posed BVP'. This is an attempt to demonstrate the robustness of the mathematical framework and the computational infrastructure. The results presented here are to be viewed within the context discussed above. We consider flow of air (at NTP) past a circular cylinder at Mach 1 with the following properties of the medium.

$$\rho_0 = 1.12254\ \mathrm{Kg/m^3}\ ;\ \mu_0 = 0.1983 \times 10^{-4}\ \mathrm{Pa-s}\ ;\ \mathrm{T}_0 = 410.52\ \mathrm{K}$$

$$c_{v0} = 717.0\ \mathrm{J/Kg/K}\ ;\ \hat{\mathrm{R}} = 286.9965\ \mathrm{J/kg/K}\ ;\ \mathrm{k}_0 = 0.028854\ \mathrm{N/Kg/K}$$

we choose the following reference quantities and their values,

$$L_0 = 1.0\ \mathrm{m}, \rho_0 = \hat{\rho}, \mu_0 = \hat{\mu}, \mathrm{k}_0 = \hat{\mathrm{k}}, \mathrm{c_{v0}} = \hat{\mathrm{c}}_\mathrm{v}$$

$$u_0 = 343.25\ \mathrm{m/s}, \mathrm{T}_0 = 410.52\mathrm{K}, \mathrm{R}_0 = 286.99\ \mathrm{J/kg/K}$$

$$\tau_0 = p_0 = \rho_0 u_0^2 = 0.14438 \times 10^6\ \mathrm{kg/m/s^2}$$

With these reference quantities we have the following dimensionless quantities and the dimensional parameters,

$$\rho = 1.0, \mu = 1.0, k = 1.0, c_v = 1.0, R = 1.0, L = 1$$

$$Re = 0.212 \times 10^6, Br = 0.19724, Ec = 0.40027$$

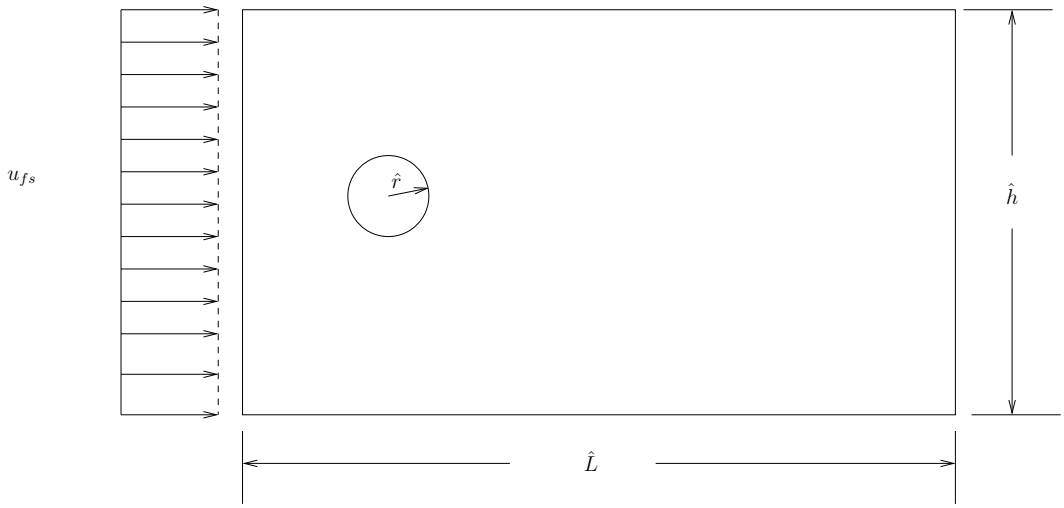

Figure 6.20: Schematic of Flow over circular cylinder

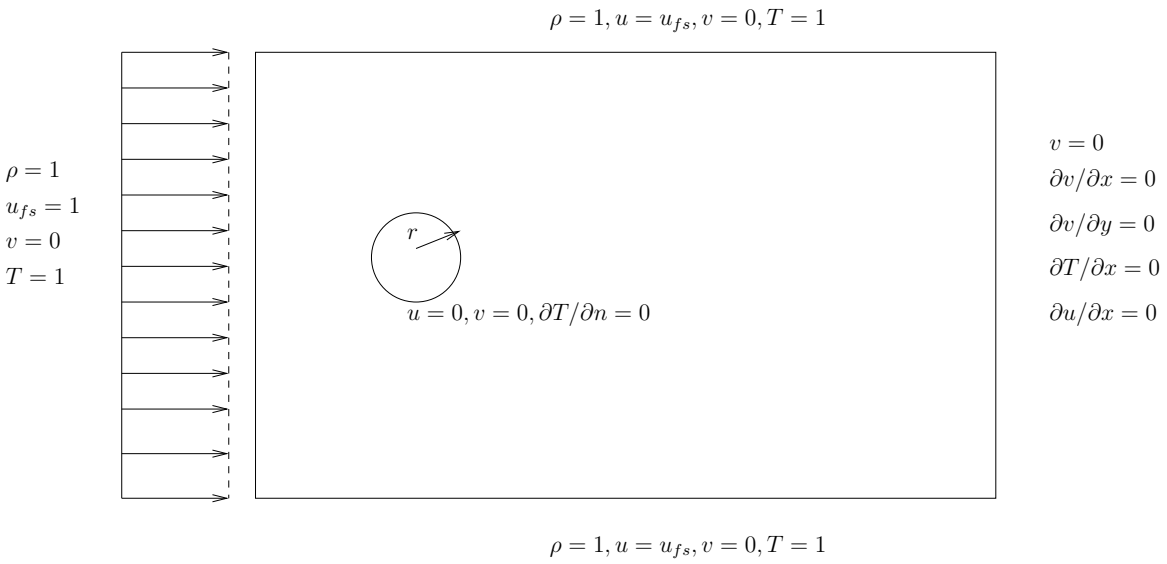

(a) Boundary Conditions for compressible flow past a circular cylinder

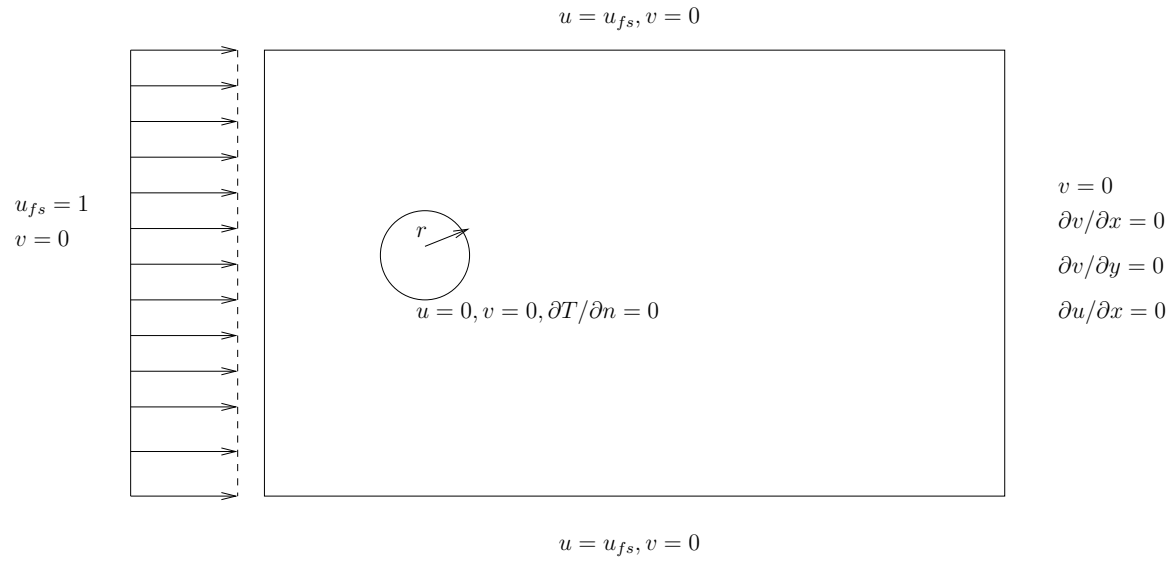

(b) Boundary Conditions for incompressible flow past a circular cylinder

Figure 6.21: Boundary conditions for flow past a circular cylinder (compressible flow)

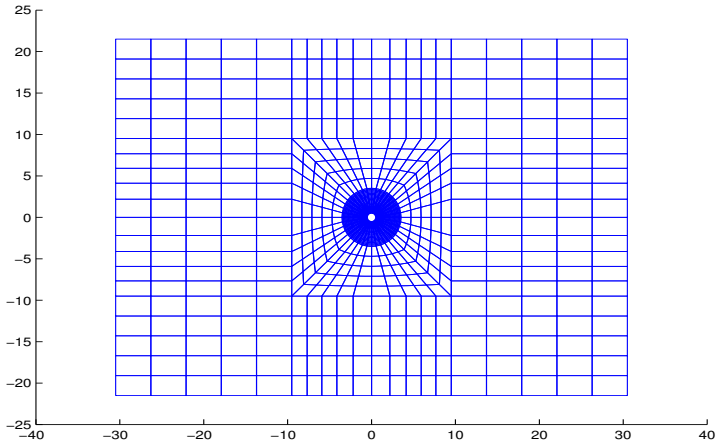

(a) Mesh of 1300 elements

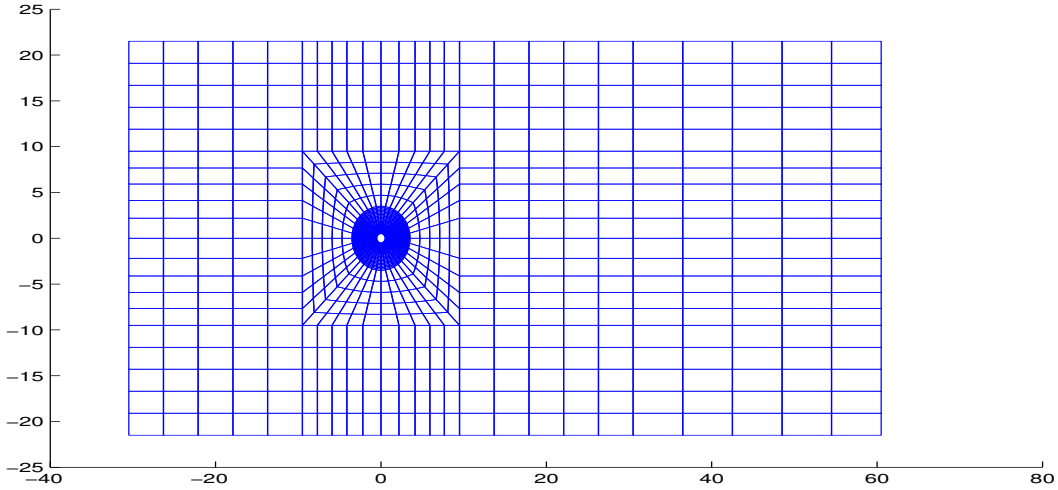

(b) Mesh of 1400 elements

Figure 6.22: Discretizations for the two different domain lengths for flow past a cylinder

Figure 6.20 shows a schematic of the problem. Since $L_0 = 1$ and the dimensionless radius of the cylinder is 1 we have $\hat{r} = 1$ meter. Flow domain consists of length L, height h and the cylinder is symmetrically located in the flow domain. Figure 6.22a show a 1300 element graded discretization for $(x \times y)$=$(-30.5, 30.5) \times (-21.5, 21.5)$. The cylinder is located at the center of the domain. Figure 6.22b showed another discretization in which the discretization of figure 6.22a remains unchanged but additional length has been added to the right of the cylinder. This discretization has 1400 elements. We choose solution of class C^{22} at p-level of 5 for ρ, u, v and T.

6.3.1 Starting or Initial solutions

From the discussion presented for Carter's plate for starting or initial solution, it is quite clear that attempts to solve this BVP with $\rho = 1, T = 1, u = 1, v = 0$ as initial solution are unlikely to succeed which infact is the case. From the preliminary studies we find that the starting solution for the velocity field is quite crucial. A starting solution (or initial solution) for velocity that replicates that similar flow features as in case of actual flow is essential to solve this problem at such high Reynolds number. For this purpose we resort to incompressible medium with isothermal flow but for exactly same geometry and discretizations. We consider water at NTP with the following properties :

$$\rho_0 = \hat{\rho} = 997.78\ \mathrm{Kg/m^3}\ ;\ \mu_0 = \hat{\mu} = 9.774 \times 10^{-4}\ \mathrm{Pa-s}\ ; \mathrm{L_0} = 1\ \mathrm{m}$$

Therefore,

$$\rho = 1, \mu = 1, L = \hat{L} \text{ and } Re = \frac{997.78}{9.774 \times 10^{-4}} u_0$$

We choose u_0 such that $Re = 10, 20, 30, 40, 60, 80, 100, 200$ and 500 are obtained and $u_{fs} = 1$ in all cases. The boundary conditions used for incompressible flow calculations are shown in figure 6.21b.

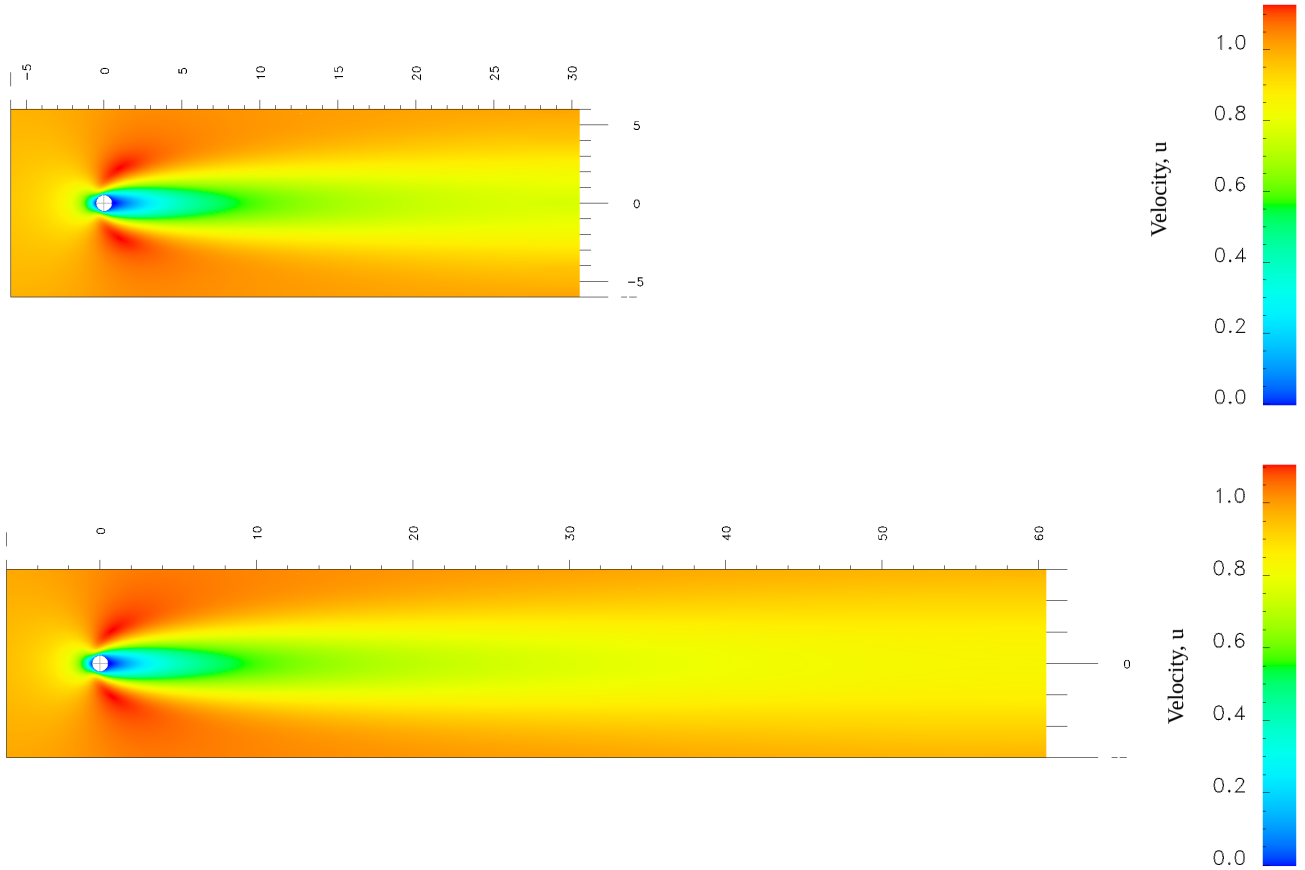

Figure 6.23: Comparison of Velocity component u for $Re = 10$ of lengths of 30.5 and 60.5 behind the cylinder (incompressible flow)

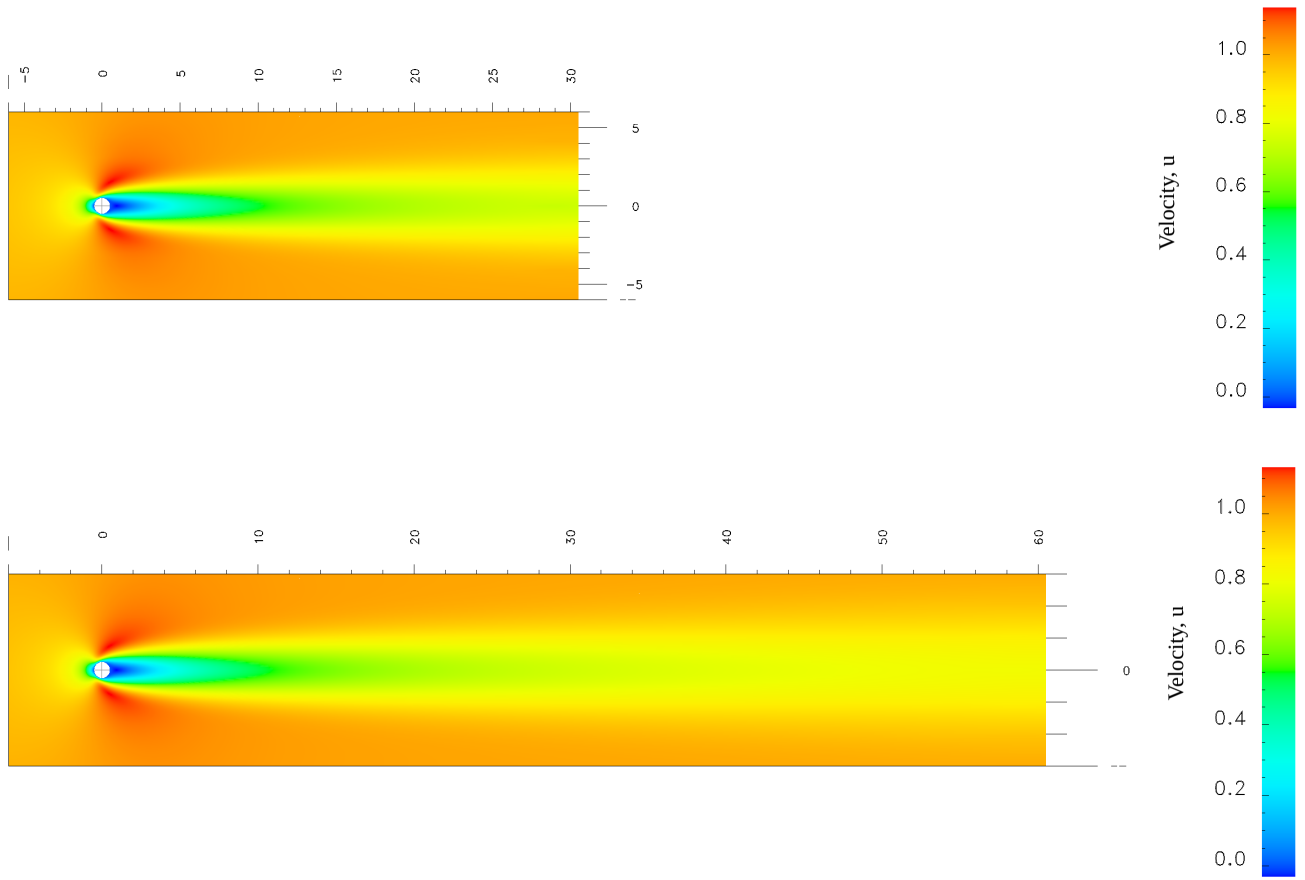

Figure 6.24: Comparison of Velocity component u for $Re = 20$ of lengths of 30.5 and 60.5 behind the cylinder (incompressible flow)

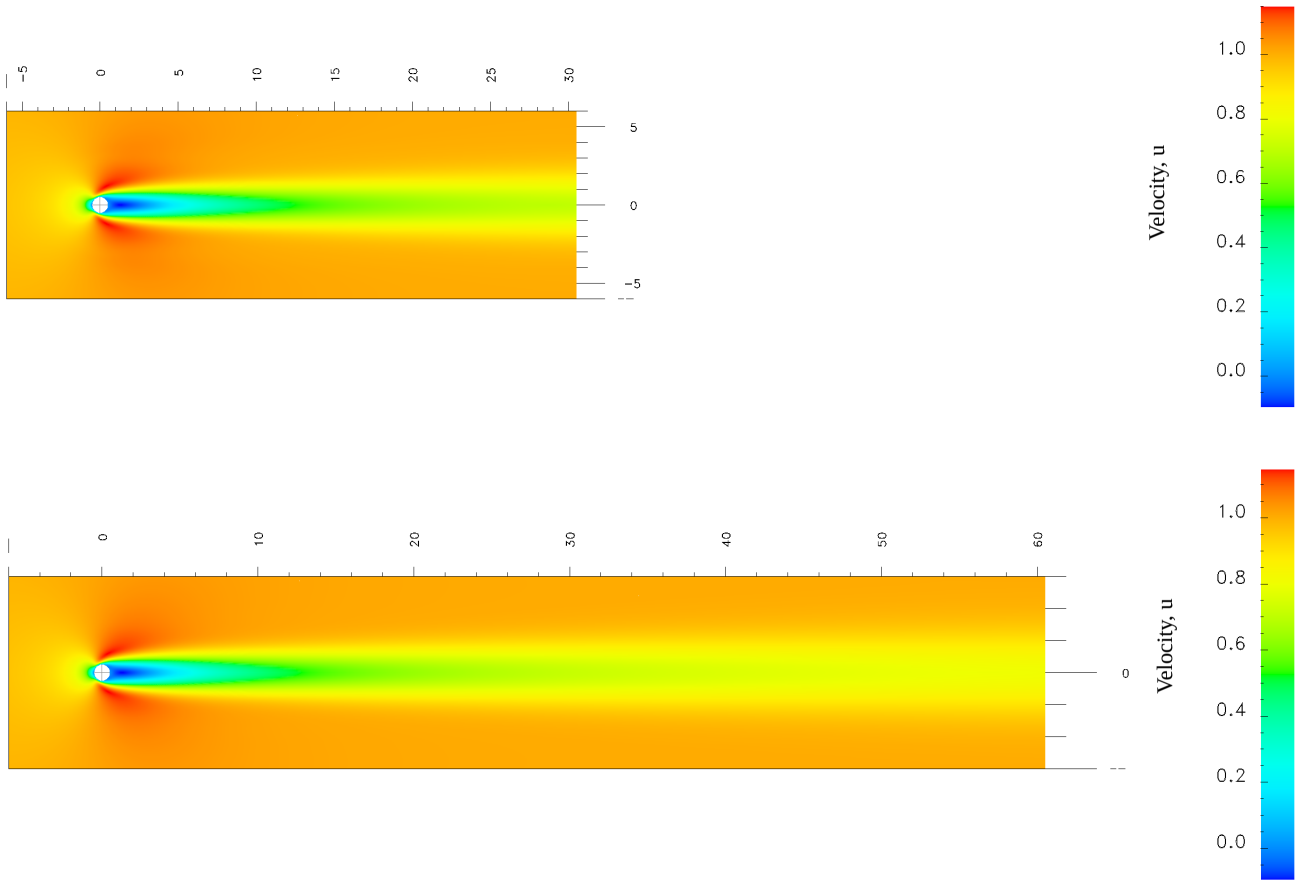

Figure 6.25: Comparison of Velocity component u for $Re = 40$ of lengths of 30.5 and 60.5 behind the cylinder (incompressible flow)

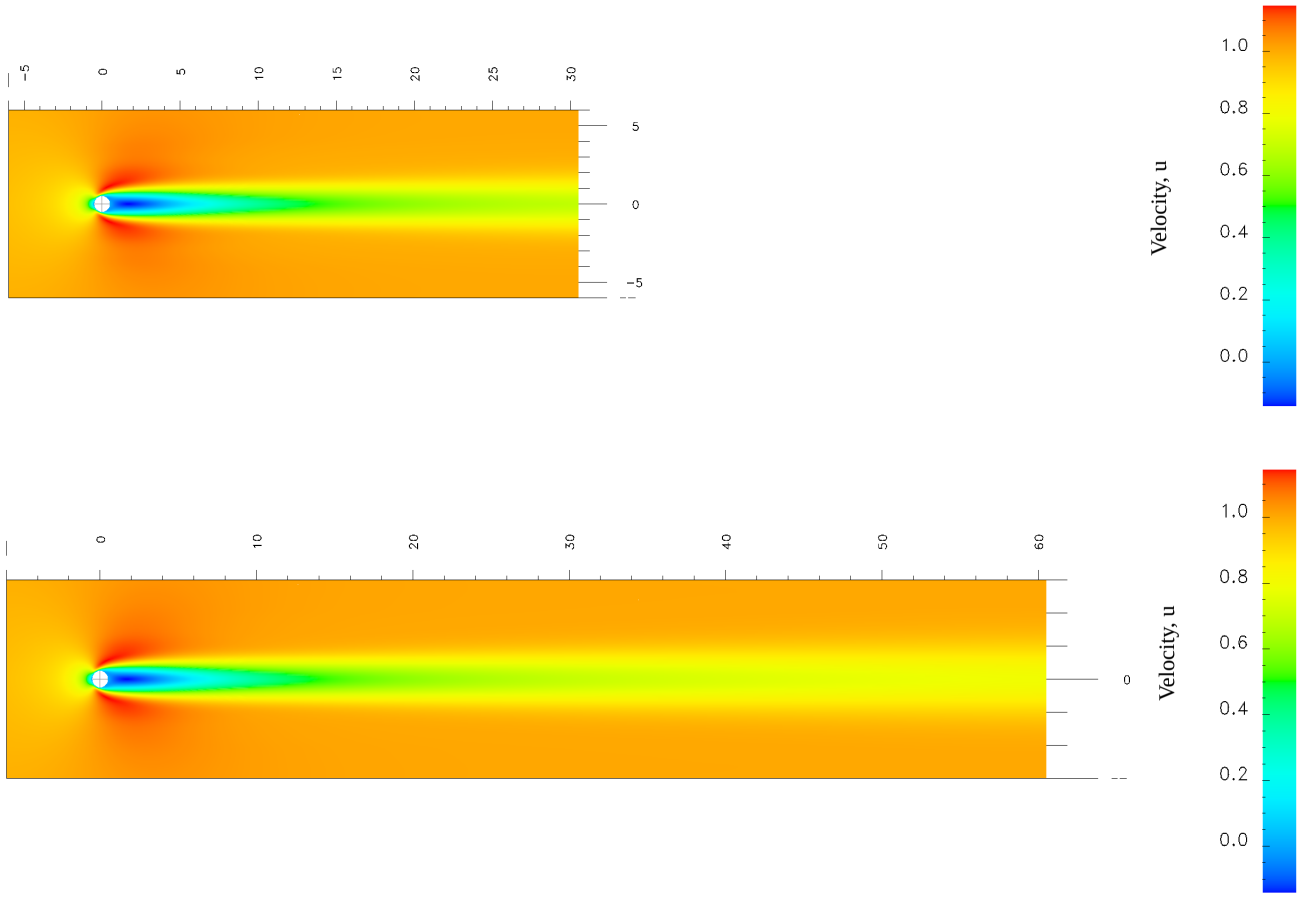

Figure 6.26: Comparison of Velocity component u for $Re = 60$ of lengths of 30.5 and 60.5 behind the cylinder (incompressible flow)

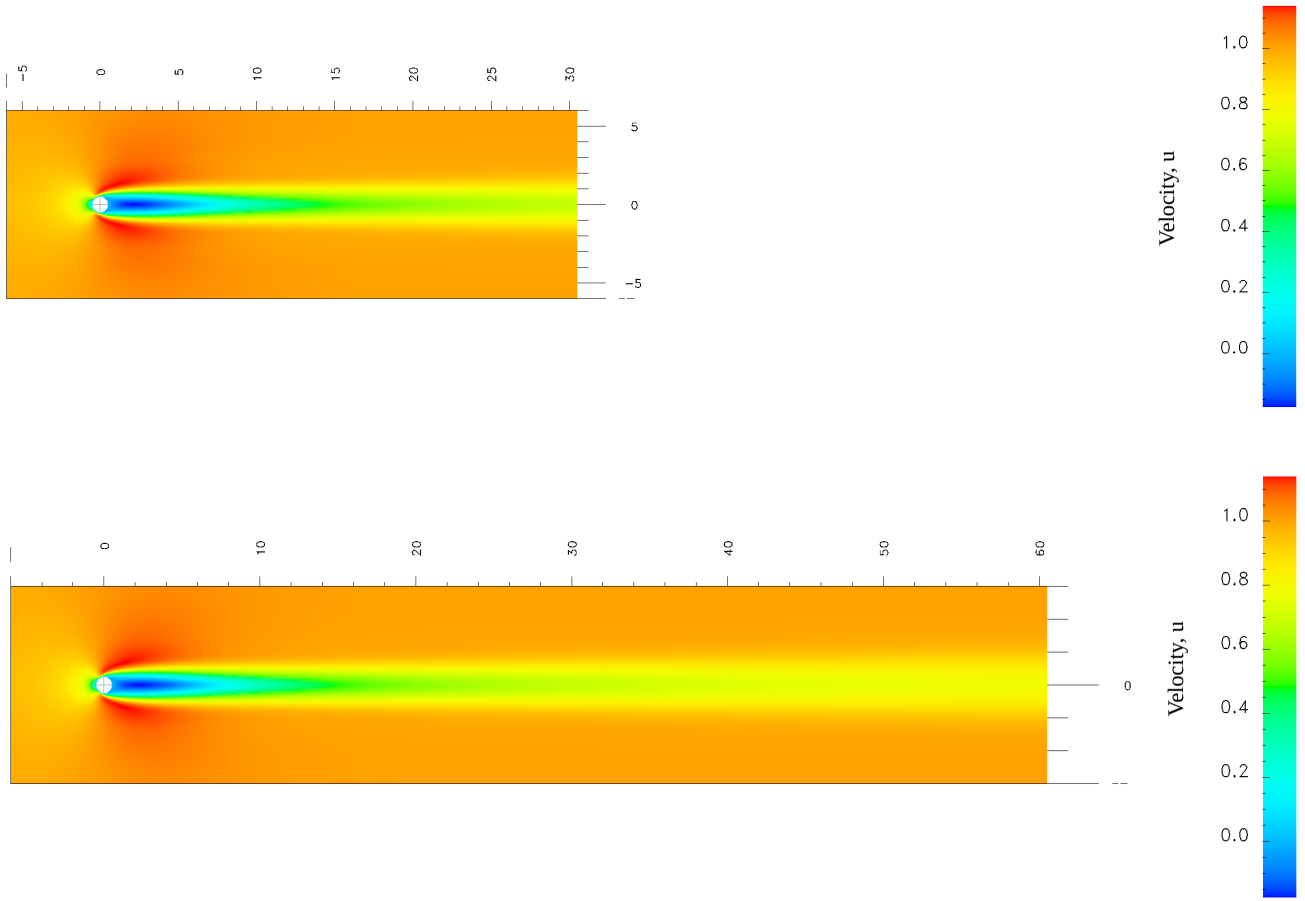

Figure 6.27: Comparison of Velocity component u for $Re = 80$ of lengths of 30.5 and 60.5 behind the cylinder (incompressible flow)

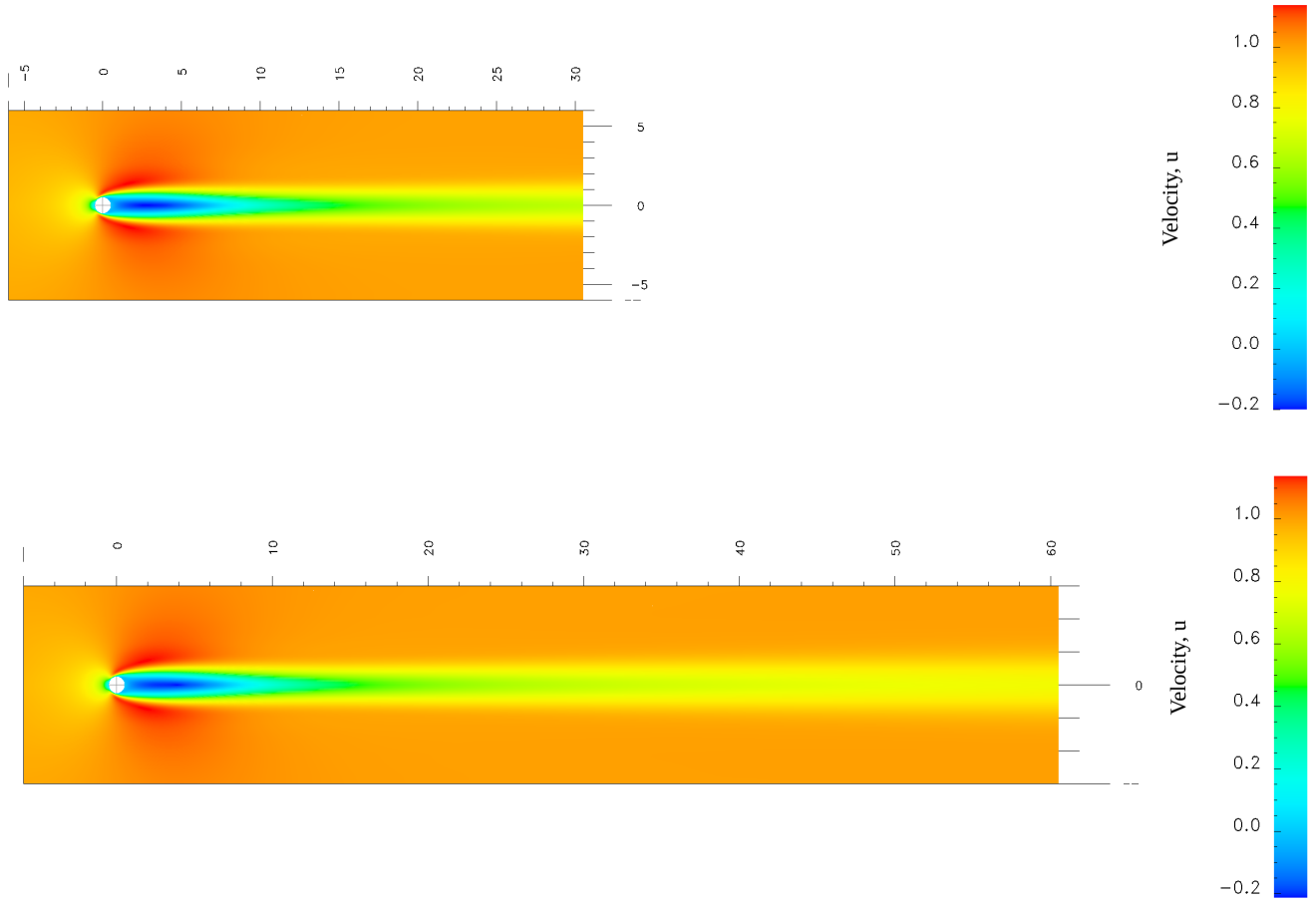

Figure 6.28: Comparison of Velocity component u for $Re = 100$ of lengths of 30.5 and 60.5 behind the cylinder (incompressible flow)

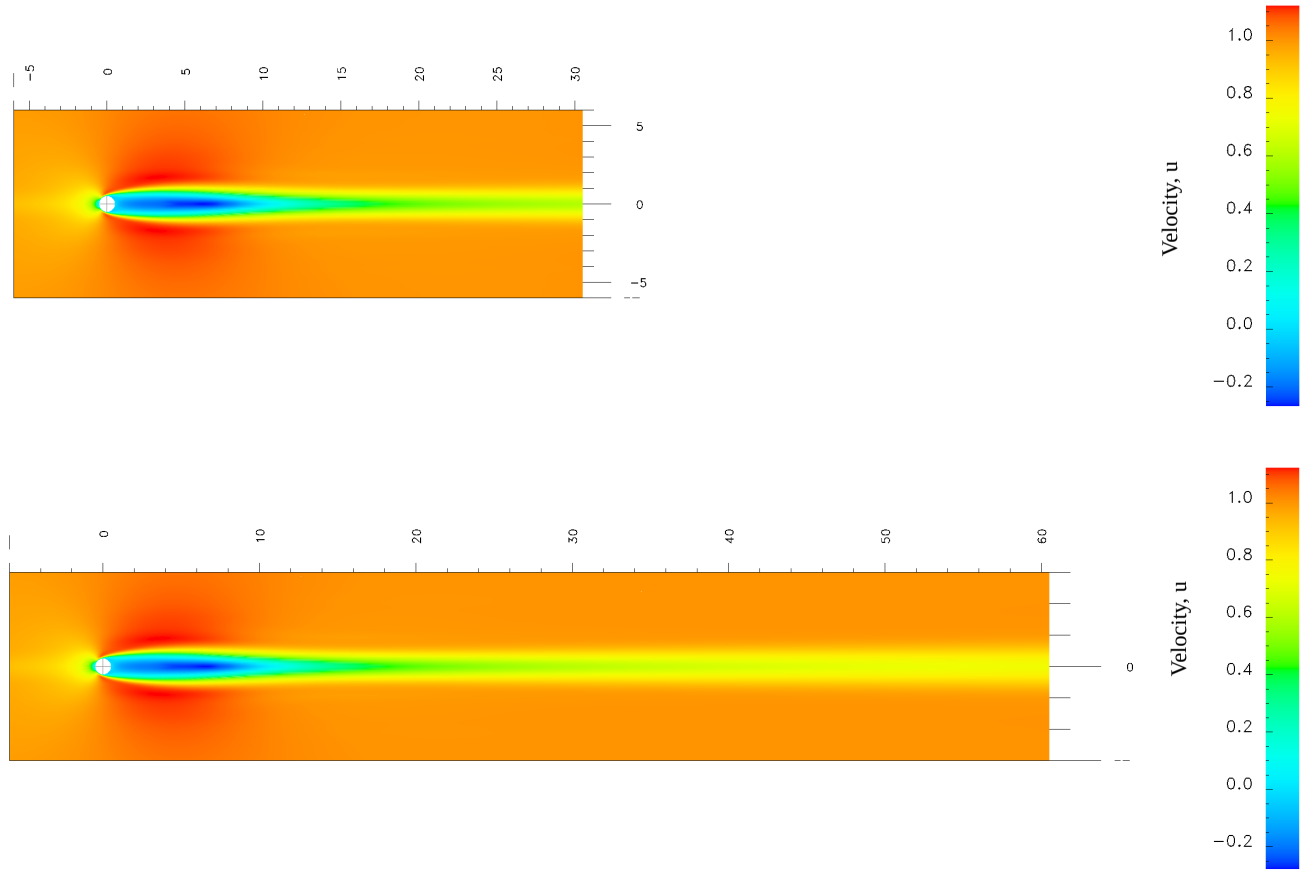

Figure 6.29: Comparison of Velocity component u for $Re = 200$ of lengths of 30.5 and 60.5 behind the cylinder (incompressible flow)

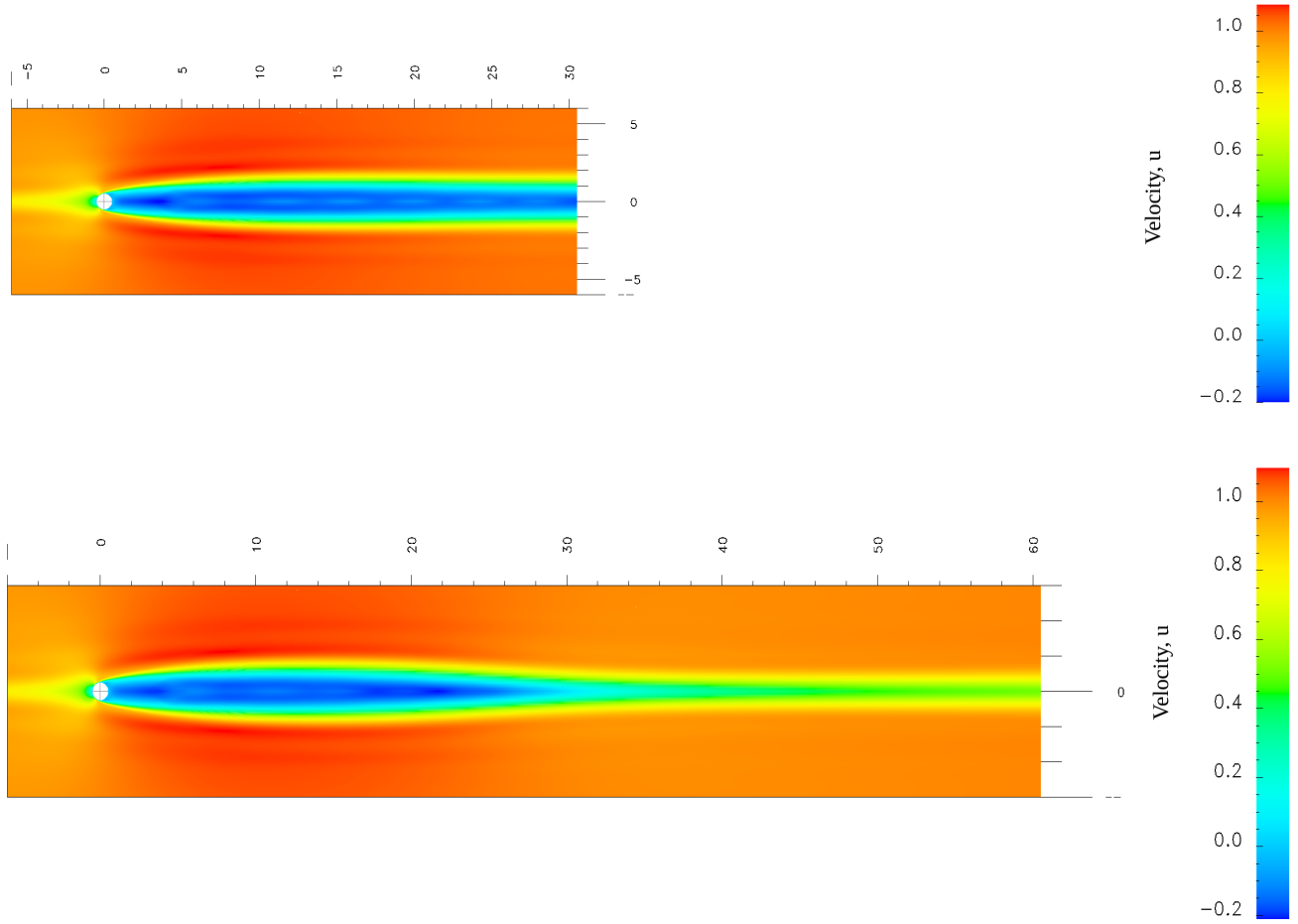

Figure 6.30: Comparison of Velocity component u for $Re = 500$ of lengths of 30.5 and 60.5 behind the cylinder (incompressible flow)

For $Re = 10$ no initial or starting solution is provided, thus Stokes flow becomes the starting solution at the end of first iteration in Newton's linear method. The convergence of the Newton's method is achieved in 5 iterations with $|g_i|_{max} = 0.332 \times 10^{-6}$ and $I = 0.213 \times 10^{-4}$. This solution is used as initial solution for $Re = 20$ (new u_0) to obtain a converged solution for $Re = 20$. This continuation process is continued until $Re = 500$ is reached for both 30.5 and 60.5 lengths of the domain past the cylinder. Table 6.1 gives details of Re, I, g and number of iterations. Contour maps of u velocity for Re=10...500 for lengths of 30.5 and 60.5 past the cylinder are shown in figures 6.23-6.30. We observe the following :

(a) For low Re (upto 200), the lengths of 30.5 and 60.5 yield same results due to the lack of influence of outflow boundar on the flow physics in the near field of the cylinder.

(b) At $Re = 500$, the length of 30.5 is obviously not sufficient where as length of 60.5 is still sufficient to capture the flow physics behind the cylinder.

(c) The importance of these studies is to provide us a good starting solution for the compressible flow at Mach 1. At Mach 1, the length required for fully developed compressible flow is obviously not known but is expected to be very large. However, if we choose a length of 30.5 behind the cylinder then we expect u velocity behavior of compressible flow to be similar in nature as in figure 6.30 (incompressible case) for 30.5 units length. In case of the length of 60.5 for compressible flow, we still expect the velocity field similar to that for 30.5 length (incompressible flow), thus for length of 60.5 behind

Re	I	$\|g_i\|_{max}$	no. of iterations
10	0.213×10^{-4}	0.332×10^{-6}	5
20	0.332×10^{-4}	0.645×10^{-6}	5
40	0.687×10^{-4}	0.159×10^{-7}	6
60	0.141×10^{-3}	0.196×10^{-6}	6
80	0.206×10^{-3}	0.598×10^{-6}	7
100	0.254×10^{-3}	0.208×10^{-6}	8
200	0.749×10^{-3}	0.510×10^{-6}	9
500	0.204×10^{-2}	0.932×10^{-6}	25

Table 6.1: Re, I, g for incompressible flow calculations

the cylinder the incompressible flow solution in figure 6.30 is not a good choice for a starting solution for compressible flow for length 60.5 behind the cylinder. Our studies infact show spurious solutions for the compressible flow of length of 60.5 when using the converged incompressible flow solution as a starting solutions. Thus for a length of 30.5 behind the cylinder the converged incompressible flow solution for $Re = 500$ should serve as a good starting solution for the compressible flow with length of 30.5 behind the cylinder.

6.3.2 Mach 1 flow past a circular cylinder

The medium is air and its properties at NTP, reference quantities etc have already been presented. We choose $u_0 = ... = u_s$, speed of sound with $u_{fs} = 1$. The domain and the discretization used is shown in figure 6.22a. The BCs used for compressible flow calculations are shown in figure 6.21a. Using the converged solution from the incompressible flow at $Re = 500$, the Newton's linear method converges in 50 iterations with $|g_i|_{max} = 0.613 \times 10^{-4}$ and $I = 0.206 \times 10^{-2}$.

Contour plots of u, v, ρ and T are shown in figures 6.31-6.34. High values of I indicate the GDEs are not satisfied accurately by the computed solution due to inadequate h and p and the length past the cylinder. Nonetheless the computational process works well in the sense that with continuation in Re, for the given h and p, the length past the cylinder and the outflow boundary conditions a solution satisfying discretized form of the GDEs is found ($\|g_i\| \leq 10^{-6}$). With h, p refinement, adequate length past the cylinder and appropriate outflow conditions we see no issues in resolving the correct physics with the laminar flow assumption. This work is currently in progress.

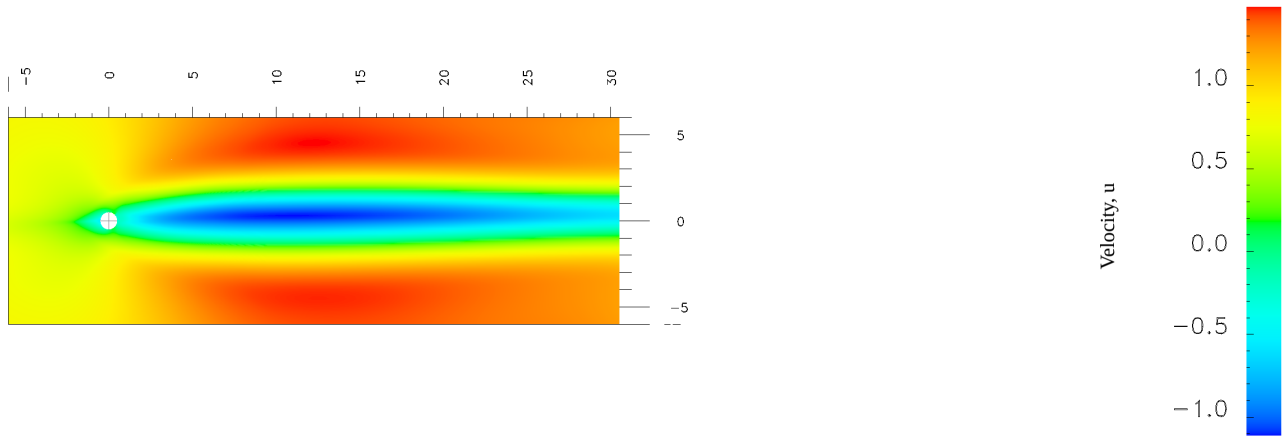

Figure 6.31: Contour plot of Velocity u for compressible flow past a cylinder of lengths of 30.5

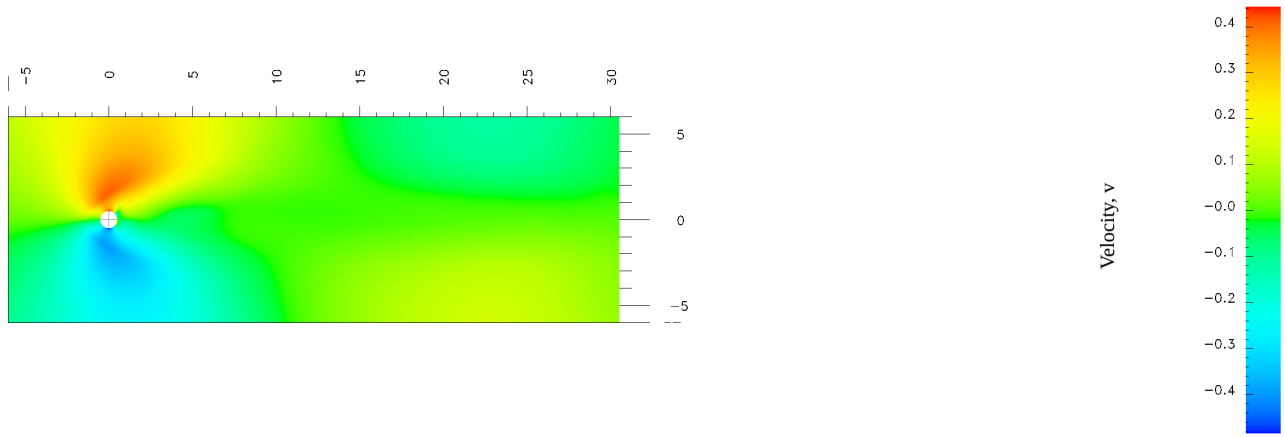

Figure 6.32: Contour plot of Velocity v for compressible flow past a cylinder of lengths of 30.5

Figure 6.33: Contour plot of Density ρ for compressible flow past a cylinder of lengths of 30.5

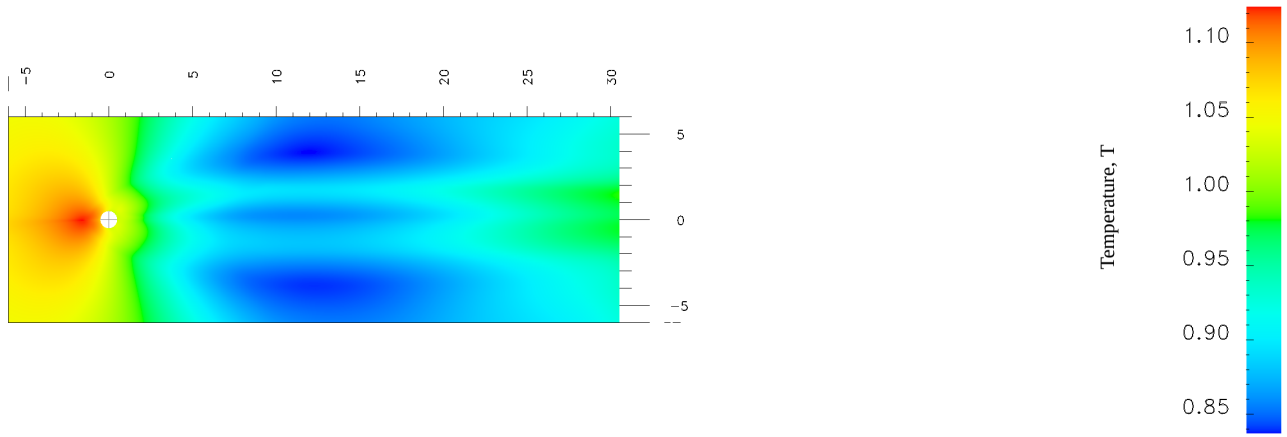

Figure 6.34: Contour plot of Temperature T for compressible flow past a cylinder of lengths of 30.5

6.4 Summary

In the following, we summarize the work presented in this chapter. Using Carter's plate for Mach 1, 2, 3 and 5 flows and Mach 1 flow past a circular cylinder as model problems, it is demonstrated that the solution of BVPs in viscous compressible flow with conducting medium is in fact possible in the h, p, k framework with variationally consistent integral forms.

(1) For Carter's plate Mach 1 flow is computed using free stream values as critical solution. For Mach 2, 3 and 5 a continuation procedure was necessary. What this means is that (for example) converged solution at Mach 1 is used as initial solution for Mach 2. For Mach 3 and 5, the Mach 1 converged solutions or the converged solutions at any other lower Mach numbers suffices as initial solution. Studies with different choices of initial solutions for higher Mach number flows yield the same converged solution, confirming its uniqueness to some extent.

(2) We like to emphasize that special care must be taken in defining boundary conditions to ensure the well posedness of BVP without over constraining. The choice of BCs here works well.

(3) Comparison of the u velocity as a function of y at outflow for different Mach numbers clearly shows progressively thinning boundary layer for increasing Mach numbers. Free stream $u_{fs} = 1$ for $y > 0.004$ confirm that $h = 0.01$ is sufficient to eliminate interaction of top boundary with the flow physics in the boundary layer.

(4) Comparisons of ρ and T versus y at the outflow for various Mach numbers shows decreasing density at the plate with increasing Mach number and increasing temperature with increasing Mach numbers with $\rho = 1$ and $T = 1$ for $y > 0.004$ confirming the adequacy of height $h = 0.01$.

(5) Velocity v versus y at the outflow for all Mach numbers shows maximum magnitude of the order of $O(10^{-5})$ (close to zero) confirming that the outflow is close to fully developed.

(6) It is significant to remark that all these simulations for BVPs are straight forward without any special treatments. Continuation for higher Mach number flows is essential due to Newton's linear method, but is quite straight forward to use.

(7) The flow past the circular cylinder at Mach 1 is a difficult problem from the point of view of : (I) flow physics (II) the length requirement behind the cylinder (III) choice of a good initial or starting solution for Newton's linear method. Using the velocity field from the solutions of incompressible Navier-Stokes equations for the same geometry and discretization for high Re shows that such BVPs for compressible flow can be solved in a rather straight forward manner without any special treatments (such as SUPG/DC/LS etc.). By no means, the results for compressible flow are of benchmark quality, but instead their importance is in demonstrating the feasibility of solving BVPs for viscous compressible flows at reasonable Mach number.

Chapter 7

Summary and Conclusions

Numerical Simulations of time dependent and stationary viscous compressible flows has been presented in h, p, k framework utilizing finite element and space-time finite element processes with variationally consistent and space-time variationally consistent integral forms. 1-D time dependent viscous Burgers equation and 1-D Riemann shock tube with viscous and conducting medium using ideal and real gas models for air and FC70 are used as model problems for time dependent flows. Carter's plate with Mach 1, 2, 3 and 5 flows and flow past a circular cylinder are used as model problems for time independent viscous compressible flows. In all cases Navier-Stokes equations with actual viscosity, conductivities and other transport properties form the basis for mathematical models. A summary of the work and the conclusion drawn from it are presented in the following ;

(1) The h, p, k framework permits higher order global differentiability local approximations in space and time due to k, the order of the approximation space yielding global differentiability of order ($k - 1$).

(2) Variationally consistent and space-time variationally consistent integral forms ensure unconditionally stable computational processes for BVPs and IVPs

during the entire evolution.

(3) Development of h, p, k framework with space-time variationally consistent integral forms (parallel to one presented by Surana et. al. for BVPs [30]-[32]) has been presented for IVPs. The space-time differential operators are classified over a space-time strip into non-self adjoint and non-linear operators. It is established that all other space-time methods of approximations except space-time least squares processes are space-time variationally inconsistent. Space-time variationally consistent integral forms yields symmetric and positive definite coefficient matrices and hence unconditionally stable computational processes regardless of the choices of h, p, k and the dimensionless parameters in the mathematical models describing IVPs. On the other hand STVIC integral forms yield non-symmetric coefficient matrices that may posses partial or completely complex basis. In such cases the computational processes are not unconditionally stable for arbitrary choices of h, p, k and the dimensionless parameters in the mathematical models.

(4) The finite element processes based on space-time VC integral forms when used for a space-time strip or a slab with time marching yield a computationally efficient framework hence, permit computations of time response over long period of time with relative efficiency. Additionally, space-time strip with time marching permits strict control over the accuracy of the evolution due to the fact that time marching is only commenced when a converged solution is obtained for the current space-time strip.

(5) Complete details of the mathematical models are presented for the model problems : 1-D time dependent viscous Burgers equation, 1-D Riemann shock tube and 2-D compressible flows. Ideal and real gas models and variable transport properties are considered and various commonly used models are described. Dimensionless forms of the mathematical models are presented using p_0 and τ_0 as reference values of pressure and stress to permit simulations near critical point in which case p_c, the critical pressure must be used for p_0. Various real gas models and their dimensionless forms (consistent with the conservation laws and constitutive equations) are also derived.

(6) Finite element formulations for BVPs based on LSP and IVPs based on STLSP are presented for each model problem. Minimally conforming spaces are discussed and the consequences of the various choices of approximation spaces in terms of the nature of the integrals (Riemann or Lebesgue) and the physics in the computations are discussed.

(7) For 1-D transient viscous form of Burgers equation various numerical studies corresponding to different BCs and ICs are presented and the results are evaluated against those available in the literature. Numerical studies consist of : (i) evolution and stationary states of single shock for $Re = 100, 1000$ and 10000. (ii) evolution and stationary state of double shock for $Re = 1000$. (iii) evolution of a transionic shock at $Re = 1000$. In all cases the least squares functional I of the order of 10^{-8} or lower ensures good time

accuracy of the evolutions. Studies demonstrate that a simple and straight forward methodology presented here yields highly accurate simulations for the transient viscous form of Burgers equation. In the limit $Re \rightarrow \infty$, the solutions of inviscid form are approached. The solution of the inviscid form of the Burgers equation are non-unique and hence require addition of artificial viscosity either in the mathematical models or during computations which are neither mathematically justified nor necessary in view of the present work in which every Re corresponds to physical diffusion for which very accurate solutions are possible in h, p, k framework with STVC integral forms.

(8) A number of different numerical studies are presented for 1-D Riemann shock tube using ideal and real gas models (Van der Waals equation of state) for air and FC70. The main thrust in this work is to show : (i) evolution of shock (ii) steady propagation of a shock (iii) interaction and reflection of shock (iv) shock structure resolution. We summarize the work in two separate sections for ideal and real gas models. In all cases S_r, the rate of entropy production per unit volume is used to quantify formation of shocks, propagation, interaction and their reflections.

(a) *Ideal gas Law* :

(a1) Using air as a medium with density ratio of 20 and isothermal initial conditions, details of shock evolution are presented. S_r always has maximum value in the rarefaction region immediately after the diaphragm rupture and for first few initial time steps. As evolution proceeds the

compression shock formation, propagation and reflection in the low density region is clearly demonstrated based on constant S_r. Fronts in the rarefaction region continue to disperse as expected.

(a2) Repeated shock reflections from impermeable and non-conducting boundaries and their interactions are demonstrated. During the entire evolution, constant S_r demonstrate good accuracy of evolution and sustained shocks.

(b) *Real gas law* : Using Van der Waals equation of state for FC70, 1-D Riemann shock tube simulations are presented to investigate the possibility of the existence of rarefaction shocks.

(b1) When initial conditions are partially in the zone of interest (isothermal or non-isothermal) neither rarefaction nor compression shocks are observed when using actual transport properties of FC70 (especially viscosity).

(b2) For the density ratios investigated, neither rarefaction nor compression shocks are observed when the initial conditions are away from the zone of interest.

(b3) When the viscosity of FC70 is lowered by a factor of ten and when the initial conditions are partly in the zone of interest, rarefaction shock formation and sustained propagation is observed. This confirms that if Euler's equations (zero viscosity) are used to study the existence of rarefaction shock then, undoubtedly rarefaction shock will be predicted.

This prediction is obviously false due to the fact that FC70 is not inviscid. Based on the study with low viscosity, for FC70 there is a threshold artificial value of viscosity say μ^* such that for $\mu^* < \mu$ the rarefaction shock will be observed. This is obviously non-physical.

(b4) All numerical studies conducted in this work various choices of ICs show that in the presence of actual viscosity of FC70 rarefaction shocks are not possible.

(b5) When viscosity of FC70 is lowered by a factor of ten and when the initial conditions are away from the zone of interest neither rarefaction nor compression shocks are observed for density ratios studies.

(b6) In conclusion rarefaction shocks are not possible for FC70 when actual properties of the medium are used.

(b7) A significant aspect of the work presented here is that we demonstrate evolution of a shock (unlike all other published work) and its sustained propagation based on constant S_r that unquestionably establishes the legitimacy of the entire process of formation of shocks, their propagation, interactions, reflections.

(9) Numerical studies for BVPs in compressible flow are presented using Carter's plate with Mach 1, 2, 3 and 5 flows and Mach 1 flow past a circular cylinder. We make following observations.

(a) BVPs in compressible flow can be solved without any special treatments. However, Newton's linear method used for solving non-linear

algebraic equations requires a starting solution in the close proximity of the solution sought. This is accomplished by a continuation process in which low Mach number (or Reynolds number) solutions are simply used as starting solution for higher Mach numbers.

(b) Studies for Carter's plate at Mach 1, 2, 3, 5 flows clearly show progressively diminishing boundary layers, decreasing density at the plate and increasing temperatures with accurate free stream conditions in all cases as we move away from the boundary layer. Low values of $|g_i|_{max} = O(10^{-6})$ show that converged solutions satisfy nonlinear algebraic equations quite well. In all cases the least squares functional I^e for an element 'e' of the order of $10{-}6$ or lower except the space-time element at the leading edge confirm good accuracy of the computed solutions.

(c) The BVPs involving flow past a circular cylinder were done in another study to demonstrate that the complexity of the flow physics may require a more rigorous continuation procedure but posses no special difficulty.

(d) In the formulations and in the numerical studies, the GDEs are never linearized or approximated in any other way. Up-winding methods such as SUPG, SUPG/DC, SUPG/DC/LS are neither needed nor utilized in the present work.

In Conclusion Numerical simulations of BVPs and IVPs based in Navier-Stokes equations describing viscous compressible flow in conducting medium can be

accomplished in a straight forward manner in h, p, k framework using VC and STVC integral forms. The computational processes always remain unconditionally stable. For IVPs, space-time strip with time marching provides error control and hence time accuracy of evolution as well as computational efficiency. The mathematical models based in Euler's equations lack physics, computational methods for Euler's equations require use of problem dependent up-winding methods which lack mathematical basis and rigor and thus, in our view are of little merit if any at all for viscous compressible flows.

Bibliography

[1] S.K. Godunov. The Problem of a Generalized Solution in the Theory of Quasilinear Equations and in Gas Dynamics. *Russian Mathematical Surveys*, 17(3):145–156, 1962.

[2] B.L. Rozhdestvenskii. Discontinuous Solutions Of Hyperbolic Systems of Quasilinear Equations. *Russian Mathematical Surveys*, 15(6):53–111, 1960.

[3] J. Glimm. Solutions in the Large for Nonlinear Hyperbolic Systems of Equations. *Communications on Pure and Applied Mathematics*, 18(4):697–715, 1965.

[4] A.N. Brooks and T.J.R. Hughes. Streamline Upwind/Petrov-Galerkin Formulations for Convection Dominated Flows with Particular Emphasis on the Incompressible Navier-Stokes Equations. *Computer Methods in Applied Mechanics and Engineering*, pages 199–259, 1990.

[5] K.S. Surana, S. Allu, and J.N. Reddy. The k-Version of Finite Element Method for Initial Value Problems: Mathematical and Computational Framework. *International Journal for Computational Methods in Engineering Science and Mechanics*, 8(3):123–136, 2007.

[6] A. Jameson. The Present Status, Challenges and Future Developments

in Computational Fluid Dynamics. *Proceeding of the AGARD 77th Fluid Dynamics Panel Symposium, Seville, Spain*, 1995.

[7] T. Pulliam. Artificial Dissipation Models for the Euler Equations. *AIAA Journal*, 24(12):1931–1940, 1986.

[8] G. May and A. Jameson. A Spectral Difference Method for the Euler and Navier-Stokes Equations on Unstructured Meshes. *AIAA Paper*, 2006.

[9] J.A. Smoller. On the Solution of the Riemann Problem with General Step Data for an Extended Class of Hyperbolic Systems. *Mich. Math. J*, 16:201–210, 1969.

[10] E. Hopf. On the Right Weak Solution of the Cauchy Problem for a Quasilinear Equation of First Order(Right Weak Solution of Cauchy Problem for First Order Quasi-Linear Equation). *Journal of Mathematics and Mechanics*, 19:483–487, 1969.

[11] K.O. Friedrichs and P.D. Lax. Systems of Conservation Equations with a Convex Extension. *Proceedings of the National Academy of Sciences of the United States of America*, 68(8):1686–1688, 1971.

[12] S.N. Kružkov. First Order Quasilinear Equations in Several Independent Variables. *Sbornik: Mathematics*, 10(2):217–243, 1970.

[13] M.S. Mock. Discrete shocks and Genuine Nonlinearity. *Michigan Math. J*, 25(2):131–146, 1978.

[14] M.S. Mock. On Fourth-Order Dissipation and Single Conservation Laws. *Communications on Pure and Applied Mathematics*, 29:383–388, 1976.

[15] R. DiPerna. Uniqueness of Solutions to Hyperbolic Conservation Laws. *Indiana Univ. Math. J*, 28(1), 1979.

[16] B.L. Keyfitz and H.C. Kranzer. Existence and Uniqueness of Entropy Solutions to the Riemann Problem for Hyperbolic Systems of two Nonlinear Conservation Laws. *Journal of Differential Equations*, 27:444–476, 1978.

[17] W. F. Noh. Errors for calculations of strong shocks using an artificial viscosity and artificial heat flux. *journal of computational physics*, 72(1):78–120, 1987.

[18] L. Rayleigh. Aerial Plane Waves of Finite Amplitude. *Proceedings of the Royal Society of London. Series A, Containing Papers of a Mathematical and Physical Character*, 84(570):247–284, 1910.

[19] R. Menikoff. Errors When Shock Waves Interact Due to Numerical Shock Width. *SIAM Journal on Scientific Computing*, 15:1227, 1994.

[20] D. Winterscheidt and K.S. Surana. p-Version Least Squares Finite Element Formulation for Convection-Diffusion Problems. *International Journal for Numerical Methods in Engineering*, 36(1):111–133, 1993.

[21] D. Winterscheidt and K.S. Surana. p-Version Least Squares Finite Element Formulation for Two-Dimensional, Incompressible Fluid Flow. *International Journal for Numerical Methods in Fluids*, 18:43–69, 1994.

[22] H. De Sterck, T.A. Manteuffel, S.F. McCormick, and L. Olson. Numerical Conservation Properties of H (div)-Conforming Least Squares Finite Element Methods for the Burgers Equation. *SIAM Journal on Scientific Computing*, 26(5):1573–1597, 2005.

[23] Z. Cai, T.A. Manteuffel, S.F. McCormick, and J. Ruge. First-Order System (FOSLL): Scalar Elliptic Partial Differential Equations. *SIAM Journal on Numerical Analysis*, 39:1418, 2001.

[24] P. Glaister. An Approximate Linearised Riemann Solver for the Euler Equations for Real Gases. *Journal of Computational Physics*, 74(2):382–408, 1988.

[25] K.S. Surana and D.G. Van Dyne. Non-Weak/Strong Solutions in Gas Dynamics: A C^{11} p-Version STLSFEF in Lagrangian Frame of Reference Using ρ, u, T Primitive Variables. *International Journal of Computational Engineering Science*, 2(3):357–382, 2001.

[26] K.S. Surana and D.G. Van Dyne. Non-Weak/Strong Solutions in Gas Dynamics: A C^{11} p-Version STLSFEF in Eulerian Frame of Reference Using ρ, u, p Primitive Variables. *International Journal for Numerical Methods in Engineering*, 53:1051–1099, 2002.

[27] K.S. Surana, S. Allu, P.W. Tenpas, and J.N. Reddy. k-Version of Finite Element Method in Gas Dynamics: Higher-Order Global Differentiability Numerical Solutions. *International journal for numerical methods in engineering*, 69(6):1109–1157, 2007.

[28] Argrow B.M. Fergason S.D., Ho T.L. and Emanuel G. Theory for Producing a Single-Phase Rarefaction Shock Wave in a Shock Tube. *Journal of Fluid Mechanics*, 445:37–54, 2001.

[29] I.M. Gel'fand and S.V. Fomin. *Calculus of Variations*. Courier Dover Publications, 2000.

[30] K.S. Surana, A.R. Ahmadi, and J.N. Reddy. The k-version of Finite Element Method for Self-Adjoint Operators in BVP. *International Journal of Computational Engineering Sciences*, 3(2):155–218, 2002.

[31] K.S. Surana, A.R. Ahmadi, and J.N. Reddy. The k-Version of Finite Element Method For Non-Self adjoint Operators in BVP. *International Journal of Computational Engineering Sciences*, 4(4):737–812, 2003.

[32] K.S. Surana, A.R. Ahmadi, and J.N. Reddy. k-version of Finite Element Method for Non-Linear Differential Operators in BVP. *International Journal of Computational Engineering Sciences*, 5(1):133–207, 2004.

[33] T.J.R. Hughes, L.P. Franca, and G.M. Hulbert. A new Finite Element Formulation for Computational Fluid Dynamics: VIII. The Galerkin/Least-Squares Method for Advective-Diffusive Equations. *Computer Methods in Applied Mechanics and Engineering*, 73(2):173–189, 1989.

[34] D.G. Van Dyne. Non-Weak/Strong Solutions in Gasdynamics. 1999.

[35] F. Shakib and T.J.R. Hughes. A New Finite Element Formulation for Computational Fluid Dynamics: IX. Fourier Analysis of Space-

Time Galerkin/Least-Squares Algorithms. *Computer Methods in Applied Mechanics and Engineering*, 87(1):35–58, 1991.

[36] R.W. Lewis and J.C. Bruch Jr. An Application of Least Square to One Dimensional Transient problems. *International Journal for Numerical Methods in Engineering*, 8:636–647, 1974.

[37] J. Donea. A Taylor-Galerkin Method for Convective Transport Problems. *International Journal for Numerical Methods in Engineering*, 20(24):101–120, 1984.

[38] R. Lohner, K. Morgan, and O.C. Zienkiewicz. The Solution of Non-Linear Hyperbolic Equation Systems by the Finite Element Method. *International Journal for Numerical Methods in Fluids*, 4:1043–1063, 1984.

[39] J. Kujawski and N.E. Wiberg. Least-Squares Schemes for Time Integration. *International Journal for Numerical Methods in Engineering*, 24:175, 1987.

[40] G.F. Carey and B.N. Jiang. Least-squares Finite Elements for First-Order Hyperbolic Systems. *International Journal for Numerical Methods in Engineering*, 26(1):81–93, 1988.

[41] B.N. Jiang and G.F. Carey. A Stable Least-Squares Finite Element Method for Non-Linear Hyperbolic Problems. *International Journal for Numerical Methods in Fluids*, 8(8):933–942, 1988.

[42] P.A.B. De Sampaio. A Petrov-Galerkin/Modified Operator Formulation for Convection-Diffusion Problems. *International Journal for Numerical Methods in Engineering*, 30:331–347, 1990.

[43] P.A.B. De Sampaio. A Petrov-Galerkin Formulation for the Incompressible Navier-Stokes Equations Using Equal Order Interpolation for Velocity and Pressure. *International Journal for Numerical Methods in Engineering*, 31:1135–49, 1991.

[44] I. Fried. Finite-element Analysis of Time-Dependent Phenomena(Finite Element Discretization Technique Extended to Time Dependent Processes Emphasizing Dynamics and Heat Conduction, Discussing Applications to Aircraft Transient Response). *AIAA Journal*, 7:1170–1173, 1969.

[45] J.T. Oden. A General Theory of Finite Elements, Part I and Part II. *International Journal for Numerical Methods in Engineering*, 1:247, 1969.

[46] A. Cella, M. Lucchesi, and G. Pasquinelli. Space-Time Elements for the Shock Wave Propagation Problem. *International Journal for Numerical Methods in Engineering*, 15:1475–1488, 1980.

[47] J.R. Yu and T.R. Hsu. Analysis of Heat Conduction in Solids by Space-Time Finite Element Method. *International Journal for Numerical Method in Engineering*, 21(11):15–88, 1985.

[48] E. Varoglu and W.D.L. Finn. A Finite Element Method for the Diffusion-

Convection Equation with Constant Coefficients. *Advances in Water Resources*, 1(6):337–343, 1978.

[49] E. Varoglu and W.D.L. Finn. Finite Elements Incorporating Characteristics for One Dimensional Diffusion-Convection Equation. *J. Comp. Phys*, 34:371–389, 1980.

[50] E. Varoglu and W.D.L. Finn. Space-Time Finite Elements Incorporating Characteristics for the Burgers Equation. *International Journal for Numerical Methods in Engineering*, 16:171–184, 1980.

[51] D.C.L. Lam. *Comparison of Finite-Element and Finite-Difference Methods for Nearshore Advection-Diffusion Transport Models*. 1977.

[52] G.R. Richter. A Finite Element Method for Time-Dependent Convection-Diffusion Equations. *Mathematics of Computation*, 54(189):81–106, 1990.

[53] H. Nguyen and J. Reynen. A Space-Time Least-Square Finite Element Scheme for Advection-Diffusion Equations. *Computer Methods in Applied Mechanics and Engineering*, 42:331–342, 1984.

[54] H. Nguyen and J. Reynen. A Space-Time Finite Element Approach to Burgers Equation. *Numerical Methods for Non-linear Problems*, 2:718–728.

[55] I. Kececioglu and B. Rubinsky. A Mixed-Variable Continuously Deforming Finite Element Method for Parabolic Evolution Problems. Part I: The Variational Formulation for Single Evolution Equation. *International journal for numerical methods in engineering*, 28:2583–2607, 1989.

[56] I. Kececioglu and B. Rubinsky. A Mixed-Variable Continuously Deforming Finite Element Method for Parabolic Evolution Problems. III: Numerical Implementation and Computational Results. *International journal for numerical methods in engineering*, 28(12):2715–2760.

[57] B.C. Bell and K.S. Surana. A Space-Time Coupled p-Version Least Squares Finite Element Formulation for Unsteady Fluid Dynamics Problems. *International Journal for Numerical Methods in Engineering*, 37:3545–3569, 1994.

[58] B.C. Bell and K.S. Surana. A Space-Time Coupled p-Version Least Squares Finite Element Formulation for Unsteady Two-Dimensional Navier-Stokes Equations. *International Journal for Numerical Methods in Engineering*, 39(15):2593–2618, 1996.

[59] K. S. Surana and Max Bona. Nonweak/strong solutions of linear and nonlinear hyperbolic and parabolic equations resulting from a single conservation law. *International Journal of Computational Engineering Science*, 1(2):299–330, 2000.

[60] K.S. Surana and D.G. Van Dyne. Non-Weak/Strong Solutions in Gas Dynamics: A C^{11} p-version STLSFEF in Eulerian Frame of Reference Using ρ, u, T Primitive Variables. *International Journal of Computational Engineering Science*, 2(3):383–483, 2001.

[61] K.S. Surana and D.G. Van Dyne. Non-Weak/Strong Solutions in Gas Dynamics: A C^{11} p-Version STLSFEF in Lagrangian Frame of Reference

Using ρ, u, p Primitive Variables. *International Journal for Numerical Methods in Engineering*, 53(5):1025–1050, 2002.

[62] HV Nayak. Solutions of Classes C^{00} and C^{11} for Two Dimensional Newtonian and Polymer Flows, Ph. D. Dissertation, University of Kansas, 2001.

[63] S.G. Mikhlin. *Variational Methods in Mathematical Physics*. Pergamon Press, 1964.

[64] C. Johnson. *Numerical Solution of Partial Differential Equations by the Finite Element Method*. Cambridge University Press New York, 1987.

[65] J.N. Reddy. *An Introduction to the Finite Element Method*. McGraw-Hill Singapore, 1993.

[66] W.A. Strauss. *Partial Differential Equations: An Introduction*. Wiley, 1992.

[67] G.B. Folland. *Introduction to Partial Differential Equations*. Princeton University Press, 1995.

[68] G.F. Carey and J.T. Oden. *Finite Elements: A Second Course*. Prentice-Hall, 1983.

[69] J.T. Oden and G.F. Carey. Finite Elements: Mathematical Aspects. *Texas Finite Element Series*, 4, 1983.

[70] K.S. Surana, L. Anthoni Raj, S. Allu, J.N. Reddy, and P.W. Tenpas. Strong And Weak Form of the Governing Differential Equations in Least Squares Finite Element Processes in h, p, k Framework. *International Journal for*

Computational Methods in Engineering Science and Mechanics, 8(3):123–136, 2007.

[71] G. Hellwig. Partial Differential Equations. An Introduction. Translated by E. Gerlach.(A Blaisdell Book in the Pure and Applied Sciences. 1964.

[72] J.A. Smoller. Contact Discontinuities in Quasi-Linear Hyperbolic Systems. *Communications on Pure and Applied Mathematics*, 23:791–801, 1970.

[73] K.S. Surana, S.R. Petti, A.R. Ahmadi, and J.N. Reddy. On p-Version Hierarchical Interpolation Functions For Higher-Order Continuity Finite Element Models. *International Journal of Computational Engineering Science*, 2(4):653–673, 2001.

[74] K.S. Surana. ME 840 class notes. *University of Kansas*, 2007.

[75] F.M. White. *Viscous Fluid Flow*. McGraw-Hill New York, 1974.

[76] G. Emanuel. *Gasdynamics, Theory and Applications*. American Institute of Aeronautics and Astronautics, 1986.

[77] W.F. Noh. Errors for Calculations of Strong Shocks Using an Artificial Viscosity and an Artificial Heat Flux. *Journal of Computational Physics*, 72(1):78–120, 1987.

[78] J.N. Reddy K.S. Surana and P.W. Tenpas. k-Version of Finite Element Method: A New Mathematical and Computational Framework for BVP and

IVP . *DTIC*, Accession Number: ADA465662(Report Number: AFRL-SR-ARTR-07-0087), 2007.

[79] K.S. Surana and J.S. Sandhu. Investigation of Diffusion in p-Version LSFE and STLSFE Formulations. *Computational Mechanics*, 16(3):151–169, 1995.

[80] Y.B. Zel'dovich. *Physics of Shock Waves and High-Temperature Hydrodynamic Phenomena*. Courier Dover Publications, 2002.

[81] H.A. Bethe. The Theory Of Shock Waves for an Arbitrary Equation of State. *US Army report*, pages 421–492, 1942.

[82] P.A. Thompson. A Fundamental Derivative in Gasdynamics. *Physics of Fluids*, 14:1843, 2003.

[83] M.S. Cramer and L.M. Best. Steady, Isentropic Flows of Dense Gases. *Physics of Fluids A: Fluid Dynamics*, 3:219, 1991.

[84] P.A. Thompson and K.C. Lambrakis. Negative Shock Waves. *Journal of Fluid Mechanics Digital Archive*, 60(01):187–208, 2006.

[85] M.S. Cramer. Shock Splitting in Single-Phase Gases. *Journal of Fluid Mechanics Digital Archive*, 199:281–296, 2006.

[86] P.A. Thompson, G.C. Carofano, and Y.G. Kim. Shock Waves and Phase Changes in a Large-Heat-Capacity Fluid Emerging From a Tube. *Journal of Fluid Mechanics Digital Archive*, 166:57–92, 2006.

[87] M.S. Cramer and A. Kluwick. On The Propagation of Waves Exhibiting Both Positive and Negative Nonlinearity. *Journal of Fluid Mechanics Digital Archive,* 142:9–37, 2006.

[88] M.S. Cramer and R. Sen. Exact Solutions for Sonic Shocks in Van Der Waals Gases. *Physics of Fluids,* 30:377, 1987.

[89] B.P. Brown and B.M. Argrow. Nonclassical Dense Gas Flows for Simple Geometries. *AIAA Journal,* 36(10):1842–1847, 1998.

[90] A. Kluwick. Transonic Nozzle Flow of Dense Gases. *Journal of Fluid Mechanics Digital Archive,* 247:661–688, 2006.

[91] J.F. Monaco, M.S. Cramer, and L.T. Watson. Supersonic Flows of Dense Gases in Cascade Configurations. *Journal of Fluid Mechanics,* 330:31–59, 1997.